Quantum versus Chaos

Questions Emerging from Mesoscopic Cosmos

by

Katsuhiro Nakamura

Kluwer Academic Publishers

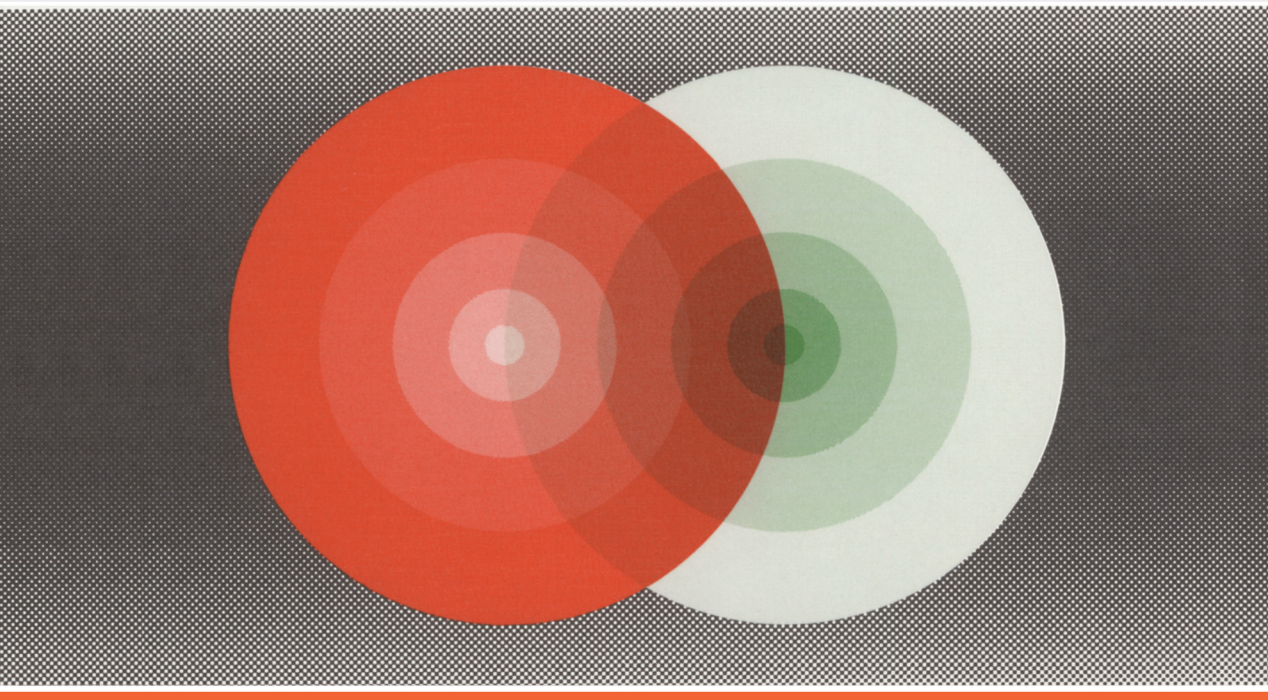

Fundamental Theories of Physics

Quantum versus Chaos

Fundamental Theories of Physics

An International Book Series on The Fundamental Theories of Physics: Their Clarification, Development and Application

Editor: ALWYN VAN DER MERWE
University of Denver, U.S.A.

Editorial Advisory Board:

LAWRENCE P. HORWITZ, *Tel-Aviv University, Israel*
BRIAN D. JOSEPHSON, *University of Cambridge, U.K.*
CLIVE KILMISTER, *University of London, U.K.*
PEKKA J. LAHTI, *University of Turku, Finland*
GÜNTER LUDWIG, *Philipps- Universität, Marburg, Germany*
ASHER PERES, *Israel Institute of Technology, Israel*
NATHAN ROSEN, *Israel Institute of Technology, Israel*
EDUARD PRUGOVECKI, *University of Toronto, Canada*
MENDEL SACHS, *State University of New York at Buffalo, U.S.A.*
ABDUS SALAM, *International Centre for Theoretical Physics, Trieste, Italy*
HANS-JÜRGEN TREDER, *Zentralinstitut für Astrophysik der Akademie der Wissenschafen, Germany*

Volume 87

Quantum versus Chaos

Questions Emerging from Mesoscopic Cosmos

by

Katsuhiro Nakamura

Faculty of Engineering,
Osaka City University,
Osaka, Japan

KLUWER ACADEMIC PUBLISHERS
NEW YORK / BOSTON / DORDRECHT / LONDON / MOSCOW

eBook ISBN: 0-306-47121-3
Print ISBN: 0-792-34557-6

©2002 Kluwer Academic Publishers
New York, Boston, Dordrecht, London, Moscow

All rights reserved

No part of this eBook may be reproduced or transmitted in any form or by any means, electronic, mechanical, recording, or otherwise, without written consent from the Publisher

Created in the United States of America

Visit Kluwer Online at: http://www.kluweronline.com
and Kluwer's eBookstore at: http://www.ebooks.kluweronline.com

Table of Contents

Preface ix

Chapter 1. Genesis of chaos and breakdown of quantization of adiabatic invariants 1
1.1. Introduction 1
1.2. Collapse of KAM tori and onset of chaos 2
1.3. Diagnostic characters of chaos 7
1.4. Suppression of chaos in quantum dynamics 9
1.5. Breakdown of quantization of adiabatic invariants 11
References 14

Chapter 2. Semiclassical quantization of chaos: trace formula 15
2.1. Green's function and Feynman's path integral method 15
2.2. Quantization of integrable systems 17
2.3. Quantization of chaos: trace formula 19
2.4. Application of trace formula to autocorrelation functions 22
2.5. Significance and limitation of trace formula 29
References 30

Chapter 3. Pseudo-chaos without classical counterpart in 1-dimensional quantum transport 31
3.1. Introduction 32
3.2. Quantum transport in superlattice and pseudo-chaos 32
3.3. Resonant tunneling in double-barrier structure and pseudo-chaos 39
3.4. General remarks 43
References 44

Chapter 4. Chaos and quantum transport in open magnetic billiards: from stadium to Sinai billiards 45
4.1. Introduction 46

4.2. Magneto-conductance in stadium billiard: experimental results 47
4.3. Transition from chaos to tori 50
4.4. Quantum-mechanical and semiclassical theories 54
4.5. Comparison in stadium billiards between theory and experiment 59
4.6. Open Sinai billiard in magnetic field: distribution of Lyapunov exponents and ghost orbits 66
4.7. Comparison in Sinai billiard between quantal and classical theories 70
4.8. Summary 75
References 76

Chapter 5. Chaotic scattering on hyperbolic billiards: success of semiclassical theory 79
5.1. Introduction 79
5.2. Exact quantum theory 83
5.3. Semiclassical theory 85
5.4. Distribution of complex resonances 92
5.5. Experiment on antidot arrays in magnetic field 97
References 100

Chapter 6. Nonadiabaticity-induced quantum chaos 102
6.1. Avoided level crossings and gauge structure 102
6.2. Nonadiabatic transitions and gauge structure 107
6.3. Forces induced by Born-Oppenheimer approximation 117
6.4. Nonadiabaticity-induced chaos 119
References 125

Chapter 7. Level dynamics and statistical mechanics 127
7.1. Level dynamics: from Brownian motion to generalized Calogero-Moser-Sutherland (gCM/gCS) system 127
7.2. Soliton turbulence: a new interpretation of irregular spectra 136
7.3. Statistical mechanics of gCM system 142
7.4. Statistical mechanics of gCS system in intermediate regime 151
7.5. Extension to case of several parameters 154
References 160

Chapter 8. Towards time-discrete quantum mechanics 162
8.1. Stable and unstable manifolds in time-discrete classical dynamics 162
8.2. Breakdown of perturbation theory 166
8.3. Internal equation and Stokes phenomenon 168
8.4. Asymptotic expansion beyond all orders and homoclinic structures 175
8.5. Time discretization and quantum dynamics 181
8.6. Time-discrete unitary quantum dynamics 183
8.7. Time-discrete non-unitary quantum dynamics 186
8.8. Problems to be examined 196
References 197

Chapter 9. Conclusions and prospects 198
References 207

Index 209

Preface

The framework of quantum mechanics in the adiabatic limit where no quantum transition occurs is traced back to the quantization condition of adiabatic invariants, i.e., of action variables. In fact, the interpretation of this condition as the commutation rule for a pair of canonical variables led to the construction of Heisenberg's matrix equation; another interpretation of this condition, as that for confining a standing wave, led to the birth of Schrödinger's wave mechanics. In classically-chaotic systems, however, the stable tori are broken up and we can conceive no action to be quantized. Therefore, we cannot prevent ourselves from being suspicious of using the present formalism of quantum mechanics beyond the logically acceptable (i.e., classically-integrable) regime. Actually, quantum dynamics of classically-chaotic systems yields only quasi-periodic and recurrent behaviors, thereby losing the classical-quantum correspondence. There prevails a general belief in the incompatibility between *quantum* and *chaos*. Presumably, a generalized variant of quantum mechanics should be established so as to accommodate the temporal chaos.

The range of validity of the present formalism of quantum mechanics will be elucidated by an accumulation of experiments on the mesoscopic or nanoscale cosmos. Owing to recent progress in advanced technology, nanoscale quantum dots such as chaotic stadium and integrable circle billiards have been fabricated at interfaces of semiconductor heterojunctions, and quantum transport in these systems is under active experimental investigation. Anomalous fluctuation properties as well as interesting fine spectral structures that have already been reported are indicating symptoms of chaos. Quantum transport in mesoscopic systems will serve as a nice candidate for elucidating the effectivenes and noneffectiveness of quantum mechanics when applied to classically-chaotic systems. The experimental results could even provide a clue towards the creation of a generalized quantum mechanics, just as blackbody cavity radiation at the turn of the last century did for the creation of present-day

quantum mechanics.

Therefore, in this book I shall investigate quantum transport in mesoscopic systems that are classically chaotic, showing the success and failure of theoretical trials to explain experimental issues. My basic idea is as follows: Our inability to explain anomalous quantum effects in mesoscopic systems is due partly to our formalism's inability to describe situations sensitive to initial conditions and partly to technological weakness in making fine-grained predictions without being affected by extrinsic noises and random potentials.

Despite active research on the *semiclassical quantum theory of chaotic systems,* most of the semiclassical treatment of bounded and open systems have not fully succeeded to capture the clear signatures of chaos because of wave diffraction effects, the difficulty of systematic enumeration of scattering and/or periodic orbits, etc. I shall also develop the semiclassical theory (i.e., scattering theory for open systems and trace formula for bounded systems) and raise some unsatisfactory points involved in this traditional theory. The existing semiclassical theory could not be the ultimate theory of quantization of chaos. There is thus a need to go in a radically new direction to accommodate a genuine temporal chaos in quantum dynamics.

In an attempt to see the unambiguous quantum-classical correspondence in the semiclassical realm of chaotic systems, we shall come to question the continuity of the time variable. With the help of recent progress in nonlinear classical dynamics, I have dared to hint at a slightly portentous proposal to construct a generalized quantum mechanics by discretizing the *"time"* and to describe interesting outcomes emerging from the procedure of time discretization in quantum dynamics.

It is our hope that, through the insights gained from studying the chapters that follow, readers would be greatly encouraged to comprehend the incompatibility between *quantum* and *chaos* and to start their own speculation on a new framework of quantum mechanics that would unify these two key concepts in contemporary science.

I am grateful to many people, including J. P. Bird, A. Bulgac, P. Gaspard, S. Kawabata, C. M. Marcus, S. A. Rice, and Y. Takane for stimulating discussions that have sharpened my ideas as embodied in the present book. I wish to thank Alwyn van der Merwe for his critical reading of the manuscript and improving its grammatical errata.

Chapter 1

Genesis of Chaos and Breakdown of Quantization of Adiabatic Invariants

Key words and key concepts required to understand the following chapters are explained below. With increase of perturbations, resonances break the Kolmogorov-Arnold-Moser (KAM) tori, leading to a genesis of chaos. Characterization of chaotic behaviors is achieved by using Lyapunov exponent and the Kolmogorov-Sinai entropy. We consider how chaos affects quantum mechanics by addressing the breakdown in the quantization of adiabatic invariants.

1.1. Introduction

Over the past decades, an increasing number of researchers have taken up studies of chaos. Most nonlinear dynamical systems, from driven pendulum to fluid turbulence, display chaotic behaviors. It is rather difficult to address, among diverse systems in nature, those that cannot exhibit chaos. The concept of chaos is, however, inherently relevant to classical dynamics. Standard diagnostic characters such as sensitivity to initial conditions and a nonvanishing Kolmogorov-Sinai entropy are meaningful only in classical dynamical systems.

On the other hand, we all recognize that quantum mechanics, the greatest theory constructed in the 20th century, can explain a lot of microscopic phenomena, such as superconductivity, superfluidity, and the quantum Hall effect, and moreover serve as an indispensable

guiding principle for today's science and technology. The genesis of chaos, however, is disturbing the foundation of the quantum theory. Researchers in the forefront have begun to reveal the quantum-mechanical fingerprints of chaos and even to contemplate the invention of a generalized version of quantum mechanics which would have an unambiguous correspondence with chaos.

In classical mechanics, the Hamilton equation is nonlinear in general. In the case of chaotic systems, the stretching and folding (Smale's horse-shoe) mechanism gives rise to a phase droplet (i.e., a cluster of initial points in phase space) that evolves into self-similar structures on infinitely small scales in phase space. In the corresponding quantum dynamics, however, the wavefunctin Ψ will show a recurrent (time-periodic) phenomenon, i.e., suppression of chaotic diffusion because of the linearity of the time-dependent Schrödinger equation. From a viewpoint of measurement, Heisenberg's uncertainty principle imposes a limitation of the order of Planck constant $\hbar$ in the resolution of phase space, leading to the unavoidable incompatibility between quanta and chaos.

In this book we shall describe this incompatibility in detail and present some challenging attempt to reconcile or unify these contradictory concepts. To begin with, standard diagnostics of chaos will be sketched.

1.2. Collapse of KAM Tori and Onset of Chaos

To explain the mechanism for the onset of chaos, we choose a two-dimensional oscillator (without dissipation) described by the Hamiltonian

$$H_0 = \sum_{i=1,2} (p_i^2 + \omega_i^2 q_i^2)/2 \ . \tag{1.1}$$

A canonical transformation from $\{p_i, q_i\}$ to $\{J_i, \varphi_i\}$ with the action $J_i = (2\pi)^{-1} \oint p_i \mathrm{d}q_i$ and angle $\varphi_i = \omega_i t$ converts (1.1) into

$$H_0 = \sum_{i=1,2} \omega_i J_i \equiv H_0(J_1, J_2) \ . \tag{1.2}$$

The $\{J_i\}$ are obviously constants of motion, i.e., $\mathrm{d}J_i/\mathrm{d}t = -\partial H_0/\partial \varphi_i = 0$. Any orbit is either periodic or quasi-periodic, and confined on the

surface of the torus characterized by a suitable set of radii J_1 and J_2; see Fig. 1.1.

On introduction of nonintegrable perturbation V, the Hamiltonian becomes

$$H = H_0(J_1,J_2) + \varepsilon \sum_{m,n} f_{mn}(J_1,J_2)\cos(m\varphi_1 + n\varphi_2), \tag{1.3}$$

where ε is a constant of O(1) and m, n run over the set of integers. The stability of the torus will be examined below.

Using a generating function

$$W = J_1'\varphi_1 + J_2'\varphi_2 + \varepsilon \sum_{m,n} g_{mn}(J_1',J_2')\sin(m\varphi_1 + n\varphi_2), \tag{1.4}$$

we consider the canonical transformation

$$J_i = \partial W/\partial \varphi_i = J_i' + \varepsilon \sum_{m,n} \begin{Bmatrix} m \\ n \end{Bmatrix} g_{mn}\cos(m\varphi_1 + n\varphi_2), \tag{1.5a}$$

$$\varphi_i' = \partial W/\partial J_i' = \varphi_i + \varepsilon \sum_{m,n} (\partial g_{mn}/\partial J_i')\sin(m\varphi_1 + n\varphi_2). \tag{1.5b}$$

Then the Hamiltonian (1.3) is transformed into

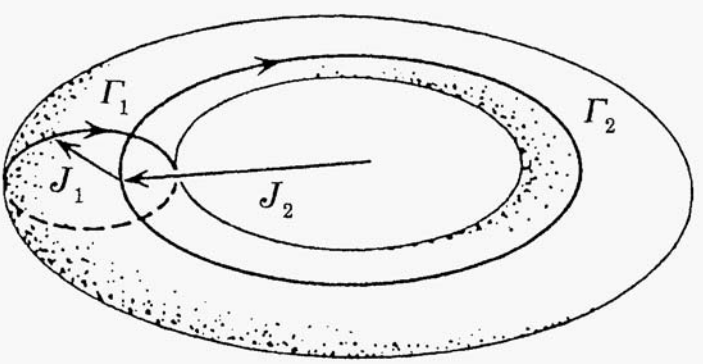

Fig. 1.1. 2-dimensional torus with action variables J_1 and J_2. Γ_1 and Γ_2 are mutually irreducible closed paths.

$$H = H_0(J_1', J_2') + \sum_{i=1,2} (\partial H_0/\partial J_i)(J_i - J_i') + \cdots$$

$$= H_0(J_1', J_2') + \varepsilon \sum_{m,n} [(m\omega_1 + n\omega_2) g_{mn} + f_{mn}] \cos(m\varphi_1' + n\varphi_2') + O(\varepsilon^2), \quad (1.6)$$

where $\omega_i = \partial H_0/\partial J_i$ are exploited. The method for treating the term linear in ε depends on the magnitude of f_{mn}

If the magnitude of the perturbation is small enough to ensure $|f_{mn}| << |m\omega_1 + n\omega_2|$ for an arbitrary set of m and n, we can choose

$$g_{mn} = -f_{mn}/(m\omega_1 + n\omega_2) \quad (<<1), \quad (1.7)$$

eliminating the ε-linear term in (1.6). In fact, in case of the nonresonant tori with the irrational winding number $\gamma = \omega_2/\omega_1$, any rational number m/n can not fall within the small but finite range around γ and thereby we can obtain (1.7). Rigorously speaking, the resonant tori with the rational number γ also exist, making the denominator of (1.7) vanishing, but most of the tori are irrational and the fraction of the resonant tori is negligible as a whole. Higher-order terms in ε in (1.6) can also be made to vanish by repetition of the same procedure as (1.4) through (1.7). Finally the Hamiltonian is written as

$$H = H_0(J_1^{(\infty)}, J_2^{(\infty)}) \quad . \quad (1.8)$$

We again obtain the torus. Therefore, as long as the perturbation V is small enough, most of the tori are stable though slightly deformed. These invariant tori are called as Kolmogorov-Arnold-Moser or KAM tori.

On the other hand, in the case of the large perturbation, one sees that $|f_{mn}| >> |m\omega_1 + n\omega_2|$ even for the nonresonant tori. Consequently one fails to get a generating function with $|g_{mn}| << 1$ to suppress the ε- linear term in (1.6): We get extremely wide resonant regions. The original torus will now collapse or be broken into pieces, and any orbit wanders in an erratic way over an infinitely large number of these pieces. This completes a scenario for the collapse of KAM tori.

We shall proceed with providing a mechanism for the genesis of chaos. A picture by which the most unstable torus (i.e., a separatrix)

collapses will be shown vividly by resorting to the Poincare' mapping. This map establishes a relation between succcessive discrete points constructed every time that the trajectory generated by time-continuous classical dynamics crosses a suitable cross section (i.e., Poincare' section) from a definite side. For instance, an arbitrary cross section of the torus discussed above is the Poincare' section, and each point in this section is generated by the area-preserving 2 x 2 mapping F obtained from a Hamiltonian system with 2 degrees of freedom. The KAM tori are represented by line manifolds (e.g., curved lines). When the system is integrable, F depicts the Poincare' section filled by KAM tori that generally involve fixed points, i.e., points $\{Q^*\}$ satisfying $FQ^*=Q^*$. Each fixed point has a pair of stability eigenvalues Λ Λ^{-1}. The fixed points with Λ (real) >I and those with $\Lambda=e^{i\theta}$ are called hyperbolic and elliptic fixed points, respectively. For the hyperbolic fixed points, in particular, the pair of stability eigenvectors $\mathbf{v}_s$ and $\mathbf{v}_u$, characterize interesting flows around the fixed points. By successive operation of F, the point on v_s approaches the fixed point, say Q_0, whereas the point on v_u moves away from Q_0. More globally, there exist stable and unstable manifolds Γ_s and Γ_u extending from $\mathbf{v}_s$ and $\mathbf{v}_u$, respectively. For any point Q on Γ_s, $\lim_{n\to\infty} F^n Q \to Q_0$; by contrast, for any point Q on Γ_u, $\lim_{n\to\infty} F^{-n} Q \to Q_0$. Away from the fixed point Q_0, both Γ_s and Γ_u are curved owing to nonlinearity of the mapping F. In case the mapping is integrable, both kind of manifolds emanating from the common hyperbolic fixed point Q_0 connect smoothly and form a doubly-degenerate separatrix segregating between localized tori around an elliptic fixed point and extended orbits (see Fig. 1.2). The separatrix is the most unstable against perturbation.

If the mapping becomes nonintegrable by switching on a perturbation, the degeneracy of separatrices is removed, and Γ_s and Γ_u will cross each other at a point P_0 called the homoclinic point. Once a single homoclinic point is available, an infinite number of similar points can be found. In fact, let us assign the location of the new point $P_1=FP_0$. P_1 is located on Γ_s if P_0 is regarded as belonging to Γ_s. P_1 should simultaneously be the point on Γ_u if P_0 is regarded as lying on Γ_u. To resolve this dilemma, P_1 has to be another homoclinic point in which Γ_s and Γ_u intersects. By repetition of this procedure, Γ_u becomes oscillating around Γ_s and an infinite number of homoclinic points are generated. Since F is area-preserving, the black area, e.g., inside Γ_s in Fig. 1.3, has to be kept on each mapping. Therefore, as the

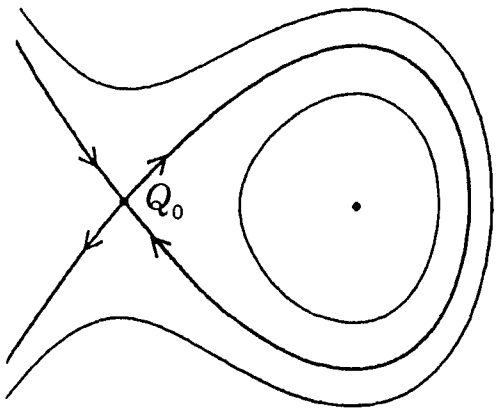

Fig. 1.2. Separatrices and hyperbolic fixed point Q_0.

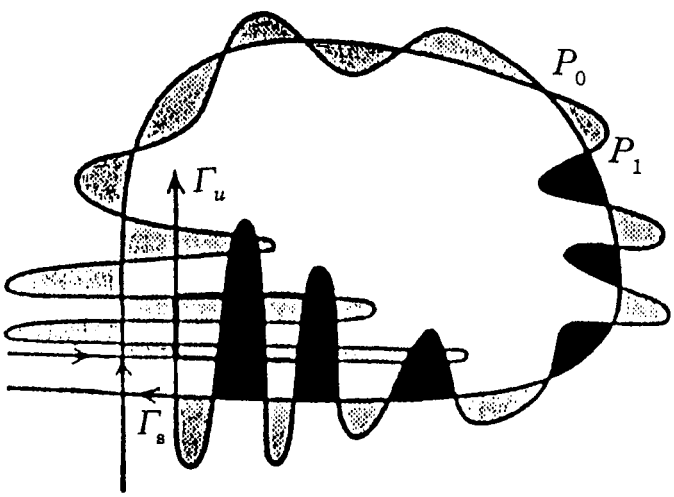

Fig. 1.3. Homoclinic structures and Smale's horse shoe.

fixed point Q_0 is approached, the black area is exponentially stretched and folded (i.e., via Smale's horse-shoe mechanism) .

The same argument holds for the inverse map F^{-1} applied to P_0. In this case Γ_s shows a violent undulation around Γ_u as Q_0 is approached. (It should be noted that the stable manifold does not cross itself and the same is true for the unstable manifold.) Consequently, as we approach the hyperbolic fixed point, the intersection of Γ_s and Γ_u generates a complicated homoclinic strucuture consisting of an infinitely large number of homoclinic points (see Fig. 1.3). This provides a mechanism for generating chaos (Poincare' , 1890). We therefore understand that textures of manifolds Γ_s and Γ_u should be woven on infinitely small scales in phase space which, as we shall see later, will be impossible in the case of quantum dynamics which poses a limitation of order of Planck constant $\hbar$ in the resolutiuon of phase space due to the *uncertainty principle.*

1.3. Diagnostic Characters of Chaos

The Standard diagnostics for characterizing chaotic behaviors are Lyapunov exponent and the Kolmogorov-Sinai entropy, whose concepts will be explained in the following:

Lyapunov Exponent

This is a quantity that describes the extreme sensitivty to initial conditions. For a given orbit in phase space, consider its variation with the initial value $\delta(0)$ at time $t=O$. The variation grows exponentially as $\delta(t) \propto \exp(\lambda t)$ in case of chaotic orbits. The positive constant λ is called the Lyapunov exponent. We also have $\lambda>0$ for isolated unstable periodic orbits embedded in the chaotic sea, which will be essential in the semiclassical theory of chaos. In case of stable regular orbits, $\delta(t)$ obeys the power law $\delta(t) \propto t^{\alpha}$, which implies $\lambda=0$.

More generally, in conservative systems with s degree of freedom, both positive $(\lambda_1 \geq \lambda_2 \geq \cdots \geq \lambda_p)$ and nonpositive $(\lambda_{p+1} \geq \lambda_{p+2} \geq \cdots \geq \lambda_{2s-1})$ Lyapunov exponents are available, satisfying the condition $\sum_{i=1}^{2s-1} \lambda_i = 0$. Note that the dimensionality of the 2s-dimensional phase space is decreased by unity owing to the presence of energy, i.e., of the self-evident constant of motion.

Let us now consider a droplet consisting of an assembly of initial points in phase space. Each point in the droplet begins to move following the deterministic law, i.e., Hamilton's equations. Keeping its phase volume, this phase droplet is then stretched in directions

with positive Lyapunov exponents and squeezed in directions with negative ones. Owing to the compactness of the phase space, the stretching mechanism is succeeded by a folding one. By repeating two distinct mechanisms, finer and finer structures are formed on infinitely small scales. This is the Smale's horse-shoe mechanism generating the chaos.

Kolmogorov-Sinai Entropy

This entropy characterizes the degree of randomization of chaotic orbits. Consider an assembly of orbits with a duration T starting from various points in phase space. By discretizing the time as $t=j\,\Delta t$ $(j=0, \bullet\,\bullet\,\bullet, n\text{-}1)$, with $\Delta\, t=T/n$, each orbit is represented by the time sequence of n points in phase space. We thus have an ensemble of discretized orbits. On the other hand, we shall divide phase space into small cells with identical volume Δu and choose an arbitrary sequence of n cells $i_0, i_1, \bullet\,\bullet\,\bullet, i_{n-1}$ (see Fig. 1.4).

Let $P_{i_0 i_1 \cdots i_{n-1}}$ be a probability of finding discretized orbits in the cells $i_0, i_1, \bullet\,\bullet\,\bullet, i_{n-1}$ and define the entropy

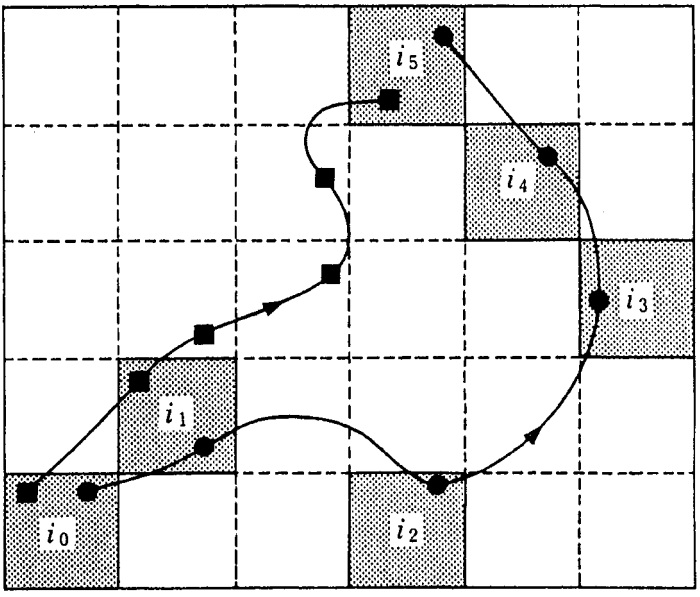

Fig. 1.4. Cell partition of phase space and cellular chain $i_0 \sim i_5$ Discrete orbits matching (circle) and not matching (square) with the celluar chain.

$$K_n = -\sum_{i_0 \cdots i_{n-1}} P_{i_0 i_1 \cdots i_{n-1}} \ln P_{i_0 i_1 \cdots i_{n-1}} \,. \tag{1.9}$$

If the phase space is occupied by KAM tori, the probability $P_{i_0 i_1 \cdots i_{n-1}}$ will be zero except for a fixed sequence of cells and then K_n will actually be vanishing. By contrast, K_n grows with time for an assembly of chaotic orbits. Then the significant quantity is the degree of randomization, characterized by the entropy production rate per unit time:

$$\Delta K_n / \Delta t = (K_n - K_{n-1})/\Delta t. \tag{1.10}$$

The Kolmogorov-Sinai entropy is defined as the limit ($\Delta t \to 0$ and $\Delta v \to 0$) of the time-averaged value of (1.10):

$$h_{KS} = \lim_{\Delta v \to 0} \lim_{\Delta t \to 0} \lim_{N \to \infty} N^{-1} \sum_{n=1}^{N} \Delta K_n / \Delta t = \lim_{\Delta v \to 0} \lim_{\Delta t \to 0} \lim_{N \to \infty} K_N / (N \Delta t). \tag{1.11}$$

It assumes the values 0 and $+\infty$ for periodic orbits and Brownian motions, respectively. For chaotic orbits, $0 < h_{KS} \leq +\infty$.

The quantities λ and h_{KS} are complementary but independent. In the case of $\lambda > 0$, h_{KS} may be vanishing. An example of this case is a point-particle scattering on two defocusing disks, where no confining of a particle is expected.

1.4. Suppression of Chaos in Quantum Dynamics

All the diagnostic features of chaos addressed above are meaningful only when the dynamics can continue to organize structures on infinitely small scales as time elapses. The present formalism of quantum mechanics, however, fails to guarantee such a kind of dynamics. To understand this point, let us investigate wavefunction features in quantum dynamics. To describe the wavefunction, we choose a minimum uncertainty state, i.e., a coherent state $|\mathbf{p},\mathbf{q}\rangle$. Then the probability density function for a system with N degrees of freedom is given by

$$P(\mathbf{p},\mathbf{q}) = (2\pi\hbar)^{-N} |\langle \mathbf{p},\mathbf{q} | \Psi \rangle|^2 \,, \tag{1.12}$$

which is a quantum analog of the classical distribution function in phase space.

The problem of representation is important. By a Fourier transformation of the position representation of the density operator $\langle \mathbf{q}''|\Psi\rangle\langle\Psi|\mathbf{q}'\rangle$ with respect to the relative coordinate $\zeta(=\mathbf{q}''-\mathbf{q}')$, one may obtain the Wigner representation of the wave function at p and $\mathbf{q}(=(\mathbf{q}''+\mathbf{q}'>/2)$ as

$$P_{\mathrm{W}}(\mathbf{p},\mathbf{q})=(2\pi\hbar)^{-N}\int \mathrm{d}\zeta\langle \mathbf{q}-\zeta/2|\Psi\rangle\langle\Psi|\mathbf{q}+\zeta/2\rangle \exp(\mathrm{i}\mathbf{p}\zeta/\hbar). \quad (1.13)$$

While $P_{\mathrm{W}}(\mathbf{p},\mathbf{q})$ has a monumental significance, it can take negative values and show violent undulation of $\mathrm{O}(\hbar)$ in phase space. Even in the semiclassical limit, therefore, the Wigner function in (1.13) can neither assimilate the classical distribution function (except for a very few linear systems like harmonic oscillators and noninteracting free particles) nor satisfy the Liouville equation even approximately. Because of its occasional negative values, $P_{\mathrm{W}}(\mathbf{p},\mathbf{q})$ does not qualify as a probability. This deficiency can be overcome by means of appropriate coarse graining guided by Heisenberg's uncertainty principle. Making a Gaussian smoothing of $P_{\mathrm{W}}(\mathbf{p},\mathbf{q})$ in (1.13) at every point $(\mathbf{p},\mathbf{q})$ in phase space, we can finally arrive at (1.12).

To make this statement concrete, a Gaussian wave packet will be chosen as an initial state. In general, up to the time of $\mathrm{O}(\hbar)$, $P(\mathbf{p},\mathbf{q})$ in (1.12) proves to mimic a (coarse-grained) classical distribution function, obeying the Liouville equation. In classically integrable and regular systems, the wave packet shows a simple (homogeneous or inhomogeneous) diffusion. In classically nonintegrable and chaotic systems, however, the profile of $P(\mathbf{p},\mathbf{q})$ develops Smale's horse-shoe (i.e., stretching and folding) mechanism. Consequently, the wavepacket deforms to finer and finer textures, suggesting a formation of a fractal object. To proceed to a more quantitative description, we define contour lines $C(t)$ and a phase space area enclosed by C such that the integrated probability takes a fixed (arbitrary) value. The area $A(t)$ constitutes an incompressible phase liquid, in which every point executes its own classical motion. Corresponding to the wavepacket dynamics of the classically chaotic system, the pattern of $A(t)$ deforms from a single spherical droplet to a finer and finer maze-like structure. The phase volume $\Gamma(t)$ for the overall structure deduced by coarsening of fine textures is given by

$$\Gamma(t)=\Gamma_0\exp(\lambda t)\,. \quad (1.14)$$

This formula is a result of the fact that one direction of the phase liquid is maximally extended as $l^{//}=l_0^{//}\exp(\lambda t)$ due to the exponential growth in the difference of nearby orbits. On the other hand, Liouville's theorem (i.e., the incompressibility of the phase liquid) imposes another direction orthogonal to $l^{//}$ to be contracted as $l^{\perp}=l_0^{\perp}\exp(-\lambda t)$.

In quantum mechanics, however, there exists a lower limit in the resolution of phase space because of the uncertainty principle: The linear dimension of each phase-space cell is of $O(\hbar^{1/2})$. Therefore the classical-quantum correspondence is broken at the cross-over time,

$$\tau_c \sim \lambda^{-1}\ln(\hbar^{-1}), \tag{1.15}$$

when quantum dynamics inevitably fails to assimilate the classical dynamics any further. For $t>\tau_c$, quantum dynamics will develop interference between nearby fine textures with a resultant diffusion behavior thoroughly different from that for $t<\tau_c$. The argument above is justified for $\tau_c<<\hbar^{-1}$, namely, so long as the similarity between $P(\mathbf{p},\mathbf{q})$ in (1.12) and the (coarse-grained) classical distribution function is ensured up to the cross-over time.

To conclude, the long-time quantum dynamics is governed by a quantum analog of Poincare' 's recurrence theorem: Both wavefunctions and energies reassemble themselves infinitely often in the course of long-time evolution. This phenomenon is called *quantum recurrence.*

1.5. Breakdown of Quantization of Adiabatic Invariants

The onset of chaos will greatly affect quantum mechanics, which describes both bounded and open (scattering) systems. The Bohr-Sommerfeld quantization condition for action lays the foundation of the present formalism of quantum mechanics in the limit where quantum transitions can be ignored. In fact, this condition, taken as the noncommutativity of canonical variables $([x, p]=i\hbar)$, led to the birth of Heisenberg's matrix mechanics; the same condition, taken as that for the existence of a standing wave, following the de Broglie's wave-particle dualism, gave rise to Schrödinger's wave mechanics. The emergence of chaos, however, renders meaningless the quantization of action.

The quantization condition for action is traced back to the

experimental discovery of the quantization of adiabatic invariants. So, let us review a historical route to this discovery. Following Ehrenfest (1916), we shall concentrate upon the problem of the radiation from a blackbody cavity. By the latter, we mean the cavity enclosed by a wall at temperature T that contains electromagnetic waves (i.e., an assembly of energy resonators) and emits radiation through a small hole to the outside. If one could move the wall adiabatically (very slowly) to expand or contract, the cavity volume V, frequency ν_i and energy E_1 of each energy resonator would change as well. Einstein proved in 1911, however, that the ratio

$$E/\nu \tag{1.16}$$

remains unchanged under the adiabatic change; this ratio is therefore called as the adiabatic invariant.

On the other hand, another kind of adiabatic invariant found by Wien is ν/T, which represents the displacement law. Combining these two invariants, one has the adiabatically-invariant equality $E/\nu = F(\nu/T)$ for a given arbitrary function $F(x)$. Noting the state density $\rho(\nu)=8\pi V\nu^2/c^3$ for the electromagnetic wave, the blackbody radiation rate in the frequency range $\nu \sim \nu+\delta\nu$ is seen to obey a scaling formula:

$$\rho(\nu)E\mathrm{d}\nu = (8\pi V\nu^3/c^3)F(\nu/T)\mathrm{d}\nu\ . \tag{1.17}$$

Equation (1.17) was in fact verified by experiments.

It should be emphasized that (1.17) was derived within a framework of classical theory. While Planck assumed E to be an integer multiple of $h\nu$ to explain the experimental curve F in terms of statistical mechanics, this assumption implies the quantization of the adiabatic invariant in (1.16), i.e., $E/\nu = nh$ with $n = 1,2,\bullet\bullet\bullet$. The adiabatic invariant is thus a cornerstone leading to the birth of quantum theory. The quantization of the adiabatic invariant formally reduces to that of the action $J=(2\pi)^{-1}\oint p\mathrm{d}q=n\hbar$, since the adiabatic invariant turns out to be the action J (more precisely, $2\pi J$). To state this explicitly, for a harmonic oscillator, with energy $E=(p^2+w^2q^2)/2$, we see that $2\pi J=\oint p\mathrm{d}q$ = area of ellipse $=E/\nu$

Extending the quantization condition for action to systems with N (>1) degrees of freedom, one gets

$$J_k = \frac{1}{2\pi} \oint_{\Gamma_k} \mathbf{p}(E) \cdot \mathrm{d}\mathbf{q} = (n_k + m_k/4)\hbar, \tag{1.18}$$

with k =1,2•••,M and n_k =0,1,2,•••. Γ_k and m_k represent mutually-independent closed paths (see Fig. 1.1) and Maslov index, respectively. In the completely-integrable case with the number of constants of motion M equal to N, N-dimensional tori are formed and all N actions $\{J_k\}$ are calculable. We are then able to proceed to quantum theory. In nonintegrable case with $M<N$, the torus will collapse and is replaced by chaos, making it impossible to quantize actions, which was first pointed by Einstein as early as 1917. In these nonintegrable cases, both matrix mechanics and wave mechanics are not able to find their logical foundation any more. One may now suspect de Broglie's relation $\lambda = h/p$ and $\nu = E/h$, since the characteristic wave length λ and frequency ν are not conceivable for the classically chaotic systems. Even if de Broglie's relation remained valid, there exsists no quantization rule of chaos because of the absence of adiabatic invariants. So, the very idea to interpret the quantization rule from the view point of wave mechanics would become groundless. This point will be investigated in detail in Chap. 8.

The new criteria for quantization of chaos should be searched for by examining the experiments on systems exhibiting chaos, e.g., complicated energy spectra of diamagnetic Rydberg atoms and the rich fluctuation features of quantum transport in stadium or crossroads billiards at the interfaces of semiconductor heterojunctions (Marcus *et al.,* 1992). In particular, rapid progress in modern high technology has made it possible to fabricate nanoscale structures and mesoscopic devices (Beenakker and van Houten, 1991; Akkermans *et al.,* 1995). For instance, in conducting disks at the interface of GaAs/AlGaAs heterostructures, the mean free path of electron is much larger than the system's size, and the concentration of electrons is less than 10^{12} cm^{-2} . Then the electron correlation is irrelevant and ballistic chaotic motions of individual electrons in billiards play an essential role in quantum transport. Since the motion of electrons obeys quantum mechanics, the quantum analog of chaos, or so-called quantum chaos, emerging from mesoscopic systems has become a target of intensive theoretical and experimental researches (Gutzwiller, 1990; Giannoni *et al.,* 1991; Nakamura, 1993, 1995; Chirikov and Casati, 1995).

In the experiments done so far on the mesoscopic (nanoscale)

cosmos, fluctuations caused by impurity potentials and thermal noises are competitive with those caused by deterministic chaos. So it would not be right to emphasize the limitation of the present formalism of quantum mechanics. As is understood from the arguments above, however, the genesis of chaos is clearly disturbing the foundation of quantum mechanics in the adiabatic regime where the quantum transition is suppressed. In the following chapters, bearing in mind a future subject of constructing a generalized quantum mechanics that could reconcile *quantum* with *chaos,* we shall discuss a variety of interesting quantum and semiclassical features of systems exhibiting chaos.

References

Akkermans, E., Montambaux, G., Pichard, J.-L., and Zinn-Justin, J., eds. (1995). *Mesoscopic Quantum Physics, Proceedings of Les Houches Summer School.* Amsterdam: North Holland.

Beenakker, C. W., and van Houten, H. (1991). In *Solid State Physics: Advances in Research and Applications,* H. Ehrenreich and D. Turnbull, eds. New York Academic.

Chirikov, B. V., and Casati, G., eds. (1995). *Quantum Chaos: Order and Disorder.* Cambridge: Cambridge University Press.

Ehrenfest, P. (1916). *Ann. Phys. (Leipzig)* **51,** 327.

Einstein, A. (1917). *Verh. Dtsch. Phys. Ges.* **19,** 82.

Giannoni, M. J., Voros, A., and Zinn-Justin, J., eds. (1991). *Chaos and Quantum Physics, Proceedings of the NATO ASI Les Houches Summer School.* Amsterdam: North-Holland.

Gutzwiller, M. C. (1990). *Chaos in Classical and Quantum Mechanics.* Berlin: Springer.

Marcus, C. M., Rimberg, A. J., Westervelt, R. M., Hopkins, P. F., and Gossard, A. C. (1992). *Phys. Rev. Lett.* **69,** 506.

Nakamura, K. (1993). *Quantum Chaos : A New Paradigm of Nonlinear Dynamics.* Cambridge: Cambridge University Press.

Nakamura, K., ed. (1995). *Quantum Chaos : Present and Future, Special issue of Chaos, Solitons and Fractals* **5** (7).

Poincare', H. (1890). *Acta Math.* **13,** 1.

Chapter 2

Semiclassical Quantization of Chaos: Trace Formula

One of the most fundamental tasks of quantum chaos is to explore the semiclassical quantization for chaotic systems. Assuming the validity of the existing formalism of Schrödinge-Feynman's quantum mechanics, a semiclassical quantization rule of chaos or the so-called Gutzwiller's trace formula is derived. Its application to persistent currents and the extension to S matrices and conductance fluctuations are presented. A number of questions around the trace formula are raised.

2.1. Green's Function and Feynman's Path Integral Method

In the previous chapter we have indicated that the genesis of chaos is destabilizing the foundation of the contemporary form of quantum mechanics. The question to be naturally addressed is how to generalize quantum mechanics so that it will become viable in chaotic systems. The answer will be given by designing experiments to capture chaos-induced quantum fluctuations and by deriving an experimental formula for the quantization of chaos. (One should recall that Bohr-Sommerfeld's quantization rule for actions can be traced back to the Wien-Planck's scaling formula for the blackbody radiation and therefore be guided by experiments.) One of the promising experiments to respond to this situation is quantum transport in mesoscopic systems wherein both thermal noise and impurity potential are well suppressed.

On the other hand, Schrödinger's quantum mechanics, which is

also supported by an accumulation of experimental results on both closed and open systems, should include this quantization condition of actions (adiabatic invariants) in the semiclassical limit. Confining ourselves to a stationary problem, we shall first illustrate this point and then derive the semiclassical quantization condition of chaos *by assuming a priori the validity of quantum mechanics for chaotic systems* (Gutzwiller, 1990).

The stationary state of a particle with mass m moving in N dimensions is described by the time-independent Schrödinger equation

$$H(\mathbf{q})\Psi_n(\mathbf{q}) = E_n\Psi_n(\mathbf{q}) , \tag{2.1}$$

where $H(q) = -(\hbar^2/2m)\sum_{j=1}^{N} \partial^2/\partial q_j^2 + V(q_1,q_2,\cdots,q_N)$ is a time-independent Hamiltonian. The corresponding Green function is defined by

$$G(\mathbf{q}'',\mathbf{q}';E) = \sum_n \Psi_n(\mathbf{q}'')\Psi_n^*(\mathbf{q}')/(E-E_n) , \tag{2.2}$$

which stores all the knowledges of eigenvalues $\{E_n\}$ and eigenfunctions $\{\Psi_n\}$. In fact, the E_n can be obtained from the poles of

$$\mathrm{Tr}G(E)\left(\equiv \int d\mathbf{q}G(\mathbf{q},\mathbf{q};E)\right) = \sum_n \frac{1}{E-E_n} . \tag{2.3}$$

And, noting $(x+i\varepsilon)^{-1} = \wp x^{-1} - i\pi\delta(x)$, we get the spectral density $p(E)$ from

$$-\pi^{-1}\mathrm{Im}(\mathrm{Tr}G(E)) = \sum_n \delta(E-E_n) \ (\equiv \rho(E)) . \tag{2.4}$$

Since the Green function (2.2) is nothing but the Laplace transform of the time evolution propagator

$$K(\mathbf{q}'',\mathbf{q}';t) \equiv \langle \mathbf{q}''|e^{-iHt/\hbar}|\mathbf{q}'\rangle , \tag{2.5}$$

the problem of solving (2.1) is eventually reduced to obtaining the propagator K. According to Feynman's path-integral formalism of quantum mechanics, K is expressed only in terms of classical terminology:

$$K(\mathbf{q}'',\mathbf{q}';t) = \int_{\mathbf{q}(0)=\mathbf{q}'}^{\mathbf{q}(t)=\mathbf{q}''} D[\mathbf{q}] \exp\{(i/\hbar) W[\mathbf{q}]\} \quad , \tag{2.6}$$

where W is a classical action functional described by a Lagrangian as

$$W[\mathbf{q}] = \int_0^t L(\mathbf{q},\dot{\mathbf{q}})dt \, . \tag{2.7}$$

Although (2.6) implies the sum of integrations over an innumerable number of classical paths, the great simplification in the calculation occurs in the semiclassical limit ($\hbar \to 0$), where the integrand in (2.6) is highly oscillating and its integration leads to a mutual cancellation. In this case, we can take a stationary phase approximation in the neighborhood of the saddle point

$$\delta W[\mathbf{q}] = 0, \tag{2.8}$$

having

$$K(\mathbf{q}'',\mathbf{q}';t) = (2\pi i\hbar)^{-N/2} \sum_j |\Im_j|^{1/2} \exp\{iW_j/\hbar - i\mu_j\},$$

where j denotes the classical orbits satisfying Hamilton's principle, (2.8), with boundary conditions $\mathbf{q}(0)=\mathbf{q}'$ and $\mathbf{q}(t)=\mathbf{q}''$. The values W_j, $\Im_j$, and μ_j are defined for each orbit j: $\Im_j = \det(-\partial^2 W_j / \partial \mathbf{q}'' \partial \mathbf{q}')$ is the inverse of a Jacobian; the phase shift $\mu_j (= m_j \pi/2)$ is the Morse-Maslov index m_j (the number of singular points of $\Im_j$ between $\mathbf{q}'$ and $\mathbf{q}''$) multiplied by the phase jump $\pi/2$.

As noted above, the Laplace transform of the propagator K yields the Green function. In particular, its trace is

$$\mathrm{Tr}G(E) = \int d\mathbf{q} \left\{ -(i/\hbar) \int dt \, \exp(iEt/\hbar) K(\mathbf{q},\mathbf{q};t) \right\} . \tag{2.9}$$

The explicit evaluation of (2.9) strongly depends on the integrability or nonintegrability of the underlying classical system. Therefore we shall investigate (2.9) in these distinctive cases separately.

2.2. Quantization of Integrable Systems

In the completely integrable case when the number of constants of motion accords with the degree of freedom N, phase space is occupied by invariant tori, as in Fig. 1.1, and adiabatic invariants given by the

irreducible actions

$$S_k = \oint_{\Gamma_k} \mathbf{p} \cdot \mathrm{d}\mathbf{q} \qquad (k = 1,2,\cdots, N) \tag{2.10}$$

are essential. In (2.10) Γ_k implies an irreducible closed contour in Fig. 1.1. After integration over t in (2.9), we transform from the dynamical variables **p, q** to the action-angle variables. Then any periodic orbit proves to be topologically equivalent to a suitable sequence of Γ_ks (see Fig. 2.1), and the effective action can be written as a sum of the winding numbers l_k times the irreducible actions S_k. Eventually (2.9) becomes

$$\begin{aligned} \mathrm{Tr}G(E) &\cong V \sum_{l_1=0}^{\infty} \cdots \sum_{l_N=0}^{\infty} \prod_{k=1}^{N} \exp[\mathrm{i}l_k(S_k/\hbar - \mu_k)] \\ &= V \prod_{k=1}^{N} (1 - \exp[\mathrm{i}(S_k/\hbar - \mu_k)])^{-1}, \end{aligned} \tag{2.11}$$

where μ_k now comes from the Morse-Maslov index for Γ_k and V is the volume of the N-dimensional torus characterized by $\{\Gamma_k\}$. Poles of (2.11) yield

$$\frac{1}{2\pi} \oint_{\Gamma_k} \mathbf{p}(E) \cdot \mathrm{d}\mathbf{q} = (n_k + m_k/4)\hbar \qquad (n_k = 0,1,2,\cdots). \tag{2.12}$$

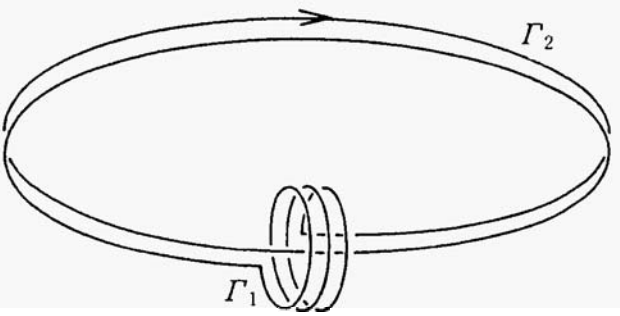

Fig. 2.1. Periodic orbit consisting of irreducible closed paths. In this example, the winding numbers are $l_1 = 3$ and $l_2 = 2$ for closed paths Γ_1 and Γ_2, respectively.

This is just Einstein's quantization rule, improved so as to include the Morse-Maslov indices. Since the rule in the form (2.12) was found originally by Brillouin and Keller, noting the single-valuedness of semiclassical wavefunctions, it is called the Einstein, Brillouin, and Keller, or EBK, quantization rule. The semiclassical limit of quantum mechanics has thus turned out to reproduce a result of "old" quantum theory, thereby unambiguously establishing a one-to-one correspondence between the invariant tori and quantum eigenvalues.

The rule (2.12) is by its nature traceable to experimental evidence (i.e., the Wien-Planck scaling formula). It holds good only for completely integrable systems. When the number of constants of motion M is less than N, the torus will collapse and become replaced by chaos. The EBK quantization rule cannot be justified any more.

2.3. Quantization of Chaos: Trace Formula

By still assuming the validity of the Schrödinger-Feynman formalism of quantum mechanics for classically-chaotic systems, Gutzwiller (1971, 1990) proceeded to look for a correspondence between the semiclassical quantum "irregular" spectra and chaotic orbits in nonintegrable systems. Because his intensive study was motivated by a theoretical curiosity to understand quantum symptoms of chaos in the semiclassical region, his final result (i.e., the trace formula) should not be understood as a new framework of quantum mechanics corresponding to chaos.

Since the invariant tori have now collapsed, it is meaningless to imagine a transformation from **p,q** coordinates to action-angle variables. Instead we again carry out the saddle-point approximation in the **q** integration of (2.9), using the equality

$$\partial W(\mathbf{q},\mathbf{q})/\partial \mathbf{q} \equiv \partial W(\mathbf{q}'',\mathbf{q}')/\partial \mathbf{q}'' + \partial W(\mathbf{q}'',\mathbf{q}')/\partial \mathbf{q}' \Big|_{\mathbf{q}''=\mathbf{q}'=\mathbf{q}}$$
$$= \mathbf{p}''-\mathbf{p}' = 0. \qquad (2.13)$$

The condition for momenta in (2.13), together with the condition for tracing (i.e., $\mathbf{q}''=\mathbf{q}'=\mathbf{q}$), manifests that only periodic orbits can contribute to the $\mathrm{Tr}G(E)$, to which, paradoxically, chaotic orbits make no contribution. Typically, in chaotic systems without any bifurcation, there exist isolated and unstable periodic orbits bearing

the positive Lyapunov exponents. Although the Lebesgue measure of periodic orbits is vanishing in the chaotic sea, their number is infinite.

Collecting all periodic orbits in (2.9), we find

$$\mathrm{Tr}G(E)=\sum_{\alpha}\sum_{l=0}^{\infty} f_{\alpha}(E)\exp\{il[S_{\alpha}/\hbar-\mu_{\alpha}]\}, \tag{2.14}$$

where

$$f_{\alpha}(E)=(2\pi i\hbar)^{-(N-1)/2}T_{\alpha}\left|\Im_{\alpha}^{\perp}\right|^{1/2}. \tag{2.15}$$

Here α denotes a primitive periodic orbit with energy E and l the number of its repetition; the reduced action and period for α are $S_{\alpha}(E)$ $(=\oint_{c}\mathbf{p}\cdot d\mathbf{q})$ and $T_{\alpha}(E)(=\partial S_{\alpha}/\partial E)$, respectively; $\Im_{\alpha}^{\perp}$ is an exponent responsible for the transverse orbital stability:

$$\Im_{\alpha}^{\perp}=\det(-\partial^{2}S_{\alpha}/\partial\mathbf{q}''_{\perp}\partial\mathbf{q}'_{\perp})\Big|_{\mathbf{q}''=\mathbf{q}'=\mathbf{q}}. \tag{2.16}$$

From (2.14)-(2.16), we finally reach Gutzwiller's trace formula:

$$\mathrm{Tr}G(E)-\mathrm{Tr}G_{0}(E)=(i\hbar)^{-1}\sum_{\alpha}T_{\alpha}\sum_{l=1}^{\infty}\{\det(M_{\alpha}^{l}-1)\}^{-1/2}\times\exp\{il(S_{\alpha}/\hbar-\mu_{\alpha})\}. \tag{2.17}$$

Tr $G_0(E)$ comes from a contribution from zero-length orbits. M_{α} is a linearized Poincare' map, i.e., a Monodromy matrix describing the time evolution of a transverse displacement from the orbit α:

$$\delta\mathbf{q}'_{\perp}=M_{\alpha}\delta\mathbf{q}_{\perp}. \tag{2.18}$$

The stability exponent Λ_{α} available from the eigenvalue of M_{α} depends on the type of fixed points. Corresponding to unstable and stable periodic orbits, one has $\Lambda_{\alpha}=\exp(\pm u_{\alpha})$ and $\exp(iu_{\alpha})$, respectively. Typically, for homoclinic orbits with hyperbolic fixed points, we get a positive Lyapunov exponent $\lambda_{\alpha}=u_{\alpha}/T_{\alpha}$ and thereby

$$\det(M_{\alpha}^{l}-1)=4\sinh^{2}(lu_{\alpha}/2)=4\sinh^{2}(\lambda_{\alpha}lT_{\alpha}/2). \tag{2.19}$$

The formula (2.17) indicates that semiclassical eigenvalues (and

eigenstates) are constructed through complicated interference among a set of periodic orbits. A serious problem we encounter here is that, due to the absence of a KAM torus, the sum in (2.17) includes arbitrarily-long periodic orbits. Introducing the KS entropy $h_{KS}(=\lambda_\alpha$ for bounded systems), the number of orbits with a period less than a given period $T(>>1)$ is $N(T)\ \exp(h_{KS}T)\ /T$ (see Sinai, 1976), i.e., exponentially proliferating, while the amplitude of terms with a period $T(=T_\alpha)$ is $A(T) \cong T_\alpha [2\sinh(\lambda_\alpha T_\alpha/2)]^{-1} \cong T \exp(-h_{KS}T/2)$. Hence the contribution of orbits with periods less than T is given by $A(T)$ x $N(T) \cong \exp(h_{KS}T/2)$, which brings about a serious problem of nonconvergence in (2.17). It is inevitable to devise a method to make (2.17) "conditionally convergent."

To resolve this problem, new developments appeal to the theory of Riemann's zeta function together with the invention of a novel resummation of series expansion called a Riemann-Siege1 type resurgence (Berry and Keating, 1990). This idea can be applied to Gutzwiller's trace formula. By simple integration and exponentiation of (2.17), together with an expansion

$$[2\ \sinh\ (lu_\alpha/2)]^{-1} = \sum_{k=0}^{\infty} \exp[-l(k+\frac{1}{2})u_\alpha]$$

in (2.19), one obtains (Gutzwiller, 1990)

$$\mathrm{Tr}G(E) - \mathrm{Tr}G_0(E) \cong -\frac{\mathrm{d}}{\mathrm{d}E}\ln\zeta(E)\ , \tag{2.20}$$

where $\zeta(E)$ is the Ruelle zeta function, defined as

$$\zeta(E)=\prod_\alpha\prod_{k=0}^{\infty}(1-t_\alpha\Lambda_\alpha^{-k})^{-1}\ , \tag{2.2 la}$$

with quantum weights

$$t_\alpha = |\Lambda_\alpha|^{-1/2}\exp[\mathrm{i}(S_\alpha/\hbar - m_\alpha\pi/2)]\ . \tag{2.21b}$$

From (2.21), one recognizes that poles of $\zeta(E)$ lead to the quantum eigenvalue.

Expanding the product sum in (2.21a) up to terms of relatively short periodic orbits, one obtains well-converging results. In fact, using periodic orbits thus organized, Gutzwiller applied his trace

formula to the calculation of irregular spectra of donors with anisotropic effective mass in silicon, obtaining eigenvalues in good agreement with exact quantum eigenvalues. But the eigenvalues derived from poles of $\zeta(E)$ are always accompanied by small imaginary components.

Another formidable problem around the trace formula is to find all periodic orbits without missing any one of them. For some fully chaotic systems without any bifurcation, the symbolic coding of periodic orbits ensures the successful counting of all periodic orbits. For generic Hamiltonian systems, from which both chaos and KAM tori emerge, however, complexity in symbolic coding of periodic orbits prevents us from our reaching the formulae (2.20) and (2.21).

Furthermore, some far more important issues should be addressed: The trace formula is valid up to the second leading order in $\hbar$. No resurgence for suitable zeta functions can therefore produce eigenvalues with precisions higher than the order of $\hbar^N$. If one were to resolve rigorously the problem of conditional convergence, the trace formula should be improved so as to incorporate all orders in $\hbar$. Such attempts, however, will lead us into the forest of complicated mathematics, which is not compatible with our aim to achieve simplicity of the fundamental law.

2.4. Application of Trace Formula to Autocorrelation Functions

While the computation of the trace formula is practically difficult, the calculation of its autocorrelation function is feasible on having recourse to some approximate methods. These correlation functions are important in the physics of mesoscopic phenomena in the ballistic regime, where the elastic mean-free path of electrons is larger than the linear dimension of the system, and a deterministic law is operative. Below we shall apply the trace formula to persistent currents and S matrices in chaotic systems.

Persistent Currents

The correlation function of the persistent current was studied by several groups (Szafer and Altshuler, 1993; Berry and Keating, 1994). We shall here introduce Berry and Keating's work (1994). Owing to the Aharonov-Bohm effect, the persistent current appears in normal conductors in mesoscopic scales. Consider the noninteracting electron

gas confined in a conducting ring threaded by an Aharonov-Bohm magnetic flux ϕ. We choose the ring shape that guarantees complete chaos in the classical motion of a point particle. For instance, one may mention the Sinai billiard, i.e., a square conductor with a circular hollow in its inside (see Fig. 2.2). The contribution of a single-particle energy level $E_n(\phi)$ to the persistent current is given by $p\ \mathrm{d}E_n/\mathrm{d}\phi$, where the mean density state ρ is the inverse of mean level separation. The flux ϕ will now be scaled by flux quanta $\phi_0=hc/e$. Taking $\{E_n\}$ as a set of energy levels near the Fermi level, the autocorrelation function of the persistent current in the ground state is given by

$$C(\phi) = \rho^2 \int_0^1 \mathrm{d}\phi' \langle \mathrm{d}E_n/\mathrm{d}\phi|_{\phi=\phi'+\phi} \mathrm{d}E_n/\mathrm{d}\phi|_{\phi=\phi'} \rangle_n \quad , \tag{2.22}$$

where ϕ integration and $\langle \bullet \bullet \bullet \rangle_n$ imply the averages for one period ϕ_0 and for levels lying below the Fermi level ε_F, respectively.

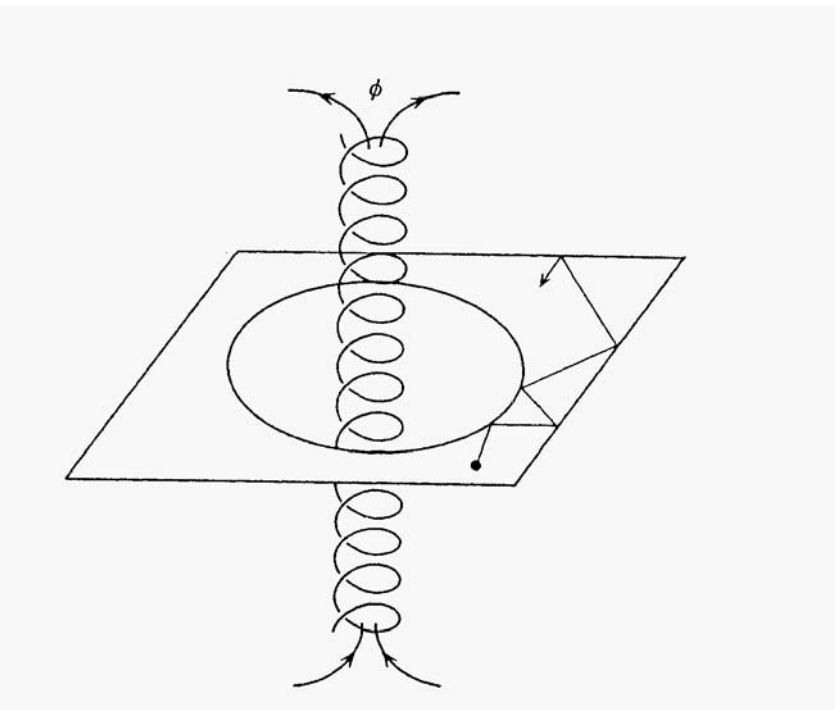

Fig. 2.2. Aharonov-Bohm flux ϕ and Sinai billiard with persistent current.

Here we introduce the integrated density of states in terms of stair-case functions:

$$N_\varepsilon(E,\phi) = \sum_n \Theta_\varepsilon(E - E_n(\phi)) \ . \tag{2.23}$$

In (2.23), the suffix ε signifies the additional procedure of coarse-graining the fine structures less than the mean level spacing (ε=(2πp)-1) ; $\rho_\varepsilon(E,\phi)=\partial N_\varepsilon/\partial E$ is just the density of states with its average given by ρ. With use of the identity $\partial N_\varepsilon/\partial\phi=-\partial N_\varepsilon/\partial E \cdot dE/d\phi=-\rho\, dE/d\phi$, the calculation of $C(\phi)$ turns out to be reduced to that of the correlation function of $\partial N_\varepsilon/\partial\phi$:

$$F(\phi) = \int_0^1 d\phi' \langle \partial N_\varepsilon/\partial\phi|_{\phi=\phi'+\phi} \partial N_\varepsilon/\partial\phi|_{\phi=\phi'} \rangle_E \ , \tag{2.24}$$

where the average on E is that over levels below ε_F.

We proceed to apply the trace formula (2.17). Deriving the state density from (2.17) and integrating it over E, we find

$$N_\varepsilon(E,\phi) = N_0(E) + \sum_j B_j(E)\exp\{i[S_j(E)/\hbar + 2\pi w_j\phi]\}\exp\{-\varepsilon T_j(E)/\hbar\}, \tag{2.25}$$

with $B_j = (2\pi)^{-1}\exp(i\mu j)\{\det(M_j - 1)\}^{-1/2}$; $\{j\}$ denotes periodic orbits. In (2.25) the action is supplemented by the Aharonov-Bohm term proportional to the winding number w_j around the flux. The ε dependent factor, originating from the coarse-graining procedure, will render (2.25) absolutely convergent.

On substitution of (2.25) into (2.24), one obtains double summations over periodic orbits. Once ϕ '-integration has been been carried out, however, diagonal terms alone survive:

$$F(\phi,\varepsilon) = 4\pi^2 \sum_j |B_j|^2 w_j^2 \cos(2\pi w_j\phi)\exp(-2\varepsilon T_j/\hbar) \ . \tag{2.26}$$

If the summation in (2.26) is taken in order of increasing periods T_j , $\sum_j |B_j|^2 \cdots$ can be replaced by $(2\pi^2)^{-1}\int_0^\infty dT/T \cdot 1\,1$.

Assume a set of winding numbers $\{w_j\}$ for orbits with period $T\sim T+dT$ to obey a Gaussian distribution with zero mean and with

variance of $\langle w_j^2 \rangle = \gamma T/T_0$, where T_0 is the period of the shortest orbit. We can then carry out the T integration in (2.26), after replacing the w_j-dependent factor in each of intervals $T \sim T+dT$ by its Gaussian average. As a result we find

$$C(\phi) = F(\phi,\varepsilon) = -[\sin^2(\pi\phi) - w_\varepsilon^{-2}]/[\sin^2(\pi\phi) + w_\varepsilon^{-2}]^2 \qquad (2.27)$$

in the limit of the characteristic winding number $w_\varepsilon = (\gamma\hbar/(\varepsilon T_0))^{1/2} \gg 1$. For a ring in d dimensions, $\rho \cong \hbar^{-d}$ and $\varepsilon = (2\pi\rho)^{-1} \cong \hbar^d$, yielding $w_\varepsilon^2 \cong \hbar^{(d-1)}$. Hence (2.27) shows asymptotic behaviors $C(0) = w_\varepsilon^2 \cong \hbar^{-(d-1)}$ and $C(\phi) \cong -(\pi\phi)^{-2}$ in the limits of $\phi = 0$ and $(\pi w_\varepsilon)^{-1} \ll \phi \ll 2^{-1}$, respectively.

S Matrices

Electric conductance, Hall resistance, and so on are being intensively measured on the interface layer of GaAs/AlGaAs systems. Their observables are related to S matrices in scattering theory. The semiclassical theory of scattering, e.g., a general calculation of S matrices was developed by Miller (1975) and by Jalabert *et al.(1990).*

In view of the analogy between the unitary transformation in quantum mechanics and canonical transformation in classical mechanics, the semiclassical expression for S-matrices is given by

$$S_{nn'}(E) = (2\pi)^{-1/2} \sum_s |\partial I'/\partial\theta|_s^{-1/2} \exp[(i/\hbar)(\Phi^{(s)}(I, I') - \hbar\mu_s)], \qquad (2.28)$$

where I and I' are action variables associated with initial (n) and final (n') channels, respectively, and θ is the angle variable conjugate to I, while $\Phi(s)$ and $2\mu s\pi$ are reduced action and Maslov index, respectively, with $\{s\}$ representing all scattering orbits connecting I and I'. The pre-exponential factor is understood as a square-root of a classical transition probability, $P^{(s)}(I, I') = (2\pi)^{-1} |\partial I'/\partial\theta|_s^{-1}$.

While in the attempt to evaluate (2.28) we shall meet the problem of the exponential proliferation, just as encountered in the trace formula, it is feasible to compute the autocorrelation function (Blumel and Smilansky, 1988; Jalabert *et al.,* 1990; Lai *et al.,* 1992) $C_{nn'}(\varepsilon) = \langle S_{nn'}^*(E) S_{nn'}(E+\varepsilon) \rangle_E$. In fact, for $\varepsilon \ll 1$,

$$C_{nn'}(\varepsilon) = \langle \sum_s P^{(s)}(I, I') \exp\{(i/\hbar)\varepsilon\partial\Phi^{(s)}/\partial E\} \rangle_E$$

$$+ \left\langle \sum_{s \neq s'} [P^{(s)}(I, I')P^{(s')}(I, I')]^{1/2} \exp\{(\mathrm{i}/\hbar)[(\Phi^{(s)} - \Phi^{(s')}) - \hbar(\mu_s - \mu_{s'})]\} \right\rangle_E . \tag{2.29}$$

In the limit $\hbar \to 0$, the double summation in the 2nd term on the r.h.s. becomes vanishing small owing to the destructive phase interference. Putting in (2.29) $\partial \Phi^{(s)} / \partial E = t$ (i.e., time for a particle staying inside the collision region), we get

$$C_{nn'}(\varepsilon) = \int \mathrm{d}t \langle P_{II'}(E,t) \rangle_E \exp(\mathrm{i}\varepsilon t/\hbar) , \tag{2.30}$$

where $P_{II'}(E,t)\ \mathrm{d}t$ is the probability of a sojourn time falling between $t \sim t + \mathrm{d}t$ and shows a mild dependence on E.

In the case of fully chaotic (hyperbolic) scattering not accompanied by any torus, $\langle P_{II'}(E,t) \rangle E \sim \mathrm{e}^{\gamma t}$ for $t >> 1$, giving a Lorentzian correlation

$$C_{nn'}(\varepsilon) = 1/[\varepsilon/\hbar + \mathrm{i}\gamma]. \tag{2.31}$$

In the case of nonhyperbolic chaotic scattering with KAM tori, on the other hand, $\langle P_{II'}(E,t) \rangle E \sim t^{-z}$, since orbits are often pulled into the surface of KAM tori. Consequently,

$$C_{nn'}(\varepsilon) \sim c_0 - c_1(\varepsilon/\hbar)^{z-1} , \tag{2.32}$$

with c_0, $c_1 > 0$ showing around $\varepsilon = 0$ a peak of cusp type which is reminiscent of the Ericson's fluctuation in the random systems. For further details, see Lai *et al.* (1992).

Fractal Conductance Fluctuations

As will be described both intensively and extensively in the coming chapters, recent experimental and theoretical work put emphasis on ballistic transport in mesoscopic semiconductor heterojunctions. While studies on conductance fluctuations have rather focused on hyperbolic systems, where the escape from the billiard is exponentially fast, phase coherent phenomena in the generic case of systems with a mixed (chaotic and regular) classical phase space are much less trivial. Since in the generic systems there exist an infinite hierarchy of cantori (see Fig. 2.3), the escape from such a system is much slower than from hyperbolic systems and follows a power law. What will be a consequence of the conductance if the underlying classical dynamics

bears such a mixed phase? A brief answer was given by Ketzmerick (1996), as follows:

The two-probe conductance G is given in terms of the sum of flux-normalized transmission amplitudes $t_{nm}=(k_n/k_m)^{1/2}S^{(2)}{}_{nm}$ as

$$G=\frac{e^2}{h}\sum_{n,m}|t_{nm}|^2 \ . \tag{2.33}$$

Here n and m denote modes of lead wires 1 and 2, respectively. (Details will be given in Chap. 4.) In the semiclassical approximation, t_{nm} is given, just as in (2.28), by

$$t_{nm}=\sum_s \sqrt{P_s}\exp(\frac{\mathrm{i}}{\hbar}S_s-\mathrm{i}\mu_s), \tag{2.34}$$

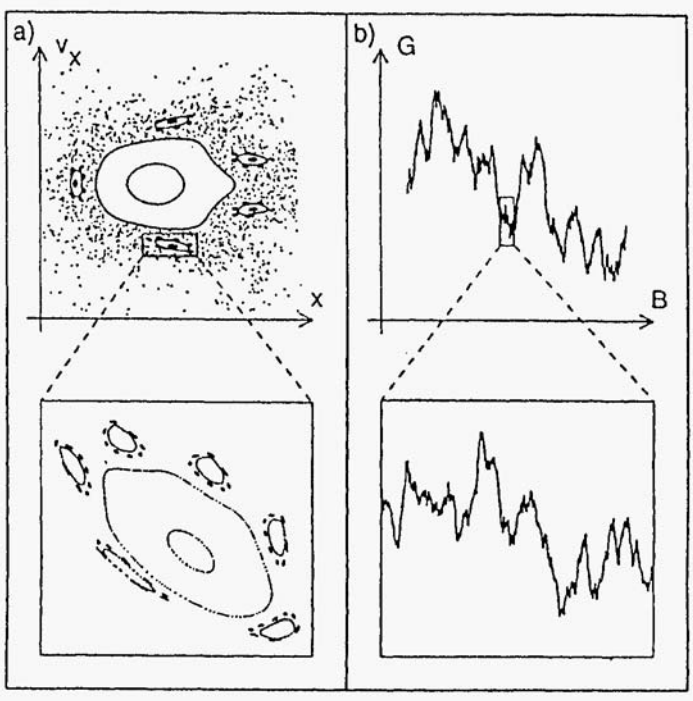

Fig. 2.3. (a) The self-similar phase space structure of a mixed system (i.e., 2-d antidot array in a magnetic field). (b) Ballistic conductance fluctuations reminiscent of fractional Brownian motion. (Courtesy of R. Ketzmerick.)

where S_s and $2\mu_s/\pi$ are the classical action and Maslov index of the *scattering path* s traversing the cavity with classical transmission probability P_s (Miller, 1975; Jalabert *et al.,* 1990). For a small change in magnetic field B, the reduced action is expanded in ΔB as

$$S_s(E, B+\Delta B) \sim S_s(E, B)+\frac{h\theta_s \Delta B}{\phi_0}, \tag{2.35}$$

where $\phi_0=hc/e$ is the magnetic flux quantum and $\theta_s=\frac{1}{2\pi}\int_s \frac{\partial \mathbf{A}}{\partial \mathbf{B}} \cdot d\boldsymbol{l}$, with $\nabla \times \mathbf{A}=\mathbf{B}$, is the accumulated area enclosed by the scattering orbit s.

The change in the conductance for a small change ΔB is found to be

$$\Delta G=G(E, B+\Delta B)-G(E, B)=\frac{e^2}{h}\sum_{n,m}\sum_{s,u}\sqrt{P_s P_u}\,[\exp(2\pi i(\theta_s-\theta_u)\frac{\Delta B}{\phi_0})-1]$$

$$\times \exp[\frac{i}{\hbar}(S_s-S_u)-i(\mu_s-\mu_u)]\,. \tag{2.36}$$

In the semiclassical limit, S_s and $S_u >> \hbar$ is guaranteed. In averaging ΔG over (Fermi) energy, therefore, the last exponential factor in (2.36) can be regarded as a complex random number ξ_{su} with mean $\langle \xi_{su} \rangle = 0$ and variance $\langle \xi_{su} \xi_{su}^* \rangle = \delta_{ss'}\delta_{uu'}$. Accordingly, ΔG has a vanishing mean value, and its variance is given by

$$\langle (\Delta G)^2 \rangle = \left(\frac{e^2}{h}\right)^2 \sum_{n,m}\sum_{s,u} P_s P_u \left| \exp[2\pi i(\theta_s-\theta_u)\frac{\Delta B}{\phi_0}]-1 \right|^2$$

$$=2\left(\frac{e^2}{h}\right)^2 \sum_{n,m}\left(\left(\sum_s P_s\right)^2-\left|\sum_s P_s \exp(2\pi i \frac{\theta_s \Delta B}{\phi_0})\right|^2\right)\,. \tag{2.37}$$

Replacing the sum in (2.37) over paths s by an integral over the (n, m-independent) area distribution proper to *mixed* systems as

$$\sum_s p_s \longrightarrow \int_{-\infty}^{\infty} \frac{dP(\theta)}{d\theta} d\theta\,, \tag{2.38a}$$

with

$$P(\theta) \sim \theta^{-\gamma}\,, \tag{2.38b}$$

one finds

$$\langle(\Delta G)^2\rangle \sim (\Delta B)^{\gamma}, \qquad \text{for } \gamma \leq 2, \tag{2.39a}$$

$$\langle(\Delta G)^2\rangle \sim (\Delta B)^{2}, \qquad \text{for } \gamma > 2. \tag{2.39b}$$

Thus, for $\gamma \leq 2$, conductance vs. magnetic field shows a feature of the same stochastic process as a fractional Brownian motion (Mandelbrot, 1982) with mean zero and and variance $(\Delta B)^{\gamma}$ (see Fig. 2.3).

Although examples in this section are intriguing, the semiclassical theory of chaotic scattering will not be satisfactory at all unless it can explain the transport properties in real experiments. Consider, for instance, the ballistic crossroad problem at the interface of GaAs/AlGaAs heterostructures. We shall meet there the serious problem of wave diffraction at junction points between lead wires and the confining cavity region. The wave diffraction will affect locations of scattering resonances and thereby autocorrelation functions. Several other interesting experiments are also being designed that measure conductance and its fluctuations in mesoscopic solid state devices and aim at elucidating a quantum-mechanical symptom of chaos. In particular, as we shall describe in the later chapter, Marcus *et al.* (1992) exploited circle and stadium billiards at the interface of the above heterostructures, measuring the electric resistance as a function of magnetic field. The fluctuation features reported by them have a rich structure, which awaits challenging analyses beyond both the periodic orbit theory and the calculation of correlation functions: Both semiclassical and exact quantum-mechanical theories are not successful in explaining the complicated experimental results.

2.5. Significance and Limitation of Trace Formula

So long as one stays within the framework of Schrödinger-Feynman's quantum mechanics, Gutzwiller's trace formula remains one of the most valuable procedures for exposing the ambiguities obscuring the borderline between quantum and classical mechanics for chaotic systems. As seen in the previous section, the autocorrelation function of the trace formula can be calculated approximately. The calculation of the trace formula itself, however, will encounter serious fundamental problems. In generic systems with elliptic islands coexisting with chaotic sea, symbolic coding of periodic orbits is much less obvious.

Even if one could achieve this coding, one would meet another difficulty, namely that of nonconvergence in the Gutzwiller series due to the exponential proliferation of periodic orbits. This problem may be partly overcome either by smoothing the density of states or by inventing a way of conditional convergence by means of the Ruelle zeta function. There remains, however, a more troublesome problem: For bounded systems, the eigenvalues computed from the trace formula are not real! To resolve this problem, one should improve the trace formula so as to include higher-order terms in $\hbar$, which will demand more and more complicated mathematics. Since the fundamental law should be as simple as possible, we are here tempted to re-examine the validity of the Shrödinger-Feynman formalism of quantum mechanics for classically chaotic systems the hope of inventing its more general version.

References

Berry, M. V., and Keating, J. P. (1990). *J. Phys.* **A23,** 4839.

Berry, M. V., and Keating, J. P. (1994). *J. Phys.* **A27,** 6167.

Blumel, R., and Smilansky, U. (1988). *Phys. Rev. Lett.* **60,** 177.

Gutzwiller, M. C. (1971). *J. Math. Phys.* **12,** 343.

Gutzwiller, M. C. (1990). *Chaos in Classical and Quantum Mechanics.* Berlin: Springer.

Jalabert, R. A., Baranger, H. U., and Stone, A. D. (1990). *Phys. Rev. Lett.* **65,** 2442.

Ketzmerick, R. (1996). Preprint.

Lai, Y. C., Blumel, R., Otto, E., and Grebogi, C. (1992). *Phys. Rev. Lett.* **68,** 3491.

Mandelbrot, B. B. (1982). *The Fractal Geometry of Nature.* San Francisco: Freeman.

Marcus, C. M., Rimberg, A. J., Westervelt, R. M., Hopkins, P. F., and Gossard, A. C. (1992). *Phys. Rev. Lett.* **69,** 506.

Miller, W. H. (1975). *Adv. Chem. Phys.* **30,** 77.

Sinai, Y. G. (1976). *Introduction to Ergodic Theory.* Princeton: Princeton University Press.

Szafer, A., and Altshuler, B. L. (1993). *Phys. Rev. Lett.* **70,** 587.

Chapter 3

Pseudo-Chaos Without Classical Counterpart in One-Dimensional Quantum Transport

While there exists no genuine chaos in quantum systems due to the linearity of Schrödinger equation, we show in this chapter two interesting examples of pseudo-chaos in 1-dimensional (1-*d*) quantum transport. These phenomena arise from quantum-mechanical tunneling through potential barriers and have no classical counterpart. First we consider quantum transport in the 1-*d* Kronig-Penny model in a static electric field. The S matrix as a function of the number of barriers is examined in the complex plane. Although no positive Lyapunov exponent is available, it shows a stagnant chaos around a torus in the weak field case, while, in the strong field case, wandering from one stagnant region to another in an unpredictable way. The power spectra of transmission coefficients show a universal $1/f^2$ behavior, which will be pointed out to be caused by a breakdown of the law of large numbers. Second, we shall investigate pseudo-chaos in multiple resonant tunnelings through a double-barrier structure. Both phenomena will be realized by using GaAs/AlAs heterostructures. The origin of pseudo- chaos will be revealed.

3.1. Introduction

Due to the linearity of the Schrödinger equation, the quantum system exhibits no chaos characterized by the standard diagnostics of Kolmogorov-Sinai entropy or positive Lyapunov exponents. We can therefore envisage merely a quantum analogue of chaos, i.e., quantum chaology, rather than genuine quantum chaos. Before beginning to elucidate many features of the quantum analog of chaos, we shall introduce interesting examples of pseudo-chaos in quantum systems which have no classical counterpart.

Rapid progress in the fabrication of nanoscale structures has made it possible to see typical quantum-mechanical effects such as tunneling (Esaki, 1985; Mendez *et al.,* 1988). In particular, growing attention has been paid to (1) superlattices (e.g., GaAs/AlAs) with alternating sequence of potential barriers and wells and (2) double-barrier structures through which resonant tunneling occurs.

In this chapter, we shall first analyze pseudo-chaos accompanying quantum transport in a strictly regular superlattice, i.e., the Krönig-Penny model, in a constant electric field (Nakamura *et al.,* 1994) and then another pseudo-chaos in multiple resonant tunnelings through double-barrier structures (Jona-Lasinio *et al.,* 1992).

3.2. Quantum Transport in Superlattice and Pseudo-Chaos

Model Hamiltonian

The superlattice is a nano-scale periodic structure composed of alternate arrays of potential barriers and quantum wells. For the 1-d superlattice with period a and barrier width d in the presence of electric field (see Fig. 3.1), the Hamiltonian is given by

$$H = -\frac{\hbar^2}{2m}\frac{\mathrm{d}^2}{\mathrm{d}x^2} + V(x) - \mathcal{F}x \ , \tag{3.1}$$

with the periodic potential: $V(x)=V_0$ for $(j\text{-}1)\alpha \le x \le (j\text{-}1)\alpha + d$ and $V(x)=0$ for $(j\text{-}1)\alpha + d \le x \le ja$ with $j=1,2,\bullet\bullet\bullet$. In (3.1), the last term of r.h.s. represents the coupling with an electric field $\mathcal{F}$. For simplicity, $\mathcal{F}x$ is here replaced by a stair-wise function $\mathcal{F}\hat{x} = \mathcal{F}\sum_{j=1}^{n}\theta(x - Ja)$, with $\theta(x)$ denoting the step function. Contrary to some recent studies on

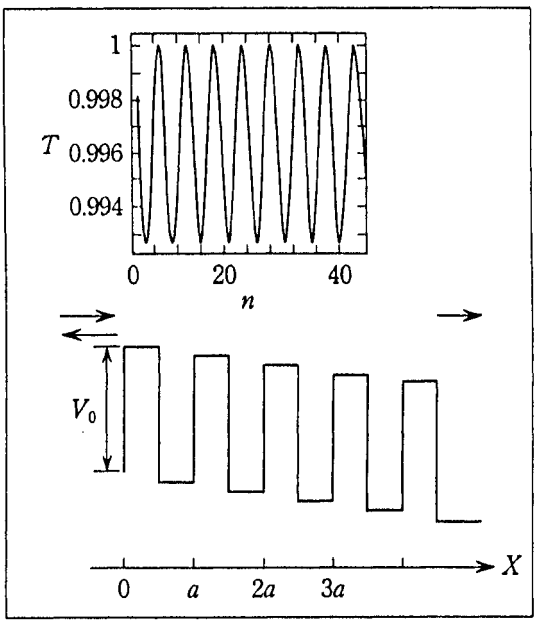

Fig. 3.1. Kronig-Penny model in the presence of electric field. Inset: T_n in case of F=0. (k0=10 is used throughout in Figs. 3.1–3.4.)

quantum transport in 1-*d* complicated structures, we assume neither artificial hierarchical (e.g., Fibonacci-type) nor random potentials.

Let us write the wavefunction

$$\Psi_0=\exp(ik_0x) + S_{11}(n)\exp(-ik_0x)$$

as a sum of the incident and reflected waves for $x<0$ and $\Psi_n=S_{12}(n)\exp(ik_nx)$ as the transmitted wave after the n-th barrier. Considering over-barrier tunneling throughout, the wave functions at the j th ($1 \le j \le n$) barrier and well are given by $\Psi_j=C_je^{iK_jx} + D_je^{-iK_jx}$ and $A_je^{ik_jx} + B_je^{-ik_jx}$, respectively, where $K_j=\sqrt{\kappa_0^2 + F(j-1)}$ and $K_j=\sqrt{k_0^2 + Fj}$ with $F=2m\mathcal{F}/\hbar^2$ and $(K_0)^2=(k_0)^2-2mV_0/\hbar^2$. Owing to the continuity and smoothness conditions at the barrier-well boundary points, we have a conservative discrete map between successive set of coefficients as

$$\begin{pmatrix} A_j \\ B_j \end{pmatrix} = M_j \begin{pmatrix} A_{j-1} \\ B_{j-1} \end{pmatrix} \quad , \tag{3.2a}$$

where the transfer matrix M_j is expressed by

$$M_j = \begin{pmatrix} e^{-ik_j(j-1)a} & 0 \\ 0 & e^{ik_j(j-1)a} \end{pmatrix} \begin{pmatrix} \alpha_{1j} & \beta_{1j} \\ \beta_{1j} & \alpha_{1j} \end{pmatrix} \begin{pmatrix} e^{i\kappa_j d} & 0 \\ 0 & e^{-i\kappa_j d} \end{pmatrix} \begin{pmatrix} \alpha_{2j} & \beta_{2j} \\ \beta_{2j} & \alpha_{2j} \end{pmatrix}$$

$$\times \begin{pmatrix} e^{ik_{j-1}((j-1)a-d)} & 0 \\ 0 & e^{-ik_{j-1}((j-1)a-d)} \end{pmatrix} \quad , \tag{3.2b}$$

with

$$\alpha_{1j}=(k_j+\kappa_j)/(2k_j)\ ,\ \alpha_{2j}=(\kappa_j+k_{j-1})/(2\kappa_j)\ ,$$

$$\beta_{1j}=(k_j-\kappa_j)/(2k_j)\ ,\ \beta_{2j}=(\kappa_j-k_{j-1})/(2\kappa_j).$$

It should be noted that in the limit of δ-function walls ($d \to 0$ with $V_0 d=1$), the map in (3.2) reduces to a greatly simplified version identical to that for barrier penetrations (Jauslin, 1991). By iterating (3.2) under the boundary condition $A_0=1$, $B_0=S_{11}$ and $A_n=S_{12}$, $B_n=0$ one obtains

$$S_{12}(n) = \det Q_n / (Q_n)_{22} \quad ,$$

$$S_{11}(n) = -(Q_n)_{21} / (Q_n)_{22} \quad ,$$

with $Q_n = \prod_{j=1}^{n} M_j$. The transmission and reflection coefficients are given by $T_n = \frac{k_n}{k_0} |S_{12}(n)|^2$ and $R_n = |S_{11}(n)|^2$, respectively. The electric conductance is simply $\sigma_n=(2e^2/h)T_n$. The validity of our computations will be justified by noting the unitarity ($T_n + R_n=1$).

Numerical Results

Keeping fixed both the periodicity $a(=1)$ and the area of each barrier $V_0 d(=1)$, we shall present numerical results first in the limiting case $d/a \to 0$ and then in general cases $d/a \neq 0$. In the absence of an electric

field, Bloch bands are formed due to the translational lattice symmetry. The transmission coefficient T_n exhibits periodic oscillations for energies $(\hbar k_0)^2/2m$ belonging to allowed bands. When the electric field is switched on, the following features emerge.

(I) ***Weak field case*** $F<<F_c\ (=(\pi/a)^2)$ Here Bloch bands are slightly tilted and kn value increases within a single band. The number of Zener tunnelings at the zone boundary $k_{BZ}(=\pi l/a$ with $l=1,2,\bullet\bullet\bullet)$ is practically vanishing. T_n shows, however, a nonstationary erratic behavior around the plateau value, as displayed in Fig. 3.2(a). The reflection component of the S matrix, $S_{11}(n)$, wanders in an erratic way (see Fig. 3.2(b)) in the complex plane. Its motion is stagnant around the torus rather than exhibiting a global chaos. This fact leads to the absence of the positive Lyapunov exponent, although the distribution function of local Lyapunov exponents (values evaluated in finite time intervals) will have positive components. We shall call this marginal chaos *pseudo-chaos* . Corresponding to this peculiar feature, the power spectra for the time sequence $\{T_n\}$, defined by

$$P(f)=\left|N^{-1}\sum_{n=1}^{N}T_n e^{-2\pi i f n/N}\right|^2 ,$$

exhibit a $1/f^{\nu}$ law (Voss and Clarke, 1976; Dutta and Horn, 1981; Weissman, 1988) with the integer exponent ν =2.000± 0.001 (see Fig. 3.2(c)), which is reminiscent of Brownian motions. The $1/f^{\nu}$ law with ν >0 is often generated in classical dynamical systems of weakly ergodic class, e.g., in the intermittent chaos and general Hamiltonian systems, and is called simply as $1/f$ fluctuation. Despite recent active works on $1/f$ fluctuation in classical systems (e.g., Geisel et al., 1987, 1990), little attention has been given to $1/f$ *fluctuation in quantum systems*.

The results in Fig. 3.2 are mysterious, if one recalls the lack of extrinsic randomness introduced into the system and the linearity of the Schrödinger equation. (In a mean-field approximation, to be mentioned in the next section, a nonlinear Hartree-like equation can be available, showing chaotic phenomena. The present scheme has nothing to do with this artificial introduction of nonlinearity.) With increase of the field strength, however, more interesting issues will come to the fore, as described below.

(II) ***Strong field case*** **($F>>F_c$)** T_n shows a sequence of steadily-elongated plateaus that are connected by bursts. (See Fig. 3.3(a).) Both

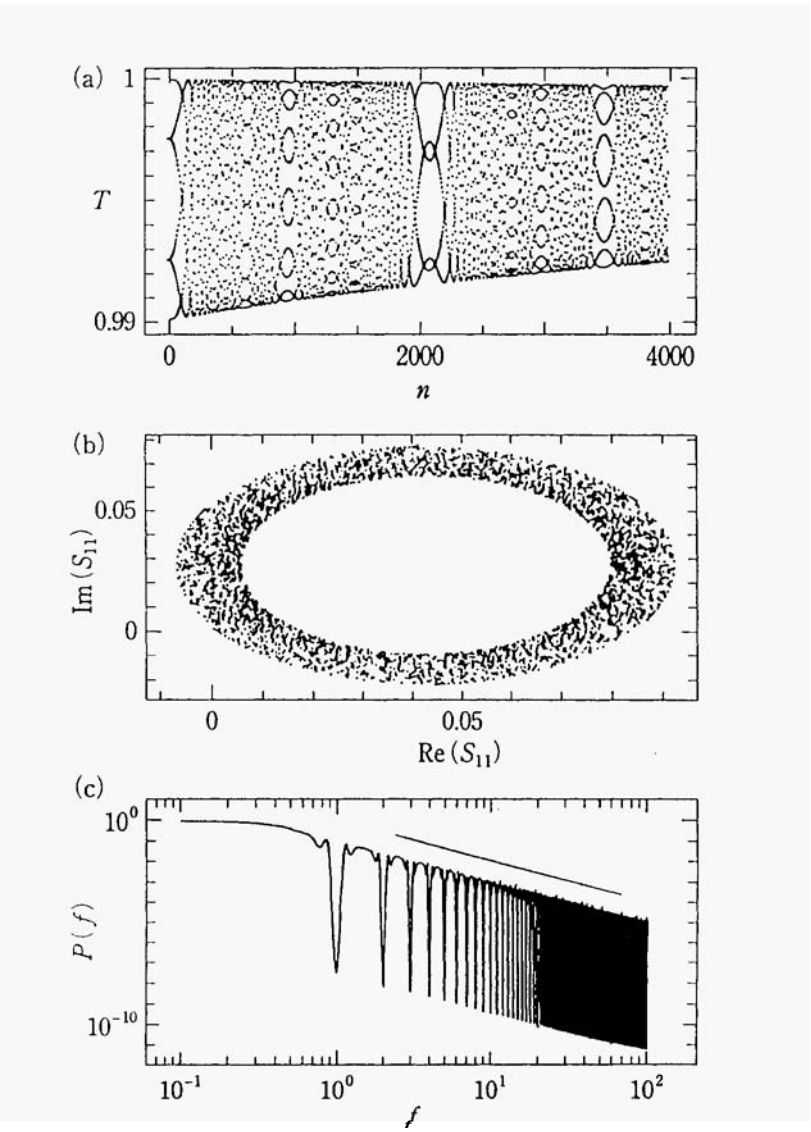

Fig. 3.2. Transport properties of δ--function model for F =0.001: (a) T_n, (b) $S_{11}(n)$, (c) power spectrum $P(f)$ of (a) in logarithmic scales, including a reference line corresponding to $P \propto f^{-2}$.

the direction (upwards or downwards) and the magnitude of each burst are unpredictable, which is in marked contrast with the feature of the intermittent chaos, where only the location of bursts is erratic.

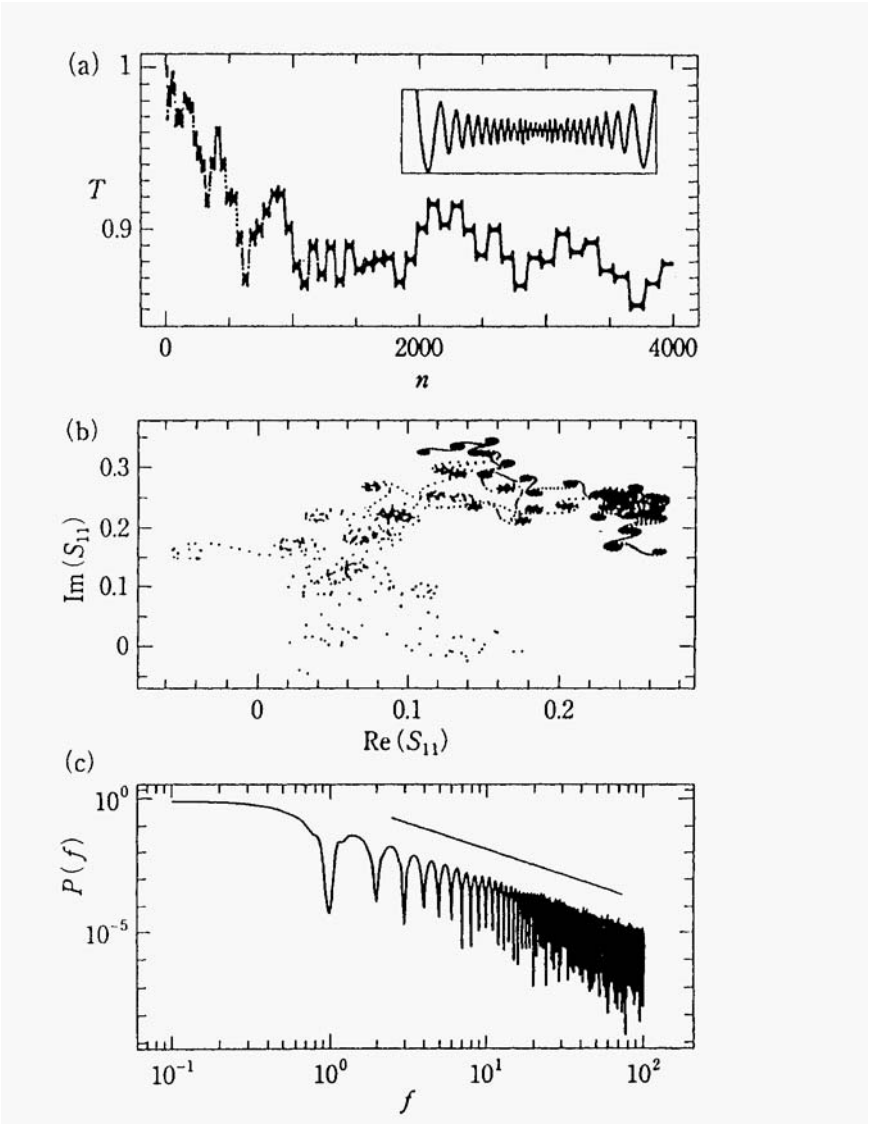

Fig. 3.3. Same as in Fig. 3.2, but for F =10.

The component S_{11} (n) in Fig. 3.3(b) wanders from one stagnant region to another in an unpredictable way, whose overall feature looks like a living animal. As in the case (I), however, the positive Lyapunov exponent is vanishing. The power spectrum of Fig. 3.3(a) again shows the $1/f^2$ law (Fig. 3.3(c)). Locally, a picture of the tilted band structure

is meaningful. Laminar oscillations in the plateaus (see the inset of Fig. 3.3(a)) are caused by the increase of k_n values within each band, whereas bursts are due to the Zener tunneling to adjacent bands at the zone boundaries. In fact, we recognize that the burst occurs regularly whenever $k_n = k_{BZ}$ be satisfied, which is also distinct from the feature of ordinary intermittent chaos.

We can further proceed to examine the transport properties in generic systems with barriers of finite width for the cases of $d/a = 0.1$ and 0.5. In this instance the problem is actually the over-barrier transmission. Despite this fact, a gross feature of T_n for $F = 10$ has proved identical to Fig. 3.3(a) and the corresponding power spectrum obeys the $1/f^2$ law. Thus the integer exponent in the $1/f^2$ law holds universally for periodic superlattices in the electric field, irrespective of the field strength and the width of barriers.

To characterize the nonstationary behavior of T_n, we shall calculate the Allan variance (Allan, 1966; Mandelbrot, 1968; Aizawa *et al.,* 1989)

$$\sigma_A^2(N) = \frac{1}{2}\left\langle \left(\frac{1}{N}\sum_{n=1}^{N} T_{n+(l-1)N} - \frac{1}{N}\sum_{n=1}^{N} T_{n+lN} \right)^2 \right\rangle_l . \tag{3.3}$$

In the Markovian process, the variance in (3.3) tends to zero as N is increased, satisfying a scaling law $\sigma_A^2 = N^y$ with $y < 0$. In the $1/f^v$ cases, however, an additional scaling region to break the law of large number is proposed, viz. the fractional noise regime with $y = v - 1$. Figure 3.4 shows that, besides the Markovian regime, there generally appears this novel scaling regime with the exponent $y = 1 (= 2 - 1)$. (In another special case of v-1, the novel scaling regime shows a *flicker floor* with $\gamma = 1 - 1 = 0$.) Finally the result provides an additional justification of the universality of $1/f^2$ law in the present system and also indicates the breakdown of the law of large number.

To design the experiments, we should systematically change quantum systems by increasing the length of superlattices by a step of a, against repeated injections of electrons with the fixed k_0. We have also analyzed the transmission coefficient as a function of k_0 for a fixed number of walls, finding again the $1/f^2$ law.

In conclusion, the electric conductance as a function of the number of barriers shows a nonstationary weak chaos characterized by both the $1/f^v$ law and anomalous Allan variance. In particular, we have

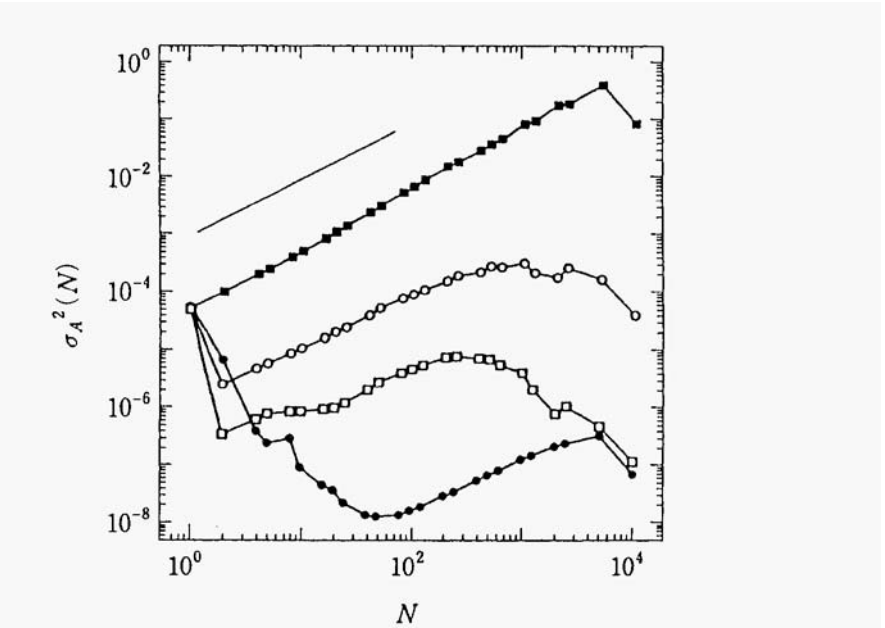

Fig. 3.4. Allan variance $\sigma_{A}^{2}(N)$ in logarithmic scales, including a reference line corresponding to $\sigma_A^2(N) \propto N^1$. Symbols are used for a δ-function model with F=0.001 (filled circle) and F=10 (open circle) and for d/a=0.1 with F=0.001 (filled square) and F=10 (open square).

found the integer exponent ν =2 and also showed the universality of this integer exponent by tuning both the width of barriers and strength of the applied field. We should emphasize many puzzling features of S matrices in tunneling-induced pseudo-chaos in quantum systems.

3.3. Resonant Tunneling in Double-Barrier Structure and Pseudo-Chaos

Heterostructures provide another example of pseudo-chaos. This model (Jona-Lasinio *et al.,* 1992) bears an effective nonlinearity arising from the mean-field approximation of many-body interactions involved in resonant tunneling through a double-barrier structure.

Let us consider the external potential consisting of double wells b_1 and b_2 surrounded by semi-infinite barriers B_1 and B_2 (see Fig. 3.5):

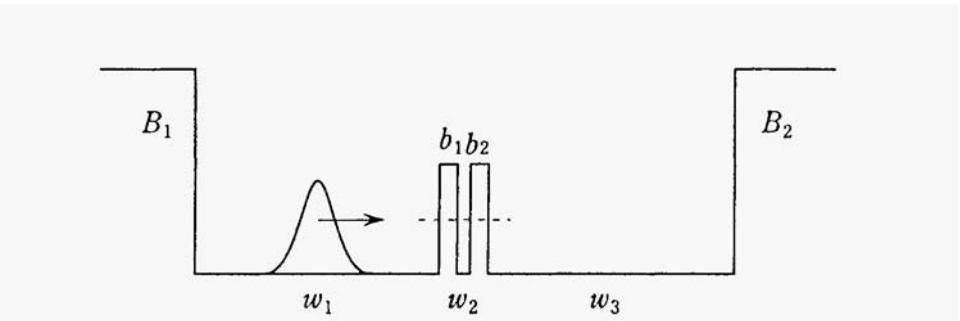

Fig. 3.5. Schematic diagram of a three-well two-barrier heterostructure. An electron cloud initially localized in the well w_1 moves towards the well w_3 with a mean kinetic energy close to the resonance.

$$V(x) = [\eta(x;b_1) + \eta(x;b_2)]V_0 + [\eta(x;B_1) + \eta(x;B_2)]V_1 \ , \tag{3.4}$$

where the positive constants V_0 and V_1 with $V_1 > V_0$ denote the height of barriers of b_1, b_2 and B_1, B_2, respectively. The semi-infinite barriers serve to confine the electrons. The term $\eta(x;A)$ is a characteristic function defined by

$$\eta(x;A) = \begin{cases} 1, & \text{if } x \in A, \\ 0, & \text{if } x \notin A. \end{cases} \tag{3.5}$$

In a mean-field approximation, one may resort to a Hartree-like equation describing the motion of the electron cloud. In terms of a single-body wavefunction $\Psi(x,t)$, the dimensionless charge inside the well w_2 is given by

$$Q(t) = \int_{w_2} |\Psi(x, t)|^2 dx \ . \tag{3.6}$$

We then obtain the time-dependent (single-body) Schrödinger equation

$$\begin{aligned} i\hbar \, \partial\Psi(x, t)/\partial t \ &= (-\hbar^2/(2m)) \, \partial^2\Psi(x, t)/\partial x^2 \\ &+ [V(x) + \kappa \, Q(t)\eta(x; w_2)]\Psi(x, t) \ , \end{aligned} \tag{3.7}$$

which is obviously nonlinear with respect to Ψ. The coupling constant κ measures the strength of the mean field acting on each electron. As an initial state, let us choose the wave packet located inside the well w_1 and moving towards the well w_2 with mean momentum $\hbar k_0$:

$$\Psi(x,0) = \sigma^{-1/2}\,\pi^{-1/4}\,\exp[-(x-x_0)^2/(2\sigma^2) + ik_0x] \quad . \tag{3.8}$$

If $\sigma/w_1<<1$, then $Q(0)=0$, and (3.8) satisfies (3.7). Parameter values employed in the numerical simulations are $w_1=w_3=1100\,a_0$ $w_2=15a_0$, $b_1=b_2=20\,a_0$, $=110\,a_0$ with Bohr radius a_0=0.529A. Others are V_0=0.3eV and E_R=0.15eV, with V_1 being large enough to confine the electron cloud between B_1 and B_2. If the mean kinetic energy $(\hbar k_0)^2/(2m)$ is chosen close to the resonance energy E_R, the wave packet will diffuse

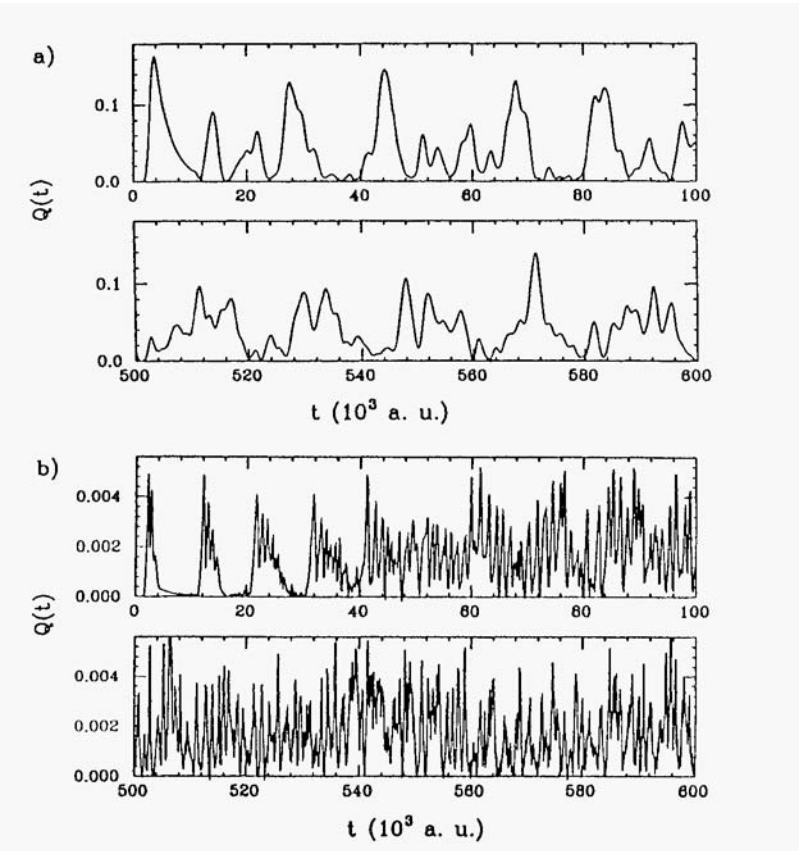

Fig. 3.6. Time evolution of the charge $Q(t)$. (a) κ=0, (b) κ=3, (Courtesy of G. Jona-Lasinio *et al.)*

by repeating a round trip through the double barriers.

Results of numerical iteration of (3.6) and (3.7) indicate a chaotic oscillation of the charge $Q(t)$; the details are as follows:
Figure 3.6 shows the erratic behavior of $Q(t)$ as a function of time for the case κ=3. A convenient tool to quantify chaotic behaviors is the autocorrelation function defined by

$$C(t) = \int_T \delta Q(t')\delta Q(t'+t)\mathrm{d}t' / \int_T \delta Q(t')\delta Q(t')\mathrm{d}t', \tag{3.9}$$

with $\delta Q(t)=Q(t) - T^{-1}\int_T Q(t')\mathrm{d}t'$. C(t) in Fig. 3.7 shows a rapid decay of the correlation, followed by noisy ripples in the nonlinear ($\kappa \neq 0$) cases, whereas it retains a long-time correlation in the linear (κ = 0) case. Other diagnostic quantities such as KS entropy and Lyapunov exponent (not displayed here) also guarantee the chaotic behavior of the system under consideration.

The origin of chaos resides in the nonlinearity of the Hartree equation, i.e., the mean-field model in (3.6) and (3.7). One should note that quantum systems evolve according to a linear Schrödinger equation, and all the nonlinear features arising from the many-body

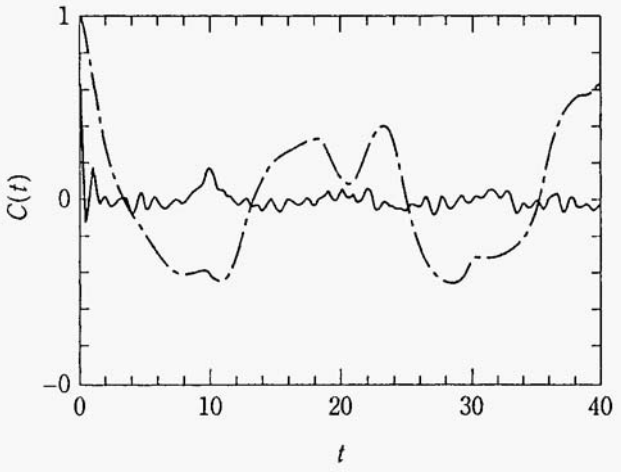

Fig. 3.7. Autocorrelation functions $C(t)$ for $\kappa \neq 0$ (solid line) and κ=0 (dashed dotted line). (Courtesy of G. Jona-Lasinio *et al.*)

effect are absorbed into the Hamiltonian, i.e., a linear operator acting on the many-body wave function. This means that chaotic behavior is not possible in the time dependence of either wavefunction or observables. If the many-body effect is taken into consideration in the Hartree approximation, however, artificial nonlinearity appears and thereby one obtains the nonlinear Schrödinger equation. Therefore the chaos demonstrated above is not a genuine chaos, but merely a *pseudo-chaos caused by the artifact.* One must recognize that the rigorous treatment of the many- body effect will smear out any signature of chaos.

3.4. General Remarks

Despite the absence of genuine chaos in quantum systems, we have shown some examples of pseudo-chaos in 1-*d* quantum transport. This transport, induced by quantum tunneling, has no classical counterpart. The pseudo-chaos has no positive Lyapunov exponent but bears a positive component in the distribution of the local Lyapunov exponent. The pseudo-chaos of the Krönig-Penny model in the applied electric field breaks the law of large numbers, leading to 1/*f* fluctuations. Chaos resulting from double-barrier structures has proved to be of the virtual reality, since it is traced back to the artificial nonlinearity as a consequence of the mean-field approximation of the many-body interaction.

In general, the quantum dynamics of systems with a few degree of freedom demonstrates periodic or quasi-periodic oscillations characterized by discrete energy spectra. On the other hand, there is a general belief that the quantum dynamics of many-body open systems has (i) no positive Lyapunov exponent but (ii) may have a nonzero generalized KS entropy extended to systems obeying the non-commutative algebra (Connes *et al.,* 1987), although it is not easy to construct an explicit example exhibiting the latter property. Eventually one should confirm that the present framework of quantum mechanics cannot yield genuine chaos characterized by positive Lyapunov exponents.

References

Aizawa, Y., *et al.* (1989). *Prog. Theor. Phys. Suppl.* **99,** 149.
Allan, D. W. (1966). *Proc. IEEE* **54,** 221.
Connes, A., Narnhofer, H., and Thirring, W. (1987). *Commun. Math. Phys.* **112,** 691.
Dutta, P., and Horn, P. M. (1981). *Rev. Mod. Phys.* **53,** 497.
Esaki, L. (1985). In *The Technology and Physics of Molecular Beam Epitaxy,* E. H. C. Parker, ed. New York Plenum.
Geisel, T., et al. (1987). *Phys. Rev. Lett.* **59,** 2503.
Geisel, T., et al. (1990). *Phys. Rev. Lett.* **64,** 1581.
Jauslin, H. R. (1991). *Physica* **D51,** 200.
Jona-Lasinio, G., etal. (1992). *Phys. Rev. Lett.* **68,** 2269.
Mandelbrot, B. B. (1968). *SIAM Review* **10,** 422.
Mendez, E. E., et al. (1988). *Phys. Rev. Lett.* **60,** 2426.
Nakamura, K., Haga, T., and Takane, Y. (1994). *Phys. Rev.* **E50,** 1700.
Voss, R. F., and Clarke, J. (1976). *Phys. Rev.* **B13,** 556.
Weissman, M. B. (1988). *Rev. Mod. Phys.* **60,** 537.

Chapter 4

Chaos and Quantum Transport in Open Magnetic Billiards: from Stadium to Sinai Billiards

Particle motion inside or outside billiards provides a prototype of chaos in conservative dynamical systems. In this chapter, chaos and quantum transport in magnetic billiards are investigated. First, theoretical and experimental studies are presented on quantum transport in weakly-opened circle and stadium billiards in the perpendicular magnetic field B. While in the circle, the magneto-conductance shows grossly regular oscillations, in the stadium it exhibits a transition from the mild to violent undulations with increase of B. The rich fluctuation features of the conductance, characterized by gradients of the cusp-like central peaks in autocorrelation functions, are attributed to the stability or instability of phase space in the underlying classical dynamics.

To see other rich aspects of quantum transport, we shall move on to classical dynamics and quantum transport in weakly-opened square and single Sinai billiards in a perpendicular magnetic field B. From comparison between the correlation field B_c of the smoothed conductance and Lyapunov exponents in wide B-field regions, it follows that fluctuation features of B_c are attributed again to the stability of the classical phase space. In the Sinai billiard case, the geometry of the billiard yields Aharonov-Bohm oscillations in a non-smoothed conductance, suppressing symptoms of chaos. Nevertheless, B_c evaluated in terms of the smoothed conductance proves to mimic nicely the scaled variance of Lyapunov exponents.

4.1. Introduction

Concave and convex billiards, together with a kicked rotator, are prototypes of conservative chaotic systems and have enjoyed a growing theoretical interest in fields of nonlinear dynamics and statistical mechanics. In the concave case, a point particle repeats alternately the free motion inside the cavity and the elasic collision (via specular reflection) at the hard wall, resulting in a complicated trajectory that is extremely sensitive to initial conditions. In the convex case, on the other hand, a particle moves between a number of convex billiards, e.g., as in case of Sinai's billiards (1979). The quantum-mechanical study of these billiards is one of the important themes of *quantum chaos* (Gutzwiller, 1990; Doron *et al.,* 1991; Nakamura, 1993). The present and next chapters will be devoted to the quantum and semiclassical analyses of concave and convex billiards, respectively.

Among concave billiards, Bunimovich's stadium billiard (Bunimovich, 1974; Benettin and Strelcyn, 1978) has received a wide attention as a paradigm of nonlinear dynamics. It belongs to the K system, showing the fully-chaotic orbits in marked contrast to regular orbits in a simple circle or rectangle. Its quantum-mechanical study showed the level statistics (McDonald and Kaufman, 1979) similar to those for the Gaussian orthogonal ensemble (GOE) and wavefunctions characterized by periodic-orbit scars (Heller, 1984), thereby heralding a new era of quantum chaos. In the presence of a perpendicular magnetic field, the stadium billiard becomes a generic system. The Meplan *et al.* treatment (1993) elucidated its characteristic classical features: The erratic and ergodic phase space in a low-field region is replaced by KAM tori via transitional unstable regions with increase of the field strength, in contrast to the circle billiard, where the phase space is always occupied by periodic (or quasi-periodic) and nonergodic orbits.

These theoretical treatments, however, have been limited to closed systems without any leaky region and, with a few exceptions, little attention has been given to corresponding studies on its open-system version. Jalabert *et al.* (1990) and Baranger *et al.* (1991; 1993a,b) indeed presented both the quantal (i.e., tight-binding calculations with Peierls' substitution) and semiclassical theories on open concave billiards (e.g., circle, stadium or wedge), but they were rather concerned with strongly opened systems where the incoming electron can bounce at the cavity wall only a few times until exit. Furthermore, their semiclassical theory does not incorporate the effect of diffraction

at holes of billiards and is limited to the weak-field region. Therefore the difference between magneto-conductances in weakly-opened circle and stadium billiards is not clear at all.

All these researches had a tendency to remain sophisticated with little relation to real systems. Dramatic progress in fabrication of nanoscale or mesoscopic structures (Beenakker and van Houten, 1991; Akkermans *et al.,* 1995) has, however, been establishing a nice bridge between high technology and fundamental researches of nonlinear dynamics. Both concave and convex billiards, around which studies of chaos are being accumulated, can be fabricated at the interface layer of semiconductor heterojunctions, e.g., GaAs /AlGaAs. Finally Marcus *et al.* (1992; 1993a,b) performed a striking experiment on the magneto-conductance of the nanoscale stadium billiard. This experiment has opened a way for us to study the quantum theory of chaos through advanced electron transport devices.

4.2. Magneto-Conductance in Stadium Billiard: Experimental Results

At the interface of GaAs /$Al_xGa_{1-x}As$, Marcus et al. fabricated stadium-shaped quantum dots of linear dimension ~0.5μm connected via point contacts with a pair of right-angled quantum wires of width ~0.14μm ; see Fig. 4.1. They also made circular quantum dots. Since a 2-dimensional electron gas in these nanoscale billiards has a very low concentration (n=3.6 x 1011 cm^{-2}) with average distance between electrons ~ 10-2μm, one may suppress many-body effects. Further, owing to a relatively long mean free path ~1 μm, the electronic motion between successive bouncings is ballistic rather than diffusive. The magnetic field B applied perpendicularly to the billiard plane is weak (e.g., B=0~2.2 T [Tesla]) so as to induce the chaotic cyclotron motion of electrons. In fact, with a choice B =0.3T, the cyclotron radius $R=\hbar(2\pi n)^{1/2}/eB$ is comparable to the billiard size, yielding the motion sensitive to both the system size and shape. We should note that, for the gate voltage V_g ~ -6.0V in the experiment, the incident wave with the corresponding Fermi wave number consists of a few fundamental modes.

Figure 4.1 shows the magneto-conductance as a function of B. Common to both the circle and stadium, the anomalous fluctuations are evident, strongly reminiscent of the universal conductance

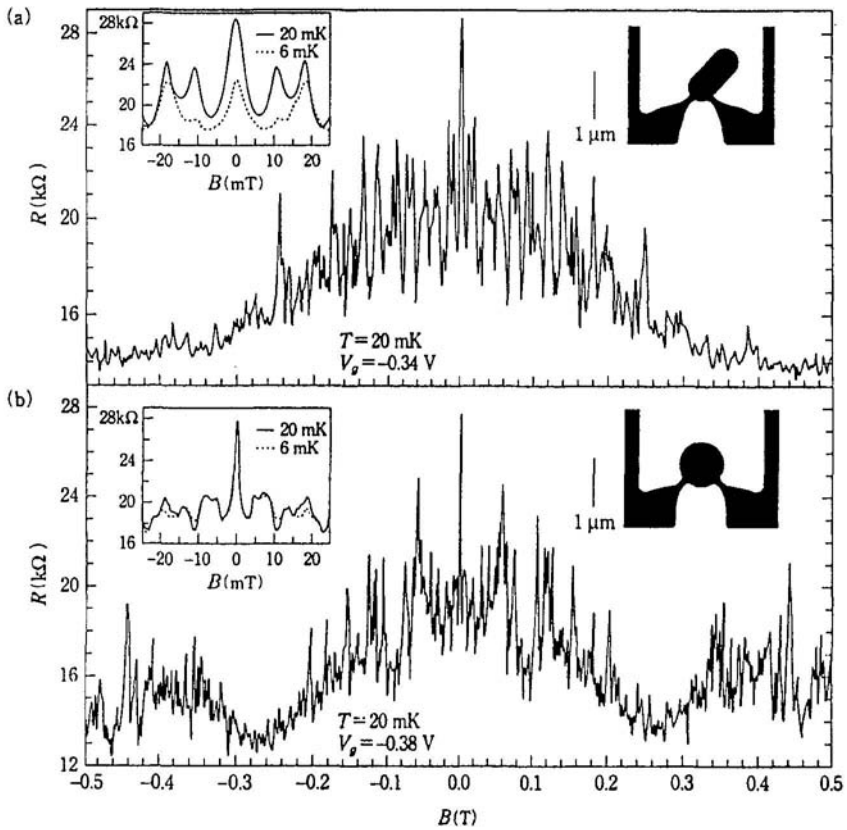

Fig. 4.1. Experimental result for resistance as a function of magnetic field. Only N=1 mode contributes to propagation: (a) stadium; (b) circle. Inset on upper left in each panel is a magnification of the vicinity of zero field. (Courtesy of C. Marcus *et al.*)

fluctuations (UCF) in dirty metals. Insight into more details reveals abundant sharp peaks corresponding to scattering resonances, i.e., electronic states confined to billiards. Marcus *et al.* assert: For B>1.5T, in both types of billiards, edge states are essential and Aharonov-Bohm oscillation commonly appears; for $B< B^{exp}_{th}$ (~0.3T), circle maintains regular oscillations whereas stadium demonstrates mild but aperiodic oscillations. Their interpretation of the intermediate region 0.3T<B<1.5T is not obvious. In the vicinity of a zero field, the gradient

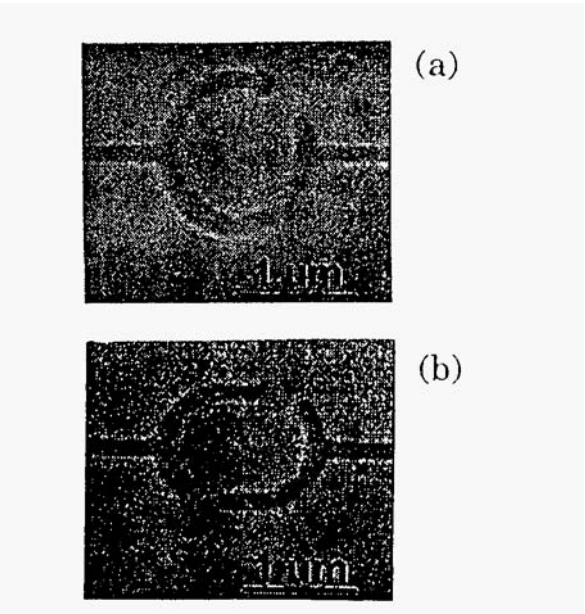

Fig. 4.2. Chang *et al's* billiards, (a) circle, (b) stadium. (Courtesy of A. M. Chang *et al.*)

of the resistance peak is much smaller in stadium than in circle.

On the other hand, by manipulating the wire-like walls (wires themselves are void of electrons), Chang *et al.* (1994) fabricated stadium-shaped and circle-shaped conducting cavities (see Fig. 4.2), in which they measured the magneto-conductance in the weak-field range $B<10^{-2}$T. In Fig. 4.2, an electron incident from the upper hole escapes to either one of the upper or lower holes after significant collisions with the cavity wall. In their experiment the resistance peak near the zero field shows the same behavior as Marcus *et al.'* s.

Baranger *et al.* (1991; 1993a,b) have performed theoretical studies of BCF (ballistic conductance fluctuation) and BWL (ballistic weak-localization). Their analytical semi-classical theory predicts that the autocorrelation function $C(\Delta B)$ of the magneto-conductance for chaotic systems has a universal form $C(\Delta B)=C(0)/[1+(\Delta B/(\alpha\phi_0))^2]^2$, assuming an exponential distribution of classical trajectory areas A within the structure: $N(A) \propto \exp(-\alpha A)$ with α denoting the r.m.s. of areas A. (Note: $\phi_0=hc/e$.) This prediction has indeed been confirmed in experiments (Marcus *et al.*, 1992, 1993a, b; Bird *et al.,* 1994, 1995). However, their semi-classical theory has been limited to a weak B-field

region, where the cyclotron radius of an electron is much larger than device dimensions, and to high energy regions where the number of injected modes is large. Therefore, the quantum-classical correspondence in wider field regions is far from obvious. Lin and Jensen (1996) studied the BCF of the open circle billiard by using the numerical semi-classical scattering theory. However, the application of their theory to billiards with tunable magnetic field is extremely complicated. At present, systematic studies on transport in open systems characterized by *mixed phase space* (e.g., open stadium and Sinai billiards in a magnetic field) are inevitably restricted only to classical phenomelogical and quantal analyses.

4.3. Transition from Chaos to Tori

While the experiments above are concerned with open billiards, we shall in this section pay some attention to closed magnetic billiards with no wires, investigating the cyclotron motion of an electron inside the cavity in terms of classical dynamics and showing its chaotic behavior. In this regard, we shall follow the analysis by Meplan *et al.* (1993).

Bearing a stadium shape in mind, let us denote the length of a straight line segment by b and the radius of a semicircle by α; $b=2\alpha$ and $b=0$ correspond a stadium and a circle, respectively. The frequency and Larmor radius of cyclotron motion are given by $w = eB/m$ and $R=mv/eB=v/w$, respectively. For convenience, the angular velocity vector is prescribed as $\omega=w\,\mathbf{e}_z$ with $\mathbf{e}_z$ the unit vector perpendicular to the billiard plane.

Now suppose that the electron reflected at P_0 on the wall impinges at P_1 (see Fig. 4.3). Noting the rotation of the velocity vector by $2\varphi_0$ during the above flight,

$$\mathbf{v}_0 - \boldsymbol{\omega} \times \mathbf{r}_1 = \mathbf{v}_1 - \boldsymbol{\omega} \times \mathbf{r}_2 \ , \tag{4.1}$$

where $\mathbf{r}_1$ and $\mathbf{r}_2$ denote the position vectors for P_0 and P_1 respectively, measured from an arbitrarily fixed origin on the plane. We introduce next unit vectors $\mathbf{e}_x$ and $\mathbf{e}_y$ which are parallel and perpendicular to $\mathbf{r}_2$-$\mathbf{r}_1$, respectively. Making the projection of (4.1) onto $\mathbf{e}_x$ and $\mathbf{e}_y$, we obtain the Poincare' map for a pair of variables, i.e., the angle α

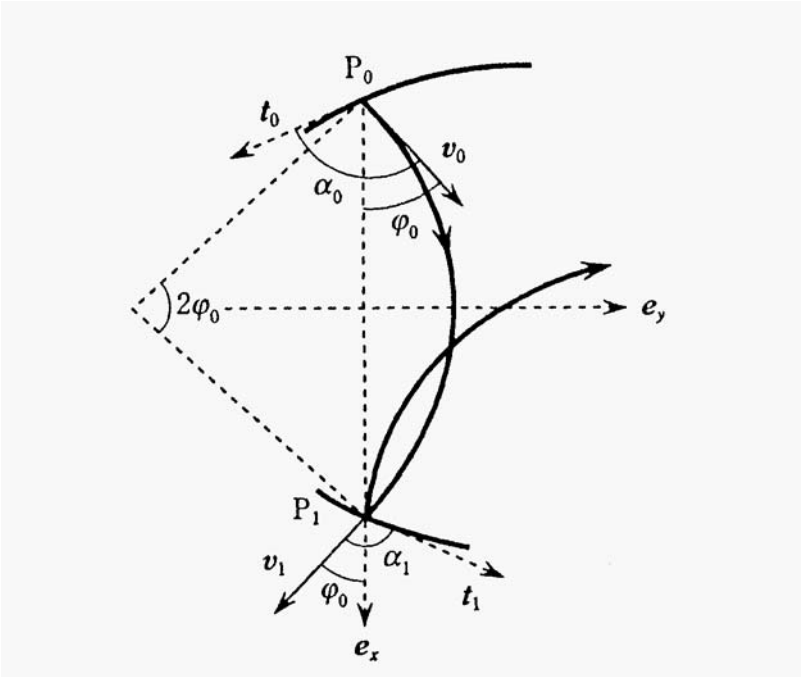

Fig. 4.3. Notation of relevant vectors and angles for successive bouncings. **t** is tangent vector defined in counter-clockwise direction.

between the tangent vector and velocity vector just after each bouncing and the distance s of the bouncing point measured along the billiard boundary.

The variation of (4.1) gives the linearized Poincare' map

$$(\delta\alpha_0 + \delta\Psi_0)\,\mathbf{e}_z \times \mathbf{v}_0 - \delta s_0\,\boldsymbol{\omega} \times \mathbf{t}_0 = (\delta\alpha_1 + \delta\Psi_1)\,\mathbf{e}_z \times \mathbf{v}_1 - \delta s_1\,\boldsymbol{\omega} \times \mathbf{t}_1 \tag{4.2}$$

with Ψ denoting the angle between **t** and an arbitrarily fixed axis on the billiard plane. The orbital stability analysis will be made in terms of (4.2). Taking a projection of (4.2) onto $\mathbf{e}_x$ and $\mathbf{e}_y$, we get the tangent map for the variation of a pair of Birkhoff coordinates (1927) s (i.e., length along the boundary of the cavity) and q (=cos α) :

$$\begin{pmatrix} \delta s_1 \\ \delta q_1 \end{pmatrix} = \mathbf{M}_{1,0} \begin{pmatrix} \delta s_0 \\ \delta q_0 \end{pmatrix}, \tag{4.3a}$$

where $\mathbf{M}_{1,0}$ is a transfer matrix with elements

$$(\mathbf{M}_{1,0})_{11} = \frac{\sin(\alpha_0 - 2\varphi_0)}{\sin\alpha_1} - \frac{R\sin 2\varphi_0}{\rho_0 \sin\alpha_1},$$

$$(\mathbf{M}_{1,0})_{12} = \frac{R\sin 2\varphi_0}{\sin\alpha_0 \sin\alpha_1},$$

$$(\mathbf{M}_{1,0})_{21} = \frac{\sin(\alpha_0 - 2\varphi_0)}{\rho_1} - \frac{R\sin 2\varphi_0}{\rho_0\rho_1} - \frac{\sin(\alpha_1 + 2\varphi_0)}{\rho_0} - \frac{\sin(\alpha_1 + 2\varphi_0 - \alpha_0)}{R},$$

$$(\mathbf{M}_{1,0})_{22} = \frac{R\sin 2\varphi_0}{\rho_1 \sin\alpha_0} + \frac{\sin(\alpha_1 + 2\varphi_0)}{\sin\alpha_0}\ ; \qquad (4.3b)$$

herein $p = 1/\kappa = ds/d\Psi$ is the radius of curvature at the bouncing point. (Note: $p = \infty$ at a square wall and $\rho = -a$ at a circular wall.) $\mathrm{Det}\mathbf{M}_{1,0}=1$ ensures the mapping to be area-preserving. For a trajectory executing n bouncings, a product sum of the transfer matrices gives the monodromy matrix,

$$\mathbf{M}_n = \mathbf{M}_{n,n-1} \bullet \mathbf{M}_{n-1,\,n-2} \cdots \mathbf{M}_{2,1} \bullet \mathbf{M}_{1,0}\ . \qquad (4.4)$$

The Lyapunov exponent is given by the logarithm of the larger eigenvalue λ_n of $\mathbf{M}_n$:

$$\lambda_n = \frac{1}{L}\ln\Lambda_n\ , \qquad (4.5a)$$

with

$$\Lambda_n = \left(\mathrm{Tr}M_n + \sqrt{(\mathrm{Tr}M_n)^2 - 4}\right)\Big/2, \qquad (4.5b)$$

where L, the length of an orbit, is identified with the flight time for unit velocity. For $\mathrm{Tr}\mathbf{M}_n > 2$, the Lyapunov exponent λ_n is positive, ensuring chaotic motion; for $\mathrm{Tr}\mathbf{M}_n \leq 2$, it is nonpositive, which reflects regular ones. Equations (4.1)-(4.4) are valid so long as the closed boundary of the billiard is smooth everywhere.

In case of circle, the phase space is occupied by tori whatever value R takes. By contrast, in case of stadium, the phase space becomes *mixed* when the B field is switched on: For $R = \infty$ (i.e., $B=0$), an electron repeats alternately the free straight motion and the specular reflection at the hard wall, resulting in chaotic motion irrespective of initial conditions; for $R<\infty$, however, the orbit is bent and the

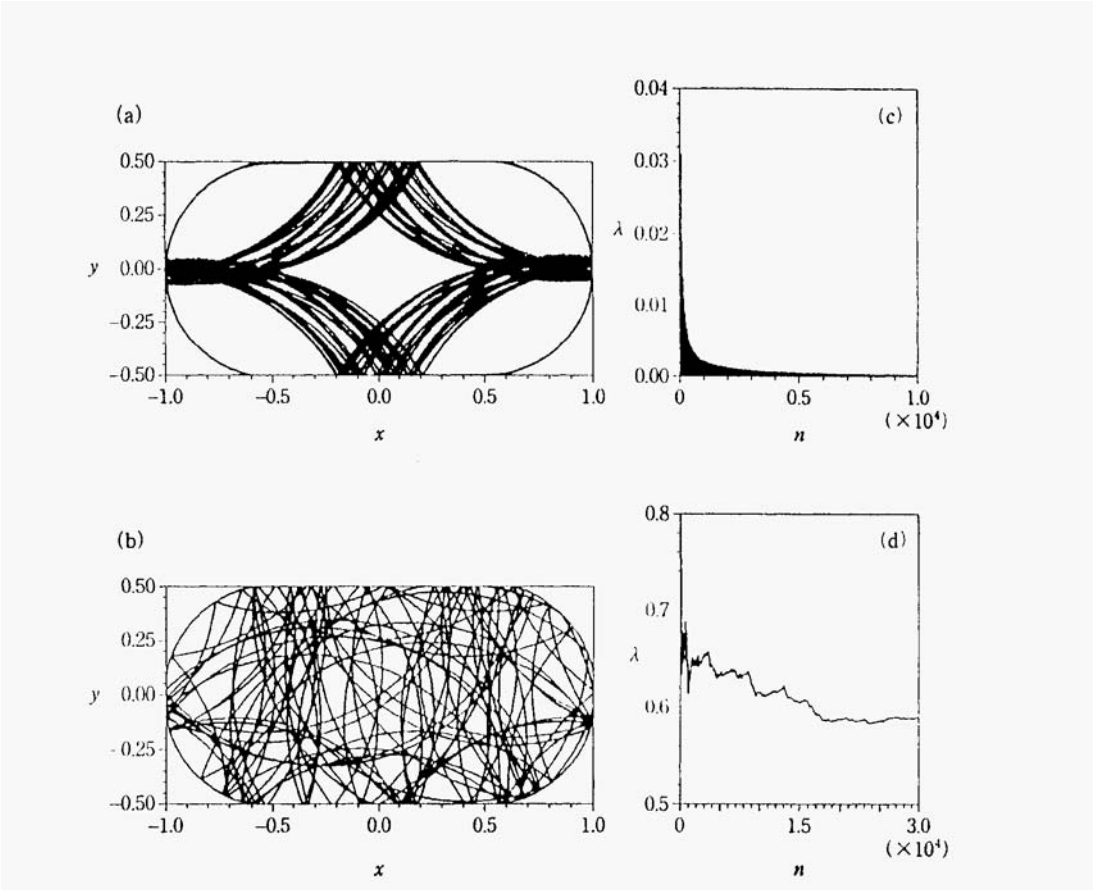

Fig. 4.4. Left panel for cyclotron motion within stadium. Right panel for convergence of Lyapunov exponent. $R= a$=1/2: (a), (c) regular orbit; (b), (d) chaotic orbit. (Courtesy of O. Meplan *et al.)*

electron launched at a left edge of the stadium executes either regular (Fig. 4.4(a)) or chaotic (Fig. 4.4(b)) motion, depending on the direction of the initial velocity vector. Figures 4.4(c) and (d), which correspond to Figs. 4.4(a) and (b), respectively, show the Lyapunov exponent λ_n in (4.5a) as a function of the bouncing number n. For the regular orbit, λ_n turns out tending to zero in the limit $n \to \infty$ (see Fig. 4.4(c)). Extensive numerical analyses suggest that, in the case of stadium, the global chaos persists in the range ∞ $>R>R^{cl}{}_{th}$ with $R^{cl}{}_{th}$~1.53a or, more precisely, the measure of KAM tori begins to take a finite value

at $R=R^{cl}_{th.}$ A question naturally arises: How is the (continuous) transition from chaos to tori in the classical dynamics reflected in the spectrum of Fig. 4.1 ? Before investigation of this intriguing problem, we should also get acquainted with the quantum-mechanical results described below.

4.4. Quantum-Mechanical and Semiclassical Theories

To examine the implication of the Marcus *et al.* 's experiment, we shall here present quantum theory on the transport in open concave billiards in a perpendicular magnetic field (Nakamura *et al.,* 1994). A pair of semi-infinite lead wires j =1 and 2 are joined to the leaky holes of the billiard on its right and left sides, respectively (see Fig. 4.5(b)). [Although this wire geometry which was also used in the open billiards

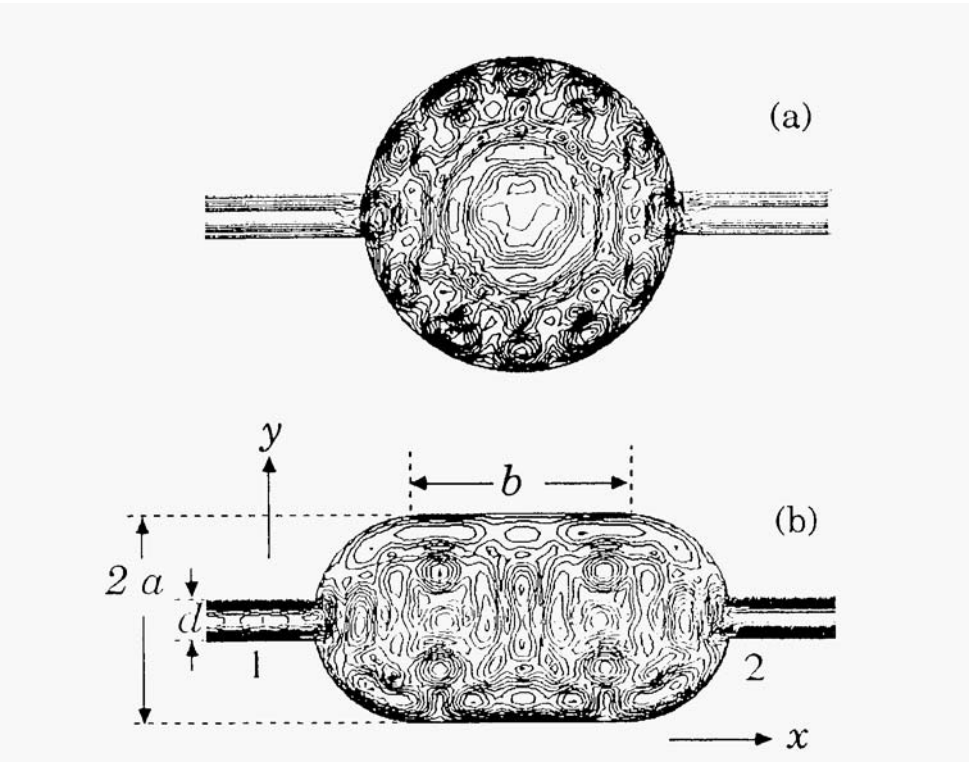

Fig. 4.5. Contour map for wavefunction $|\Psi|$ in case of complete transmission: (a) circle with B/B_0=12.2604, (b) stadium with B/B_0=12.6489.

without magnetic field (Nakamura and Ishio, 1992) is different from the one in Marcus *et al.* 's experiments, qualitative features of the magneto-conductance will depend on the billiard's shape rather than the wire geometry.] This open system is characterized by *a, b,* and *d* for semicircle radius, line segment length, and width of holes at $x=a'_j=(-1)^j a'$, respectively, taking the origin at the center of the billiards. Note $a'=b/2+(a^2-d^2/4)^{1/2}$. We shall choose the stadium with $b=2a$, where the maximum Lyapunov exponent is available, and the circle with $b=0$, while keeping fixed the area of the billiard $\mathcal{A}(=\pi a^2+2ab)$ and the degree of opening $d/\mathcal{A}^{1/2}=0.1497$ common to both types. (In this case, $d/(2a)=0.2$ and 0.1327 for the stadium and circle, respectively.) This degree corresponds to a weakly-opened situation suitable to uncover the ample fluctuation properties of quantum transport. We shall be concerned with tuning the strength of magnetic field. For convenience, the circle and stadium will be abbreviated hereafter as *Cl* and *Sd,* respectively. The region inside the billiard wall and within $|x|<a'$ will be prescribed as the cavity region. Nonlinear dynamics of electrons in this region will have an outstanding effect on the *S* matrix and quantum transport, and our major interest lies in this effect.

For brevity, suppose the field *B* applied only to the cavity region and no field in the wire regions. We prescribe the velocity of light $c=1$. The essential quantities are cyclotron frequency and magnetic length given by $w=eB/m$ and $l_c=(\hbar/(eB))^{1/2}$, respectively. We choose the gauge potential in the Landau gauge, $\mathbf{A}=(0,-Bx,\ 0)$, which continuously changes to the constant value $\mathbf{A}=(0,\ -Ba'_j,\ 0)$ at the wires.

For an electron with Fermi energy $E=(\hbar k_F)^2/2m$, the wavefunction Ψ satisfies Schrödinger equation

$$(2m)^{-1}[-i\hbar\nabla + eA(\mathbf{r})]^2\Psi(\mathbf{r}) = E\Psi(\mathbf{r}). \tag{4.6}$$

For the incident propagating mode *n* at the wire 1, $\Psi(r)$ at wires $j=1$ and 2 is written in terms of *S* matrix $\{S^{(j)}_{mn}\}$ as

$$\Psi^{(j)}(x, y; n) = \delta_{j1}\exp[ik_n(x - a'_j)]\phi_n(y) + \sum_{m=1}^{M} S^{(j)}_{mn}\exp[(ieBa'_j/\hbar)y]\exp[(-1)^j ik_m(x-a'_j)]\phi_m(y), \tag{4.7}$$

with the transverse component

$$\phi_m(y) = (2/d)^{1/2} \sin\{(m\pi/d)(y + d/2)\}. \tag{4.8}$$

Here the wave vector is defined by $\mathbf{k}=(k_m, m\pi/d)$, with $m\pi/d$ and $k_m=[k_F^2-(m\pi/d)^2]^{1/2}$ for the transverse and longitudinal components, respectively. Modes m for $1 \le m \le N$ and for $m > N$ with N $[k_F d/\pi]$ correspond to propagating and evanescent waves, respectively.

In the cavity region, on the other hand, the Green function is given by (Feynman and Hibbs, 1965; Ueta, 1992)

$$G(\mathbf{r}, \mathbf{r}';\varepsilon) = (-m\pi/(2\pi\hbar^2))\ \{\exp[i(x'y - xy' + xy - x'y')/2l_c^2]\}$$
$$\times\ [(\cos\pi\varepsilon)\Gamma(\varepsilon+1/2)]^{-1} W_{\varepsilon,0}(z)/z^{1/2}, \tag{4.9}$$

where $\varepsilon = (E + i\delta)/\hbar w$ is a scaled energy and $W_{\varepsilon,0}$ is the Whittaker function of $z\ (=|\mathbf{r}-\mathbf{r}'|^2/(2l_c^2))$.

To determine the values for *S* matrix, we exploit Green's theorem which yields the equation including integrations along the closed boundary *C* of the cavity region:

$$\frac{\theta(\mathbf{r})}{2\pi}\Psi(\mathbf{r}) = -\frac{\hbar^2}{2m}\wp\oint_C \left[G(\mathbf{r},\mathbf{r}')\frac{\partial\Psi(\mathbf{r}')}{\partial n'} - \Psi(\mathbf{r}')\frac{\partial G(\mathbf{r},\mathbf{r}')}{\partial n'}\right] ds'$$
$$-2\frac{i\hbar e}{2m}\wp\oint_C G(\mathbf{r},\mathbf{r}')\mathbf{A}(\mathbf{r}')\cdot\mathbf{n}'\Psi(\mathbf{r}')ds', \tag{4.10}$$

where **r** and **r'** lie on *C* and $\partial/\partial n'$ signifies the outward-normal derivative on *C;* $\wp$ and θ **(r)** denote Cauchy's principal value and the interior angle at **r,** respectively. In (4.10), no contribution from the bulk integration arises, since **r** also locates along *C.*

We shall here apply the boundary element method: The boundary of the cavity region is approximated by a sequence of small line segments. Then functions in the integrand along each integration segment in (4.10) are approximated by their linear interpolations: For a segment connecting $\mathbf{r}_i$ and $\mathbf{r}_{i+1}$, for instance,

$$\mathbf{r}(\xi) = F_1(\xi)\mathbf{r}_i + F_2(\xi)\mathbf{r}_{i+1},$$
$$\Psi(\mathbf{r}(\xi)) = F_1(\xi)\Psi_i + F_2(\xi)\Psi_{i+1},$$
$$\partial\Psi(\mathbf{r}(\xi))/\partial n' = F_1(\xi)\partial\Psi_i/\partial n' + F_2(\xi)\partial\Psi_{i+1}/\partial n', \tag{4.11a}$$

where

$$F_1(\xi) = (1 - \xi)/2, \quad F_2(\xi) = (1 + \xi)/2 , \tag{4.11b}$$

with $-1 \le \xi \le 1$. Substituting into (4.10) $G(\mathbf{r}, \mathbf{r}'; \varepsilon)$ from (4.9), its normal derivative, and expressions from (4.11), we find

$$J_i \Psi_i = \sum_{l=1}^{L} P_{i\,l} \Psi_l - \sum_{l=1}^{L} Q_{i\,l} \partial \Psi_l / \partial n' \qquad (1 \le i \le L) , \tag{4.12}$$

where J, P and Q are numerical coefficients and the boundary condition $\mathbf{r}_{L+1} = \mathbf{r}_1$ is imposed. Among unknown variables Ψ and $\partial \Psi / \partial n'$, $\Psi = 0$ is satisfied at the wall and Ψ and $\partial \Psi / \partial n'$ at the holes j=1 and 2 are rewritten in terms of S matrix as:

$$\Psi^{(j)}(a'_j, y;\ n) = \delta_{j1} \phi_n(y) + \sum_{m=1}^{M} S_{mn}^{(j)} \exp\{(\mathrm{i}e B a'_j / \hbar) y\} \phi_m(y) ,$$

$$\partial \Psi^{(j)}(a'_j, y;\ n) / \partial n' = -\mathrm{i} k_1 \delta_{j1} \phi_n(y) - \sum_{m=1}^{M} S_{mn}^{(j)} (-1)^j (\mathrm{i} k_m) \exp\{(\mathrm{i}e B a'_j / \hbar) y\} \phi_m(y) . \tag{4.13b}$$

Using these notions in (4.12), we eventually obtain a set of linear equations for unknown variables $S^{(1)}$, $S^{(2)}$, and $\partial \Psi / \partial n' \mid_{wall}$, whose solutions lead to the flux-normalized transmission coefficient $t_{mn} = (k_m / k_n)^{1/2} S^{(2)}_{mn}$ and the magneto-conductance $g(B) = (2e^2/h) \sum_{1 \le n, m \le N} |t_{mn}|^2$.

Similarly, wavefunctions are available by substituting the solution for $S^{(j)}$ and $\partial \Psi / \partial n' \mid_{wall}$ into (4.10) with $\mathbf{r}$ taken inside the cavity region together with a new choice $\theta(\mathbf{r}) = 2\pi$.

Semiclassical Treatment

Before proceeding to the numerical analysis, we shall mention a way of deriving the *semiclassical formula* for S matrix. In open billiards, a point particle escapes to exit wires after being temporarily confined within the cavity, which is distinct from situations in closed billiards. Owing to this fact, one will be free from the problem of the divergence (i.e., exponential proliferation coming from summation over infinitely-long periodic orbits) proper to Gutzwiller's semiclassical trace formula (1990). Since our major concern in this chapter lies in the quantum-mechanical explanation of the experimental results, the semiclassical

approach will be briefly presented below.

Suppose an electron enter in mode n from the wire 1 and escape in mode *m* to the wire 2. The quantum-mechanical expression for a transmission element of the *S* matrix is then given by (Baranger *et al.,* 1991; 1993a,b)

$$t_{mn} = i\hbar (v_m v_n)^{1/2} \int_{-d/2}^{d/2} dy'' \int_{-d/2}^{d/2} dy' \phi_m^*(y'') G(y'',y') \phi_n(y') \ , \qquad (4.14)$$

where y' and y'' are coordinates at the entrance and exit, respectively, on the boundary *C,* with corresponding x coordinates fixed as ~~x'=a'~~ and x''= a'. The symbols $\{\phi_n(y)\}$ and $G(y'', y')$ denote transverse components of the wavefunctions at junction points (see (4.8)) and the Green function through the cavity, respectively. Finally, $v_n(v')$ and $v_m(v'')$ are parallel (to wires) components of velocities for modes *n* and *m,* respectively.

The semiclassical ($\hbar \to 0$) approximation to (4.14) will be made as follows: We first replace $G(y'', y')$ by the semiclassical Green function:

$$G^{scl}(y'', y') = 2\pi (2\pi i\hbar)^{-3/2} \sum_{j(y',y'')} |\Im_j|^{1/2} \exp[iS_j/\hbar - i\mu_j] \ , \qquad (4.15)$$

where the summation is taken over all the classical orbits starting at y' and ending at y''. In (4.15), S_j $(=\int_{q'}^{q''} \mathbf{p}\bullet \, d\mathbf{q})$, $\Im_j (= \det(-\partial^2 S_j/\partial y'' \partial y')/|v'v''|)$, and $2\mu_j/\pi$ are reduced action, inverse of the Jacobian, and Morse-Maslov index, respectively. Using (4.15) in (4.14) and evaluating the double integrals in (4.14) by a saddle-point method, we reach the semiclassical result

$$t_{mn} = (i\lambda_F)^{1/2} (2d)^{-1} \sum_j \mathrm{sgn}(\bar{n})\mathrm{sgn}(\bar{m}) D_j \exp[2\pi i(l_j/\lambda_F + y_j'/\lambda_{\bar{n}} - y_j''/\lambda_{\bar{m}}) - i\nu_j], \qquad (4.16)$$

where $D_j = \left| (\partial \cos\alpha'' / \partial y')_{p_y} \right|^{-1/2}$ and $\lambda_{\bar{m}} = 2d/\bar{m}$, with $\bar{m} = \pm m$; l_j and λ_F are length of orbit *j* and Fermi wavelength, respectively. The summation in (4.16) is taken over all the isolated open orbits satisfying the saddle-point condition $(p_{y'} = h/\lambda_{\bar{n}}, p_{y''} = h/\lambda_{\bar{m}})$.

For the actual computation of (4.16), one should vary the value y' and have an assembly of orbits that satisfy $p_{y'} = h/\lambda_{\bar{n}}$ and $p_{y''} = h/\lambda_{\bar{m}}$ at the entrance and exit, respectively. The Poincare' map in (4.1) will be a convenient tool for obtaining these orbits. After finding orbits, we

should resort to the linearized Poincare' map connecting between variations at the initial and final points (see (4.3) and (4.4)), obtaining the derivatives as $(\partial\alpha''/\partial y')_{py}$. For instance, noting $\kappa_0=0$, $\alpha_0=\alpha$ at the entrance and $\kappa_n=0, \alpha_n=\alpha'$ at the exit, one finds $D_j=|M_{n}^{21}|^{-1/2}$. All these results will be used as input in (4.16). A further explanation of details will be omitted here.

4.5. Comparison in Stadium Billiard between Theory and Experiment

We shall now embark upon describing the numerical issue derived from quantum theory and interpreting Marcus *et al.* 's experimental results. Assume an injection of a single-mode (N=1) by choosing $k_F d/\pi$ =1.2. Taking $B_0=(hc/e)/A$ as a unit of the magnetic field, the scaled magnetic field B/B_0 will be varied between 1.72 and 27.62. In terms of Larmor radius $R(=\hbar k_F/(eB)=(2\varepsilon)^{1/2} l_c)$ this regime corresponds to 0.39<R/α<6.23, which obviously covers both fully-chaotic and transitional regions in case of *Sd* billiard (Meplan *et al.,* 1993).

Figure 4.5 shows typical wavefuction features in the case of the complete transmission. In the *Cl* billiard, $|\Psi|$ consists of structures with a partially-broken circular symmetry (see Fig. 4.5(a)). The circularly-symmetric pattern changes regularly as B is varied. In the *Sd* billiard, by contrast, $|\Psi|$ shows no symmetric patterns (Fig. 4.5(b)), indicating the aperiodic variation of patterns with change of B. As seen below, this variation yields a rich structure of $g(B)$.

Figure 4.6 displays the conductance $g(B)$. Both billiard types commonly exhibit very noisy fluctuations, reminiscent of the universal conductance fluctuations in dirty metals. These anomalous fluctuations, regardless of the integrability and nonintegrability, are a typical feature of weakly-opened systems where locations of highly concentrated poles for S matrix in the complex k plane are sensitive to the change of B field. On closer examination, however, we find a clear difference between two billiard types: In *Cl* billiard, the frequency of fluctuations of $g(B)$ remains unchanged throughout the B-field range in Fig.4.6(a). This result is consistent with the feature of the underlying classical dynamics where the phase space is occupied by tori whose structure is displaced regularly with a B field. In *Sd* billiard, on the other hand, $g(B)$ exhibits slow and extremely rapid oscillations in the low and higher field regions, respectively (see Fig.

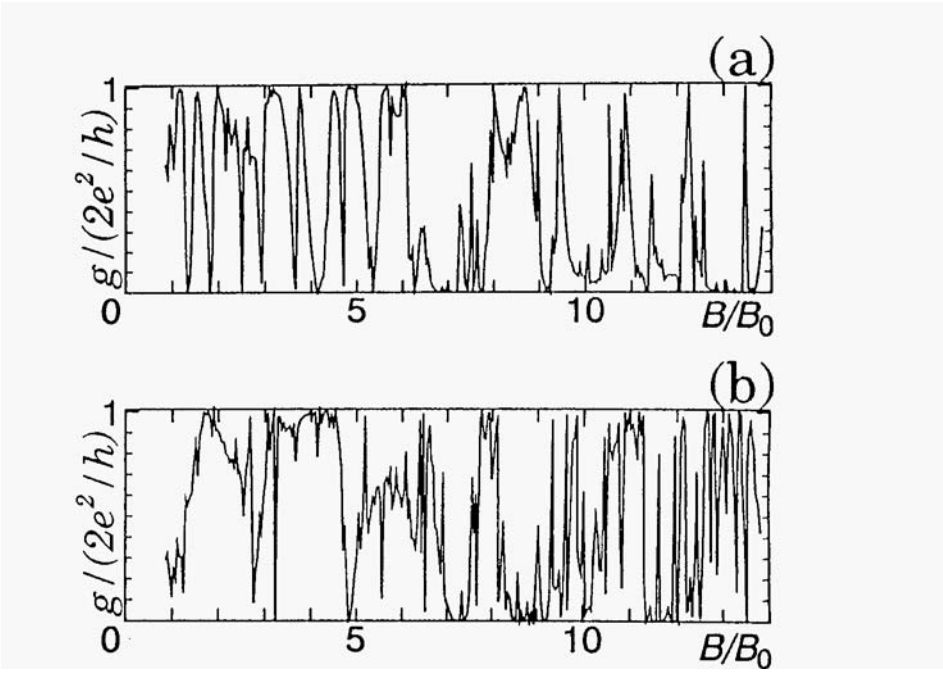

Fig. 4.6. Quantum conductance *g(B):* (a) circle, (b) stadium.

4.6(b)). This qualitative feature is in an excellent agreement with the experiments of Marcus *et al.* on a right-angled wire geometry. The threshold distinguishing two distinct oscillations lies around B/B_0=7.0. This result can be understood by noting the structural stability of the classical phase space. In fact, for $B< 7B_0$, $R >1.53a$ and orbits are fully chaotic. As a result, the phase space is globally occupied by the ergodic sea which feature is insensitive to the variation of *B,* consistent with the insensitivity of the quantum transport against *B.* On the other hand, for $B>7B0$, the ergodic part begins to be replaced successively by the KAM tori and thereby the phase space shows an extreme sensitivity to the variation of *B,* which explains a rapid variation of *g(B).*

To characterize the fluctuation of *g(B),* the autocorrelation functions $\Gamma(\Delta B) = \langle \delta g(B)\delta g(B+\Delta B)\rangle_B / \langle (\delta g(B))^2\rangle_B$ have been computed for both the low and high reference fields (see Fig. 4.7); $\langle \bullet\bullet\bullet \rangle_B$ means the average over referenced *B* fields. Both *Cl* and *Sd* billiards are commonly accompanied by the cusp-like central peaks proper to

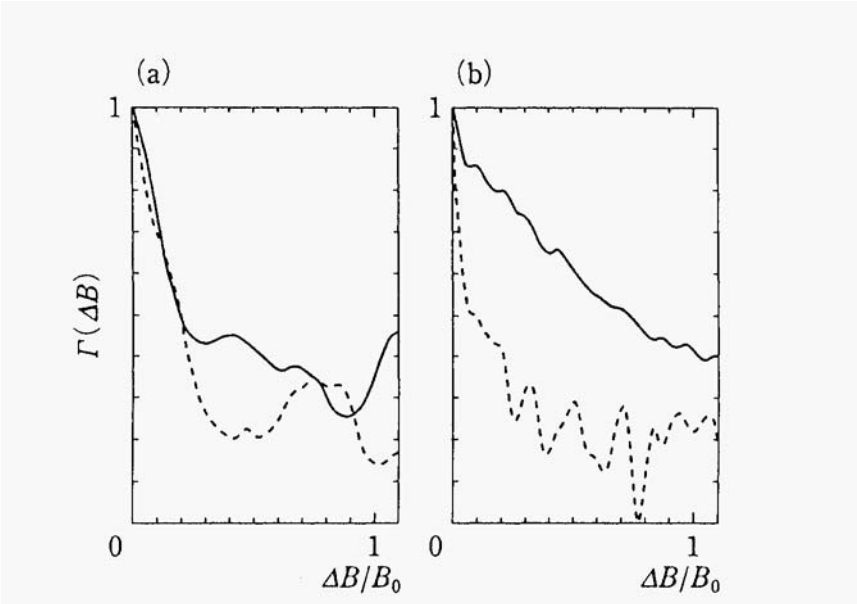

Fig. 4.7. Autocorrelation functions $\Gamma(\Delta B)$. Reference ranges are $0<B/B_0<7$ (solid line) and $7<B/B_0$ (broken line): (a) circle, (b) stadium.

generic systems (see Chap. 2 and Lai et al.(1992)). While for *Cl* billiard (see Fig. 4.7(a)) the gradients of the cusps are the same in both the low and higher field regions, for *Sd* billiard (see Fig. 4.7(b)) the obvious difference exists between the gradients in low and higher reference fields: A long-range correlation and a rapid decrease of the correlation are obvious in the low-field and higher-field regions, respectively.

In order to see the quantum-classical correspondence, we calculate the classical conductance $g_{cl}(B)$: In accordance with the transverse component of the incident propagating mode in (4.7) and (4.8), an electron is supposed to lie at the hole 1 with the occupation probability $|\phi_1(y)|^2$. We then compute the rate of its escaping to the wire 2 after significant classical bouncings off the wall, and finally obtain $g_{cl}(B)$ in Fig. 4.8. For comparison, we also construct a smoothed version $g_{qt}(B)$ by coarse-graining of $g(B)$. (Smoothing is done here by averaging $g(B)$ over each interval of $\Delta B/B_0=0.7$, with successive intervals chosen by shifting the preceding one by $\Delta B/B_0=0.1$.) The quantity $g_{qt}(B)$ more

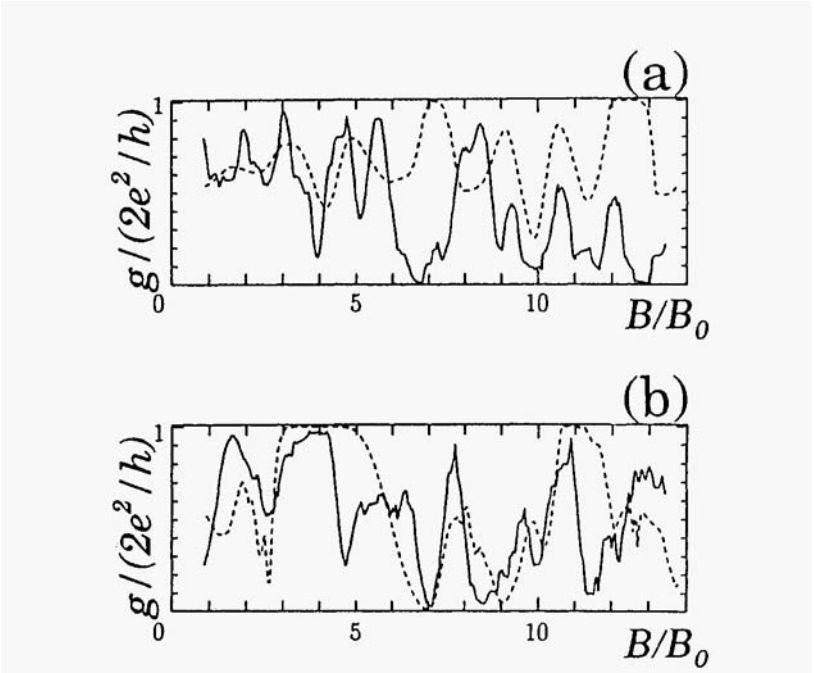

Fig. 4.8. Coarse-grained quantum conductance g_{qt} (solid line) and classical conductance g_{cl} (broken line): (a) circle, (b) stadium.

evidently shows periodic (Fig. 4.8(a)) and a periodic (Fig. 4.8(b)) alignment of peaks in *Cl* and *Sd* billiards, respectively, while $g_{cl}(B)$ proves to reproduce a gross feature of $g_{q_t}(B)$. In particular the location of peaks in g_{q_t} are mostly identical with those of $g_{cl}(B)$ in both of *Cl* and *Sd* billiards except for the peaks around B/B_0=5.5 and 8.5 in Fig. 4.8(a). Thus the bouncing Larmor-orbit picture recovers a gross feature of the quantum conductance.

Let us consider a stadium with semicircle radius a=0.1μm. Then A=7.14x 10-2 μm2 and B_0=0.058T, and the transition point corresponds to $7B_0$~0.3T, in nice agreement with Marcus *et al.'* s assertion. In a real experiment, on the other hand, a=0.5μm and therefore B_0 =0.0023T. The transition point is now $B^{qt}{}_{th}$ ~7B$_0$ ~0.016T, less than the experimental value $B^{exp}{}_{th}$~0.3T by more than an order of magnitude. It is not easy, however, to clearly specify the transition point by glancing over the spectrum in Fig. 4.1. In fact, one might assign a transition point less than 0.3T. Although a quantitative

agreement between theory and experiment has not yet been attainable, behaviors in Figs. 4.6-4.8 are in accord with those in Fig. 4.1, at least qualitatively, and it is true that Marcus *et al* 's experiment should have captured a quantum signature of chaos.

The magneto-conductance *g(B)* in open *Cl* and *Sd* billiards has proved to be related to the behaviors of classical dynamics. It shows fluctuations dependent largely on the stability of phase space in the underlying classical dynamics of closed billiards. While in the *Cl* billiard the regular modulation of periodic orbits in the phase-space structure gives rise to regular oscillations of *g(B),* the global chaos and genesis of successive tori with increase of *B* in the *Sd* billiard are responsible for slow and rapid variations of quantum conductance, respectively. The gradient of the cusp-like central peak in the autocorrelation function characterizes rich fluctuation properties of *g(B).* The present result is qualitatively consistent with Marcus *et al* .'s experiment on a different wire geometry. Further, using the bouncing Larmor-orbit picture, we have derived the classical conductance, which turns out to reproduce most of the locations of peaks in the coarse-grained version of *g(B).*

Real nanoscale structures are accompanied by extrinsic randomness, e.g., corrugation of walls, impurities and thermal noises. The rapid progress of advanced technology will smear out these obstacles that prevent us from a simple comparison between theory and experiment. The quantum theory of chaos is thus entering an era which will see its experimental test in stages for quantum transport in mesoscopic devices fabricated by the present-day high technology. Currently, theoretical interests focus on: (1) showing a universality of conductance fluctuations on the basis of random matrix theory; (2) deriving the *S* matrices directly by extending the Gutzwiller's semiclassical trace formula to open systems.

Nevertheless, the observed magneto-conductance would demand much deeper insight: The discrepancy of the transition point by more than order of magnitude between theory and experiment is serious, and one should meet the challenge to solve this puzzle which can be explained by neither the semiclassical nor quantum theory.

Before closing this section, we should mention the latest progress in measurements of mesoscopic conductance fluctuations in quantum dots. Chang *et al.* (1995) provided the experimental test on the statistical distribution of peak heights in the conductance inside the Coulomb blockade regime. This regime, where lifetime broadening is

less than the mean level spacing and the electrostatic energy e^2/C of the dot with capacitance C is larger than the applied bias, differs from the one treated hitherto, where many electronic levels contribute to the tunneling process. On the contrary, they observed the transport mediated by quantum tunneling through a single eigenstate of the dot. Since the Coulomb interaction in these region is comparable to the level spacing, the essential statistical quantity is the peak heights G_{max} rather than the level spacings, while the peak positions are absolutely stable and reproducible. Chang *et al.* observed Coulomb blockade peak heights as a function of magnetic field and gate voltage by tuning the temperature and coupling to leads. Then they proceeded to examining the statistical properties of the peak heights. The non-Gaussian distribution they elucidated is amazing (see Fig. 4.9); it has not been seen in the case of level spacing distribution. To be explicit, let us introduce the scaled height α by

$$G_{max}=(e^2\pi/(2hkT))\Gamma_L\Gamma_R/(\Gamma_L+\Gamma_R)=(e^2\pi/(2hkT))\,\overline{\Gamma}\,\alpha\ , \tag{4.17}$$

where $\Gamma_L(\Gamma_R)$ is the partial decay width into the left (right) lead. For B=0, the distribution $P_{B=0}$ (a) has proved to obey

$$P_{B=0}(\alpha) = (2/\pi\alpha)^{1/2}\mathrm{e}^{-2\alpha}\ , \tag{4.18}$$

exhibiting the square-root singularity near zero. In a magnetic field greater than the correlation field, the breaking of time-reversal symmetry reduces the number of near-zero values of G_{max}. Nevertheless, the distribution is still non-Gaussian and peaked near zero:

$$P_{B\neq 0}(\alpha) =4\alpha\,[K_0(2\alpha) + K_1(2\alpha)]\mathrm{e}^{-2\alpha}\ , \tag{4.19}$$

where K_n are the modified Bessel functions. This contrasts with the Gaussian distribution of peak heights for typical metallic dots, where many levels are involved in the tunneling.

Folk *et al.* (1995), besides confirming the above issue, showed that the autocorrelation function of peak height fluctuations agrees with the Lorentzian-squared form for the unitary ensemble.

These results address several interesting issues to be explored further by theoreticians. However, a question should be raised: The word *"quantum chaos"* should be used in cases where the underlying

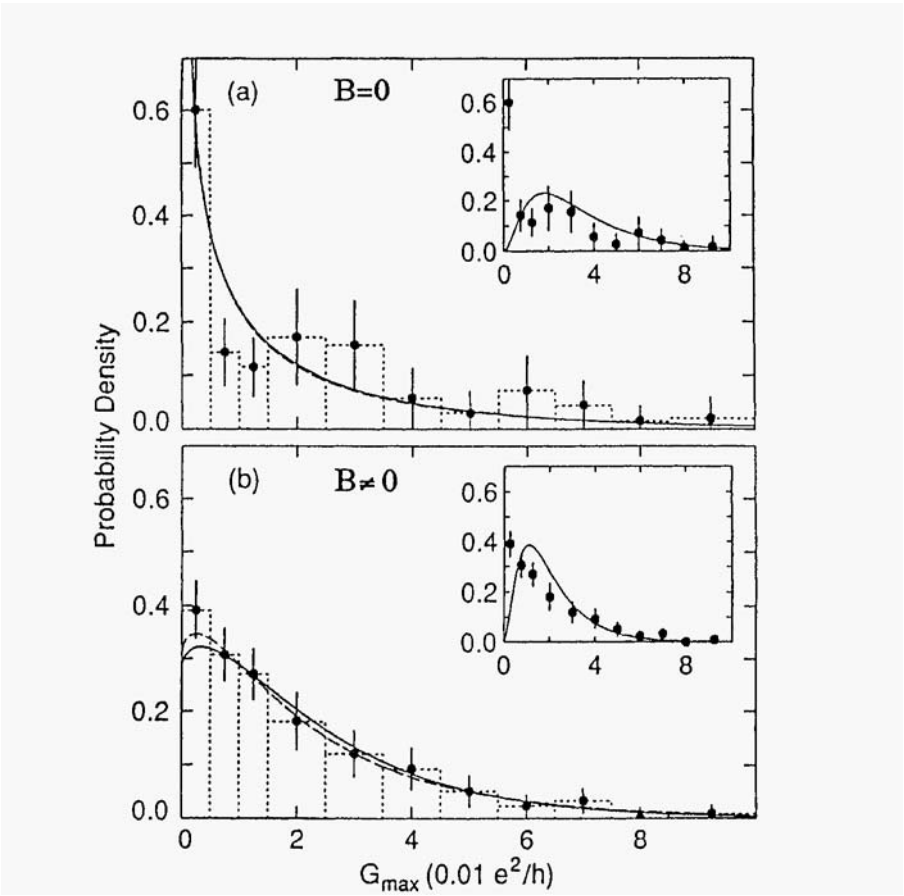

Fig. 4.9. Histograms of conductance peak heights for (a) B=0 and (b) $B \neq 0$. Note the non-Gaussian shape of both distributions and the strong spike near zero in Fig. 4.9(a). Fits to the data using both the fixed pincher theory (solid) and the theory averaged over pincher variation (dashed) are excellent. The insets show fits to a more Gaussian distribution $\chi_6^2(\alpha)$ averaged over the pincher variation; the fit is extremely poor. (Courtesy of A. M. Chang *et al.)*

classical dynamics exhibits chaos characterized by a positive Lyapunov exponent and a non-zero Kolmogorov-Sinai entropy. In the present Coulomb blockade case where Coulomb interaction gives rise to the many-body effect, what is the origin of chaos? One reasonable answer would be that both the many-body effect and the boundary effect of the small dot will be responsible for the genesis of chaos.

4.6. Open Sinai Billiard in Magnetic Field: Distribution of Lyapunov Exponents and Ghost Orbits

As stated in the introduction of the present chapter, recent advances in microfabrication technology have allowed physicists to study the conducting properties of ultra-small electrical circuits with length scale much shorter than both elastic and inelastic mean free paths but larger than the Fermi wave length (Beenakker and van Houten, 1991). These ballistic electron devices have attracted much interest as a probe of *"quantum chaos," i.e.,* the quantum signature of classical chaotic scattering. The transport properties of ballistic conductors are strongly influenced by geometrical features of the system. In these devices aperiodic fluctuations of conductance as a function of magnetic field B have been observed (Marcus *et al.,* 1992, 1993a,b; Bird *et al.,* 1994, 1995), which are reminiscent of UCF (universal conductance fluctuation) in diffusive regimes. The fluctuation is caused by the frequent resonant scattering proper to weakly opened devices.

In the remaining part of this chapter, we shall present quantum and classical analyses of transport in the open square and single Sinai billiards (Fig. 4.10) in a perpendicular magnetic field B (Kawabata and Nakamura, 1997). (The phase space of a classical particle moving

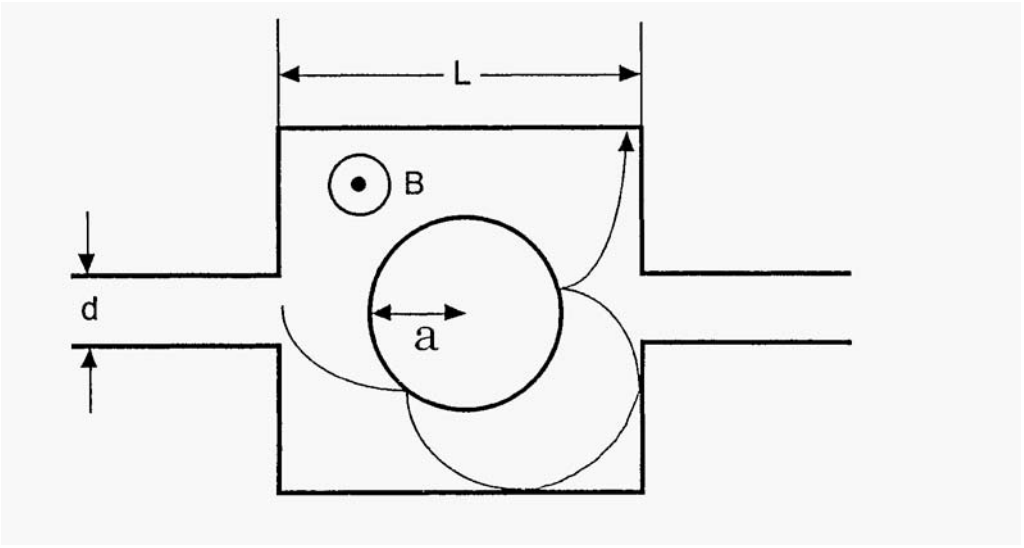

Fig. 4.10. Open Sinai billiard in magnetic field and bouncing orbit.

in the closed Sinai billiard is always ergodic and chaotic for B =0 (Sinai, 1979) but becomes mixed for $B \neq 0$.) We concentrate on a single mode injection and explore the quantum-classical correspondence. This open system is characterized by the parameters L, a, and d for dimension of square wall, radius of circle wall, and width of a pair of conducting quantum wires attached to the square walls, respectively. The Aspect ratio σ is defined by $\sigma = a/L$, and the degree of opening ξ is given by $\xi = d/(L^2 - \pi a^2)^{1/2}$. For comparative study, we shall choose σ= 0 (for square billiard) and σ=11/36 (for Sinai billiard) with ξ~0.1 for each. This degree of opening corresponds to a weakly-opened situation suitable to uncover the ample fluctuation properties of quantum transport.

First, in order to examine the features of classical billiards, we calculate the dwelling time distribution. Figure 4.11 shows a spectrum of the time τ (or path length l ($\propto \tau$)) during which an electron with a given injection angle θ_0 incident from the left lead wire, dwells inside the billiard until exit. We take ϕ_0/L^2 as a unit of the magnetic field, where ϕ_0 *(=hc /e)* is the magnetic flux quantum. For the square billiard, the spectrum exhibits a simple structure which consists of a few plateaus in a weak B field region (Fig. 4.11(a)). As B is increased, however, the spectrum exhibits, besides plateaus, fine comb-like structures responsible for chaotic motion (Fig. 4.11(b)). The plateaus here are concerned with a family of the short dwelling time orbits bouncing off the wall only a few times until exit. These orbits, which provide anomalous Lyapunov exponents (see below), are characteristic of open systems and hereafter will be called as *"ghost orbits."* In the high field region, electron orbits are restricted to the vicinity of the wall. Therefore their classical phase space is occupied by K.A.M. tori, so that no fine structure can be perceived in the spectrum (Fig. 4.11(c)). On the other hand, in the case of Sinai billiard, the spectrum shows fine comb-like structures already in a weak field region (Fig. 4.11(a')), in contrast to the case of square billiard. As B is increased, plateau structures intervene fine comb-like structures (Fig. 4. 11(b')), which is similar to Fig. 4.11(b). A further increase of B smears out any fine structure in the spectrum (Fig. 4.11 (c')).

Next, in order to quantify the degree of non-integrability, we calculate the B dependence of Lyapunov exponents for an assembly of scattering (not periodic) orbits. The Lyapunov exponent of any classical trajectory is calculated from the tangent map which corresponds to the linearized Poincare' map. The tangent map for a charged particle

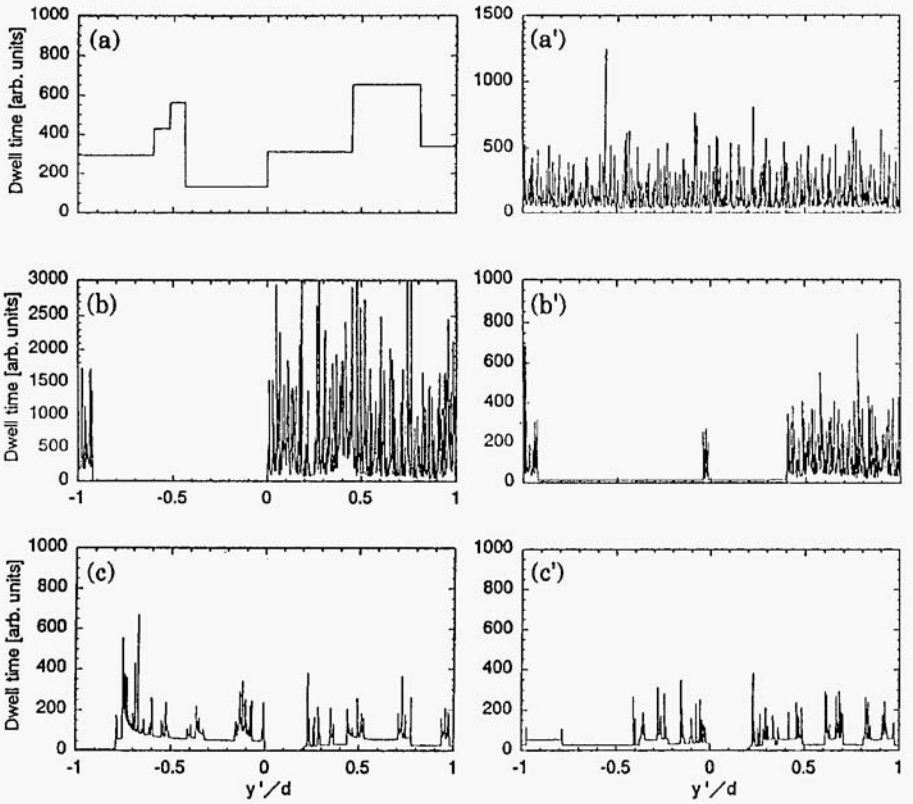

Fig. 4.11. Dwelling time spectrum for open billiards. Abcissa denotes initial location (vertical coordinate $|y|<d/2$) of electron. Data on positive ($0 < y'(=y+d/2) < d$) and negative ($-d<y'(=y-d/2) < 0$) regions correspond to θ_0 =0.337rad and −0.337rad, respectively. Left panel for open square billiard: (a), (b), and (c) are for BL^2/ϕ =0.1646, 81.38, and 325.7, respectively; right panel for open Sinai billiard: (a')- (c') are the same as (a)-(c).

inside the present Sinai billiard in a perpendicular magnetic field is already given in (4.3) with Larmor radius $R=mv_f/eB$. While (4.3) was originally invented for billiards with continuous boundary, it holds as well for the present Sinai billiard by taking the radius of curvature at each bouncing point as $\rho_i = \infty$ at a square wall and $\rho|_i = a$ at a circle wall. For a trajectory that takes n steps before exit, the monodoromy matrix is given by $\mathbf{M}_n$ in (4.4). The Lyapunov exponent is given by $\lambda_n=(1/l)\ln\Lambda_n$ (see (4.5)), where l, the length of an orbit, is

identified with the dwelling time for unit velocity.

In order to calculate the average Lyapunov exponent $\langle\lambda\rangle$, we inject 2000 particles which start in equal spacing at the left lead wire. Here the average and variance (see below) of Lyapunov exponents are calculated directly without resorting to Ruelle-Bowen's pressure function (Bowen, 1975; Ruelle, 1978). Figure 4.12 shows the B dependence of $\langle\lambda\rangle$. In the case of square billiard without the circular obstacle (Fig. 4.12(a)), as B is increased, $\langle\lambda\rangle$ is vanishing for $B < B_{th}$ (-1.3) and suddenly increases at $B=B_{th}$. The global feature is accompanied by a dip at B~4.536 and by a hump at B~54.43. This complicated structure is attributable to the existence of ghost orbits

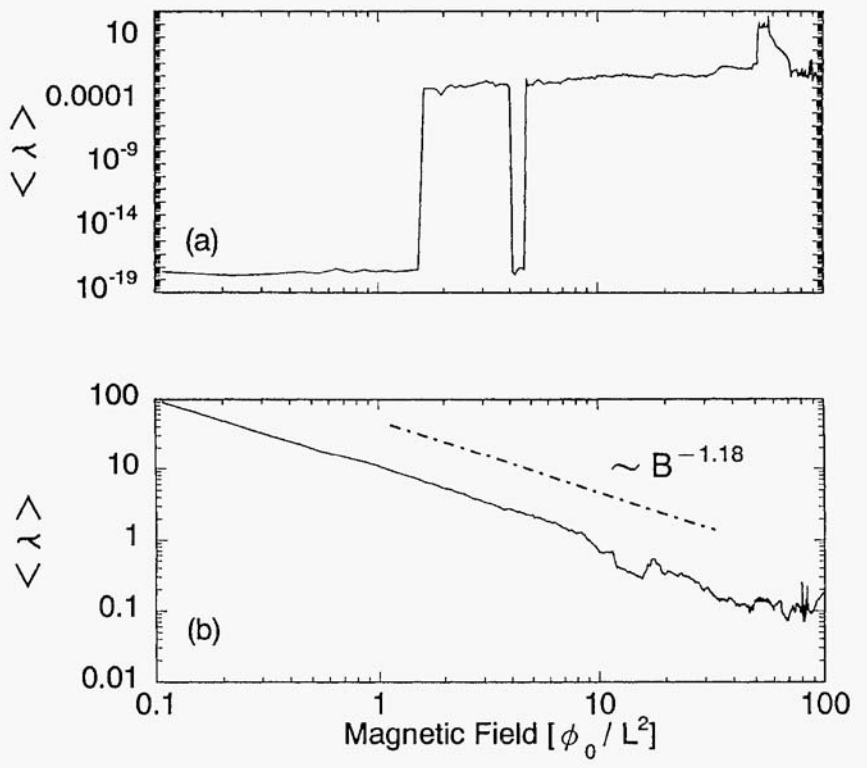

Fig. 4.12. Average Lyapunov exponent as a function of magnetic field: (a) open square billiard (σ=0), (b) open Sinai billiard (σ=11 /36). The dashed-dotted line represents a power-law fitting for the numerical curve (solid line).

which stay for a short time in the billiard and therefore have ill-converged small and large Lyapunov exponents for a dip and a hump, respectively. By contrast, in the case of Sinai billiard (Fig. 4.12(b)), $\langle\lambda\rangle$ decreases monotonically with increasing B, describing a continuous transition from chaos to tori. We obtain a power law B^{-n} with n=1.18 from the power-law fitting to the numerical curve. The average $\langle\lambda\rangle$ is much larger here than for the square billiard. Ghost orbits have proved to play a minor role in the stadium billiard.

The above fact indicates that in the Sinai billiard case the classical phase space is globally stable against B, while in the square billiard it is globally unstable.

4.7. Comparison in Sinai Billiard between Quantal and Classical Theories

To see the quantum-classical correspondence, we consider a two-dimensional tight binding model of width L, connected to perfect lead wires across point contacts. We assume hard-wall confinement in the transverse direction of the wire. A single antidot potential with diameter a is placed at the middle of the square billiard (quantum dot). The Hamiltonian of the model is given by (Kawabata and Nakamura, 1997)

$$\mathcal{H}=\sum_{n}\sum_{m=1}^{M}(-te^{2\pi i\overline{H}m}c^{+}_{n+1,m}c_{n,m}+h.c.)+\sum_{n}\sum_{m=1}^{M-1}(-tc^{+}_{n+1,m}c_{n,m}+h.c.)$$
$$+\sum_{n}\sum_{m=1}^{M}\varepsilon_{n,m}c^{+}_{n,m}c_{n,m}\quad, \tag{4.20}$$

where $c_{n,m}$ and $c_{n,m}^{+}$ are creation and the annihilation operators for an electron at the lattice site (n,m) and t is the transfer integral. A magnetic field B is included in a Peierls phase factor of the transfer integral as $\overline{H}=Ba_0^2/\phi_0$, where a_0 is the lattice constant. We calculate the transmission coefficient by use of the recursive Green function method (Fisher and Lee, 1981; Lee and Fisher, 1981). The conductance $G(B)$ is calculated by the Landauer formula (Landauer, 1957; Buttiker *et al.,* 1985). (Note: A capital letter G will be used hereafter so as to be distinct from the designation for the stadium billiard in the first half of this chapter.) The length of the dot is chosen as L=36a_0. We concentrate on a single mode injection and choose $k_F \cong 1.2/a_0$ in order

to identify the incident angle from the lead with the one used in the classical analysis. Figure 4.13 shows the B dependence of $G(B)$. Both billiard types commonly exhibit aperiodic fluctuations, reminiscent of the universal conductance fluctuation in dirty metals. These anomalous fluctuations are typical features of weakly opened systems regardless of their integrability and nonintegrability. In the case of Sinai billiard (Fig. 4.13(b)), the geometry forms an Aharonov-Bohm ring, so that A-B oscillation is observed in a weak field region. This feature is more pronounced in the Sinai billiard with σ=14/36 (see Fig. 4.13(b')). The regular A-B oscillation has a tendency to smear out the quantum analogue of the transition between chaos and tori. In order to see the global variation of conductance, we, therefore, shall calculate the coarse-grained conductance. Coarse-graining is achievedby by averaging $G(B)$ over the interval $(\Delta B)L^2/\phi_0$=3.24 around each value B. Generally speaking, coarse-grained conductance corresponds to low frequency components of $G(B)$. Let us denote low frequency components of $G(B)$ as $G_{cb}(B)$ and high frequency components of $G(B)$ as $G(B)$-G_{cg} (B). In the square billiard (σ=O), $G_{cg}(B)$ shows a large-amplitude oscillation in a regime B<25 [ϕ_0/L^2]. On the other hand, in the Sinai Billiard (σ=11/36), G_{cg} (B) keeps a mild modulation as B increases in the same B region. This difference is relates to the feature of the underlying classical dynamics, that will be described below.

To characterize the fluctuations, we have calculated the auto-correlation function

$$C(\Delta B)=\langle \delta G(B)\, \delta G(B+\Delta B)\rangle_B \tag{4.21}$$

with $\delta G(B) = G(B)-\langle G(B)\rangle_B$. The angular bracket indicates an average over a suitably large field range. The correlation field B_c is then defined as the half-width of the correlation function $C(B_c)$=C(0)/2. There exist two kind of B_c s. Firstly, B_c of G_{cg} (B) is concerned with the strength of long-range correlation of $G(B)$. On the other hand, the global stability of the classical phase space against B is represented by the average Lyapunov exponent $\langle\lambda\rangle$, by taking the initial variation of each orbit as induced by a small change of B. Therefore, B_c of $G_{cg}(B)$ is expected to be comparable to $\langle\lambda\rangle$. Figure 4.14(a) shows the B dependence of B_c. In the case of a square billiard, as B is increased, B_c varies irregulary. By contrast, in the case of a Sinai Billiard, B_c decreases monotonicaly with increasing B and therefore captures a

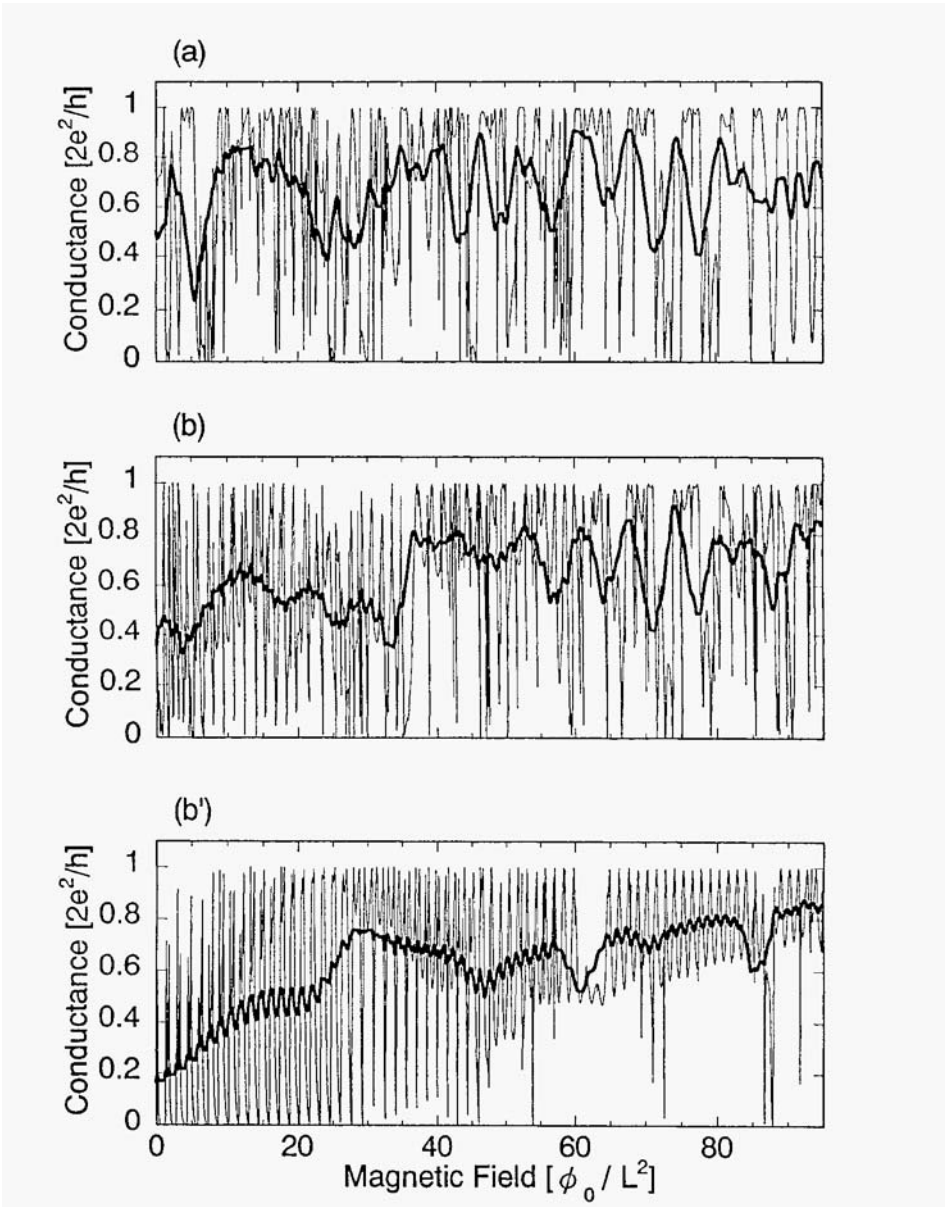

Fig. 4.13. Magneto-conductance as a function of magnetic field. Thick solid line represents coarse-grained conductance: (a) square billiard (σ=0), (b) Sinai billiard (σ=11/36), (b') Sinai billiard (σ=14/36).

continuous transition from chaos to tori. In Fig. 4.14 we show comparison between B_c and $<\lambda>$ both as a function of B. The B dependence of B_c is in good agreement with that of $\langle\lambda\rangle$ in both billiard cases. However, there is a quantitative discrepancy between classical and quantal peak positions in the case of a square billiard. This discrepancy is caused by quantum-mechanical effects, *e.g.,* finiteness of the Fermi wave number or diffraction at holes of billiards.

Secondly, B_c for $G(B)$-G_{cg} (B), corresponding to the high frequency component of conductance fluctuation, is much smaller than the period of A-B oscillation (~1.7[$\hbar$ /L^2]) and related to the strength of

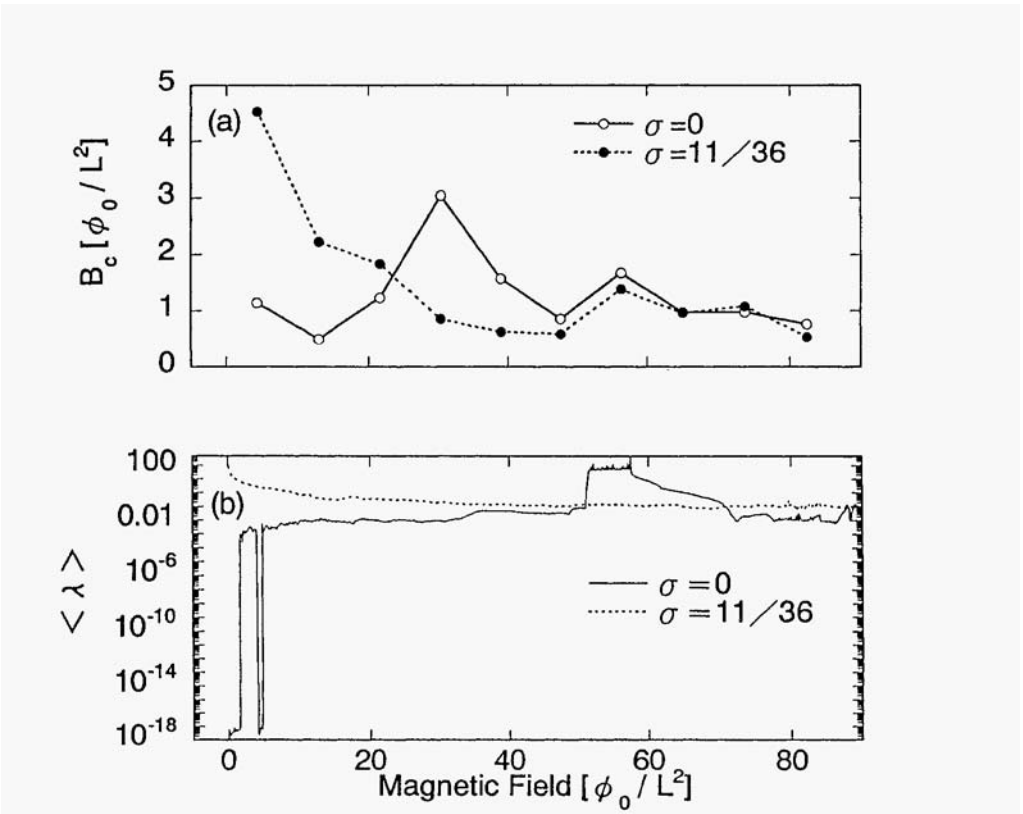

Fig. 4.14. (a) Correlation field of G_{cg} (B) as a function of the magnetic field. Solid line with open circles for square billiard (σ=0) and dotted line with filled circles for Sinai billiard (σ=1 1 /36). (b) Average Lyapunov exponent as a function of magnetic field. Solid line for square billiard (σ=0) and dotted line for Sinai billiard (σ= 11/36).

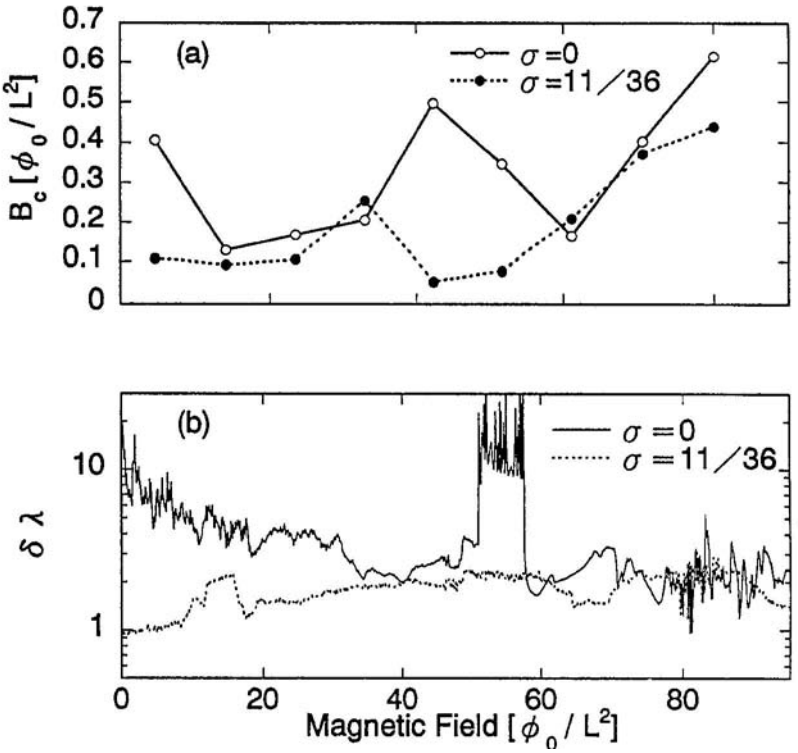

Fig. 4.15. Same as in Fig. 4.14 but for correlation field of $G(B) - G_{cg}(B)$ (Fig.4.15(a)) and for scaled standard deviation of Lyapunov exponents (Fig.4.15(b)).

short-range correlation of $G(B)$. Meanwhile, the local stability of the classical phase space against B is represented by the scaled standard deviation of Lyapunov exponents

$$\delta\lambda \equiv (\mathrm{var}(\lambda))^{1/2} / \langle\lambda\rangle . \tag{4.22}$$

Therefore, B_c of $G(B) - G_{cg}(B)$ is expected to be comparable with $\delta\lambda$. Figure 4.15 shows the comparison between B_c and $\delta\lambda$. In Fig. 4.15(b) we show the B dependence of $\delta\lambda$. On comparison of square and Sinai billiards, $\delta\lambda$ of the square billiard turns out to be larger than that of the Sinai billiard. Moreover, noisy fluctuations and a hump structure

can can be perceived only in the square billiard case. The origin of noisy fluctuations lies in the extreme sensitivity of local phase structures with respect to B, while a hump can be explained as an influence of the ghost orbits. In the case of a Sinai billiard, conversely, we can recognize that the local structure of phase space is stable again against B and that both B_c and $\delta\lambda$ do not show significant variations with respect to B. One may conclude that, as a whole, the behavior of B_c nicely mimics that of $\delta\lambda$. Quantitative discrepancy of the position of a hump can also be interpreted in terms of quantum mechanical effects.

The latest and most interesting discovery concerning the single Sinai billiard is that of the semiclassical formula for the Al'tshuler-Aronov-Spivak effect in the magneto-conductance for the Sinai billiard with Aharonov-Bohm flux threaded only through the hollow. For details, see Kawabata and Nakamura (1996).

4.8. Summary

The conductance $g(B)$ in weakly-opened *Cl* and *Sd* billiards has been shown to reflect the phase-space structure of classical dynamics. Fluctuations of $g(B)$ depend largely on the stability and instability of phase space in the underlying classical dynamics of closed billiards. The global chaos and genesis of successive tori in the Sd billiard with increasing B are related to slow and rapid variations of quantum conductance, respectively. The autocorrelation function characterizes rich fluctuation of $g(B)$. Although the classical and quantal results are qualitatively consistent with Marcus *et al* .'s experiment on a different wire geometry, the observed magneto-conductance would demand a much deeper insight: The discrepancy between $B^{qt}{}_{th}$ ($\sim B^{cl}{}_{th}$) and $B^{exp}{}_{th}$ in spectral properties is very serious, and some challenge is required to solve this puzzle.

In this chapter, the comparative studies on the Lyapunov exponents and magneto-conductance $G(B)$ in open square and Sinai billiards have also been developed. They show that conductance fluctuations depend largely on the stability of a *mixed phase space* in underlying classical dynamics. In the Sinai billiard case the classical phase space is globally stable against B, while for the square billiard it is globally unstable. The smoothed (coarse-grained) conductance $Ge_g(B)$ reveals a continuous transition between chaos and tori. In the

case of a square billiard, the correlation field B_c of the smoothed conductance is shown to vary irregularly with respect to B, while in the case of a Sinai billiard it decreases monotonically with increasing B. To be precise, two kinds of correlation fields B_c s are relevant: B_c of $G_{cg}(B)$ (low frequency component) and that of $G(B)$ - $G_{cg}(B)$ (high frequency component) have turned out to mimic the average Lyapunov exponent $<\lambda>$ and scaled standard deviation of Lyapunov exponent $\delta\lambda$, respectively. The fluctuation of B_c in the case of a square billiard is attributed to the *ghost orbits* proper to a scattering (not periodic) orbit. In the Sinai billiard case, the geometry of the billiard forms an Aharonov-Bohm ring so that an A-B oscillation is observed in a weak field region. While the A-B effect suppresses a symptom of chaos, both B_c s for $G_{cg}(B)$ and $G(B)$ - $G_{cg}(B)$ nicely capture the quantum-classical correspondence. These results are anticipated to be observed experimentary in nanoscale quantum dots. Research in many other directions, both theoretical and experimental, is also in progress. Readers are encouraged to refer to a collection of reviews by many active scholars in this field (Nakamura, 1997).

References

Akkermans, E., Montambaux, G., Pichard, J.-L., and Zinn-Justin, J., eds. (1995). *Mesoscopic Quantum Physics, Proceedings of Les Houches Summer School.* Amsterdam: North Holland.

Baranger, H. U., DiVincenzo, D. P., Jalabert, R. A., and Stone, A. D. (1991). Phys. Rev. **B44,** 10637.

Balanger, H. U., Jalabert, R. A., and Stone, A. D. (1993a). *Chaos* **3,** 665.

Balanger, H. U., Jalabert, R. A., and Stone, A. D. (1993b). *Phys.Rev.Lett.* **70,** 3876.

Beenakker, C. W., and van Houten, H. (1991). In *Solid State Physics: Advances in Research and Applications,* H. Ehrenreich and D. Turnbull, eds. New York: Academic.

Benettin, G., andStrelcyn, J. M. (1978). *Phys. Rev.* **17A,** 773.

Bird, J. P., Ishibashi, K., Aoyagi, Y., Sugano, T., and Ochiai, Y. (1994). *Phys.Rev.* **B50,** R18678.

Bird, J. P., Ishibashi, K., Ferry, D.K., Aoyagi, Y., and Sugano, T. (1995). *Phys. Rev.* **B51,** R18037.

Birkhoff, G. D. (1927). *Acta Math.* **50,** 359.
Bowen, R. (1975). *Equilibrium States and the Ergodic Theory of Anosov Differeomorphisms.* Berlin: Springer.
Bunimovich, L. A. (1974). *Func. Anal. Appl.* **8,** 254.
Buttiker, M., Imry, Y., Landauer, R., and Pinhas, S. (1985). *Phys. Rev.* **B31,** 6207.
Chang, A. M., Baranger, H. U., Pfeiffer, L. N., and West, K.W. (1994). *Phys. Rev. Lett.* **73,** 8857.
Chang, A. M., Baranger, H. U., Pfeiffer, L. N., and West, K. W., and Chang, T. Y. (1996). *Phys. Rev. Lett.* **76,** 1695.
Doron, E,, Smilansky, U., and Frenkel, A. (1991). *Physica* **D50,** 367.
Feynman, R. P., and Hibbs, A. R. (1965). *Quantum Mechanics and Path Integrals.* New York McGraw-Hill.
Fisher, D. S., and Lee, P. A. (1981). *Phys. Rev.* **B23,** 6851.
Folk, J. A,, et al. (1996). *Phys. Rev. Lett.* **76,** 1699.
Gutzwiller, M. C. (1990). *Chaos in Classical and Quantum Mechanics.* Berlin: Springer.
Heller, E. J. (1984). *Phys. Rev. Lett.* **53,** 1515.
Jalabert, R. A., Baranger, H. U., and Stone, A. D. (1990). *Phys. Rev. Lett.* **65,** 2442.
Kawabata, S., and Nakamura, K. (1996). *J. Phys. Soc. Jpn.* **65,** 3708.
Kawabata, S., and Nakamura, K. (1997). *J. Phys. Soc. Jpn.* **66** (3).
Lai, Y. C., Blumel, R., Ott, E., and Grebogi, C. (1992). *Phys. Rev. Lett.* **68,** 3491.
Landauer, R. L. (1957). IBM *J. Res. and Deu.* **1,** 223.
Lee. P. A,, and Fisher, D. S. (1981). *Phys. Rev. Lett.* **47,** 882.
Lin, W. A., and Jensen, R. V. (1996). *Phys. Rev.* **B53,** 3638.
Marcus, C. M., Rimberg, A. J., Westervelt, R. M., Hopkins, P. F., and Gossard, A. C. (1992). *Phys. Rev. Lett.* **69,** 506.
Marcus, C. M., Westervelt, R. M., Hopkins, P. F., and Gossard, A. C. (1993a). *Phys. Rev.* **B48,** 2460.
Marcus, C. M., Westervelt, R. M., Hopkins, P. F., and Gossard, A. C. (1993b). *Chaos* **3,** 643.
McDonald, S. W., and Kaufman, A.N. (1979). *Phys. Rev. Lett.* **42,**1189.
Meplan, O., Brut, F., and Gignoux, C. (1993). *J. Phys.* **A26,** 237.
Nakamura, K. (1993). *Quantum Chaos: A New Paradigm of Nonlinear Dynamics.* Cambridge: Cambridge University Press.
Nakamura, K., ed. (1997). *Chaos and Quantum Transport in Mesoscopic Cosmos, Special issue of Chaos, Solitons and Fractals* **7.** In press.

Nakamura, K., and Ishio, H. (1992). *J. Phys. Soc. Jpn.* **61,** 3939.
Nakamura, K., Ito, K., and Takane, Y. (1994). *J. Phys.* **A27,** 5889.
Ruelle, D. (1978). *Themodynamic Formalism.* Reading, Massachusetts: Addison- Wesley.
Sinai, Y. G. (1979). *Russ. Math. Surv.* **25,** 137.
Ueta, T. (1992). *J. Phys. Soc. Jpn.* **61,** 4314.

Chapter 5

Chaotic Scattering on Hyperbolic Billiards: Success of Semiclassical Theory

In this chapter we present semiclassical and exact quantum theories of a point particle bouncing off C_{4v} four-disk billiards which exhibits chaotic scattering in classical dynamics. It is demonstrated how the semiclassical theory is superior to conventional quantum theory. The zeta function in the semiclassical trace formula is calculated by using cycle expansions with respect to periodic orbits up to period three in the number of bounces. Its complex poles provide resonances which are in excellent agreement with the exact quantum resonances in a wide range of wave numbers k. An assembly of resonances lying parallel and close to the real k axis indicates that the distribution of the imaginary part of the resonances presents a threshold and consists of a sequence of small bands below the threshold. Consequences of these resonances on the dynamical behavior of mesoscopic devices are discussed. A survey on the monumental experiment by Weiss *et al.* (1991, 1993) on the Sinai billiard in the presence of magnetic field is also given.

5.1. Introduction

N. Krylov, a Russian sientist, was the first to study the chaotic scatterring of a point particle on the surfaces (with negative curvature) of convex billiards (Krylov, 1979). The motivation for his reasearch was to give

a proof of the ergodicity and mixing which constitute a foundation of statistical mechanics. While he died young at age 29, in 1947 and three quarters of a century have since passed, the chaotic scattering by hyperbolic (defocusing) billiards is nowadays widely studied in physics and advanced high technology as well as in mathematics. As examples of convex billiards, one may discuss Sinai's billiard, i.e., a triangular array of identical hard disks (Fig. 5.1(a)) and a crossroad where four hard disks are placed with C_{4v} symmetry with four wires inserted between disks (Fig. 5.1(b)). Both examples can be fabricated at interface layers of nano-scale semiconductor hetero-junctions, once the hard disks are regarded as regions void of electrons. In fact, regular arrays of hard disks are called as anti-dot systems in advanced technology of electron transport devices (Beenakker and van Houten, 1989). In this context, the semiclassical and quantum analogue of chaotic scattering constitutes a challenging subject of *"quantum chaos* " (Gutzwiller, 1990; Giannoni et al., 1991; Nakamura, 1993).

On the other hand, measurements of electric conductance, Hall resistivity, and other quantum transport properties have accumulated on the so-called crossroad in the GaAs/AlGaAs interfaces (see Fig. 5.1(b)). The four corners of the crossroad consist of electron depletion regions which correspond to C_{4v} four convex hard-disks in the limit where the potential at the border of the circuit is very steep. While some theoretical studies aim at applying Gutzwiller's semiclassical trace formula to the crossroad problem, their outcome (e.g., on conductance) is not in good agreement with experimental results (Beenakker and van Houten, 1989). This discrepancy would be due to the serious diffraction effect at the leaky regions connected with straight lead wires.

In this chapter, to capture the fluctuation properties truly attributable to chaotic scattering, we shall develop both semiclassical and exact quantum theories for a point particle scattered by a model system consisting of C_{4v} -symmetric four identical hard disks (radii a and inter-disk distances R) with all its attachments discarded so as to suppress the effect of diffraction (see Fig. 5.1 (c)). In this simplified system, the semiclassical theory of chaos or the so-called Gutzwiller's trace formula is extremely powerful. The reason is: (1) The system is fully chaotic without exhibiting any bifurcation, and therefore the symbolic dynamics predicts all the periodic orbits systematically; (2) due to the open-system nature, only short-periodic orbits contribute substantially to the trace formula, suppressing a serious problem of exponential proliferation described in Chap. 2.

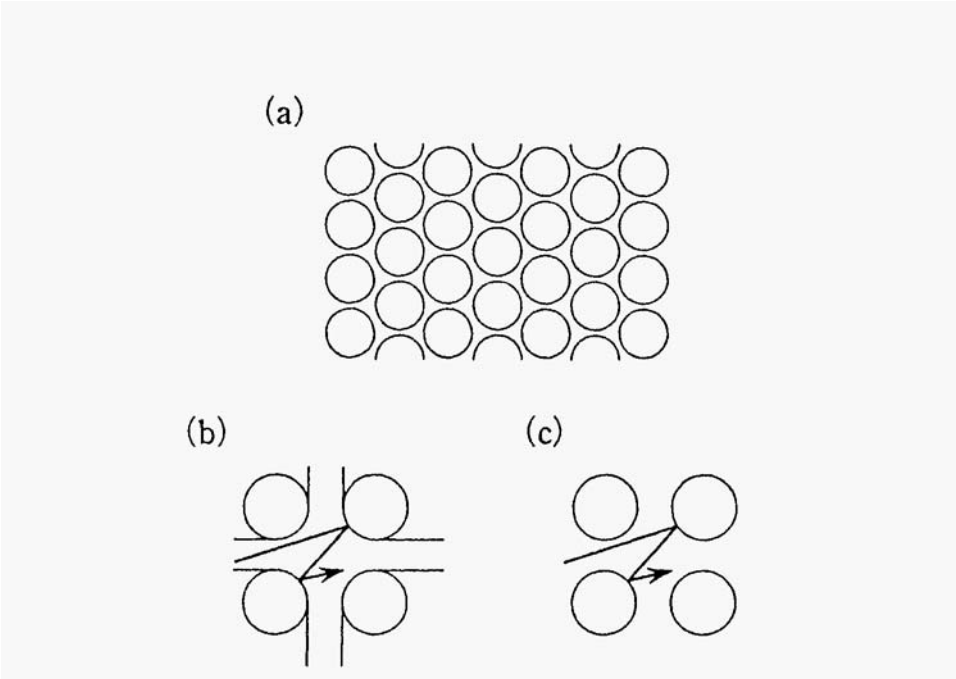

Fig. 5.1. (a) Sinai billiard, (b) Crossroad, (c) C_{4v} hard disk system.

Before developing the quantum and semiclassical theories, we should note that the classical properties of hard-disk systems are well characterized by mathematical tools like the Perron-Frobenius operator, topological pressure functions, and other characteristic quantities (Ruelle, 1978, 1986; Walters, 1981; Gaspard and Rice, 1989 a, b, c; Doron, Smilansky and Frenkel, 1991; Gaspard, Nakamura, and Rice, 1991; Rice, Gaspard and Nakamura, 1992). In particular, in systems with more than two hard disks, unstable orbits trapped between disks constitute a fractal set with zero Lebesgue measure in three-dimensional phase space. (Three coordinates are, for instance, particle positions x, y, and the angle of the velocity vector with respect to x axis.)

Assume a system of convex hard disks lying within the large circular area $\mathcal{B}$ with radius $\mathcal{R}$. The escape rate γ of a point particle moving outside of $\mathcal{B}$ is expressed, in terms of KS entropy h_{KS} and the sum of positive Lyapunov exponents λ, as

$$\gamma = \lambda - h_{\mathrm{KS}} \tag{5.1}$$

(Eckmann and Ruelle, 1985). y >0 is guaranteed, since $\lambda > h_{\mathrm{KS}}$. This implies the existence of an upper limit for the confining time. On the other hand, let us consider a gas of particles confined initially between disks inside $\mathcal{B}$ and eventually escaping outside $\mathcal{B}$. The particle density function f satisfies inside $\mathcal{B}$ a diffusion equation (with diffusion coefficient *D)*

$$\partial_t f = D\nabla^2 f \ , \tag{5.2}$$

with the boundary condition f=0 outside $\mathcal{B}$. By assuming a long-time behavior with the solution, f~exp(-y t), one obtains the relationship

$$\gamma \sim D/\mathcal{R}^2 \ . \tag{5.3}$$

Combining (5.1) and (5.3), one arrives at (Gaspard and Nicolis, 1990)

$$D \sim \mathcal{R}^2(\lambda - h_{\mathrm{KS}}) \ . \tag{5.4}$$

D proves to be nonvanishing owing to the presence of the lower limit for y.

The Lyapunov exponent λ strongly depends on the degree of opening of the system, $\sigma = R/a$: Figure 5.2 shows the σ dependence of λ_p for several unstable periodic orbits p in the four-disk system to be explained in Table 1 below. We find A decreases with increase of σ. In case $\sigma >> 1$, $\lambda >> h_{\mathrm{KS}}$, and hence γ $(\sim\lambda)$ decreases with increase of σ.

In our study below on the semiclassical and quantum-mechanical counterparts of these properties, we shall evaluate wavenumbers k_{res} associated with scattering resonances. The scattering resonance means a state in which an incident electron is transiently trapped within the quasi-closed region surrounded by disks. The imaginary part of k_{res} is related to the inverse life time of the electron. (Note: In case of closed systems, all the eigenstates are absolutely stable and $\{k_{res}\}$ have no imaginary component.) We shall elucidate the interesting distribution of k_{res}, corresponding to the classical outcomes, e.g., the presence of the lower limit of γ and its σ dependence. The following description is based on the work by Gaspard *et al.* (1994).

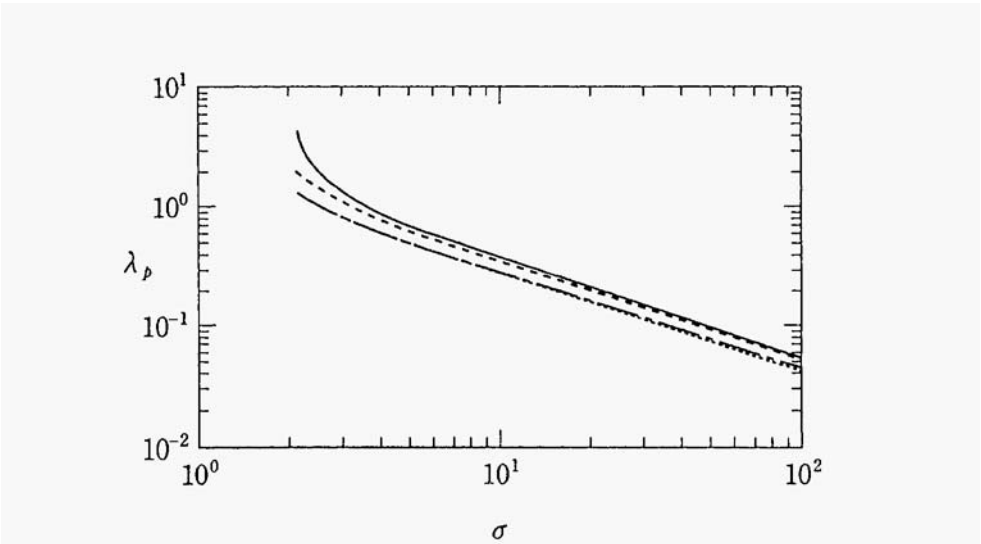

Fig. 5.2. σ dependence of Lyapunov exponent λ_p. a=1 (this value are used also in Figs. 5.3 and 5.4): "0" orbit (solid line), "2" orbit (dotted line), "01" orbit (broken line), "12" orbit (dotted broken line).

5.2. Exact Quantum Theory

In the scattering problem, the S matrix is a fundamental quantity giving the electric conductance and scattering cross section. The values of k_{res} will be derived from poles of S matrices. Before entering into the semiclassical theory we shall describe the method and results within the framework of the exact quantum theory.

Let us suppose that the four disks $\{d_1, d_2, d_3, d_4\}$ are of unit radius $(a=1)$ and are surrounded by a large circle $\mathcal{B}$ of radius R which is arbitrary. Denoting the inter-disk distance by R, we assume $2a<R<<\mathcal{R}$. (Note: In this chapter, R_c will denote to the Larmor radius (see Sec. 5.5).) The $\sigma = R/a$ ratio represents the degree of opening: $\sigma \sim 2$ and $\sigma >> 2$ correspond respectively to a weakly-open scatterer with a bulky repeller and to a strongly-open scatterer with a filamentary repeller. When $\sigma > 2.5$, the symbolic dynamics controlling the trapped orbits of the repeller does not demand special pruning rules. We shall focus on the case $\sigma >>$ 2.5 when the corresponding classical dynamics is fully and strongly chaotic.

Consider an incident particle with energy $E=\hbar^2k^2/2m$. The S matrix is introduced in the asymptotic expansion of the wave function in the angular momentum representation as

$$\Psi_{kl}(\mathbf{r}) \sim \sum_{l'=-\infty}^{\infty} (2\pi kr)^{-1/2}[\delta_{ll'}\exp\{-\mathrm{i}(kr - l'\pi/2 - \pi/4)\} + S_{ll'}\exp\{\mathrm{i}(kr - l'\pi/2 - \pi/4)\}]\exp(\mathrm{i}l'\phi). \tag{5.5}$$

At the boundaries of $(d_1, \cdots, d_4)$, the wave function satisfies

$$\Psi_{kl}(\mathbf{r}_j) = 0, \tag{5.6a}$$

with its normal derivatives expressed as

$$\mathbf{n}_j \cdot \nabla\Psi_{kl}(\mathbf{r}_j) = \sum_{m=-\infty}^{\infty} A_{ljm}\exp(\mathrm{i}m\theta_j), \tag{5.6b}$$

where $j = 1, \cdots, 4$.

The unknown quantities $\{S_{ll'}\}$ and $\{A_{lj\ m}\}$ can be obtained by substituting (5.5), (5.6) and the expression for a free-particle Green function $G(\mathbf{r},\mathbf{r}') = -(\mathrm{i}/4)\mathrm{H}_0^{(1)}(k|\mathbf{r}-\mathbf{r}'|)$ into Green's theorem, which transforms the volume integral into a surface integral:

$$\int_D \mathrm{d}^2\mathbf{r}'\left[\Psi_{kl}(\mathbf{r}')(\Delta'+k^2)G(\mathbf{r},\mathbf{r}') - G(\mathbf{r},\mathbf{r}')(\Delta'+k^2)\Psi_{kl}(\mathbf{r}')\right]$$
$$= \oint_{\partial D}\mathrm{d}s'\left[\Psi_{kl}(\mathbf{r}')\nabla' G(\mathbf{r},\mathbf{r}') - G(\mathbf{r},\mathbf{r}')\nabla'\Psi_{kl}(\mathbf{r}')\right], \tag{5.7}$$

where ds' is the line element along the boundary ∂D and primes in (5.7) mean the value at ∂D. Choosing $\mathbf{r}$ on the boundary of disks we have, from (5.7), AM = C. Similarly, when $\mathbf{r}$ is taken very distant from disks, $S = I - \mathrm{i}AD$ is derived. Eliminating A between these two equations, the S matrix is obtained as

$$S = I - \mathrm{i}CM^{-1}D, \tag{5.8}$$

where C, M and D are biinfinite matrices whose elements contain Bessel functions. This matrix equation is decomposed by using the irreducible representation of the C_{4v} point group. Noting that $A_{l1m} = A_{l2m} = A_{l3m} = A_{l4m}$, with $A_{ljm} = A_{lj\text{-}m}$ for the A_1-representation, the components of $M^{(A_1)}$ are given as follows:

$$M_{00}^{(A_1)} = \frac{\pi a}{2i}\left[1 + 2\frac{J_0(ka)}{H_0(ka)}H_0(kR) + \frac{J_0(ka)}{H_0(ka)}H_0\left(\sqrt{2}kR\right)\right],$$

$$M_{0m'}^{(A_1)} = \frac{\pi a}{2i}\left[4\frac{J_0(ka)}{H_{m'}(ka)}H_{-m'}(kR)\cos\left(\frac{\pi m'}{4}\right) + \frac{J_0(ka)}{H_{m'}(ka)}H_{-m'}\left(\sqrt{2}kR\right)\right],$$

$$M_{m0}^{(A_1)} = \frac{\pi a}{2i}\left[4\frac{J_m(ka)}{H_0(ka)}H_{-m'}(kR)\cos\left(\frac{3\pi m}{4}\right) + 2\frac{J_m(ka)}{H_0(ka)}H_m\left(\sqrt{2}kR\right)\cos(\pi m)\right],$$

$$M_{mm'}^{(A_1)} = \frac{\pi a}{2i}\left[2\delta_{mm'} + 4\frac{J_m(ka)}{H_{m'}(ka)}\right.$$

$$\times\left\{H_{m-m'}(kR)\cos\frac{(3m-m')\pi}{4} + (-1)^{m'}H_{m+m'}(kR)\cos\frac{(3m+m')\pi}{4}\right\}$$

$$\left.+2\frac{J_m(ka)}{H_{m'}(ka)}\left\{H_{m-m'}\left(\sqrt{2}kR\right)\cos(m\pi) + (-1)^{m'}H_{m+m'}\left(\sqrt{2}kR\right)\cos(m\pi)\right\}\right], \quad (5.9)$$

where $H_m(z)=H_m^{(1)}(z)$ is the first Hankel function and $m,m'>0$.

Confining ourselves to the A_1 representation throughout the present chapter, the resonance of the S matrix are determined by

$$\det M^{(A_1)}(k) = 0 \quad (5.10)$$

in the complex plane of the wave number k. We shall examine the ranges $-0.4<\mathrm{Im}\,k<0$ with $0<\mathrm{Re}\,k<20$ and $0<\mathrm{Re}\,k<5$ for the ratios $\sigma=6$ and $\sigma=12$, respectively. The size of the matrix $M_{(A1)}$ amounts to a dimension of 50x50, for us to obtain well-converged values of its (scaled) determinant for any fixed k value. The computed results are given in Figs. 5.3 and 5.4 for the case of $\sigma=6$ and 12, respectively. These figures will be used for comparison with the semiclassical results in the next section.

5.3. Semiclassical Theory

Let us define a relative density of states $\rho(E)$ as the difference between the state densities of free and scattering systems, both confined in the

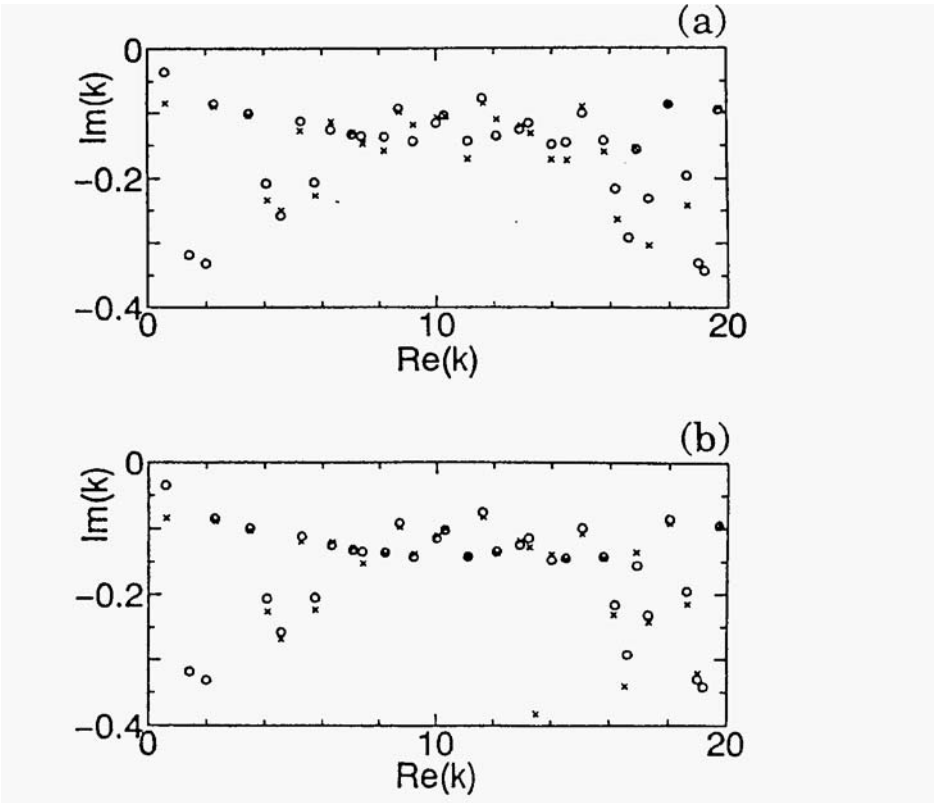

Fig. 5.3. Exact quantum (○) and semiclassical(x) resonances in case of σ=6. Semiclassical results using: (a) 6 orbits with periods 1 an 2, (b) 14 orbits with periods 1,2, and 3.

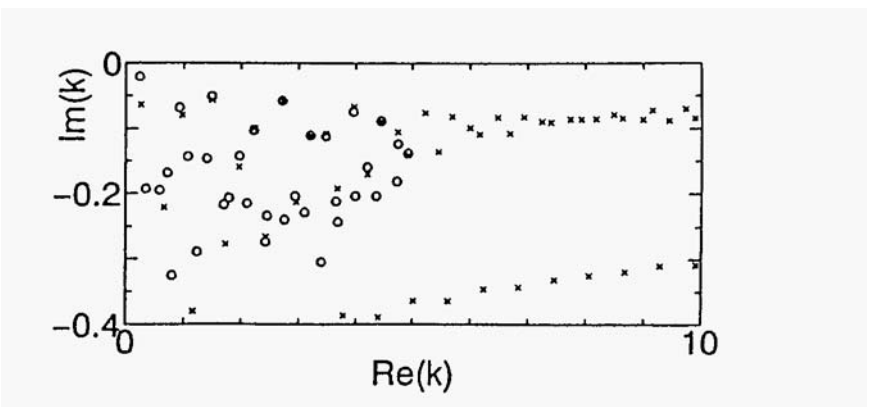

Fig. 5.4. Same as in Fig. 5.3 but σ=12. The semiclassical result consists of orbits with periods 1, 2, and 3.

very large circle $\mathcal{B}$. The function $\rho(E)$ is asymptotically independent of the radius of $\mathcal{B}$ and is related to the S matrix as (Balian and Bloch, 1974)

$$\rho(E) = (2\pi i)^{-1} \mathrm{Tr}\{S^{\dagger}(E)\, \mathrm{d}S(E)/\mathrm{d}E\}. \tag{5.11}$$

Therefore, the density $\rho(E)$ *and the S-matrix share the same poles.* The function $p(E)$ itself is written as $\rho(E) = -\pi^{-1}\mathrm{Im}\, g(E)$, with $g(E)$ being the trace of the difference between the Green functions with and without the four disks.

In the semiclassical limit, $g(E)$ is expressed as a sum over periodic orbits, i.e., by Gutzwiller's trace formula:

$$g(E) = g_0 + \sum_p \frac{T_p(E)}{i\hbar} \sum_{r=1}^{\infty} \frac{\exp(\frac{i}{\hbar} rS_p(E) + i\pi rL_p)}{2\sinh(ru_p/2)}, \tag{5.12}$$

where g_0 is E-independent and given by the difference between Thomas-Fermi state densities with and without four disks:

$$g_0 = \frac{m}{2\pi\hbar^2}\left(\int_{\mathcal{B}-4disks} \mathrm{d}^2q - \int_{\mathcal{B}} \mathrm{d}^2q\right) = -\frac{m}{2\pi\hbar^2}\int_{4disks} \mathrm{d}^2q = -4a^2m/(2\hbar^2).$$

Here p and r denote any unstable and isolated prime periodic orbit and the number of its repetition, respectively. With l_p signifying the length of the periodic orbit, $S_p(E) = \oint_p \mathbf{p}\cdot\mathrm{d}\mathbf{q} = \hbar k l_p$ and $T_p(E) = \mathrm{d}Sp(E)/\mathrm{d}E = l_p/v$ are the reduced action and the period, respectively. (For convenience, we rescale the velocity to a unit value v=1.) Lp is the number of collisions of the orbit p with disks. The stability exponent μ_p is derived from the stability eigenvalue Λ_p via $u_p = \ln\Lambda_p$. (The Lyapunov exponent λ_p, is given by $=u_p/T_p$.) Λ_p is the larger eigenvalue of the monodromy matrix Mp constructed from the linearized Poincare' map for coordinates perpendicular to the trajectory. The advantage of the present system lies in the E independency of Λ_p due to the constancy of the particle velocity (v=l), which greatly simplifies the summation in (5.12). Equations (5.11) and (5.12) indicate that *the scattering resonances can be obtained from poles of g(E).*

With a help of symbolic codings, we can get all the periodic orbits

period 1	0	12	
	1	1234	
	2	13	
period 2	01	1214	
	02	1243	
	12	12413423	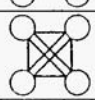
period 3	001	121232343414	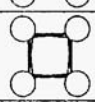
	002	121343	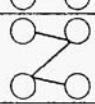
	011	121434	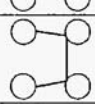
	012	121323	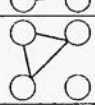
	021	124324	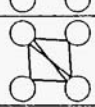
	022	124213	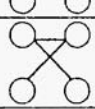
	112	123	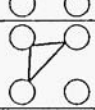
	122	124231342413	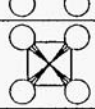

Table 1. Periodic orbits up to period 3. The 3rd column represents a sequence of disk numbers in the order of bouncings.

without missing any one of them, pictures of 14 periodic orbits up to the period 3 in the number of bounces being listed in Table 1. As pointed out in Chap. 2, the trace formula in (5.12) is not convergent as it stands, i.e., conditionally convergent. Using the expansion

$$2\sinh^{-1}(x/2) = \sum_{j=0}^{\infty} e^{-(1/2+j)x} ,$$

one can write the trace function in terms of the Ruelle zeta function ζ as

$$g(E) = g_0 - \sum_{j=0}^{\infty} \frac{\partial}{\partial E} \ln \zeta_{1/2+j}(-ik) , \tag{5.13a}$$

with

$$\zeta_{1/2+j}(-ik) = \prod_p \left[1 - \frac{(-1)^{L_p} \exp(ikl_p)}{|\Lambda_p|^{1/2} \Lambda_p^{\,j}} \right]^{-1} , \tag{5.13b}$$

where $\Lambda_p = \exp(\mu_p)$. The form of product sum in (5.13) guarantees the better convergence. Finally, the complex poles of the Ruelle zeta function yield resonances of the S matrix.

Noting the C_{4v} symmetry of the system, the ζ function can be factorized as $\zeta = \zeta_{A_1}\zeta_{A_2}\zeta_{B_1}\zeta_{B_2}\zeta_E^2$, with each factor corresponding to the irreducible representations A_1, A_2, B_1, B_2 and E. This symmetry-induced factorization further simplifies the procedure of taking the product over periodic orbits in (5.13b). We have, for instance (Cvitanovic and Eckhardt, 1989, 1993),

$$\begin{aligned} \zeta_A^{-1} &= \prod_p (1 - t_p) \\ &= 1 - t_0 - t_1 - t_2 - (t_{01} - t_0 t_1 + t_{02} - t_0 t_2 + t_{12} - t_1 t_2) - \cdots , \end{aligned} \tag{5.14a}$$

where t_p is given by

$$t_p = (-1)^{L_p} |\Lambda_p|^{-1/2} \exp[ikl_p] , \tag{5.14b}$$

so long as we restrict ourselves to the resonances with the longest lifetimes, which are given by the first Ruelle zeta function with j=0.

How can we compute Λ_p and l_p necessary to evaluate t_p in (5.14) ?

The answer is as follows: Let (ξ,γ) be coordinates on the Poincare' surface of section for the periodic orbit p and then derive the Poincare' map for the flow in the phase space. By linearizing this map, we obtain the map for variations of the orbit p:

$$\delta\xi' = M_{11}\delta\xi + M_{12}\delta\eta ,$$
$$\delta\eta' = M_{21}\delta\xi + M_{22}\delta\eta .$$

The eigenvalue of the monodromy matrix M is nothing but the stability eigenvalue Λ_p, which are

$$\Lambda_p = (\mathrm{Tr}M + ((\mathrm{Tr}M)^2 - 4)^{1/2})/2 . \tag{5.15}$$

[Note that u_p below (5.12) is $u_p=\ln\Lambda_p$ and the Lyapunov exponent is $\lambda_p=u_p/T_p=u_p/l_p$.]

The explicit form of M is available from a simple geometrical inspection as

$$\mathrm{Tr}M=(-1)^n\,\mathrm{Tr}\begin{pmatrix} 1+\dfrac{2\ell_{n1}\kappa_n}{\cos\varphi_n} & \ell_{n1} \\ \dfrac{2\kappa_n}{\cos\varphi_n} & 1 \end{pmatrix}\begin{pmatrix} 1+\dfrac{2\ell_{n-1n}\kappa_{n-1}}{\cos\varphi_{n-1}} & \ell_{n-1n} \\ \dfrac{2\kappa_{n-1}}{\cos\varphi_{n-1}} & 1 \end{pmatrix}\cdots\begin{pmatrix} 1+\dfrac{2\ell_{12}\kappa_1}{\cos\varphi_1} & \ell_{12} \\ \dfrac{2\kappa_1}{\cos\varphi_1} & 1 \end{pmatrix}, \tag{5.16}$$

where $\{l_{n-1,n}\}$ and $\{\varphi_{n-1}\}$ are the length of the flight between disks and the reflection angle, respectively, and are found from the profile of periodic orbits in Table 1. The quantity $\kappa_n(=1/a$ for all $n)$ is the curvature of the disks where a particle bounces.

For illustration, let us choose the n=1 orbit "0." Then, $\cos\varphi_1=\cos\varphi_2=1$ and $l_{12}=l_{21}=R-2a$, leading to $\Lambda_p=(\sigma-1+(\sigma^2-2\sigma)^{1/2})^2$ and $l_p=2(R-2a)$ with the degree of opening σ. As a little more complicated example, we consider the n=3 orbit "022" (see Fig. 5.5). By application of Pythagoras' theorem and the sine formula to right-angled triangles, OPP' and OPP", respectively, one gets

$$y=\sqrt{[\sqrt{2}R-a\cos(\pi/4-\varphi)]^2+[a\sin(\pi/4-\varphi)]^2},$$

$$\frac{y}{\sin(\pi/2)}=\frac{R-a\sin\varphi}{\sin 2\varphi} .$$

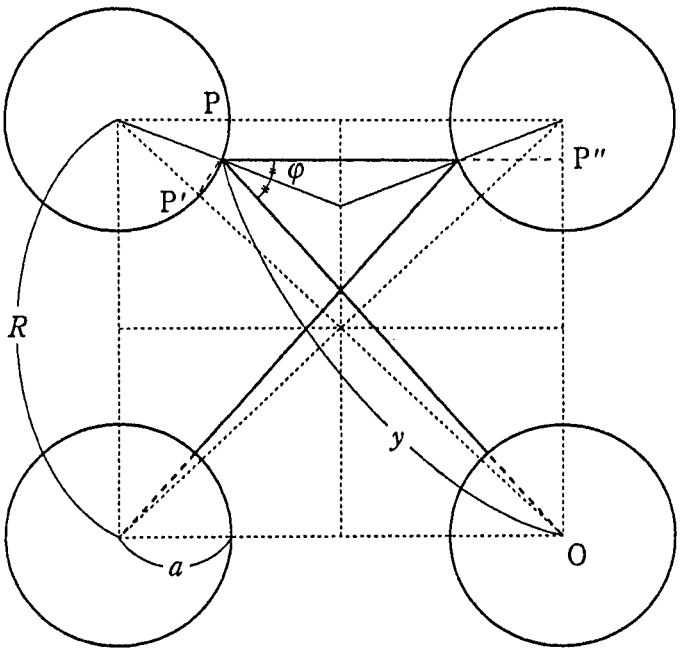

Fig. 5.5. Flight distances and incident angles of period-3 orbit "022" in Table 1.

By solving these equations simultaneously, values of y and $x=\cos\varphi$ are determined, and other variables are given by $\cos(\varphi_1)=1$, $\cos(\varphi_2)=\cos(\varphi_3)=x$, $l_{12}=l_{31}=y-a$, $l_{23}=R-ax$ and $l_{31}=y-a$. Substituting these results into (5.15) and (5.16), we obtain both Λ_p and $l_p=2(R-2ax+2(y-a))$. For other periodic orbits in Table 1, similar calculations as above are possible. Finally, with use of the values Λ_p and l_p, t_p in (5.14) is determined for any periodic orbit p. It should be noted that the Bunimovich-Sinai curvature formula (1980) can also be used to obtain the Lyapunov exponents.

We are concerned with the A_1 representation which proves to include the scattering resonance with the longest lifetime bordering a *"gap"* void of resonances formed just below the real k axis. The resonances for the A_1 sector are given by complex k values satisfying

$$\zeta_{A_1}^{-1}(-ik) = 0. \tag{5.17}$$

In a quantum-mechanical treatment, the computation of scattering resonances demands an excessively long cpu time and a large region size for storage of memories. By contrast, the computation of (5.14) and (5.17) is not laborious, and one may promptly get a large number of resonances by which one is able to analyze their statistical properties. For the present system, therefore, the semiclassical theory is superior to the exact quantum theory.

5.4. Distribution of Complex Resonances

The location of poles, i.e., of complex resonances are given in Figs. 5.3 and 5.4 in the cases σ =6 and 12, respectively. While the resonances $\{k_{res}\}$ lie on the real k axis in closed systems, they have nonvanishing imaginary components in open scattering systems. The semiclassical resonances based on 6 orbits with periods 1 and 2 and those based on 14 orbits with periods 1, 2, and 3 are displayed in Figs. 5.3(a) and 5.3(b), respectively.

From Fig. 5.3(b), we learn the following:

(i) In a wide window of $0<\mathrm{Re}\,k<20$ and $-0.4<\mathrm{Im}\,k<0$, a remarkable agreement is obtained between locations of the semiclassical and exact quantum-mechanical resonances. While the semiclassical resonances have also been obtained by using orbits up to period 4, no noticeable improvement has been found. Therefore the semiclassical theory with orbits up to the period 3 is extremely effective in reproducing the quantum resonances. (There remains, however, the difference for the resonance close to k=0. Since the de Broglie wavelength for this special resonance is larger than the system's characteristic lengths, a and R, and invalidates the semiclassical theory, the difference is inevitable.)

(ii) The distribution of resonances has a gap below the real k axis. The semiclassical gap law shows that the resonances obey $\mathrm{Im}\,k_{res}<-x_{gap}$ at large wave numbers $Re\,k_{res}>>1$, with x_{gap} =0.03796 in the case σ=6. The afore-mentioned resonance close to k=0 is however ruled out because it is strongly affected by a diffraction effect. For repellers with σ=6 but consisting of more than four disks, the gap will be diminished owing to the increase in the effective trapping region (more quantitatively, to the increase of Hausdorff and information dimensions of the corresponding classical fractal repellers). The nonvanishing gap is a quantum-mechanical manifestation of the presence of the finite upper limit of the trapping time for a classical particle (see (5.1)). On

the other hand, the quantum-mechanical asymptotic theorem (Lax and Phillips, 1967) states that, for repellers with more than two disks and $\sigma >> 1$, the region satisfying

$$-\mathrm{Im}k < \alpha \ln(|k| + 1) + \beta \tag{5.18}$$

with $\alpha, \beta > 0$ is void of scattering resonances. The present issue is consistent with this theorem.

(iii) The distribution consists of periodic structures parallel to the real k axis. The periods can be attributed to combinations of two length scales $\sim R$ and $\sim 2\frac{1}{2} R$ characterizing the square geometry.

Let us proceed with the case of a strongly-opened scatterer with $\sigma = 12$, whose resonance spectrum is shown in Fig. 5.4. While the semiclassical resonances are displayed in the window $0 < \mathrm{Re}k < 10$ and $-0.4 < \mathrm{Im}k < 0$, their comparison with the exact quantum counterparts has been done in the limited range $\mathrm{Re}k < 5$ because of the too large size of $M^{(A_1)}$ required to get converged values of $\det M^{(A_1)}$ in the quantal treatment. Nevertheless the results in (i)-(iii) are also valid here.

A careful insight into the periodic structures in Figs. 5.3(b) and 5.4 reveals that they are composed of several oscillating strings which lie parallel to the real k axis and merge into narrow bands in higher energies. To characterize these structures, we shall now analyze dh/dx, i.e., the distribution function of the imaginary parts ($x = -\mathrm{Im}k$) of the semiclassical resonances near the gap. Here $h(x)$ is the cumulative distribution function per unit $y = \mathrm{Re}k$ (Jessen and Tornehave, 1945):

$$h(x) = \lim_{(y_2 - y_1) \to \infty} [\arg f(x + \mathrm{i}y_2) - \arg f(x + \mathrm{i}y_1)] / [2\pi (y_2 - y_1)], \tag{5.19}$$

where $f(x+\mathrm{i}y) = \zeta_{A_1}^{-1}(-ik)$. (5.19) is derived by noting that the number N of zeros of $f(x+\mathrm{i}y)$ within a loop C on the complex k plane is given (see Fig. 5.6) by

$$\begin{aligned} N(x_1, x_2; y_1, y_2) &= \frac{1}{2\pi \mathrm{i}} \oint_C d \ln f(x + \mathrm{i}y) \\ &= \frac{1}{2\pi \mathrm{i}} \oint_C d\left[\ln |f(x + \mathrm{i}y)| + \mathrm{i} \arg f(x + \mathrm{i}y)\right] \\ &= \frac{1}{2\pi} \oint d \arg f(x + \mathrm{i}y) \quad . \end{aligned}$$

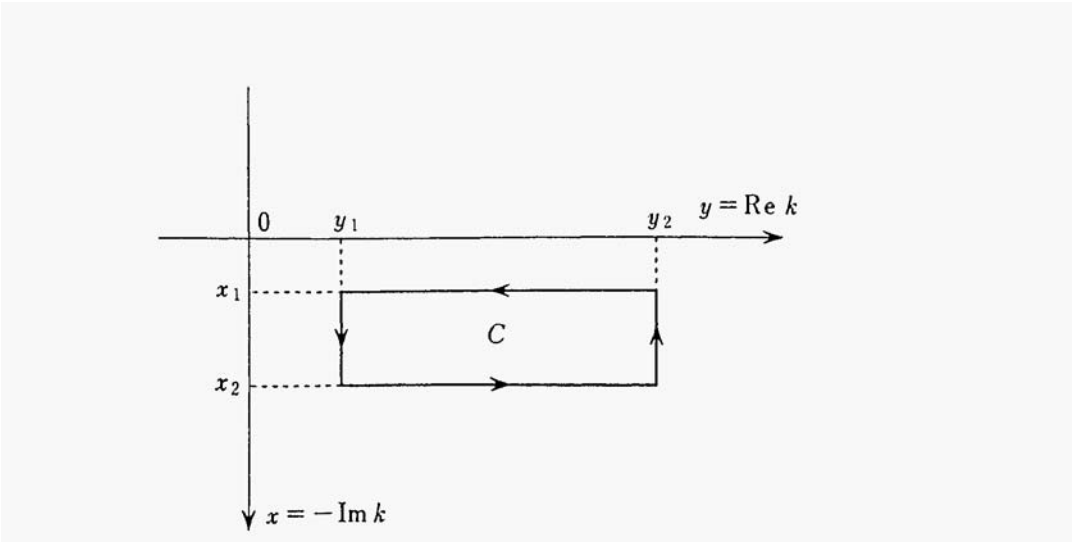

Fig. 5.6. Closed loop C in the complex k plane.

We choose the case α =12 where the beating of oscillating strings is more evident (see Fig. 5.4). The density distribution dh/dx per unit Rek is depicted in Fig. 5.7 for increasing sampling range (y_2-y_1) used in the average (5.19), with y_1(=8) fixed. The density distribution consists of a sequence of stable bands with fine structures near the threshold fluctuating as y_2 increases. The formation of bands is caused by bunching of several oscillating strings parallel to the real k axis. The location of a threshold (at x_{gap}=0.0509) in the distribution is extremely stable against increasing the sampling range, ensuring the resonance gap in the semi-infinite range Rek>8 We should note that, for the separable two-disk billiards (Miller, 1975), we have (instead of a band structure) only a single discrete spectrum because of the regular arrangement of resonances parallel to the real k axis at large values of Rek: dh/dx= $\delta(x-x_{gap})$, with $x_{gap}=\ln|\Lambda_p|/(2l_p)$. On the other hand, the random-matrix theory suggests a distribution with the density dh/dx $\propto$ $x^{\nu/2-1}\exp(-x/2)$ for ν (>2) open channel systems. This density is the derivative of the generalized Porter-Thomas cumulative distribution function (Porter and Thomas, 1956; Porter, 1965, showing a monotonic growth, starting from Imk=0 (i.e., with no gap) for ν >2. Because the density of the four-disk scatterer in Fig. 5.7 shows a behavior which is more complex than in these two special limits, the result of Fig. 5.7 suggests a new universality

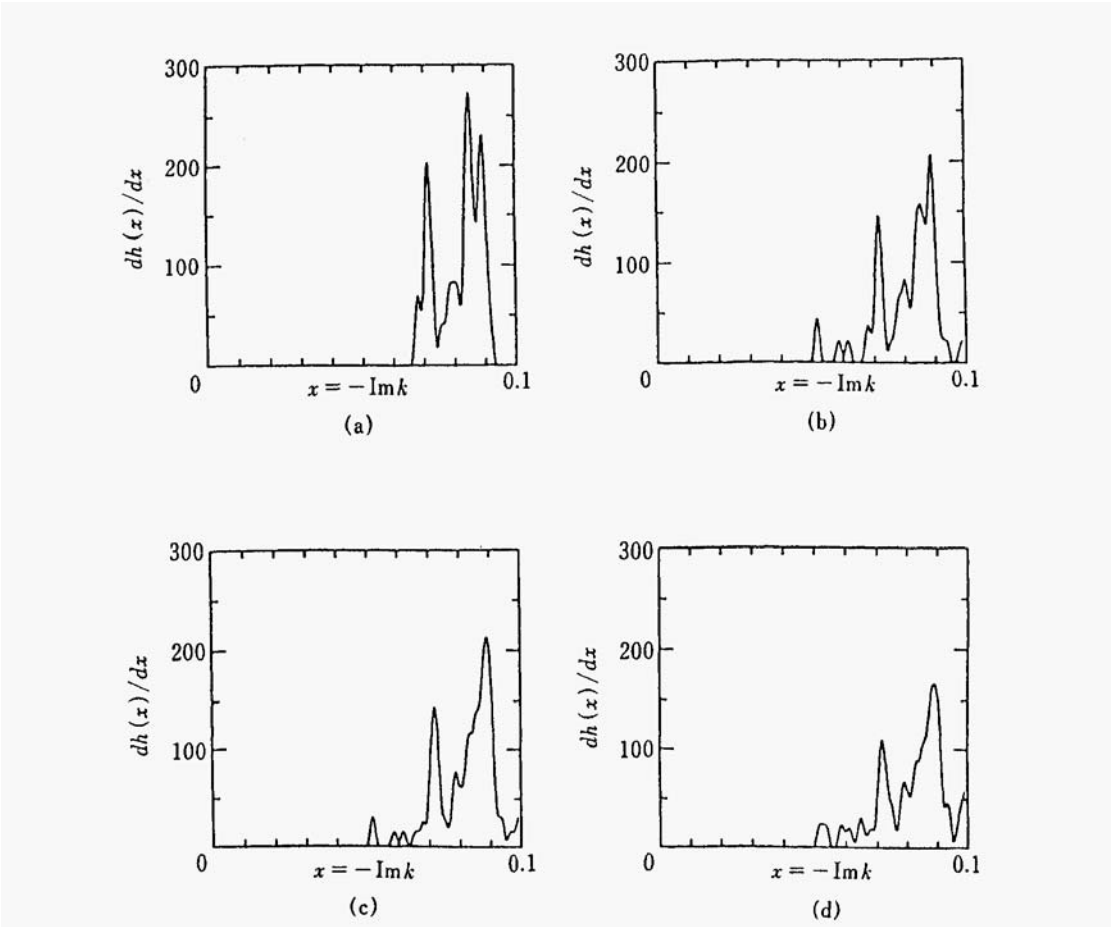

Fig. 5.7. Distribution function of imaginary part of semiclassical resonances dh/dx with x=-IMk. y_1=8: (a) y_2=20, (b) y_2=30, (c) y_2=40,)d) y_2=50..

class of the distribution of x=−Imk.

For C_{4v} four-disk systems, we showed that the exact quantum resonances can be nicely reproduced by the semiclassical theory, using the cycle expansion of the Ruelle zeta function with a finite set of periodic orbits, up to period 3 in the number of bounces. Small differences remaining between the quantum and the semiclassical resonances may be attributed to higher-order $\hbar$ corrections to be incorporated in the periodic-orbit quantization. Near the resonance gap, the statistical distribution per unit Rek of the imaginary parts of the semiclassical resonances turns out to consist of a sequence of bands

with small peaks near the threshold. Any finite truncation of the inverse zeta function should lead to a stable asymptotic distribution $h(x)$ when $\mathrm{Re}k \to \infty$. However, it seems that the asymptotic distribution is reached only at high values of $\mathrm{Re}k$. On the other hand, there is presently no rigourous result (other than the inequality in (5.18)) on the existence of this distribution $h(x)$ for the quantum-mechanical system. Besides this question, our results show that the distribution $h(x)$ considerably differs from the prediction of random matrix theories. This difference holds irrespective of the degree of opening of the scatterer and strongly indicates a nonuniversality of the distribution function near the threshold.

The present theory may also be a vehicle for studies on more complicated open systems like the crossroad, where the effect of diffraction should be incorporated. Indeed, the classical repeller of the crossroad billiard differs from that of the four-disk billiard at the level of the periodic orbit "12" of Table 1 (see Fig. 5.1). The periodic orbit "12" is bouncing just at the matching points between the straight lead wires and the circular corners. The contribution of such periodic orbits bouncing at discontinuites of the border of the billiard needs to be modified due to special diffraction effects (Alonso and Gaspard, 1994). Such modifications may lead to quantitative differences in the distribution of the resonances between the crossroad and the four-disk billiards, but our study indicates that both billiards should share the same qualitative properties.

The resonances studied in this chapter can provide information on the dynamical behavior of a semiconductor mesoscopic device like the crossroad. The reaction time of the device may be estimated from the size of the aforementioned gap in the distribution of resonances. Indeed, according to Schrödinger's equation applied to scattering systems, the time evolution of an electronic wavepacket is given by a linear superposition of damped exponentials, $\exp(\mathrm{Im}E_n t/\hbar)$, controlled by imaginary parts of the complex energies of the resonances. In the present system, we have shown that imaginary parts of the wavenumbers are bounded by the value of the gap according to $\mathrm{Im}k_n < -x_{gap}$. Using the relation between energy and wavenumber, we infer that the probability for the electron to remain in the scatterer decays like $\exp(-t/\tau_{gap})$. The upper bound on the lifetimes is given by $\tau_{gap} = 1/(2u_F x_{gap})$ in terms of the semiclassical gap and the Fermi velocity of the electron gas. Since the gap is related to the Lyapunov exponents of the periodic orbits, our analysis shows how the reaction time of the

device depends on the geometry of the system:

$$\tau_{gap} \sim \frac{R}{v_F \ln(R/a)}, \tag{5.20}$$

which is valid in the regime kR, ka >>1 where diffraction effects can be neglected. In the case of crossroad, we see that the shortest reaction times are obtained for the smallest values of the corner radius a, assuming a fixed value for the width (=R-2a) of the lead wires. For GaAs/AlGaAs heterojunctions, the effective mass of the electrons is m=0.067m_e , and an electron density of n_s=3 x 10^{11}cm^{-2} can be obtained so that the Fermi velocity would then take the value $v_F=(2\pi\hbar^2 n_s)^{1/2}/m$=2.4 x x$10^5$m/s. For a nanometric circuit of size R=100nm, the time unit is therefore of R/u_F=0.4x 10^{-12}s so that the lifetimes of the resonances are in the subpicosecond domain. We suggest that the dynamical behavior of such devices could be probed by femto-second laser experiments.

To conclude, the semiclassical theory on chaotic scattering on convex hard disk systems has the following advantages: (1) The systematic enumeration of all the periodic orbits is possible owing to the symbolic dynamics. (2) So long as one is concerned with the case of the large degree of opening (i.e., of filamentary disks), only short periodic orbits contribute substantially to the trace formula, eliminating the problem of its divergence due to exponential proliferations. (3) Since poles of *g(E)* and *S(E)* are identical, their imaginary components are significant, while they are not demanded in bounded systems.

As a consequence, the semiclassical theory of chaotic scattering has not only a conceptual significance to uncover the quantum-classical correspondence, but also an advantage to be more practical than the exact quantum theory which, in applications, meets computational limitations in both cpu time and memory area.

5.5. Experiment on Antidot Arrays in Magnetic Field

While effects of magnetic field have not been taken into consideration in the theoretical treatment above, recent experiments have accumulated around the quantum transport in regular arrays of hard disk billiards in the presence of magnetic field. Weiss *et al.* (1991, 1993), using high-mobility GaAs/AlGaAs heterojunctions having carrier density

n_8~2 x x1011 a" and mobility μ-1.0 x 10^6 cm^2 /Vs, fabricated a periodic square antidot array (: periodically-drilled holes through a two-dimensional electron gas) with the period R=200~300 nm (which should not be confused with R_c below) and with radius α of each antidot (electron depletion region) less than $R/2$. Applying a magnetic field B perpendicularly, they explored transport anomalies in a temperature region where both the electron mean free path l_e and the phase coherence length l_ϕ are of the order of 10 μm. Note the classical cyclotron radius $R_c=\hbar k_F/(eB$ at the Fermi energy. The measurement of resistivity p_{xx} for a sample with αR~0.5 at T~0.4K as a function of B shows distinct quantum oscillations in the low B regime ($2R_c>R-\alpha$), which differ from the Shubnikov-de Haas oscillations periodic in 1/B in the high B regime (see Fig. 5.8). The latter is caused by the Landau level structures. Since l_e, I_ϕ >>R and the Fermi wavelength λ_F, ~ 50nm, the quantization of chaotic motion of electrons plays a role. The quantity ρ_{xx} in Fig. 5.8 displays quantum oscillations superimposed upon the low-B resistance anomalies. These oscillations are periodic in B with periodΔB~ 0.105 T [Tesla]~h/eR^2 . The crossover from B-periodic to $1/B$-periodic oscillations, together with the fact that the antidot array is much larger than the phase-breaking length in a 2DEG, suggest that the B-periodic oscillations are not due to the Aharonov-Bohm interference of phase-shifted wave functions.

Assuming ρ_{xx}~$g^2(E,$ B), Weiss *et al.* tried to explain the experimental issue by resorting to Gutzwiller's trace formula. This system, though simulating the so-called Sinai billiard, is a generic and mixed system since electrons are subject to the magnetic field. Furthermore, not a hard but rather soft wall model is employed in their study. As a consequence both stable and unstable periodic orbits contribute to $g(E, B)$. The relevant periodic orbits are displayed in Fig. 5.8(b). Due to finite temperatures and impurity broadening effects, only the shortest periodic orbits are taken into consideration. The periodic orbits cause a modulation of $g(E, B$) with maxima given by the quantization rule

$$S(B)=\oint (m^*\mathbf{v}+e\mathbf{A})\cdot d\mathbf{r}=m^*\oint \mathbf{v}\cdot d\mathbf{r}- eB\mathcal{A}(B)=2\pi\hbar N\,, \qquad (5.21)$$

where N=(n+y/2+ α/4) in terms of the quantum number n, the winding number γ, and the Maslov index α. B$\mathcal{A}$(B) is the flux penetrating the area $\mathcal{A}$(B) enclosed by a periodic orbit. For comparison with experiment,

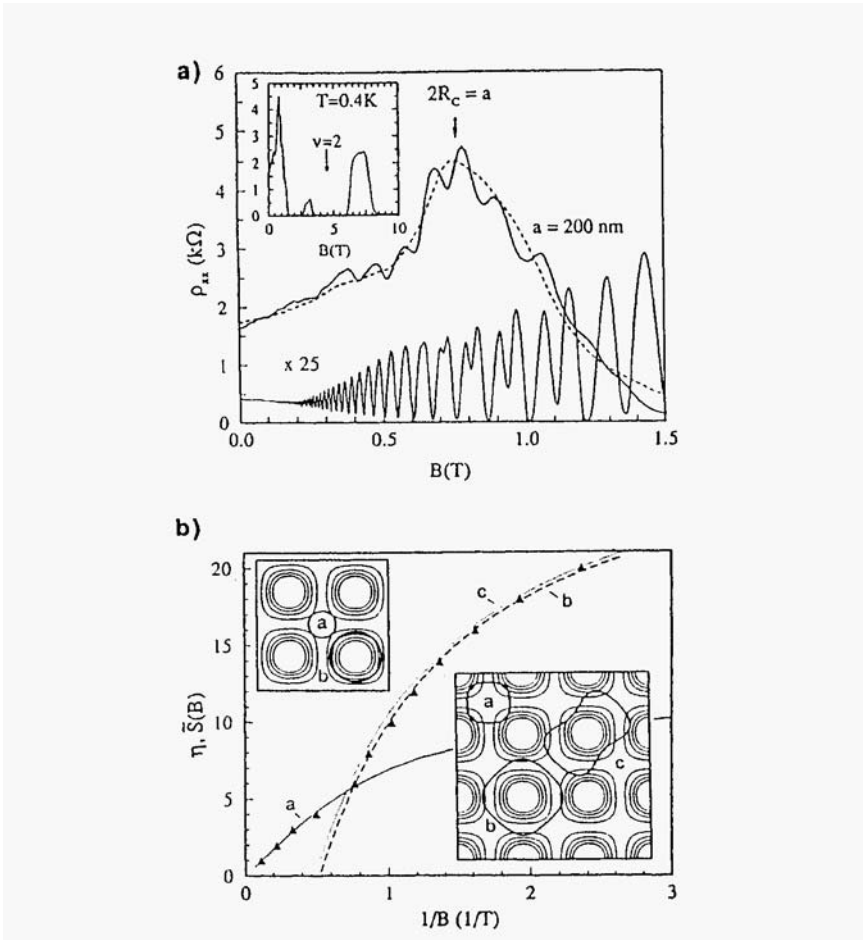

Fig. 5.8. (a) ρ_{xx} measured in the patterned (top traces) and unpatterned (bottom trace) segments of the same sample for T=0.4K (solid lines) and 4.7K (dashed line). Inset: ρ_{xx} up to 10 T with filling factor ν =2 marked by arrow.
(b) Triangles mark 1/B positions of pxx minima. Solid, dashed, and dotted lines are calculated reduced actions $\tilde{S}(1/B)$ of orbits (a), (b), and (c), respectively. These orbits are shown for 1 /B=0.6T-1 (top) and 1 /B= 2.7 T-1 (bottom inset). (Courtesy of D. Weiss *et al.*)

the reduced action

$$\tilde{S}(B) \equiv 2S(B)/\hbar - \gamma(B) - \alpha/2 - 1$$

is more advantageous: $S(\tilde{B})=2n$ with $n=1,2,\cdots$ labels *minima* of

$g(E,B)$. Three periodic orbits in Fig. 5.8(b) are sufficient to explain the minima of p_{xx} . These are: (a) an orbit between four antidots, (b) another one around a single antidot, (c) the last one emerging from a bifurcation of orbit (b). All other periodic orbits are asserted to play only minor roles. The calculated $\hat{\mathbf{S}}(B)$ traces in Fig. 5.86) highlight the dominant role of the orbits (a)-(c).

Despite an elegant interpretation of some of the fluctuations in quantum transport, there remains an open question concerning the underlying low-B field anomaly, which should be interpreted on the basis of isolated unstable periodic orbits. Specifically, it is possible to have to give alternative insight into the fluctuation in the vicinity of zero field when the system is fully chaotic and no stable periodic orbit survives. It is therefore highly desirable to extend the theory given in the present chapter to the system with more than four disks and also in the presence of magnetic field.

References

Alonso, D., and Gaspard, P. (1994). *J. Phys.* **A27,** 1599.

Balian, R., and Bloch, C. (1974). *Ann. Phys.* **85,** 514.

Beenakker, C. W., and van Houten, H. (1991). In *Solid State Physics: Advances in Research and Applications,* H. Ehrenreich and D. Turnbull, eds. New York: Academic.

Bunimovich, L. A., and Sinai, Ya. G. (1980). *Commun. Math.* Phys. **78,** 247,479.

Cvitanovic, P., and Eckhardt, B. (1989). *Phys. Rev. Lett.* **63,** 829.

Cvitanovic, P., and Eckhardt, B. (1993). *Nonlinearity* **6,** 277.

Gaspard, P., and Alonso, D., Okuda, T., and Nakamura, K. (1994). *Phys. Rev.* **E50,** 2591.

Gaspard, P., and Nicolis, G. (1990). *Phys. Rev. Lett.* **65,** 1693.

Gaspard, P., and Rice, S. A. (1989). *J. Chem. Phys.* **90,** 2225, 2242, 2255 (1989).

Gaspard, P., Nakamura, K., and Rice, S. A. (1991). *Comments Atom. Mol. Phys.* **25,** 321.

Doron, E., Smilansky, U., and Frenkel, A. (1991). *Physica* **D50,** 367.

Eckmann, J. P., andRuelle, D. (1985). *Rev. Mod. Phys.* **57,** 617.

Giannoni, M. J., Voros, A., and Zinn-Justin, J., eds. (1991). *Chaos and Quantum Physics, Proceedings of the NATO ASI Les Houches Summer School.* Amsterdam: North-Holland.

Gutzwiller, M. C. (1990). *Chaos in Classical and Quantum Mechanics.* Berlin: Springer.

Jessen, B., and Tornehave, H. (1945). *Acta Math.* **77,** 137.

Krylov, N. S. (1979). *Works on the Foundations of Statistical Physics.* Princeton: Princeton University Press.

Lax, P. D., and Phillips, R. S. (1967). *Scattering Theory.* New York: Academic.

Miller, W. H. (1975). *J. Chem. Phys.* **63,** 996.

Nakamura, K. (1993). Quantum Chaos: *A New Paradigm of Nonlinear Dynamics.* Cambridge: Cambridge University Press.

Porter, C.E. (1965). *Statistical Theories of Spectra: Fluctuations.* New York: Academic.

Porter, C. E., and Thomas, R. G. (1956). Phys. Rev. 104,483.

Rice, S. A., Gaspard, P., and Nakamura, K. (1992). In *Advances in Classical Trajectory Methods* **1,** W. L. Hase, eds. Connecticut: JAI Press.

Ruelle, D. (1978). *Thermodynamic Formalism.* Reading, Massachusetts: Addison-Wesley.

Ruelle, D. (1986). *Phys. Rev. Lett.* **56,** 405.

Walters, P. (1981). *An Introduction to Ergodic Theory.* Berlin: Springer.

Weiss, D. et al. (1991). *Phys. Rev. Lett.* ***66,*** 2790.

Weiss, D. et al. (1993). *Phys. Rev. Lett.* **70,** 4118.

Chapter 6

Nonadiabaticity-Induced Quantum Chaos

To accommodate temporal chaos in quantum dynamics, we consider the dynamics beyond the Born-Oppenheimer approximation. After reviewing the fictitious gauge strucure in the adiabatic limit, we examine the role of gauge structure in nonadiabatic transitions for transport in open paths. Local features of the gauge potential modify the nature of the intersection of the adiabatic energy surfaces and thereby affect crucially the Landau-Zener formula for a single-passage transition rate. We then investigate the full dynamics of systems involving both slow (nuclear) and first (electronic) dynamical variables and demonstrate the chaotic behaviors in quantum dynamics.

6.1. Avoided Level Crossings and Gauge Structure

As we have so far insisted, the collapse of tori and onset of chaos are disturbing the foundation of the formalism of quantum mechanics in the adiabatic limit, i.e., when no quantum transition occurs. In this limit the present formalism of quantum mechanics demonstrates many puzzling features: avoided level crossing and gauge structure, commonly appearing at the level degeneracy, are the most interesting events, which we shall explain below.

The adiabatic limit correponds to stationary states, in which the major problem of quantum mechanics is to solve the eigenvalue equations

$$H(\mathbf{q})|\Psi_n(\mathbf{q})\rangle = E_n|\Psi_n(\mathbf{q})\rangle\,, \tag{6.1}$$

where in general the Hamiltonian $H(\mathbf{q})$ depends on parameters $\mathbf{R}=(R_1, R_2, \cdots, R_d)$ such as external electric and magnetic fields. Within a desymmetrized manifold, no degeneracy can be seen except for the accidental ones (von Neumann and Wigner, 1929): If a single parameter were varied, we would see only level repulsions, e.g., avoided level crossings. We shall illustrate this point by using a two-states model. Suppose that at some point $\mathbf{R}_0$ two states $|\Psi_1{}^0\rangle$ and $|\Psi_2{}^0\rangle$ are degenerate with common energy E_0. The eigenvalue problem in the vicinity of $\mathbf{R}^0$ can be solved by degenerate perturbation theory. Using as diabatic (R-independent) bases $|\Psi_1{}^0\rangle$ and $|\Psi_2{}^0\rangle$, the matrix elements of $H(\mathbf{R})$ are given as

$$\begin{bmatrix} E_0 + H'_{11}(\mathbf{R}) & H'_{12}(\mathbf{R}) \\ H'_{21}(\mathbf{R}) & E_0 + H'_{22}(\mathbf{R}) \end{bmatrix}, \tag{6.2}$$

with $H'_{ij}(R) = \langle\Psi_i{}^0|\{H(\mathbf{R}) - H(\mathbf{R}_0)\}|\Psi_j{}^0\rangle$. The energy splitting at $\mathbf{R}$ is

$$\Delta E = \{(H'_{11}(\mathbf{R}) - H'_{22}(\mathbf{R}))^2 + 4|H'_{12}(\mathbf{R})|^2\}^{1/2}\,. \tag{6.3}$$

To meet the degeneracy (or to make ΔE =0), both equalities

$$H'_{11}(\mathbf{R}) = H'_{22}(\mathbf{R}), \tag{6.4a}$$

and

$$|H'_{12}(\mathbf{R})| = 0 \tag{6.4b}$$

should be satisfied. The number s of independent equations in (6.4a) and (6.4b) is 2, 3, and 5, respectively, for real symmetric, complex Hermitian and quaternionic Hamiltonians. Hence, if $d<s$, no solution for $\mathbf{R}$ exists satisfying (6.4), and one cannot see any degeneracy except for accidental ones. For $d=s$ we can have a set of isolated degenerate points. Finally, for $d>s$ the degeneracy is not isolated, lying on a $g(=d-s)$-dimensional manifold, e.g., lines for g =1, surfaces for g =2, etc. This situation has been extensively studied by Arnold (1978) in the context of the theory on a surface of the second order (quadric): The condition for degeneracy to occur is identical to that for a given ellipsoid to become the ellipsoid of revolution.

In fully chaotic systems, we have no integral of motion other than the total energy. The corresponding quantum systems are therefore

desymmetrized at the outset. When a single quantity is vaned among $d(\geq 2)$ nonintegrability parameters, we shall see only avoided level crossings. In the semiclassical limit the level density is very high, and these avoided crossings constitute the backbone of complicated energy spectra. Below we shall examine in detail a structure of the vicinity of the avoided crossing in case of $d \geq 2$.

The eigenvalue problem (6.1) is closely related to quantum dynamics in the adiabatic limit that $\mathbf{R}$ changes very slowly as a function of time t. Let us find the corresponding adiabatic change of the electronic wavefunction $|\Psi(t)\rangle$, lying initially at by $|n(\mathbf{R}(t=0))\rangle$, investigating the time-dependent Schrödinger equation

$$i\hbar\, \mathrm{d}|\Psi(t)\rangle/\mathrm{d}t = H(\mathbf{R}(t))\,|\Psi(t)\rangle. \tag{6.5}$$

In the adiabatic limit, one may regard $\mathbf{R}$ as frozen at each moment in time. By exploiting (6.1), the solution of (6.5) is given by

$$|\Psi(t)\rangle = \exp\left[-\frac{i}{\hbar}\int_0^t E_n(t')\mathrm{d}t'\right] \cdot \exp\left[i\Gamma_n(t)\right]|n(\mathbf{R}(t))\rangle\ , \tag{6.6}$$

where $\Gamma_n(t)$, the phase that the wavefunction acquires in its adiabatic change, is defined by

$$\begin{aligned}\Gamma_n(t) &= i\int_0^t dt'\,\langle n(\mathbf{R}(t'))|\,\frac{\mathrm{d}}{\mathrm{d}t'}\,|n(\mathbf{R}(t'))\rangle \\ &= i\int_0^{\mathbf{R}(t)} \langle n(\mathbf{R}')|\nabla_{\mathbf{R}'}|n(\mathbf{R}')\rangle \cdot \mathrm{d}\mathbf{R}'\ .\end{aligned} \tag{6.7}$$

In the case $d \geq 2$, $\Gamma_n(t)$ is a path-dependent geometric phase that cannot be vanishing in general (Berry, 1984), while in the case d=1 it can always be smeared out by suitably after choosing the phase of $|n(\mathbf{R})\rangle$. This is a manifestation of the fact that eigenstates are multi-valued in the parameter space $\mathbf{R}$ in $d(\geq 2)$ dimensions, though they are single-valued in configuration space.

Let us consider a closed circuit C in $\mathbf{R}$ space (see Fig. 6.1) and introduce the fictitious gauge potential

$$\mathbf{A}_n(\mathbf{R}) = i\langle n(\mathbf{R})|\nabla_{\mathbf{R}}|n(\mathbf{R})\rangle\ . \tag{6.8}$$

For an adiabatic transport of the wavefunction along C, the geometric phase is now expressed as

$$\Gamma_n(C) = \oint \mathbf{A}_n(\mathbf{R})\cdot d\mathbf{R} = \iint_C d\mathbf{S}\cdot(\nabla_{\mathbf{R}}\times\mathbf{A}_n(\mathbf{R})) = \iint_C d\mathbf{S}\cdot\mathbf{V}_n(\mathbf{R}), \tag{6.9}$$

where $d\mathbf{S}$ denotes an area element of the surface enclosed by C, and $V_n(\mathbf{R})$ is a fictitious magnetic field defined by

$$\mathbf{V}_n(\mathbf{R}) = \mathrm{Im}\sum_{m(\neq n)} (\nabla_{\mathbf{R}}\langle n|)|m\rangle\times\langle m|\nabla_{\mathbf{R}}|n\rangle$$

$$= \mathrm{Im}\sum_{m(\neq n)} \{\langle n|\nabla_{\mathbf{R}}H(\mathbf{R})|m\rangle\times\langle m|\nabla_{\mathbf{R}}H(\mathbf{R})|n\rangle\}(E_n(\mathbf{R})-E_m(\mathbf{R}))^{-2}. \tag{6.10}$$

[The vector products in (6.9) and (6.10) follow Berry's paper (1984). They should be rewritten in general in terms of exterior differentials.] The form (6.10) indicates that $\mathbf{V}_n(\mathbf{R})$ is singular at degenerate points. For the case $d(\geq 2)$, the parametric change of an energy eigenvalue

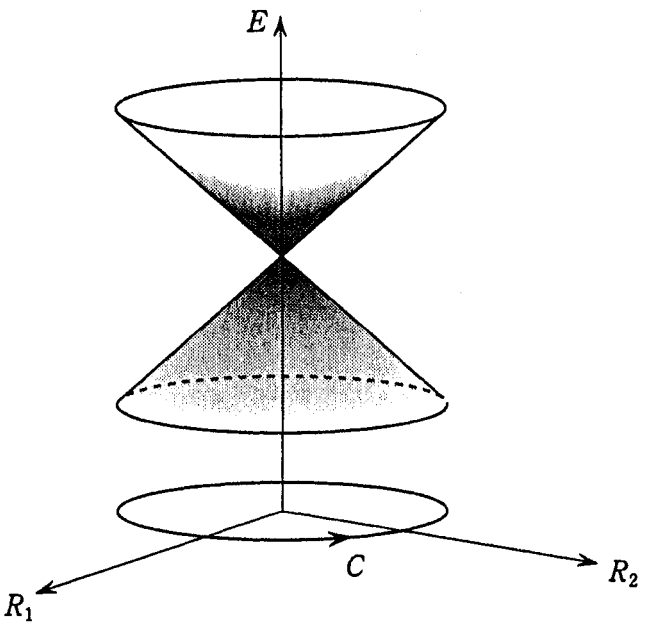

Fig. 6.1. Conical intersection of a pair of energy surfaces and closed path C.

constitutes not a line but a surface. The crossing point of a pair of adjacent energy surfaces is topologically singular and generating the fictitious gauge potential.

As a concrete example, let us take a model of a spin in the magnetic field ($\mathbf{R}=(X, Y, Z)$) described by an $SU(2)$ complex Hermitian Hamiltonian

$$H(\mathbf{R}) = \varepsilon I + \tfrac{1}{2}\ \boldsymbol{\sigma}\cdot\mathbf{R}, \tag{6.11}$$

where I and $\boldsymbol{\sigma}=(\sigma_x,\sigma_y,\sigma_z)$ denote the unit matrix and Pauli matrices, respectively. In this example, $d=s=3$. A pair of energy surfaces (eigenvalues) are represented by

$$E_{\pm}(\mathbf{R}) = \varepsilon \pm \tfrac{1}{2}(X^2 + Y^2 + Z^2)^{1/2}, \tag{6.12a}$$

and they are conically intersected at the diabolical point $\mathbf{R}=0$ (see Fig. 6.1). In terms of polar coordinates defined by $R=(\sin\theta\cos\phi,\ \sin\theta\sin\phi,\ \cos\theta)$, the corresponding eigenstates are given by

$$|\pm\rangle = e^{i\phi}\begin{pmatrix}\cos(\theta/2)\\ \sin(\theta/2)\end{pmatrix}|\uparrow\rangle + \begin{pmatrix}\sin(\theta/2)\\ -\cos(\theta/2)\end{pmatrix}|\downarrow\rangle, \tag{6.12b}$$

where $\sigma_z|\uparrow\rangle=|\uparrow\rangle$, $\sigma_z|\downarrow\rangle=-|\downarrow\rangle$. Substituting (6.12) into (6.10), we have

$$\mathbf{V}_{\pm}(\mathbf{R}) = (\pm 1/2)\mathbf{R}/R^3. \tag{6.13}$$

This is equivalent to a magnetic field induced by a monopole at $\mathbf{R}=0$ with charge $\pm 1/2$. Using (6.13) in (6.9), the geometric phase is given by $\Gamma_{\pm}(C) = \mp\Omega/2$, where Ω is the solid angle for the view of circuit C as seen from the degeneracy. When C encloses (with any plane circle including $\mathbf{R}=0$) the degeneracy, $\Omega = \pm 2\pi$; otherwise, $\Omega=0$. In the former case, $\exp\{i\Gamma_{\pm}(C)\} = -1$, which changes the sign of the eigenstates.

The phase (6.9) is a manifestation of a holonomy (i.e., failure of some variables to return to their original values after a cyclic change of other variables) for the parallel transport of quantum eigenstates (unit vectors) in parameter space (see Fig. 6.2). In the field of quantum chemistry, vibration-rotation energies of molecules are analyzed in the Born-Oppenheimer approximation, wherein electronic quantum states are assumed to follow the change of nuclear coordinates

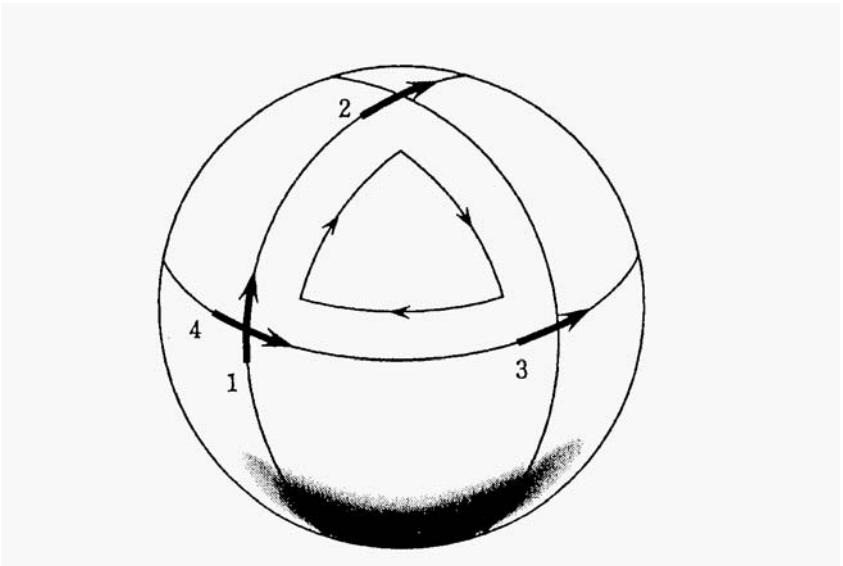

Fig. 6.2. Parallel transport of state vector along spherical surface. Path: 1 → 2 → 3 → 4.

adiabatically. Longuet-Higgins *et al.* (1958) noticed the geometric-phase-induced sign change in the electronic wavefunctions when nuclear coordinates are cycled. In the field of differential geometry, Darboux (1896) had found a similar sign change in his analysis of "umbilic points" of curved surfaces. Nevertheless, the universal gauge structure around level degeneracies was not revealed until Berry's work.

6.2. Nonadiabatic Transitions and Gauge Structure

The discovery of quantum adiabatic phase accompanying transport along closed paths has indeed had a great impact on various fields of physics and chemistry (Shapere and Wilczek, 1989). This global phase, originally discussed in connection with the intersection of molecular energy surfaces, is attributed to connections in a Hilbert bundle, i.e., to a fictitious gauge potential. This gauge structure is a consequence of the novel complex nature of the wavefunction Ψ in the time-dependent Schrödinger equation.

A generalization of the influence of the quantum adiabatic phase to

the nonadiabatic transitions is nontrivial, because we capture the local (rather than global) structure of the novel gauge potential via the transition rate. While several studies are concerned with this theme, most of the efforts have been concerned with corrections to the global geometric phase factor for closed or near-closed paths (Aharonov and Anandan, 1987; Moor, 1991; Wu and Kuppermann, 1993).

Nonadiabatic transitions, however, occur widely for both open and closed paths and they provide a key to understanding a variety of state-changing phenomena, e.g., two-level dynamics in the presence of magnetic and/or electric fields, atomic and molecular collisions, Zener tunneling, etc. (Dykhne, 1962; Mott and Massey, 1965; Pechukas, 1969; Miller and George, 1972; Child, 1974; Hwang and Pechukas, 1977; Nikitin and Umanskii, 1984). This kind of transition is induced at the avoided crossings of the potential surfaces.

In this section, we consider nonadiabatic transitions between a pair of states as a mechanism for nonadiabatic transport along open paths. In particular, following Nakamura and Rice (1994), we show the influence of the fictitious gauge potential on the transition rate. Although we use, as a prototype, the dynamics of a single spin in the presence of a time-dependent magnetic field, the present analysis is applicable to other systems, e.g., two-level systems subjected to time-dependent laser fields.

In the magnetic field $\mathbf{B}(t) = (B_x(t), B_y(t), B_{//}(t))$, the spin dynamics is described by the Schrödinger equation, $i\hbar\, d\Psi/dt = H(\mathbf{B}(t))\Psi$, with

$$H(\mathbf{B}(t)) = \frac{1}{2}\sigma \bullet \mathbf{B}(t) = \frac{1}{2}\begin{pmatrix} B_{//}(t) & B_x(t) - iB_y(t) \\ B_x(t) + iB_y(t) & -B_{//}(t) \end{pmatrix}, \qquad (6.14)$$

where the negative of the Bohr magneton μ_B has been suppressed for simplicity. With the choice $B_{//} = vt$, $B_x = \Gamma$, and $B_y = 0$, we obtain the Landau-Zener (or curve-crossing) model. Here both B_x and B_y are assumed nonvanishing and time-dependent: B(t) executes a winding (besides a translational) motion. We shall evaluate the transition amplitude from one adiabatic state at $t = -\infty$ to another at $t = +\infty$.

First we briefly summarize the existing formula (Berry, 1990) for the transition rate in the presence of winding motion. With the use of adiabatic bases $\Psi_1(t)$ and $\Psi_2(t)$, $\Psi(t)$ is written as $\Psi(t) = C_1(t)\Psi_1(t) + C_2(t)\Psi_2(t)$ and the Schrödinger equation is reduced to

$$i\hbar\dot{C}_1 = (E_1(t) - A_1(t))C_1 - i\hbar\langle\Psi_1 \mid \dot{\Psi}_2\rangle C_2 ,$$

$$i\hbar\dot{C}_2 = (E_2(t) - A_2(t))C_2 - i\hbar\langle\Psi_2 \mid \dot{\Psi}_1\rangle C_1 , \qquad (6.15)$$

with

$$A_i = i\hbar\langle\Psi_i \mid \dot{\Psi}_i\rangle , \qquad i=1, 2 , \qquad (6.16)$$

where overdots denote time derivative, the $\{E_i\}$ are the eigenvalues of H in (6.14) at particular times (adiabatic energies), and the $\{A_i\}$ are (mutually different) fictitious gauge potentials. In our notation, i =1 and 2 are associated with the lower and higher energy states, respectively. This gauge structure leads to a novel geometric phase for adiabatic transport along closed paths. As for nonadiabatic transport, use of the path-integral method and the stationary phase approximation leads to the following transition rate for a single passage of the avoided crossing: p=exp(−2δ) with

$$\delta = \frac{1}{\hbar}\mathrm{Im}\int_0^{t_c} dt(\Delta E(t) - \Delta A(t)) , \qquad (6.17)$$

where $\Delta E = E_2 - E_1$, $\Delta A = A_2 - A_1$, and t_c is the complex crossing point at which ΔE vanishes (Berry, 1990). According to the rigorous treatment given below, however, the gauge potentials enter into the phase integral in a much more intricate way, and (6.17) is valid only in a very special limit.

We now examine the quantum dynamics for the Hamiltonian (6.14) using a diabatic (time-independent) basis. Transforming to polar coordinates defined by $B_x(t) - iB_y(t) = B_\perp(t)\exp(-i\Phi(t))$ and introducing the unitary transformation

$$U(t) = \begin{pmatrix} e^{-i\Phi/2} & 0 \\ 0 & e^{i\Phi/2} \end{pmatrix} ,$$

we introduce a new wavefunction $\tilde{\Psi}$ defined by $\Psi = U\tilde{\Psi}$. Then $\tilde{\Psi}$ satisfies

$$i\hbar d\tilde{\Psi}/dt = \tilde{H}(t)\tilde{\Psi} = \frac{1}{2}\begin{pmatrix} B_{//} - \hbar\dot{\Phi} & B_\perp \\ B_\perp & -(B_{//} - \hbar\dot{\Phi}) \end{pmatrix}\tilde{\Psi} . \qquad (6.18)$$

The transformed Hamiltonian $\tilde{H}$ given by (6.18) is now analytic throughout some strip of the complex-time plane centered on the real axis, and it satisfies $I\,\tilde{H}_{12}\,|/|\,\tilde{H}_{22}-\tilde{H}_{11}\,|\to 0$ for $|t|\to\infty$ (i.e., absence of mixing between diabatic states). In this situation we can apply the phase-integral method (Stückelberg, 1932; Crothers, 1971), obtaining for the full transition rate

$$P = 4p(1-p)\sin^2(\bullet\bullet\bullet)$$

with the single-passage rate $p = \exp(-2\delta)$. (We are not interested in the phase-interference factor, $\sin^2(\bullet\bullet\bullet)$, proper to the passage of successive avoided crossings.) δ is now given by

$$\delta = \frac{1}{\hbar}\,\mathrm{Im}\int_0^{\hat{t}_c} dt(\Delta\hat{E}(t))\,, \tag{6.19}$$

where

$$\Delta\hat{E} = \sqrt{\{(B_{//}-\hbar\dot{\Phi})^2 + B_\perp{}^2\}} = \sqrt{(B_{//}{}^2 + B_\perp{}^2 - 2\hbar\dot{\Phi}B_{//} + \hbar^2\dot{\Phi}^2)}\,, \tag{6.20}$$

i.e., the difference between adiabatic energies of $\tilde{H}$ in (6.18). Note that $\hat{t}_c$ is the complex crossing point $(\Delta\hat{E}(\hat{t}_c)=0)$ nearest to real axis.

Equations (6.19) and (6.20) are exact. In the near-adiabatic region of the winding Landau-Zener model, $B_\perp\,(=\Gamma)$ is constant and predominant, whereas Φ and $B_{//}$ are slow and small variables in the transition region near the avoided crossing. In this extreme case, (6.20) is expanded in one of the slowest variables as

$$\Delta\hat{E} \sim \sqrt{B_\perp{}^2 + B_{//}{}^2} - \hbar\dot{\Phi}B_{//}\Big/\sqrt{B_{//}{}^2 + B_\perp{}^2} + O(\hbar^2\dot{\Phi}^2),\ \text{for}\ \hbar\dot{\Phi} << B_{//}\,, \tag{6.21a}$$

and

$$\Delta\hat{E} \sim \sqrt{B_\perp{}^2 + \hbar^2\dot{\Phi}^2} + O(B_{//})\,,\ \text{for}\ \hbar\dot{\Phi} >> B_{//}\,. \tag{6.21b}$$

The corresponding expansion of $\hat{t}_c$ will follow in the integration (6.19).

While the results in (6.19) - (6.21) are derived using the diabatic basis, we now rewrite them in terms of the adiabatic basis: Definition (6.16) yields $\Delta A = A_2 - A_1 = \hbar\Phi B_{//}/\Delta E$ and $\Sigma A = A_2 + A_1 = \hbar\Phi$, with $\Delta E = (B_\perp{}^2 + B_{//}{}^2)^{1/2}$. Using these expressions in (6.20), we have

$$\Delta\hat{E} = \sqrt{(\Delta E^2 - 2\Delta A\Delta E + (\Sigma A)^2)}\,. \tag{6.22}$$

With the same replacement in (6.21), the asymptotic behavior is given by

$$\Delta\hat{E} \approx \begin{cases} \Delta E - \Delta A, & \text{for } \hbar\dot{\Phi} << B_{//}, \quad (6.23a) \\ \sqrt{B_{\perp}^{\,2} + (\Sigma A)^2}, & \text{for } \hbar\dot{\Phi} >> B_{//}, \quad (6.23b) \end{cases}$$

with $\hat{t}_c$ approximated by the values at which ΔE and $\sqrt{B_{\perp}^{\,2} + (\Sigma A)^2}$ vanish in (6.23a) and (6.23b), respectively. Therefore (6.17) is justified in the special limit when the winding motion is much slower than the translational motion. In the opposite limit, the sum of gauge potentials is needed and, in the general case, we should use (6.22).

We shall now apply the results in (6.19), (6.22), and (6.23) to a winding Landau-Zener (curve crossing) model where $B_{//} = vt$, $B_x = \Gamma\cos\Phi$, and $B_y = \Gamma\sin\Phi$, with $\Phi = wt^n/n$ (n=1,2,• • •). For simplicity, v, Γ and w are assumed positive. Below we shall use $\Delta E = [\Gamma^2 + (vt)^2]^{1/2}$, irrespective of the value of n.

Case of *n*=1. In this case, the Galilean transformation $(t \rightarrow t' = t - \hbar w/v)$ smears out the phase factor, so that there is no gauge structure and the ordinary Landau-Zener transition rate $p_{LZ} = \exp[-\pi\Gamma^2/(2\hbar v)]$ is applicable

Case of *n*=2. Using in (6.23) $\Delta A = \hbar v w t^2/\Delta E$ and $\Sigma A = \hbar wt$, we find, from (6.19),

$$\delta = \begin{cases} (\pi\Gamma^2/(4\hbar v))(1 + \hbar w/v), & \text{for } \hbar w << v, \quad (6.24a) \\ \pi\Gamma^2/(4\hbar^2 w), & \text{for } \hbar w >> v. \quad (6.24b) \end{cases}$$

With the same expression for gauge potentials in (6.22), (6.19) with $\hat{t}_c = i\Gamma/|v - \hbar w|$ yields $\delta = \pi\Gamma^2/(4\hbar|v - \hbar w|)$, which recovers the two limits in (6.24). While Berry carefully analyzed the n=2 case, he was mainly concerned with (6.23a) and (6.24a), showing neither (6.22) nor (6.23b).

Case of *n*=3. In this case, $\Delta A = \hbar wvt^3/\Delta E$ and $\Sigma A = \hbar wt^2$. The formula in (6.17) or (6.23a) here yields no correction to the Landau-Zener's result, since the integration of ΔA does not have any imaginary component. On the other hand, from (6.23b) we have δ=0.61 x $(\Gamma^8/(\hbar^3 w))^{1/2}$. In terms of a scaled time τ, the most general result available from (6.22) is

$$\delta(\varepsilon) = (\Gamma^3/(\hbar^3 w))^{1/2}\,\mathrm{Im}\int_0^{\tau_c}[(\tau^2-\varepsilon)^2+1]^{1/2}\,d\tau\ ,$$

with $\varepsilon = v^2/(4\Gamma\hbar w)$ and $\tau_c = (\varepsilon+i)^{1/2}$. Noting the asymptotic expansions $\delta(\varepsilon)/(\Gamma^3/\hbar^3 w)^{1/2} \quad (\pi/8\varepsilon^{1/2})[1 - 3/(32\varepsilon^2) \quad 565/(2^{14}\varepsilon^4) + \cdots]$ for $\varepsilon >>1$, and $\sim 0.61-0.42\varepsilon$, for $\varepsilon <<1$, we get

$$p = p_{LZ}\cdot\exp\{(3\pi\hbar w^2\Gamma^4/4v^5)[1-(565/1536)(4\hbar w\Gamma/v^2)^2+\cdots]\} \qquad (6.25a)$$

and

$$p = \exp\{-2(\Gamma^3/\hbar^3 w)^{1/2}[0.61 - 0.42v^2/(4\hbar w\Gamma)+\cdots]\}\,, \qquad (6.25b)$$

for $4\hbar w\Gamma << v^2$ and $4\hbar w\Gamma >> v^2$, respectively.

The asymptotic behaviors in (6.25) are in excellent agreement with an envelope of the full transition rate $P(\cong 4p)$ in Fig. 6.3 obtained by our numerical iteration of the time-dependent Schrödinger equation (6.14) for n=3. (Spiking oscillations in P are attributed to the multiplicative phase-interference factor in the equation above (6.19).)

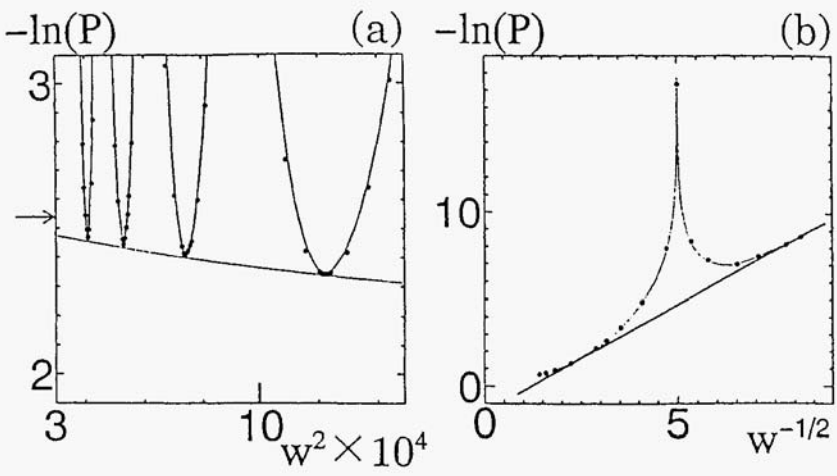

Fig. 6.3. Full transition rate P for the winding Landau-Zener model with $\hbar$=1 and Γ=1. Filled circles denote values obtained by numerical iteration of (6.14): (a) $4\hbar w\Gamma << v^2$ with v=0.4, (b) $4\hbar w\Gamma >> v^2$ with v=0. Envelope lines in (a) and (b) represent $-\ln P = -2\ln 2 - \ln(p)$ with p in (6.25a) and (6.25b), respectively. The arrow in Fig. 6.3(a) corresponds to the limit $p=p_{LZ}$.

We here assert: (i) Even when the winding motion is slower than the translational motion, the existing formula (6.17) fails in providing a leading-order correction to p_{LZ}. (ii) In the opposite case, the formula in (6.23b), consisting only of a sum of gauge potentials, can give accurate leading-order values for the transition rate. (iii) In general, (6.22) indicates the transition rate depends on the difference and sum of a pair of gauge potentials in intricate ways, according to the adiabaticity ratio of the winding and translational motions.

The present formula in (6.22) and (6.23), with a slight modification, can also be used in other winding models in the near-adiabatic region. Consider, for instance, a winding Demkov (exponential) model (Demkov, 1964) with $B_{//} = \Gamma$, $B_{\perp} = \gamma \cos\kappa \cdot \exp(-vt)$, and $\Phi(t) = (\gamma/\hbar v)$ $\sin\kappa \cdot \exp(-vt)$ in the case $\hbar v << \Gamma$. Interchanging $B_{//}$ and $B_{\perp}$, the formulas from (6.21) through (6.23) still hold; this interchange comes from the predominance of $B_{//}$ in this model. Noting the gauge potentials

$$\Delta A = -\Gamma\gamma \sin\kappa \cdot \exp(-vt)/\Delta E$$

and

$$\Sigma A = -\gamma \sin\kappa \cdot \exp(-vt)$$

with

$$\Delta E = (\Gamma^2 + \gamma^2 \cos^2\kappa \cdot \exp(-2vt))^{1/2},$$

we have, from (6.23) and (6.22),

$$p/p_{\text{Demk}} = \begin{cases} \exp[-\pi\Gamma\kappa/(\hbar v)], & \text{for } \kappa << \pi/2, \quad (6.26a) \\ \exp[-\pi\Gamma/(\hbar v)], & \text{for } \kappa \sim \pi/2, \quad (6.26b) \end{cases}$$

and

$$p/p_{\text{Demk}} = \exp[-\pi\Gamma \sin\kappa/(\hbar v)], \quad (6.27)$$

respectively, where $p_{Demk} = \exp[-\pi\Gamma/(\hbar v)]$. [Due to a finite mixing of diabatic states in the limit $t \to -\infty$, the exact expression for a single passage transition rate in the winding Demkov model is $p=(1+e^{2\delta})^{-1}$, which, however, reduces to a standard form $p=e^{-2\delta}$ in a near-adiabatic regime.] The winding Demkov model, after a unitary transformation (6.18), turns out the exactly solvable Nikitin's model (1970), whose known solution justifies (6.26) and (6.27) in the near-adiabatic region.

In conclusion, when the applied magnetic and/or electric fields show

time dependence in both amplitude and polarization vector, the local aspect of the gauge potentials greatly affects the intersection of adiabatic energy surfaces. The formula for nonadiabatic transition rate includes a pair of gauge potentials in intricate ways, depending on the ratio of the adiabaticities of the winding and translational motions of applied fields.

Experimental Evidence

The interference in transitions due to local geometric phases has been observed by Bouwmeester *et al.* (1996). They chose an optical system in which the polarization dynamics of the light can be described by a Schrödinger-like equation. Two optical levels are formed by two orthogonal polarization eigenstates of a single longitudinal mode of a ring cavity. The two adiabatic eigenstates are determined by three birefringent elements in the form of electro-optic modulators (EOMs) placed inside the optical cavity. The birefringences form *X, Y,* and *Z* coordinates of the parameter space and are controlled by time-dependent electric voltages applied to EOMs. The cavity decay time (~μs) is long enough to complete the whole process of measurement. The dynamics

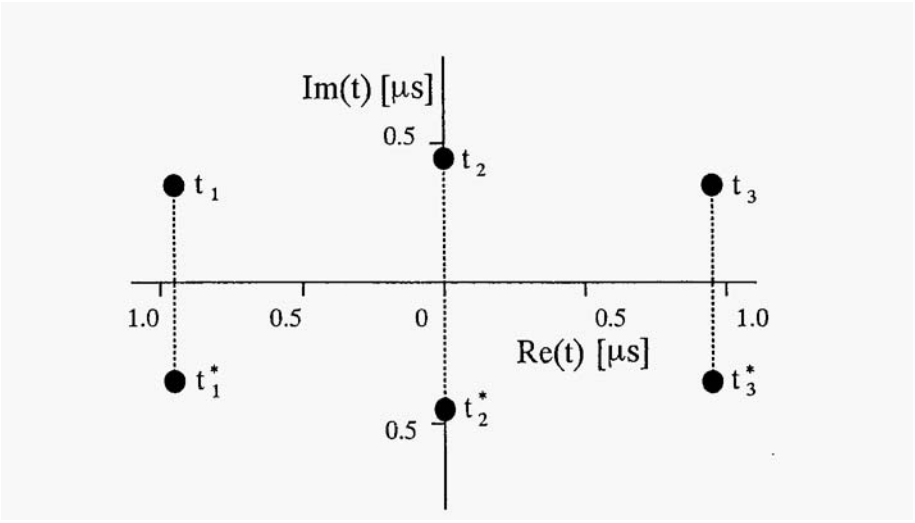

Fig. 6.4. Three pairs of branching points that dominate the transition phenomena for Gaussian twisted Landau-Zener model. α=0.44MHz/μs, Δ=0.33MHz, σ=1 μs and μ=5.4 rad. These parameter values are also used in Fig. 6.5. (Courtesy of D. Bouwmeester *et al.*)

of the intracavity field is measured by analyzing the polarization of light that leaks out through the cavity mirrors.

Bouwmeester *et al.* have examined the case of Gaussian twisted Landau-Zener (LZ) model by taking in (6.18) $B_{//}/2=\alpha t, B_{\perp}/2=\Delta$ and the phase function $\Phi(t)=\mu(1-\exp(-(t/\alpha)^2))$. The transition probability, being dominated by three pairs of branch points (see Fig. 6.4), is expected to show interference phenomena between successive avoided crossings. The approximately analytical expression for the transition probability P as a function of the adiabatic parameter $\Lambda(=\alpha/(2\pi\Delta^2))$ can be obtained by using the methodology described so far. The most essential issue is the presence of a local minimum in P for the twisted LZ model, which is a clear indication of interference between the branch points.

Figure 6.5 shows the time trace of the normalized intensity of +

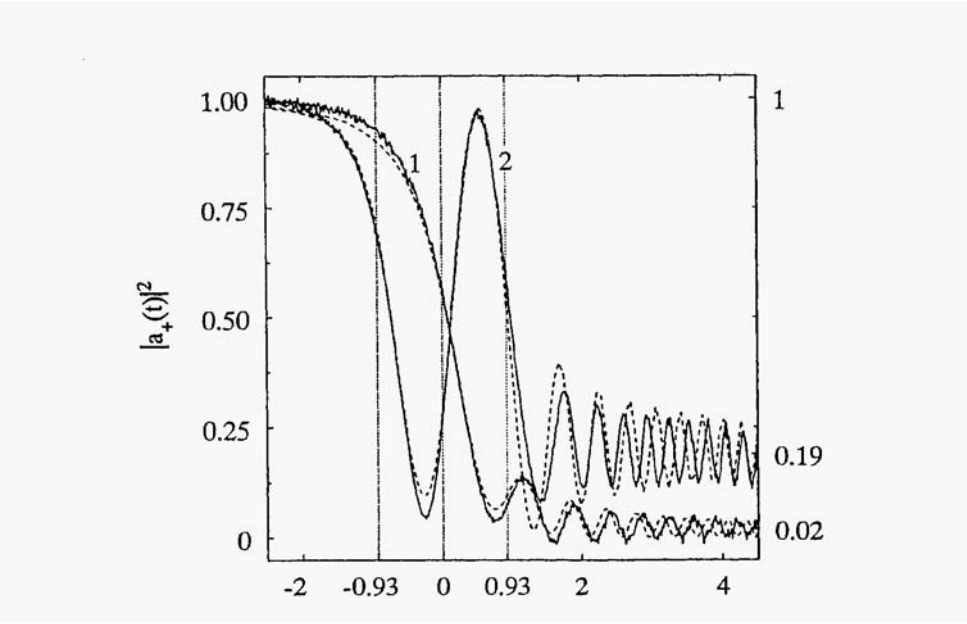

Fig. 6.5. Experimental results: curve 1 shows the time trace of $|a_+(t)|^2$ for the conventional Landau-Zener model with α=0.44MHz/μs, Δ=0. 33MHz; curve 2 shows the time trace for Gaussian twisted Landau-Zener model. Dotted curves are the corresponding traces obtained by numerical simulations. Vertical dotted lines indicate the time positions corresponding to real parts of branching points in Fig. 6.4. (Courtesy of D. Bouwmeester *et al.)*

polarization $|a_+(t)|^2$. Curve 1 is the experimental result of the ordinary LZ model in the near-adiabatic region. The oscillation after the avoided crossing at t=0 is caused by the strong mixing between + and - polarizations (i.e., a pair of adiabatic eigenstates) in the crossing region. Curve 2 is for the Gaussian twisted LZ model, indicating the influence of the three pairs of branch points in Fig. 6.4. In fact the intensity $|a_+(t)|^2$ shows radical changes at t=0 and t=± 0.93 μs which are just the real parts of the branch points in Fig. 6.4. The dotted curve is a numerically computed one which is in good agreement with the experimental issue.

Figure 6.6 shows the final transition probability P between the adiabatic energy levels as a function of the adiabatic parameter Λ. A good agreement between the experimental data and numerical and approximate-analytical results. The key point is the presence of the

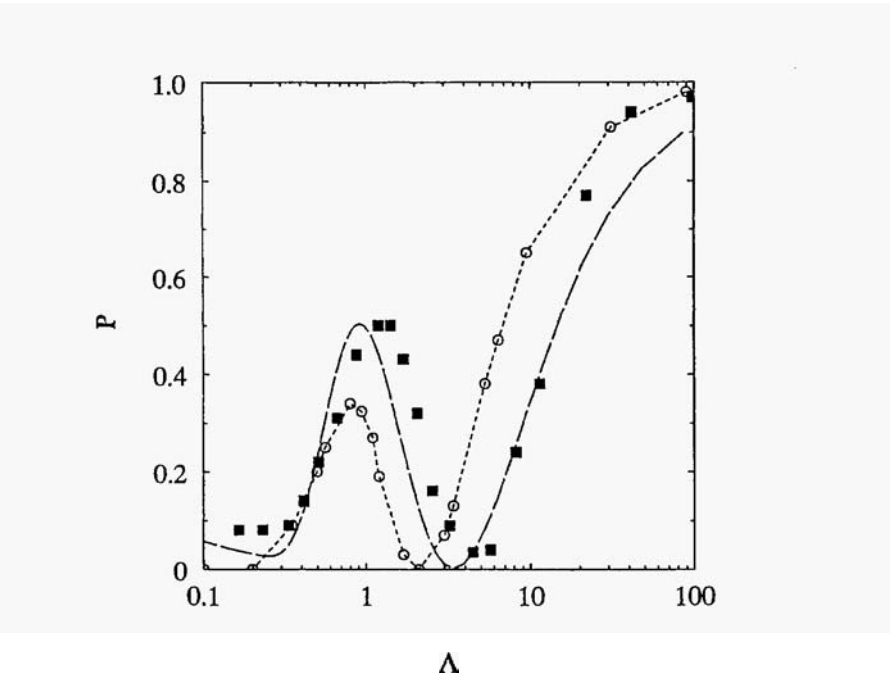

Fig. 6.6. Square points are experimental values for final transition amplitude P as a function of adiabatic parameter Λ. During the parameter change, α=0.49MHz /μs, α=0.72μs and μ=3.0rad are kept fixed. Dashed curve is the corresponding numerical result. Circles connected by dotted curve are the corresponding analytical results obtained by taking into account three pairs of branching points in Fig. 6.4. (Courtesy of D. Bouwmeester *et al.*)

minimum caused by the interference phenomena. In this way we can really observe local aspects of the gauge structure around the avoided level crossings.

6.3. Forces Induced by Born-Oppenheimer Approximation

We have demonstrated that many diabolos and avoided level crossings appear in energy spectra of the classically-chaotic systems and that they induce the fictitious gauge potential in the adiabatic limit when external parameters are taken as frozen at each time. What phenomena are expected if the external parameters are slowly-varying variables like nuclear coordinates, rather than electric or magnetic fields?

In studying the complex dynamics in microscopic cosmos, one encounters situations where a light (electronic) system with fast variables is coupled to a heavy (nuclear) system with slow variables. Since the dynamics of the whole system is quite complicated and hard to analyze, we separate fast from slow variables noting the difference in time scale of dynamical variables. Below *we shall treat fast and slow degrees of freedom in terms of quantum and classical variables, respectively.* An adiabatic approximation is first to solve the motion of fast variables for frozen values of slow variables and then to elucidate the slow dynamics under the averaged environment of the first motion. This approximation is called as the Born-Oppenheimer approximation (see also Messiah (1959)). The averaged energy of the fast system depends on the values of the slow variables so that its gradient w.r.t. slow variables provides a reaction force on the slow motion. We shall hereafter illustrate this point and then scrutinize the dynamics beyond the Born-Oppenheimer approximation to see chaos in quantum systems.

Suppose that Hamiltonian for molecules with slow (nuclear) **P, R** and fast (electronic) **p, r** variables is

$$H = \mathbf{P}^2/2M + \mathbf{p}^2/2m + V(\mathbf{R}, \mathbf{r}), \tag{6.28}$$

and apply the Born-Oppenheimer approximation to the complete eigenvalue problem $H\Psi = E\Psi$. For frozen **R,** the electronic system satisfies the eigenvalue problem

$$(\mathbf{p}^2/2m + V(\mathbf{R}, \mathbf{r}))\ |n;\mathbf{R}\rangle = \varepsilon_n(\mathbf{R})|n;\mathbf{R}\rangle$$

with $\varepsilon_n(\mathbf{R})$ and $|n;\mathbf{R}\rangle$ for the adiabatic eigenvalue and eigenstate of the fast (electronic) Hamiltonian, respectively .

If one chooses an eigenfunction of the whole system (6.28) in a factorized form

$$\Psi = \Phi(\mathbf{R})|n;\mathbf{R}\rangle, \tag{6.29}$$

$\Phi(\mathbf{R})$ proves to satisfy

$$[(\mathbf{P}-\mathbf{A})^2/2M + V_{\text{eff}}(\mathbf{R})]\Phi(\mathbf{R}) = E\Phi(\mathbf{R}) \tag{6.30a}$$

unless $|n;\mathbf{R}\rangle$ is degenerate. In (6.30a)

$$\mathbf{A}(\mathbf{R}) \equiv \mathrm{i}\langle n;\mathbf{R}|\nabla_{\mathbf{R}}|n;\mathbf{R}\rangle \tag{6.30b}$$

and

$$V_{\text{eff}}(\mathbf{R}) = \varepsilon_n(\mathbf{R}) + (\nabla_{\mathbf{R}}\langle n;\mathbf{R}|\nabla_{\mathbf{R}}|n;\mathbf{R}\rangle - \mathbf{A}^2)/2M \tag{6.30c}$$

are the fictitious gauge potential and effective potential, respectively. $\mathbf{A}(\mathbf{R})$ is essential in the vicinity of level crossings or conical intersections. $V_{\text{eff}}(\mathbf{R})$ consists of the adiabatic eigenvalue $\varepsilon_n(\mathbf{R})$ and corrections due to the slow motion. From (6.30), we observe that the slow variables are subject to three reaction forces (Jackiw, 1988; Berry and Robbins, 1993): (i) Born-Oppenheimer $(-\nabla_{\mathbf{R}}\varepsilon_n(\mathbf{R}))$, (ii) fictitious magnetic $(\mathbf{B}=\nabla_{\mathbf{R}} \times \mathbf{A})$, (iii) fictitious electric $(\nabla_{\mathbf{R}}\Phi(\mathbf{R}))$ in terms of the electrostatic potential $\Phi(\mathbf{R}) \equiv (\nabla_{\mathbf{R}}\langle n;\mathbf{R}|\nabla_{\mathbf{R}}|n;\mathbf{R}\rangle - \mathbf{A}^2)/2M$.

The Lagrangian corresponding to the Born-Oppenheimer Hamiltonian in (6.30) is straightforward: $L = M\mathbf{R}^2/2 + \mathbf{R}\cdot\mathbf{A} - V_{\text{eff}}(\mathbf{R})$. ($\mathbf{R}$ implies time-derivative.) The kinetic energy in (6.30a) resembles that of a charged particle in the presence of a magnetic field. Consequently, upon quantization, the slow variables should satisfy the anomalous commutation relation (Jackiw , 1988; Kuratsuji and Iida, 1988)

$$[P_i, P_j] = \mathrm{i}\hbar\varepsilon^{ijk}B_k, \tag{6.31}$$

where $\{B_k\}$ denote the components of $\mathbf{B}$. In the anomaly phenomena in modern quantum field theory, some symmetries of classical physics may disappear in corresponding quantum systems because of a symmetry-violating procedure exploited in quantum-mechanical

treatment. The relation (6.31) provides a typical example of this phenomenon.

From a viewpoint of nonlinear dynamics the system described by (6.30) has a possibility of exhibiting chaos if the number of degrees of freedom is larger than that of the constants of motion. Will slow (and consequently fast) degrees of freedom be able to demonstrate chaos with the help of reaction forces in (6.30)? Our special interest lies in the genesis of chaos in the *quantum* (electronic) system with the nuclear system left classical. Below we shall pursue this theme.

6.4. Nonadiabaticity-Induced Chaos

We shall show a significant consequence of the above discovery, by examining a concrete example exhibiting an isolated avoided crossing, i.e., a system of the Jahn-Teller type (Bulgac and Kusnezov, 1995). Denoting a two-level electronic system by σ, suppose the Hamiltonian for a prototype of molecules with (nuclear) slow and classical $\mathbf{P},\mathbf{Q}$ and (electronic) fast and quantum σ variables as given by

$$H = \mathbf{P}^2/(2M) + V(Q) + (\kappa/2)f(Q)\mathbf{Q}\cdot\sigma\ , \tag{6.32}$$

where on the r.h.s. the 2nd and 3rd terms designate the potential for slow variables and the interaction between slow and fast variables, respectively; κ is a coupling parameter and $f(Q)$ is a form factor. In terms of the density operator ρ, let the expectation value of σ be written as $\mathrm{Tr}(\rho\sigma) = \mathbf{r} = (x, y, z)$. Then ρ can be expressed by

$$\rho = (1/2)\begin{pmatrix} 1+z & x-iy \\ x+iy & 1-z \end{pmatrix}\ . \tag{6.33}$$

While $\rho^2=\rho$ in a pure state, the unequality $\rho^2<\rho$ is satisfied in general for mixed states.

The equation of motion for the system (6.32) can be derived from the Lagrangian

$$L = \mathbf{P}\cdot\dot{\mathbf{Q}} + z(x\dot{y}-y\dot{x})/(2(x^2+y^2)) - \{\mathbf{P}^2/(2M) + V(Q) + (\kappa/2)f(Q)\mathbf{Q}\cdot\mathbf{r}\}. \tag{6.34}$$

The first two terms represent canonical terms for slow and first

variables. Euler-Lagrange equation for (6.34) yields

$$\mathrm{d}\mathbf{Q}/\mathrm{d}t = \mathbf{P}/M, \tag{6.35a}$$

$$\mathrm{d}\mathbf{P}/\mathrm{d}t = -\mathrm{d}V(Q)/\mathrm{d}\mathbf{Q} - (\kappa/2)(\partial f(Q)/\partial \mathbf{Q})\mathbf{Q}\cdot\mathbf{r} - (\kappa/2)f(Q)\mathbf{r}, \tag{6.35b}$$

$$\mathrm{d}\mathbf{r}/\mathrm{d}t = \kappa f(Q)\mathbf{Q}\times\mathbf{r}. \tag{6.35c}$$

Equation (6.35c) is identical with the Schrö dinger equation i$\mathbf{p}$/dt = [H, $\mathbf{p}$]. The set of Eqs.(6.35) has the following constants of motion:

$$r = (x^2 + y^2 + z^2)^{1/2}, \tag{6.36a}$$

$$E = \mathbf{P}^2/(2M) + V(Q) + (\kappa/2)f(Q)\mathbf{Q}\cdot\mathbf{r}, \tag{6.36b}$$

$$\mathbf{J} = \mathbf{Q}\times\mathbf{P} + \mathbf{r}/2. \tag{6.36c}$$

The conservation of r reflects the normalization condition for the electronic wavefunction Ψ: r=1 and r<1 for pure and mixed states, respectively.

Before numerical iteration of (6.35) with (6.36), we shall see the results of the adiabatic approximation. In this approximation, one assumes the quantum system to remain in either one of the instantaneous eigenstates ((6.37b) below) of the Hamiltonian (6.32) with $\mathbf{P}$=0 and $\mathbf{Q}$ fixed, which renders $\mathbf{Q}\cdot\mathbf{r} = \pm Q$ with r =1. The resulting Lagrangian for slow variables is then obtained, by using $\mathbf{r} = \pm \mathbf{Q}/Q$ in (6.34), as

$$L_{\mathrm{BO}} = [\mathbf{P}\cdot\dot{\mathbf{Q}} \pm Q_z(Q_x\dot{Q}_y - Q_y\dot{Q}_x)/(2(Q_x^2 + Q_y^2)\sqrt{Q_x^2 + Q_y^2 + Q_z^2})] - [\mathbf{P}^2/(2M) + V_{\pm}(Q)], \tag{6.37a}$$

with

$$V_{\pm}(Q) = V(Q) \pm (\kappa/2)f(Q)Q. \tag{6.37b}$$

Equation (6.37b) represents a pair of adiabatic potential surfaces with a Mexican-hat shape for the lower one (see Fig. 6.7).

The adiabatic equation of motion is derived from (6.37) as

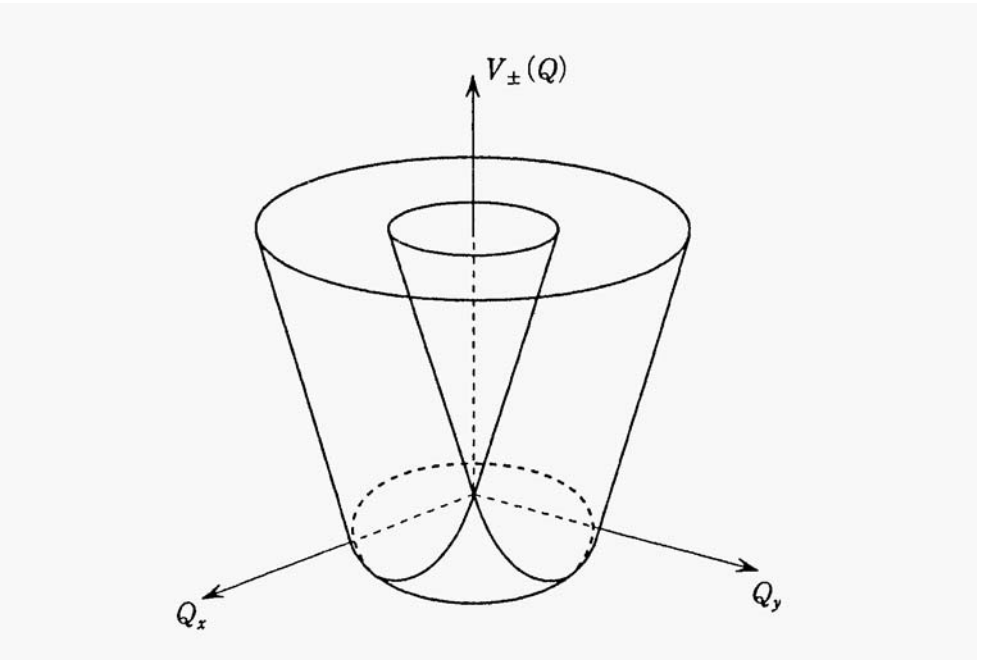

Fig. 6.7. Adiabatic potential for Jahn-Teller system.

$$d\mathbf{Q}/dt = \mathbf{P}/M, \tag{6.38a}$$

$$d\mathbf{P}/dt = -\partial V_{\pm}(Q)/\partial \mathbf{Q} \mp (\mathbf{Q}\times\mathbf{P})/(2MQ^3)\,. \tag{6.38b}$$

On the r.h.s. of (6.38b), the first and second terms represent, respectively, the Born-Oppenheimer force and the induced magnetic force arising from the Dirac monople (i.e,, conical intersection of energy surfaces) at the origin Q=0. Other induced forces are suppressed here coming from corrections higher order w.r.t. the adiabaticity parameter. While the induced magnetic force has a highly nonlinear feature, the total number of constants of motion (i.e., E and $\mathbf{J}$ in (6.36) with $\mathbf{r} = \pm\,\mathbf{Q}/Q$) is 4, rendering the effective phase space dimensionality for $\mathbf{P}$ and $\mathbf{Q}$ to 2(=6–4). Since the minimum dimension necessary to see chaos is 3, orbits predicted by (6.38) execute only regular motions along the absolute minimum of the Mexican-hat potential (6.37b), indicating no signature of chaos. Despite the highly nonlinear nature of the reaction forces, therefore, the adabatic or Born-Oppenheimer approximation suppress a symptom of chaos.

Bulgac and Kusnezov (1995), however, pointed out that the *dynamics beyond the adiabatic approximation* can lead to a genesis of chaos in quantum systems, which will be described below. We shall treat separately the closed system with the slow degree of freedom confined to a finite area and the open scattering system.

Chaos in a Bounded System

To solve the equation of motion in (6.35) beyond the adiabatic approximation, we should specify the model by taking a harmonic potential $V(Q) = Mw^2Q^2/2$ and a unit form factor $f(Q) = 1$. After additional scaling ($M = w = 1$), (6.35) becomes

$$d\mathbf{Q}/dt = \mathbf{P}, \tag{6.39a}$$

$$d\mathbf{P}/dt = -\mathbf{Q} - (\kappa/2)\mathbf{r}, \tag{6.39b}$$

$$d\mathbf{r}/dt = \kappa\mathbf{Q}\times\mathbf{r}. \tag{6.39c}$$

The nonlinearity is obvious on the r.h.s. of (6.39c) describing the torque on **r**. The system in (6.39) has 9 dynamical variables and 5 integrals of motion in (6.36). Therefore the effective phase space dimensionality is 9−5=4. For strong enough coupling κ and in most of the energy ranges other than the vicinity of the bottom of Mexican-hat potential $(V_(Q) = (Q - \kappa/2)^2/2 - \kappa^2/8)$, the trajectories of the slow variables are chaotic. The electronic variable, namely, the density matrix shows a fully ergodic behavior (see Fig. 6.8) at the same time. This outbreak of chaos in the quantum (electronic) system is not a mere reflection of chaos in the slow degree of freedom but attributed to the nonlinear interaction involved in (6.39c).

Chaos in an Open System

While the above result is interesting enough, the problem is limited to the bounded system with a harmonic potential. One can also discuss an anomalous nonadiabatic transition by choosing the potential with a finite-height barrier which allows scattering phenomena. Consider, for instance, an incident atom A to be scattered by a target atom B fixed at the origin. The electronic (quantum) system of the atom B and the (classical) nucleus of the atom A correspond to fast and slow degrees of freedom, respectively. In (6.32), we choose

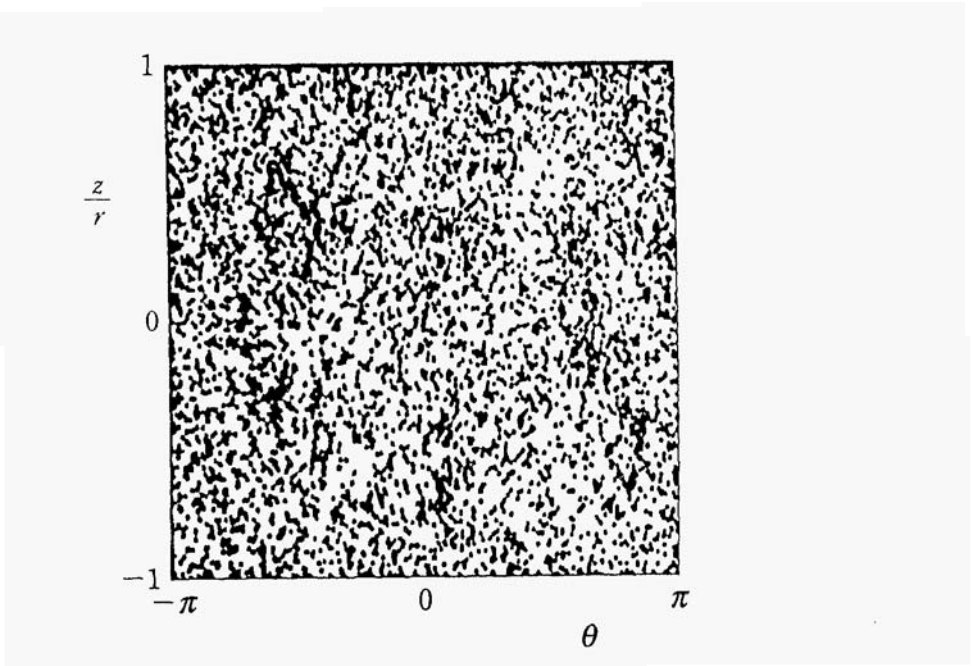

Fig. 6.8. Poincare' section for the density matrix **p**; θ and z are defined by $\mathbf{r}=((r^2-z^2)^{1/2}\cos\theta(r^2-z^2)^{1/2}\sin\theta,z)$; κ =5. (Courtesy of A. Bulgac and D. Kusnezov.)

$$V(Q) = V_0 \exp(-Q^2/(2Q_0^2)) \ , \tag{6.40a}$$

$$f(Q) = \tanh(Q)/Q \ . \tag{6.40b}$$

This model yields a conical intersection near the origin and, far from the origin, a pair of nondegenerate levels. In fact, using (6.40) in (6.32), one obtains the two adiabatic potential energy surfaces

$$V_{\pm}(Q) = V(Q) \ \pm \ (\kappa/2)\tanh(Q) \ , \tag{6.41}$$

which are reduced to $\pm \kappa/2$ in the limit $Q \to \infty$ and crosses mutually at Q=0.

Let us now launch a particle towards the center from downward (Q_z<O) with tunable impact parameter b (>0). We choose $\mathbf{Q}(t=0) = (b, 0, -100)$ and $\mathbf{P}(t=0) = (0, 0, P_0)$ with P_0>0 as an initial condition. By solving (6.35) with (6.36) exactly beyond the adiabatic approximation, the interaction between quantum (electronic) and classical (nuclear) degrees of freedom will ensure the occurrence of chaotic motion.

Figure 6.9 demonstrates the b dependence of the time during which the nucleus stays in the interaction region. The complicated spectrum reflects the sensitivity to b, a feature proper to chaotic scattering. Figure 6.10 displays the z component of the final momentum $P_z(t=\infty)$ as a function of the initial electronic state of $\mathbf{r}(t=0)=(r\cos\theta_{in}, r\sin\theta_{in}, 0)$. Its fractal feature is obvious. The P_0 dependence of the transition probability $Pr=|z(t=\infty)|^2$ is also pointed out to exhibit a fractal aspect, in contrast to a monotonous feature in the case of Landau-Zener transition described in the previous section.

In this way, so long as systems with a few degrees of freedom are concerned, we may conclude: In the adiabatic limit when the time scales between slow and fast degrees of freedom are extremely different, the reaction (e.g., virtual magnetic and electric fields) is indeed exerted on the slow degree of freedom, but quantum dynamics cannot exhibit chaos. In the dynamics beyond the adiabatic approximation, however, we can see a genesis of chaos in the *quantum (electronic) system* or the genuine quantum chaos in both bounded and open systems.

From a viewpoint of nonlinear (classical) dynamics, most of molecular kinetics in the microscopic cosmos have the possibility to

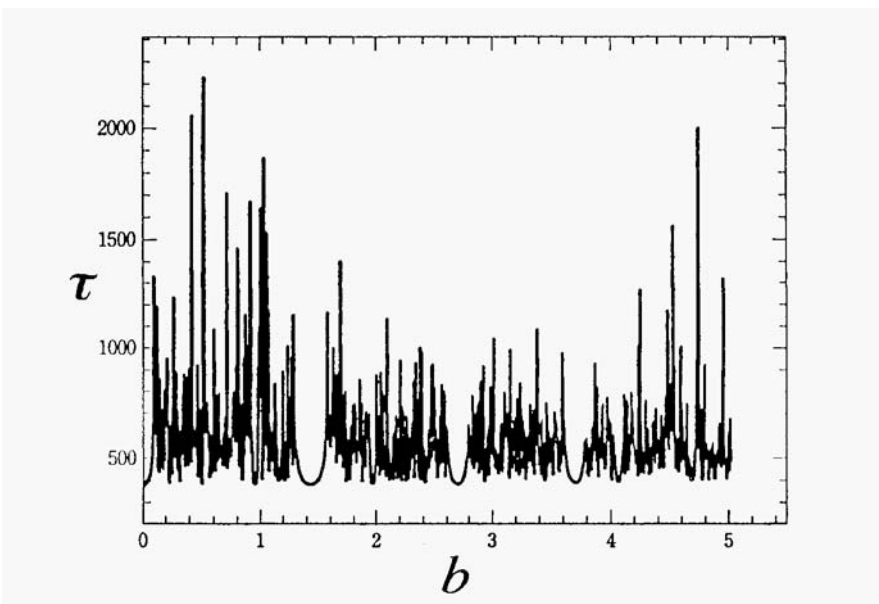

Fig. 6.9. The b dependence of the time during which the atom A stays in the interaction region. V_0=-2.5, Q_0=2, and κ=5. The lower limit for τ(~200) is the passing time in the absence of interaction. (Courtesy of A. Bulgac and D. Kusnezov.)

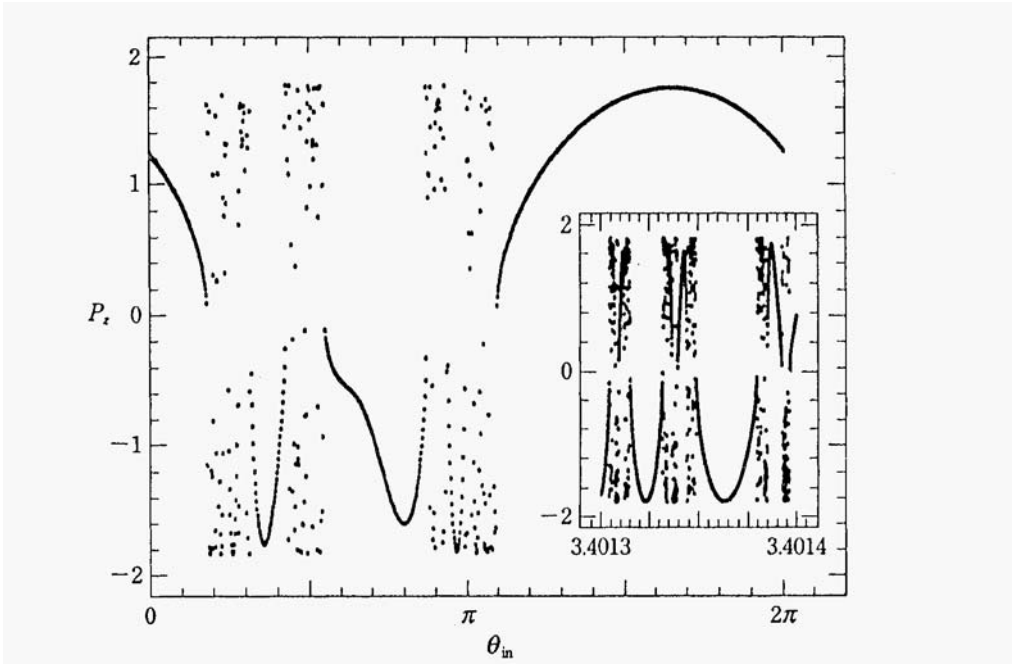

Fig. 6.10. Final momentum of the scattered atom $P_z(t=\infty)$ as a function of the initial electronic state θ_{in}. b=1 and other parameter values are the same as in Fig. 6.9. (Courtesy of A. Bulgac and D. Kusnezov.)

generate chaos. However, if each molecular system were quantized at the outset, this possibility would be smeared out. It is difficult to see chaos in quantum systems without artificial approximations. This means the present formalism of quantum dynamics should be innovated so as to accommodate temporal chaos.

References

Arnold, V. I. (1978). *Mathematical Methods of Classical Mechanics.* New York: Springer.

Aharonov, Y., and Anandan, J. (1987). *Phys. Rev. Lett.* **58,** 1593.

Berry, M. V. (1984). *Proc. R. Soc.* London **A392,** 45.

Berry, M. V. (1990). *Proc. R. Soc.* London **A430,** 405.

Berry, M. V., and Robbins, J. M. (1993). *Proc. R. Soc.* London **A442,** 659.

Bouwmeester, D., *et al.* (1996). *Phys. Rev.* **A53,** 985.

Bulgac, A., and Kusnezov, D. (1995). *Chaos, Solitons and Fractals* **5,**

1051.
Child, M. S. (1974). *Molecular Collision Theory.* New York: Academic.
Crothers, D. S. F. (1971). *Adv. Phys.* **20,** 405.
Darboux, G. (1896). *Lecons sur la theorie generale des surfaces, vol. 4.* Paris: Gauthier-Villars.
Demkov, Yu. N. (1964). *Sov. Phys. JETP* **18,** 138.
Dykhne, A. M. (1962). *Sov. Phys. JETP* **14,** 941.
Hwang, J. T., and Pechukas, P. (1977). *J. Chem. Phys.* **67,** 4640.
Jackiw, R. (1988). *Comments At. Mol. Phys.* **21,** 71.
Kuratsuji, H., and Iida, S. (1988). *Phys. Rev.* **D37,** 441.
Longuet-Higgins, H. C., et al. (1958). *Proc. R. Soc. London* **A244,** 1.
Messiah, A. (1959). *Mecanique Quantique.* Pans: Dunod.
Miller, W. H., and George, T. F. (1972). *J. Chem. Phys.* **56,** 5637.
Moore, D. J. (1991). Phys. Rep. 210, 1.
Mott, N. F., and Massey, H.S. W. (1965). *The Theory ofAtomic Collisions.* London: Oxford University Press.
Nakamura, K., and Rice, S. A. (1994). *Phys. Rev.* **A49,** R2217.
von Neumann, J., and Wigner, E. P. (1929). *Phys. Z.* **30,** 467.
Nikitin, E. E. (1970). *Adv. Quantum Chem.* **5,** 135.
Nikitin, E. E., and Umanskii, S. Ya. (1984). *The Theory of Slow Atomic Collisions.* Berlin: Springer.
Pechukas, P. (1969). *Phys. Rev.* **181,** 166, 174.
Shapere, A., and Wilczek, F., eds. (1989). *Geometric Phases in Physics.* Singapore: World Scientific.
Stückelberg, E. C. G. (1932). *Helv. Phys. Acta* **5,** 369.
Wu, Y. S. M., and Kuppermann, A. (1993). *Chem. Phys. Lett.* **201,**178.

Chapter 7

Level Dynamics and Statistical Mechanics

Statistical aspects of classically-chaotic quantum systems are described by random matrix theory and its constrained variants. These apparent irregularity can be explained more profoundly by statistical mechanics of the completely-integrable Calogero-Moser and Calogero-Sutherland systems derived from quantum-mechanical eigenvalue problems by regarding a nonintegrability parameter as a pseudo-time. The idea is traced back to Dyson's level dynamics, but the modern framework described in this chapter is based on conservative Newtonian dynamics rather than on an overdamped limit of Langevin equation.

7.1. Level Dynamics: from Brownian Motion to Generalized Calogero-Moser-Sutherland (gCM/gCS) System

In classical mechanics, the transition from regular behaviours to chaos occurs when the strength (τ) of nonintegrable perturbations is varied. In the corresponding quantum mechanics, we manage the eigenvalue problem for a τ -dependent Hamiltonian, provided the system is autonomous. Consequently we envisage multiple avoided crossings or repulsions of energy levels, which constitute a fundamental mechanism for complicated spectra with a definite symmetry in (classically-chaotic) quantum bound systems. Indeed, adiabatic-*ansatz* eigenvalue problems in (7.3) (see below) yield a new paradigm of nonlinear dynamics which bridges the gap between greatly different

theories of solitons and random matrices. The transition from Poisson to Wigner level-spacing distributions can be interpreted in terminology of nonlinear dynamics.

Taking energy levels as particle coordinates, Dyson started a level-dynamics approach to describe statistics of irregular energy spectra. He was the first to conceive the idea of deriving the joint probability density of eigenvalues from a level dynamics standpoint. Dyson (1962) remarked: "After considerable and fruitless efforts to develop a Newtonian theory of ensembles, we discovered that the correct procedure is quite different • • •. The x_j (eigenvalues) should be interpreted as positions of particles in Brownian motion. This means that the particles do not have well-defined velocities, nor do they possess inertia." So long as he confined his argument to random matrices, his remark was right. His theory of Brownian motion in the form of stochastic differential equations will be sketched below.

For a Gaussian orthogonal ensemble, the stochastic differential equation for a τ-dependent (τ is "quasi-time") real symmetric matrix H(τ) is given by

$$\mathrm{d}H(\tau) = -H\mathrm{d}\tau + \mathrm{d}V(\tau), \tag{7.1}$$

which implies that the differential d$H(\tau)$, like a differential velocity, is provided by a sum of the frictional ($-H\mathrm{d}\tau$) and random (d$V(\tau)$) forces. In (7.1), $V(\tau)$ is also a member of the Gaussian orthogonal ensemble and d$V(\tau)$ denotes a fundamental Brownian step obeying Wiener processes:

$$\langle \mathrm{d}V_{nm} \rangle = 0, \tag{7.2a}$$

$$\langle \mathrm{d}V_{nm}\,\mathrm{d}V_{n'm'} \rangle = (\delta_{nn'}\delta_{mm'} + \delta_{nm'}\delta_{mn'})\zeta^2\mathrm{d}\tau \tag{7.2b}$$

with <• • •> denoting ensemble average. The essential point is that dV is of the order $(\mathrm{d}\tau)^{1/2}$. We shall now derive the corresponding stochastic differential equations for eigenvalues and eigenvectors by investigating the eigenvalue problem

$$H(\tau)\,|\,n(\tau)\rangle = x_n(\tau)\,|\,n(\tau)\rangle. \tag{7.3}$$

Let us replace τ in (7.3) by $\tau + \mathrm{d}\tau$ and use expansions w.r.t. $(\mathrm{d}\tau)^{1/2}$:

$$H(\tau + d\tau) = H(\tau) + dH(\tau), \tag{7.4a}$$

$$x_n(\tau + d\tau) = x_n(\tau) + dx_n(\tau), \tag{7.4b}$$

$$|n(\tau + d\tau)\rangle = \sum_m c_{nm}(\tau + d\tau)|m(\tau)\rangle , \tag{7.4c}$$

with

$$dx_n = dx_n^{(1/2)} + dx_n^{(1)} + \quad , \tag{7.5a}$$

$$c_{nm} = c_{nm}^{(0)} + c_{nm}^{(1/2)} + c_{nm}^{(1)} . \tag{7.5b}$$

Then, standard perturbation theory yields equalities for each order of $(d\tau)^{1/2}$ with $l = 1,2,\cdots$. The differentials of order of $(d\tau)^{1/2}$ proves to be derived only by the random forces. The relevant equalities appear in order of $d\tau$ and are given by

$$dx_n(\tau) = -x_n d\tau + \sum \frac{\zeta^2}{\quad} d\tau + dW_{nn}(\tau) \tag{7.6a}$$

and

$$d|n(\tau)\rangle = -(1/2) \sum_{m(\neq n)} \frac{\zeta^2}{x_n - x_m} |n(\tau)\rangle d\tau + \sum_{m(\neq n)} \frac{dW_{mn}}{x_n - x_m} |m(\tau)\rangle , \tag{7.6b}$$

with dW defined by

$$\langle dW_{nm} \rangle = 0, \tag{7.7a}$$

$$\langle dW_{nm}(\tau)\, dW_{n'm'}(\tau)\rangle = (\delta_{nn'}\delta_{mm'} + \delta_{nm'}\delta_{mn'})\zeta^2 d\tau . \tag{7.7b}$$

We find that the equation for eigenvalues, (7.6a), which is decoupled from eigenstates, describes the one-dimensional Brownian motion of particles of unit charge and unit mass subject to both on-site harmonic potential and a repulsive two-dimensional (logarithmic) Coulomb potential; ζ^2 plays the role of friction coefficient which fixes the diffusion rate.

Equation (7.6a), with (7.7), is identical with the Smoluchowski or Fokker-Planck equation for the time-dependent probability density $P(\{x_n\};\tau)$:

$$\zeta^{-2}\frac{\partial}{\partial\tau}P=\sum_n\frac{\partial}{\partial x_n}\left\{\frac{\partial}{\partial x_n}-F_n\right\}P\ , \tag{7.8}$$

where $F_n(=-\partial U/\partial x_n)$ is a systematic force derived from the effective potential

$$U=(2\zeta^2)^{-1}\sum_n x_n^2-\sum_{m(\neq n)}\ln\ |x_n-x_m\ |. \tag{7.9}$$

The stationary $(\tau\to\infty)$ solution of (7.8) yields the joint probability density for a Gaussian orthogonal ensemble:

$$P(\{x_n\};\tau\to\infty)=\prod_{n<m}\ |x_n-x_m|\ \exp(-\sum_n x_n^2/(2\zeta^2))\ , \tag{7.10}$$

which, as will be explained later, belongs to the same universality class as the Legendre orthogonal ensembles encountered in quantum chaos. Similar arguments apply to Gaussian unitary and symplectic ensembles. This completes Dyson's whole story.

Dyson's Brownian motion model corresponds to the overdamped limit of Langevin's equation given by

$$\ddot{x}_n=-\zeta^2\dot{x}_n+F_n+w_n(\tau) \tag{7.11}$$

with $\langle w_n(\tau)\rangle=0$ and $\langle w_n(\tau)w_m(\tau')\rangle=2\delta_{nm}\delta(\tau-\tau')$. Here $w_n(\tau)$ represents Gaussian white noise.

Evidently there is no coupling between particle positions and internal degree of freedom (i.e., eigenstates). Although the Brownian motion model is successful in describing level correlations of irregular spectra, it originates in random matrices, failing to capture the parameter-dependent characteristics of the spectra. It is therefore highly desirable to invent a formalism of level dynamics and statistical mechanics starting from deterministic Hamiltonians.

We describe below a modern version of this analysis, by managing a conservative Newtonian system rather than the overdamped limit of a Langevin equation. Systems exhibiting chaos are classified into either one of autonomous or driven nonautonomous systems, corresponding to whether the nonintegrable perturbation V with strength τ added to the integrable unperturbed system H_0 is time-independent (for the autonomous case) or not (for the nonautonomous case). (The perturbations are, for instance, a nonlinear particle-

particle interaction, coupling of a particle with electric or magnetic field, and so on.) As far as these systems are bounded, the standard quantum-mechanical method to describe them is as follows:

(1) Autonomous systems are described by means of the time-dependent Schrödinger equation $i\hbar\, d\Psi/dt = H(\tau)\Psi$, with the *time-independent* Hamiltonian

$$H(\tau) = H_0 + \tau V, \tag{7.12}$$

where both H_0 and V are Hermitian *($H_0{}^+ = H_0$, $V^+ = V$)*. Taking a product form $\Psi = \hat{\Psi}(\tau)\exp(-iE(\tau)t/\hbar)$, the problem is reduced to the eigenvalue problem $H(\tau)\hat{\Psi}(\tau) = E(\tau)\hat{\Psi}(\tau)$ or, in Dirac's notation, to (7.3).

(2) A prototype of driven nonautonomous systems is the periodically-pulsed system, e.g., a kicked rotator, which has received a considerable interest in the area of quantum chaos. The Hamiltonian for this system is given by

$$H(t;\tau) = H_0 + \tau\mathcal{V}\sum_{j=-\infty}^{j=\infty} \delta(t - 2\pi j). \tag{7.13}$$

The problem of solving the time-dependent Schrödinger equation $i\hbar\, d|\Psi\rangle/dt = H(t;\tau)|\Psi\rangle$ is reduced as well to the eigenvalue problem

$$U(\tau)|n(\tau)\rangle = \exp[-ix_n(\tau)]\,|n(\tau)\rangle \tag{7.14}$$

for a one-period (2π) unitary operator $U(\tau)$ defined in terms of time-ordering operator $\mathcal{T}$ as

$$U(\tau) = \mathcal{T}\exp\left[\int_{+0}^{2\pi+0} (-i/\hbar)H(t')dt'\right]$$

$$= \exp(-i\tau V)U_0$$

with $V = \mathcal{V}/\hbar$ and $U_0 = \exp[(-i/\hbar)2\pi H_0]$. In fact, the quasi-energies $\{x_n(\tau)\}$ and quasi-eigenfunctions $\{|n(\tau)\rangle\}$ in (7.14) determine the wavefunction just after the jth pulse as $|\Psi_j\rangle = U^j|\Psi_0\rangle = \sum_n \exp(-ijx_n)|n\rangle\langle n|\Psi_0\rangle$.

Here we shall pose a question: If τ is taken as *"quasi-time"* with both eigenvectors $\{|n\rangle\}$ and eigenvalues (or quasi-eigenvalues) $\{x_n\}$

viewed as classical dynamical variables, what universal dynamical system would be deduced from the eigenvalue problems in (7.3) and (7.14)? The answer to this query was provided by Pechukas (1983), Yukawa (1985), and Nakamura and Lakshmanan (1986). In the following we shall follow the work of Nakamura and Lakshmanan (1986).

Let us first consider the autonomous systems. Equation (7.3) yields

$$\langle m(\tau)|H(\tau)|n(\tau)\rangle = x_n(\tau)\delta_{mn} \ . \tag{7.15}$$

Below we shall be concerned with a manifold with a set of fixed quantum numbers and assume no degeneracy of the eigenvalues. Differentiating (7.15) w.r.t. the pseudo-time τ, we have

$$(\mathrm{d}\langle m|/\mathrm{d}\tau)H|n\rangle + \langle m|\mathrm{d}H/\mathrm{d}\tau|n\rangle + \langle m|H(\mathrm{d}|n\rangle/\mathrm{d}\tau) = \delta_{mn}\,\mathrm{d}x_n/\mathrm{d}\tau \ . \tag{7.16}$$

After slightly rewriting its l.h.s., (7.16) becomes

$$(x_m - x_n)\langle m|(\mathrm{d}|n\rangle/\mathrm{d}\tau) + \langle m|\mathrm{d}H/\mathrm{d}\tau|n\rangle = \delta_{mn}\,\mathrm{d}x_n/\mathrm{d}\tau. \tag{7.17}$$

Equation (7.17) implies

$$\mathrm{d}x_n/\mathrm{d}\tau = \langle n|\mathrm{d}H/\mathrm{d}\tau|n\rangle \tag{7.18a}$$

for $m=n$, and

$$\langle m|(\mathrm{d}|n\rangle/\mathrm{d}\tau) = \langle m|\mathrm{d}H/\mathrm{d}\tau|n\rangle/(x_n - x_m) \tag{7.18b}$$

for $m \neq n$. Noting that $\{\langle m|\}$ constitutes a complete set and also that $\langle n|(\mathrm{d}|n\rangle/\mathrm{d}\tau) = 0$ does hold, due to the arbitrariness of wavefunction's phase factor, (7.18b) turns out to be identical to the equation

$$\mathrm{d}|n\rangle/\mathrm{d}\tau = \sum_{m \neq n} |m\rangle\langle m|\mathrm{d}H/\mathrm{d}\tau|n\rangle/(x_n - x_m) \ . \tag{7.18b'}$$

Equations (7.18) are just an extension of Hellmann and Feynman's theorem (Feynman, 1939).

If one were to substitute in (7.18) the concrete expression (7.12) for $H(\tau)$ and the expansions $x_n = x_n^{(0)} + \tau\, x_n^{(1)} + \cdots$, $|n\rangle = |n\rangle^{(0)} + \tau|n\rangle^{(1)} +$

•••, and then write down equalities in each power of τ, well-known formulas for the nondegenerate perturbation theory would become available.

In the following treatment, however, we shall not resort to expansions of $\{\mathbf{x}_n\}$ and $\{|n\rangle\}$ but exploit dH/d $\tau=V$ (i.e., (7.12)) with the aim of rewriting (7.18) in a form of the canonical equations of motion. For this purpose, let $\{V_{nm}\}$ be replaced by new variables: We shall introduce "momenta" $p_n=V_{nm}$ for m=n and auxiliary variables

$$\Lambda_{nm}=\mathrm{i}^{-1}V_{nm}\ (x_n-x_m) \tag{7.19}$$

for m $\neq$n. Noting the latter to be re-expressed as

$$\Lambda_{nm}=\langle n|\mathrm{i}^{-1}[H_0,V]|m\rangle\equiv\langle n|\Lambda|m\rangle\ ,$$

Λ proves to be τ-independent and Hermitian $(\Lambda^+=\Lambda)$. Let λ_0 be the lowest eigenvalue Δf; then the non-negative Hermitian operator $\Lambda-\lambda_0\mathrm{I}$ is found to be described, in terms of a suitable τ-independent operator L, as

$$\Lambda-\lambda_0\mathrm{I}=L^+L\ . \tag{7.20}$$

Replacing V_{nm} finally by

$$\langle n|L^+L|m\rangle=\mathrm{i}^{-1}V_{nm}\ (x_n-x_m) \tag{7.21}$$

in case of $m\neq n$, (7.18) is reduced to (Nakamura and Lakshmanan, 1986; Nakamura, 1993)

$$\mathrm{d}x_n/\mathrm{d}\tau=p_n\ , \tag{7.22a}$$

$$\mathrm{d}p_n/\mathrm{d}\tau=2\sum_{m\neq n}\langle n|L^+L|m\rangle/(x_n-x_m)^3\ , \tag{7.22b}$$

$$\mathrm{d}(L|n\rangle)/\mathrm{d}\tau=-\mathrm{i}\sum_{m\neq n}L|m\rangle\langle m|L^+L|n\rangle/(x_n-x_m)^2\ , \tag{7.22c}$$

$$\mathrm{d}(\langle n|L^+)/\mathrm{d}\tau=\mathrm{i}\sum_{m\neq n}\langle n|L^+L|m\rangle\ \langle m|L^+/(x_n-x_m)^2\ . \tag{7.22d}$$

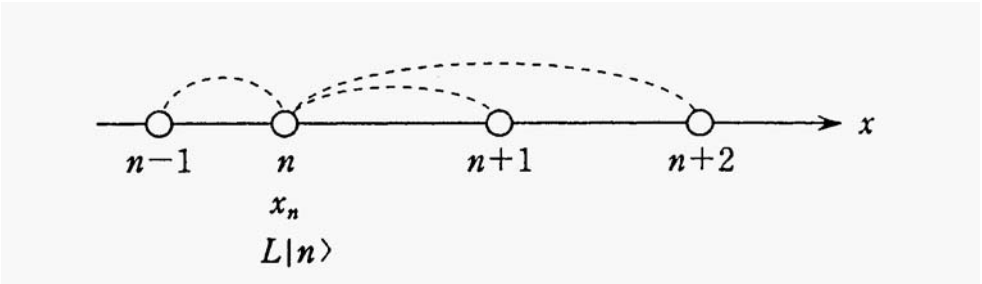

Fig. 7.1. Generalized Calogero-Moser system.

Amazingly, (7.22) proves to constitute a set of canonical equations to describe (1+1)- dimensional classical many-body system, i.e., a linear chain of particles exhibiting positions $\{x_n\}$, momenta $\{p_n\}$ and internal degrees of freedom $\{L|n\rangle\}, \{\langle n|L^+\}$. In fact, let us introduce the generalized Calogero-Moser system consisting of N "classical" particles with each possessing the internal complex-vector space in N dimensions (see Fig. 7.1), which is described by the Hamiltonian

$$\mathcal{H}_N = \sum_{1\le n\le N} \frac{p_n^2}{2} + \frac{1}{2} \sum_{1\le n,m\le N} \langle n|L^+ L|m\rangle\langle m|L^+ L|n\rangle (x_n - x_m)^{-2}, \quad (7.23)$$

with $\langle n|L^+ L|m\rangle$ defined as a scalar product of complex vectors $\langle n|L^+$ and $L|m\rangle$. By the application of Poisson brackets,

$$\{A,B\} = \sum_n \left((\partial A/\partial p_n)(\partial B/\partial x_n) - (\partial A/\partial x_n)(\partial B/\partial p_n) \right)$$
$$+ \sum_n \left((\partial A/\partial \langle n|L^+)(\partial B/\partial iL|n\rangle) - (\partial A/\partial iL|n\rangle)(\partial B/\partial \langle n|L^+) \right), \quad (7.24)$$

one obtains a set of canonical equations from (7.23) :

$$\begin{aligned} dx_n/d\tau &= \{\mathcal{H}_N, x_n\} = \partial\mathcal{H}_N/\partial p_n, \\ dp_n/d\tau &= \{\mathcal{H}_N, p_n\} = -\partial\mathcal{H}_N/\partial x_n, \end{aligned} \quad (7.25a)$$

$$\begin{aligned} d(iL|n\rangle)/d\tau &= \{\mathcal{H}_N, iL|n\rangle\} = \partial\mathcal{H}_N/\partial\langle n|L^+, \\ d(\langle n|L^+)/d\tau &= \{\mathcal{H}_N, \langle n|L^+\} = -\partial\mathcal{H}_N/\partial iL|n\rangle, \end{aligned} \quad (7.25b)$$

which are shown to reproduce (7.18) exactly.

In this way we have seen that the eigenvalue problem for autonomous systems in (7.12) is equivalent to solving the initial value problem for the gCM system. The repulsive interaction in the gCM system stems from avoided crossings proper to the quantum chaos. [Even in case of integrable perturbations where no avoided crossings would emerge, it would also be possible to map the eigenvalue problem to gCM system so long as one concentrates on the manifold with fixed quantum numbers. Singularity of the repulsive interaction will be suppressed in the integrable case, however, by weakening the coupling coefficients $\langle n|L^{+}L|m\rangle$.]

The method developed so far applies as well to driven nonautonomous systems. Here the eigenvalue problem (7.14) is reduced to the generalized Calogero-Sutherland system (Nakamura and Mikeska, 1987) which is derived from (7.23) with a replacement

$$(x_n - x_m)^2 \quad \text{-----> } \quad (2\sin[(x_n - x_m)/2])^2 \tag{7.26}$$

but with the same Poisson bracket as in (7.24).

Introducing the quaternions $\{e_\alpha\}$ (i.e., $e_1=i\sigma_x$, $e_2=-i\sigma_y$, $e_3=-i\sigma_y$, $e_0=1$ in terms of 2 x 2 Pauli matrices), one may generalize (7.12) to a symplectic Hamiltonian: $H'(\tau)=H0+\tau\sum_{\alpha=0}^{3} e_\alpha V^{(\alpha)}$. The resultant dynamical system is again given by (7.23) except for the replacement in the inter-"particle" interaction

$$L^{+}L \quad \text{-----> } \quad \sum_{\alpha=0}^{3} L^{(\alpha)+}L^{(\alpha)}e_\alpha \ , \tag{7.27}$$

with $\langle n|L^{(\alpha)+}L^{(\alpha)}|m\rangle=\langle n|i^{-1}[H_0,V^{(\alpha)}]|m\rangle$ for $m \neq n$.

The most important characteristics of gCM (gCS) system is its complete integrability, meaning that one can rewrite (7.22) in the Lax formalism and have the constants of motion with their number equal to the degrees of freedom. In fact a single soliton solution has been obtained (Gaspard *et al.,* 1989), which corresponds to an avoided crossing moving when τ is varied. One may conceive that a high density soliton gas, representing a high density avoided crossings, should serve in describing irregular spectra. Without having recource to an analytical method like the inverse scattering method, let us now demonstrate this picture vividly on the basis of a numerical calculation of a simple Hamiltonian.

7.2. Soliton Turbulence: A New Interpretation of Irregular Spectra

Most treatments of level dynamics have been directed towards confirming the random-matrix formalism of energy spectra. Generic features of quantum spectra for classically chaotic systems, however, are much more fruitful than the results of random-matrix theory. Even a coherent structure can coexist with the irregular spectra for a Gaussian orthogonal ensemble (GOE). The existence of solitonic structures (i.e., mobile avoided crossings) has been found in the experiment on diamagnetic Rydberg atoms (Iu *et al.,* 1989) and in numerical data (e.g., on a pulsed spin system). These solitons are attributed to regular orbits such as stable KAM tori (in generic systems) or (unstable) periodic orbits (in K systems, i.e., systems with positive Kolmogorov entropy) in the underlying classical dynamics.

The most astonishing aspect of the gCM system is its complete integrability. This fact implies that, for any kind of initial conditions, we should inevitably see a gas of solitons in large τ regimes; and, conversely, a gas of solitons at τ =0 will yield complicated level structures in some of the large τ (>0) regions because of many collisions among solitons. Solitons would thereby be a precursor of spectra for the Gaussian orthogonal ensemble (GOE).

By solving numerically the generalized Calogero-Moser equation corresponding to the model quantum Hamiltonian, we suggest a new interpretation of quantum irregular energy spectra from the viewpoint of nonlinear dynamics (Ishio and Nakamura, 1992). The soliton-turbulence picture is shown to be effective in describing the Gaussian orthogonal ensemble-like spectra. The transition from Poisson to Wigner level-spacing distributions can be interpreted in the terminology of nonlinear dynamics such as soliton density and fluctuation of accelerations.

To formulate our idea, we choose a model Hamiltonian involving the core of generic classically chaotic quantum systems. We introduce a set of three manifolds (diagonal block matrices) $\mathcal{M}_1$, $\mathcal{M}_2$, and $\mathcal{M}_3$. In the absence of the interaction between the manifolds, each of them may be characterized by different quantum numbers such as principal quantum numbers. For convenience, $\mathcal{M}_2$ is here assumes horizontal while $\mathcal{M}_1$ and $\mathcal{M}_3$ are solitonic: Levels in $\mathcal{M}_2$ are τ independent; levels in $\mathcal{M}_1$ which at τ = 0 lie with an energy gap ε_g above those in $\mathcal{M}_2$, show downward motions with increasing τ so as to cross the $\mathcal{M}_2$. Similarly,

levels in $\mathcal{M}_3$, lying with the gap ε_g below those in $\mathcal{M}_2$ at $\tau = 0$, show upward motions. In the presence of coupling between these manifolds, however, the quantum numbers become meaningless and mixing among manifolds is crucial, as is often encountered in generic quantum systems. Finally the effective Hamiltonian is given by

$$H(\tau) = \begin{bmatrix} A^- & W & U \\ W & A^+ & U \\ U & U & B \end{bmatrix}, \tag{7.28a}$$

with

$$A^{\pm} = \begin{bmatrix} p_{\pm 1}\tau + q_{\pm 1} & w & w \\ w & p_{\pm 2}\tau + q_{\pm 2} & w \\ w & w & \cdots \end{bmatrix}, \quad B = \begin{bmatrix} a_1 & 0 & 0 \\ 0 & a_2 & 0 \\ 0 & 0 & \cdots \end{bmatrix}, \tag{7.28b}$$

$$W = \begin{bmatrix} w & w & \cdots \\ w & w & \cdots \\ \cdots & \cdots & \cdots \end{bmatrix}, \quad U = \begin{bmatrix} u & u & \cdots \\ u & u & \cdots \\ \cdots & \cdots & \cdots \end{bmatrix}, \tag{7.28c}$$

where $\{p_{\pm i}\tau + q_{\pm i}\}$ and $\{a_i\}$ denote solitonic (crossing) and horizontal (τ-indenpendent) levels, respectively. The quantities w and u are soliton-soliton and soliton-horizontal couplings, respectively. The model (7.28) is just a generalized Demkov-Osherov Hamiltonian, originally used for the problem of multidimensional Landau-Zener transitions and belongs to the category of our concern in (7.12); from (7.28) we have $H_0 = H(\tau = 0)$, $V = (H(\tau) - H(0))/\tau$. We choose three sets $\{a_i\}$, $\{q_i\}$, and $\{q_{-i}\}$ such that the spacing distribution in each set satisfies the Poisson distribution. For values $\{p_{\pm i}\}$, we consider two different cases: (i) the Maxwell-Boltzmann distribution $P(p)\,dp \propto \exp(-p^2/2kT)dp$; (ii) the regular sequences given by $p_{\pm i} = \pm y\ (i\text{-}1) \pm \delta$ with $i = 1,2,\cdots$, where + and - are used for $\mathcal{M}_3$ and $\mathcal{M}_1$ manifolds, respectively. In case (ii) any stochasticity is thoroughly expelled.

We choose u=0.2, w=0.4, and ε_g =100 and prepare 600 horizontal levels for the $\mathcal{M}_2$ manifold with 1150 solitonic levels for each of the $\mathcal{M}_1$ and $\mathcal{M}_3$ manifolds. Furthermore, kT = 1000 [case (i)] and γ =0.02 and δ = 9.0 [case (ii)] are taken for convenience. By diagonalizing the matrix in (7.28a) at τ = 0, we obtain a complete set of initial values for $\{x_n\}$,

$\{L\,|\,n>\}$, and their canonical-conjugate variables. With these initial values we proceed to solving the gCM equation for $\tau>0$. Figure 7.2 shows, in case (i), the τ -dependent energy spectrum in some of the originally horizontal-level energy regions. We see: (1) In the small τ region [see Fig. 7.2(a)], several solitons become invading the $\mathcal{M}_2$ manifold. A

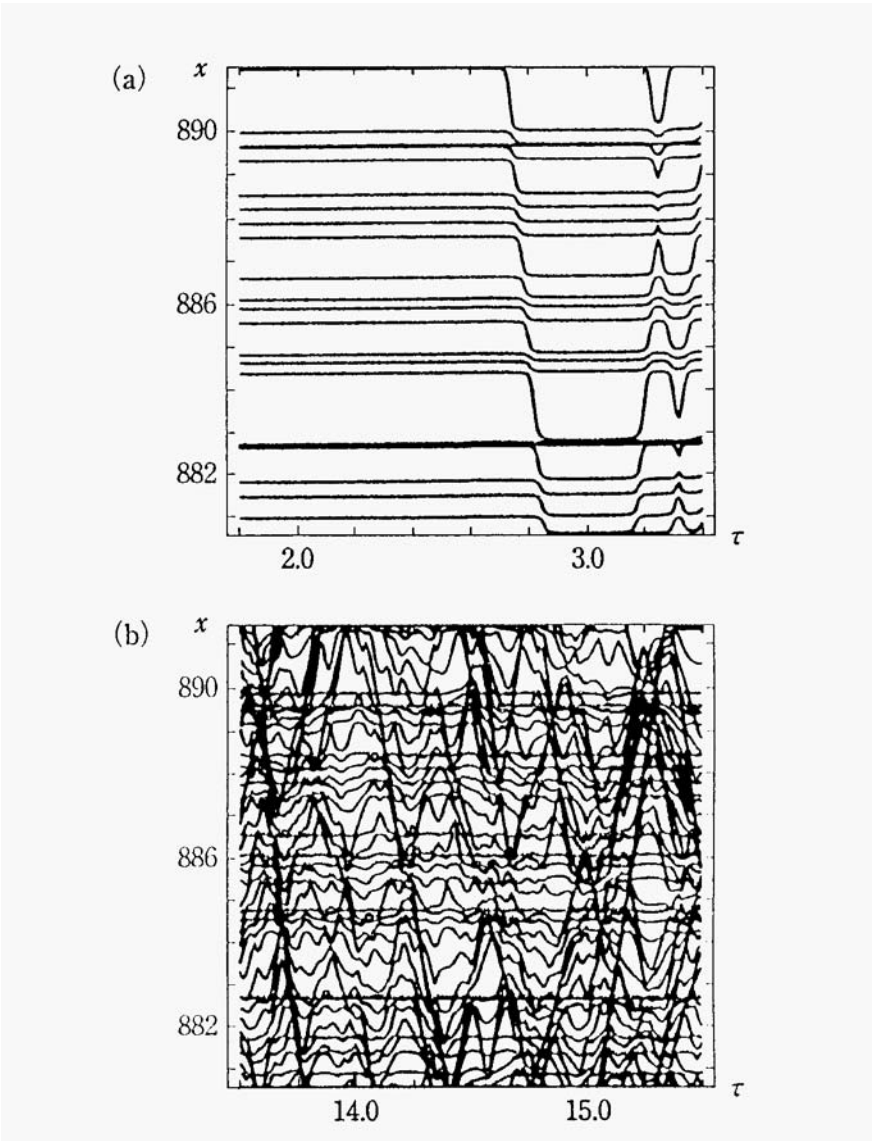

Fig. 7.2. The τ dependence of energy spectra in case (i): (a) $1.8<\tau<3.4$, (b) $13.6<\tau<15.2$.

regular feature of the spectrum is almost retained in this region. This orderly structure is quite similar to the one in the experiment by Iu et al., though it is not straightforward to reduce the Hamiltonian for the diamagnetic Rydberg atoms to the form in (7.28). (2) In some of the large τ region [see Fig. 7.2(b)], solitonic and horizontal levels can hardly be perceived. In this region the invasion by many solitons of the horizontal-level region is essential and the resultant increase in the number of collisions between solitons and between solitons and horizontal levels yields the irregular spectrum. It is worth noting that such irregularity comes from the completely integrable system.

Taking all levels included in the energy region ΔE, where the levels in the $\mathcal{M}_2$ manifold are located at τ =0, we calculate the level-spacing distribution *P(s)* and the spectral rigidity Δ_3 at some fixed τ values. The results are shown in Figs. 7.3(b) and 7.3(c) in cases (i) and (ii), respectively. Figure 7.3(a) is the near-Poisson distribution at τ= 0, which is here regarded as reflecting the classical integrability. (Since precise energy levels at τ = 0 are obtained by the diagonalization of (7.28), a slight deviation from the Poisson distribution is inevitable.) Both Figs. 7.3(b) and 7.3(c) show the Wigner distribution. We find it to be widely observed for $\tau_c<\tau<\tau'_c$ with $\tau_c \cong 5.0$ and $\tau'_c \cong 80.0$. In the other τ region, we see the intermediate distribution. On the other hand, for any value of $\tau \geq 0$, Δ_3 shows persistent $L/15$ behaviors with increasing L, which is characteristic of the Poisson distribution. Our additional data for much larger L values up to 200 (not shown here) indicate neither $\pi^{-2}\ln(L) - 0.007$ behavior for GOE nor the saturation of Δ_3.

Noting that large L behavior of Δ_3 represents the long-range level correlation, one may assert the following: As for the short-range correlation, the present model describes the transition from the Poisson to GOE statistics, but it does not for the long-range correlation. This is due to the short rangeness of the couplings (in the sense of the second-order perturbation theory) between horizontal and solitonic levels and between solitonic levels, which locally affect the level structures. In general, the large L behavior of Δ_3 is known to be nonuniversal, depending on the individual nature of the Hamiltonian. So, our concern will be limited only to the short-range correlations.

In the same energy range as considered in Fig. 7.3, we show in Fig. 7.4 the concentration of solitons (i.e., solitonic levels) $n(\tau)$ [$= (N(\tau) - N(0))/N'(\tau)$] and fluctuation of accelerations $\sigma(a) \equiv [\langle\langle(a-\langle a\rangle)^2\rangle\rangle]^{1/2}$ as a function of τ. Here $a \equiv d^2x/d\tau^2$ and $N'(\tau)$ denotes the number of levels

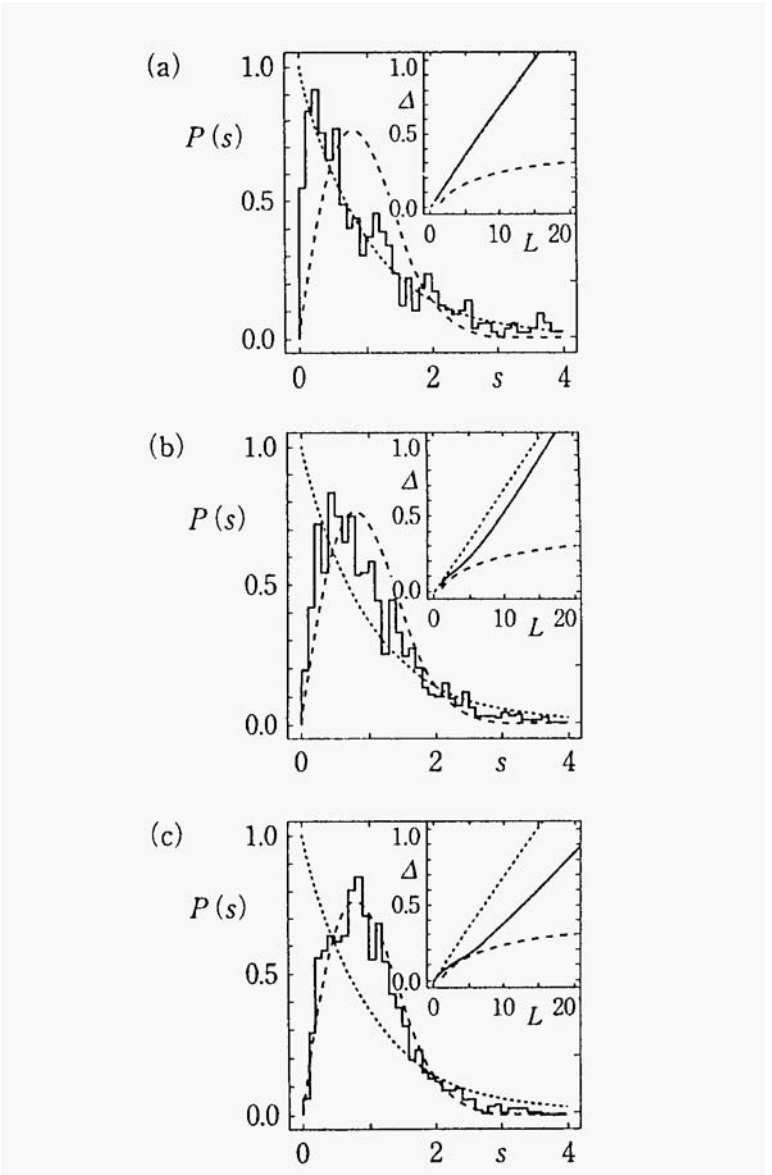

Fig. 7.3. Level-spacing distribution and corresponding spectral rigidity (inset). Δ denotes $\overline{\Delta_3}$. Dashed and dotted lines correspond to GOE and Poisson limits, respectively: (a) τ =0, (b) τ=15.0 [case(i)], (c) τ=15.0 [case (ii)].

involved in the energy range ΔE. Figures 7.4(a) and 7.4(b) correspond to cases (i) and (ii), respectively. The quantities n and $\sigma(a)$ grow

linearly with τ and decay with an accompanying long-time tail. The maximum occurs at nearly equal values τ_0^n and τ_0^a for n and $\sigma(a)$, respectively. We can identify the GOE region, $\tau_c<\tau<\tau'_c$, as a region where $\sigma(a)$ takes values above the threshold. On close inspection, however, we see $\tau_0^a<\tau_0^n$ and $n(\tau_c)<n(\tau'_c)$. Both inequalities are caused by the difference in the number of solitonic collisions between ranges below and above τ_0^a. In fact, most of the solitonic levels with large gradients invading the horizontal levels in the smaller τ region ($\tau<\tau_0^a$) and collide often with those incident from the opposite direction as well as with horizontal levels, thereby leading to the GOE spectrum even

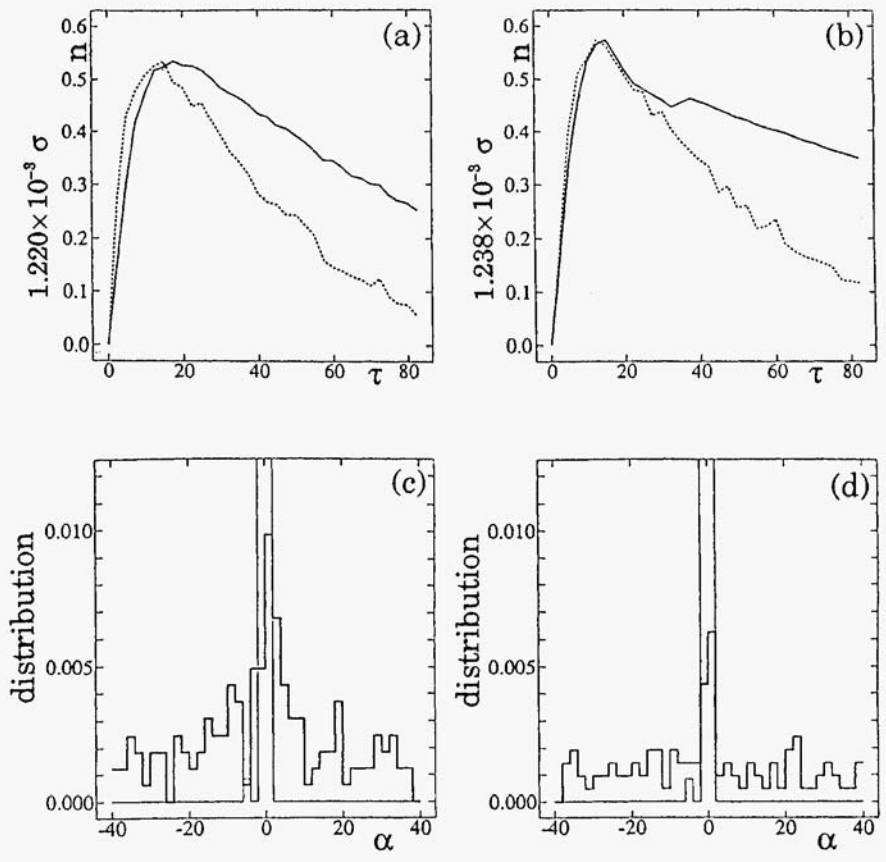

Fig. 7.4. The τ dependence of n (solid line) and $\sigma(\alpha)$ (dotted line): (a) case (i), (b) case(ii). Distribution of accelerations at τ=0 (thin histogram) and τ=15 (thick histogram): (c) case (i), (d) case (ii).

for relatively small n values. To further explore a dynamical aspect of the ensemble of levels, we also show in Figs. 7.4 (c) and 7.4 (d) the distribution function of a in the small-α region. In both cases (i) and (ii), the very narrow distribution at $\tau = 0$ well spreads at $\tau = 15$ and again narrows in the region of very large τ.

While limited data are presented, almost identical results are available for various magnitudes of w, u, and ε_g for both distributions (i) and (ii). Therefore the present findings strongly suggest the universality of the interpretation of irregular spectra in terms of nonlinear dynamics.

In conclusion, on the basis of a model Hamiltonian, a soliton-turbulence picture is shown to be effective in describing the energy spectra for classically nonintegrable and chaotic systems. Like vortices in fluid turbulence, the condensation of solitons leads to the enhanced fluctuation of accelerations of energy levels and to the Wigner level spacing distribution. In fact there is a recent experimental report that the absorption spectra for diamagnetic Rydberg atoms have a wide window of soltonic structures in the classically chaotic regime, betraying the prediction of the random matrix theory. The present soliton-gas picture will provide a new interpretation not only of the irregular spectra but also of the coexisting orderly structures in real experiments .

7.3. Statistical Mechanics of gCM System

Since the Hamiltonian operator in (7.12) works in infinite-dimensional Hilbert space, we inevitably have an infinite number of energy levels. This fact leads us to consider the statistical properties of energy levels, in particular, distributions of level spacing and curvature (see Fig. 7.5). Despite the complete integrability of the finite gCM system, statistical information is available from any finite interval in the infinite gCM system where dynamical mixing becomes possible. As for an infinite ideal gas or harmonic solid, it may have ergodic, mixing or Bernoulli properties, while its finite counterpart is completely integrable, showing no local dynamical instability (Sinai, 1976; Lanford and Lebowitz, 1975). We assume such results for an infinite gCM system.

To study the statistical mechanics of a gCM system, an invariant probability density is needed to define a canonical ensemble. To

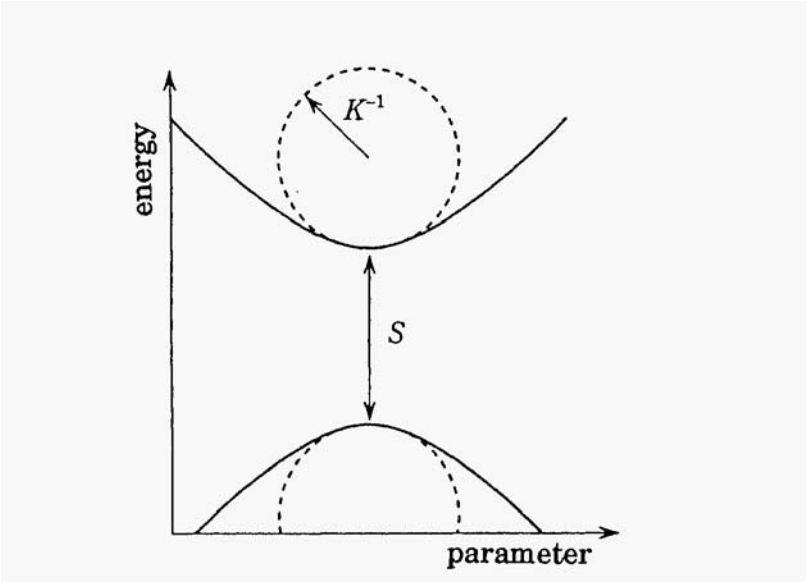

Fig. 7.5. Level spacing S and curvature K, typically at avoided level crossing.

simplify the construction, we assume that the energy spectrum $\{x_i\}$ extends from $-\infty$ to $+\infty$ and is invariant under x translations with a uniform density ρ. In actual quantum systems, the level density is usually non-uniform, but for the purpose of studying the spectral fluctuations, the uniform density is desirable. Prior to construction of the canonical ensemble, let us introduce an intermediate canonical ensemble of systems with N particles (i.e., energies) in the interval $[-L/2, +L/2]$. At the end points of this interval we place hard walls where the particles undergo elastic collisions. Between walls the particle motion is ruled by the *classical* gCM Hamiltonian (7.23) or by its extension

$$\mathcal{H}_N = \sum_{1\le n\le N} \frac{p_n^2}{2} + \frac{1}{2} \sum_{\substack{1\le n,m\le N \\ n\ne m}} \sum_{\alpha=0}^{\nu-1} \Lambda^{(\alpha)}{}_{nm} \Lambda^{(\alpha)}{}_{mn} (x_n - x_m)^{-2}, \qquad (7.23')$$

with $\Lambda^{(\alpha)}{}_{nm} = \langle n | L^{(\alpha)+} L^{(\alpha)} | m \rangle$ (see also (7.26) and (7.27)). The value of ν (=1,2 and 4) depends on the symmetry of quantum Hamiltonians under consideration. Equation (7.23') is used to define a Gibbs measure

$$\mathrm{d}M_{N,L} = (1/Z_{N,L}) \exp(-\beta \mathcal{H}_N) \prod_{1\le m<n\le N} \prod_{\alpha=0}^{\nu-1} dx_m \, \mathrm{d}p_m \, \mathrm{d}\Lambda^{(\alpha)}{}_{nm}. \qquad (7.29)$$

The canonical ensemble will then be obtained in the limit where the size L of the box increases infinitely while keeping the density p constant. The resulting measure depends on two parameters: density ρ and inverse *"temperature"* β. The value of β is determined from the variance of the velocities $\{p_n(\tau)\}$ of the energy levels: $\langle(\Delta p_n)^2\rangle = \langle p_n^2\rangle - \langle p_n\rangle^2 = 1/\beta$. Unless the mean drift is nonvanishing, it should be subtracted from the motion of individual energy levels so as to guarantee $\langle p_n\rangle$=O. To fulfill translational invariance of the canonical measure, we have to verify that a uniform density of energy levels be deduced for the canonical ensemble in the thermodynamic limit $L,N \to \infty$ with N/L kept constant.

The integration of the measure (7.29) over variables p_m and $\Lambda^{(\alpha)}_{mn}$ yields the joint probability density of energy levels:

$$f_{N,L}(x_1,\cdots,x_N) = (1/\mathcal{N}_{N,L}) \prod_{1\le i<j\le N} |x_i - x_j|^{\nu} \tag{7.30}$$

for $-L/2 < x_i < L/2$. This is just the joint probability density encountered in random matrix theory except for the weight factor. Therefore, if the uniform level density is obtained, the measure (7.29) for the gCM system is expected to reproduce known results from random matrix theory.

To be concrete, the normalizing constant $\mathcal{N}_{N,L}$ in (7.30), level density, as well as the spacing distribution will all be calculated starting from the generating functional defined by (Gaspard *et al.,* 1990; Rice *et al.* 1992),

$$I_N(u) = \int_{-1}^{1}\cdots\int_{-1}^{1} \prod_{k=1}^{N} u(x_k) \prod_{1\le i<j\le N} |x_i - x_j|^{\nu} dx_1 \cdots dx_N \ , \tag{7.31}$$

where $\{u(x_k)\}$ are arbitrary functions, and variables $\{x_i\}$ are scaled to give the size of the box $L = 2$. In case of random matrix theory, Mehta and Gaudin (1960; 1961) reduced integrals like (7.31) to the Fredholm determinant of an integral kernel composed of mutually orthogonal functions. For the Gaussian ensemble, harmonic oscillator eigenfunctions (i.e., Hermite's polynomials) are used to calculate the joint probability density (7.30) multiplied by a Gaussian weight factor, $\exp(-\Sigma_k x_k^2/2)$. For Jacobi or Laguerre ensembles, the corresponding orthogonal polynomials are used in reduction of (7.31) with a varied multiplicative factor. In this classification, (7.30) is the joint

probability density of the Legendre ensemble, since the weight factor is unity so that Legendre polynomials working in the domain [-1,1] are needed to calculate (7.31). Within the Legendre ensembles, exponents v=l, 2, and 4 define orthogonal, unitary and symplectic ensembles, respectively. The analysis of the statistical mechanics of the gCM system is thus reduced to that of the Legendre ensemble.

Level Density and Level Spacing Distribution

We shall hereafter concentrate on the case v=l for simplicity, while the extension to cases v=2 and 4 is straightforward. Let the variables $\{x_n\}$ be placed in order as

$$R=\{-1<x_1<x_2<\cdots<x_N<1\}\,. \tag{7.32}$$

Then the product $\prod_{1\le i<j\le N}|x_i-x_j|$ in (7.31) is equal to the Vandermonde determinant

$$\begin{vmatrix} 1 & 1 & \cdots & 1 \\ x_1 & x_2 & \cdots & x_N \\ \vdots & \vdots & \vdots & \vdots \\ x_1^{N-1} & x_2^{N-1} & \cdots & x_N^{N-1} \end{vmatrix} \tag{7.33}$$

multiplied by a facor $(-1)^{N(N-1)/2}$. Using (7.33) and the property

$$P_n(x)=[2^{-n}(2n)!/(n!)^2]x^n+\mathrm{O}(x^{n-1}), \tag{7.34}$$

of Legendre polynomials, Eq. (7.31) becomes

$$I_n(u)=N!A_{N-1}\int\cdots\int_R \det[u(x_i)P_{j-1}(x_i)]_{i,j=1,\cdots,N}dx_1\cdots dx_N\,, \tag{7.35}$$

with $A_{N-1}=\prod_{k=0}^{N-1}[2^k(k!)^2/(2k)!]$.

From the generating functional in (7.35), we can obtain all the necessary information on orthogonal systems with v =1: Firstly, the normalizing constant is given by

$$\mathcal{N}_{N,L}=I_N(1)(L/2)^{N(N+1)/2}=2^N A_N(L/2)^{N(N+1)/2}\,, \tag{7.36}$$

where $IN(1)$ is the integral (7.35) for $u(x)$=l. Accordingly, the partition

function becomes, for N >>1,

$$Z_{N,L} = I_N(1)2^{N/2}\,[(\pi/\beta)^{1/2}\,L/2]^{N(N+1)/2} \cong 2^{3N/2}[(\pi/\beta)^{1/2}\,L/2]^{N(N+1)/2}\,. \tag{7.37}$$

Secondly, the level density is available from the functional derivative,

$$\sigma_{N,2}(x)=\delta \ln I_N(u(x))/\delta\, u(x)\,|_{u(x)=1}\,. \tag{7.38}$$

(See Dyson (1962).) Using a large-order expansion of Legendre polynomials and after rescaling $x \to 2x/L$, the level density near $x=0$ is given by

$$\sigma_{N,L}(x) \cong (2/\pi)(N/L)[1-(2x/L)^2]^{-1/2} \tag{7.39}$$

for $N>>1$. The density (7.39) reaches a uniform value in the thermodynamic limit $N,\ L \to \infty$ with N/L a constant. In this limit, therefore, the Gibbs measure in (7.29) has proved to be successful in constructing the canonical ensemble. It should be emphasized that the present scheme has an advantage superior to Wigner's semicircle law for a Gaussian ensemble given by $\sigma_N(x)=(1/\pi)(2N-x^2)^{1/2}$, which shows an unpleasant extensive behavior $(\sim N^{1/2})$ in the thermodynamic limit.

Finally, in terms of the probability $\varepsilon(S)$ that an interval of size S is void of eigenvalues, the spacing distribution $p(S)$ is defined by

$$p(S)=\mathrm{d}^2\varepsilon(S)/\mathrm{d}S^2\,. \tag{7.40}$$

The function $\varepsilon(S)$ itself is reached (Mehta, 1967) by a limiting behavior of the probability $\varepsilon_N(\theta)$ given by

$$\varepsilon_N(\theta)=I_N(u)/I_N(1) \tag{7.41}$$

with $u(x)=0$, for $|x|<\theta$, and 1 for $|x|>\theta$. Using (7.35) in (7.41), one gets

$$\varepsilon(S)=\lim_{N\to\infty}\varepsilon_N(\pi S/2N)=\prod_{i=0}^{\infty}\,[1-S\gamma^2_{2i}(S)]\,, \tag{7.42}$$

where $\gamma_{2i}(S)=\int_{-1}^{1} f_{2i}(z;S)\mathrm{d}z/(2f_{2i}(0;S))$ in terms of the S-dependent spheroidal functions $f_0, f_2, f_4, \cdots$. From (7.40) and (7.42), we find

$$p_{\nu=1}(S) = (\pi^2/6)S - (\pi^4/60)S^3 + (\pi^4/270)S^4 + (\pi^6/1680)S^5 + \cdots, \tag{7.43a}$$

which agrees with the universal level spacing distribution *pOE(S)* obtained for the Gaussian and circular orthogonal ensembles (Mehta, 1967). The well-known Wigner distribution, $P_W(S)=(\pi/2)S\exp((-\pi/4)S^2)$, is merely an approximate distribution available from the "two-level model." The issue (7.43a) can be generalized to the cases ν =2 and 4: For ν=2,

$$p_{\nu=2}(S) = (\pi^2/3)S^2 - (2\pi^4/45)S^4 + (\pi^6/315)S^6 + \cdots, \tag{7.43b}$$

with quadratic level repulsion; for ν=4

$$p_{\nu=4}(S) = (2^4\pi^4/135)S^4 - (2^7\pi^6/4725)S^6 + \cdots, \tag{7.43c}$$

with quartic level repulsion. (7.43b) and (7.43c) are identical to *pUE(S)* for a Gaussian unitary ensemble and *pSE(S)* for a Gaussian symplectic ensemble, respectively.

The statistical mechanics of gCM systems has thus explained why level spacing distribution for classically-chaotic systems (or spectra of quantum chaos) should obey the same universal distributions as those of random matrix theory.

Curvature Distribution

Although the random matrix theory conveys only statistical information when a set of nonintegrability parameters are fixed, the statistical mechanics of gCM system can also predict distribution functions for parameter-dependent quantities. Among such quantities, the most important one is level curvature (Fig. 7.5) given by

$$K_i \equiv \lim_{\Delta\tau\to 0}\frac{\Delta^2 x_i}{\Delta\tau^2} = \ddot{x}_i(\tau). \tag{7.44}$$

Curvature in (7.44) takes large values for a pair of adjacent levels at avoided crossings and constitutes a promising indicator of quantum chaos. In practice, numerical computation of curvatures K_i can be done by using the discrete form of the second-order derivative in (7.44) with a small but finite $\Delta\tau$. (In near-integrable regimes) anomalously large values for K_i may be available which would prevent us from

constructing the curvature distribution. We shall therefore assume a fully-chaotic regime where the presence of universal curvature distribution can be expected.)

In (7.44), $\ddot{x}_i(\tau)$ is nothing but the acceleration of the *i*-th particle in gCM systems, so that

$$\ddot{x}_i(\tau) = -\partial \mathcal{H}_N / \partial x_i \tag{7.45}$$

(see (7.23')). Without loss of generality, we take x_1 as a sample level and derive the probability density for curvature $\ddot{x}_1$ to take the value *K:*

$$P(K) \equiv \lim_{\substack{N,L\to\infty \\ N/L=const}} P_{N,L}(K), \tag{7.46}$$

with

$$P_{N,L}(K) \equiv \int \delta(K+\partial \mathcal{H}_N/\partial x_1)\, \mathrm{d}M_{N,L}\,, \tag{7.47}$$

where dMN,L is the Gibbs measure (7.29). From (7.23'), the equation $K+\partial \mathcal{H}_N/\partial x_1 = 0$ possesses $N-1$ roots $\{x_1^{(k)}\}$ for any value of K. These zeros can be evaluated when *K* is large and positive, because $\partial \mathcal{H}_N/\partial x_1$ is a function of x_1 which diverges in the vicinity of levels different from x_1 (see Fig. 7.6). Choosing *K* positive, we obtain

$$x_1^{(k)} \cong x_k + \left[\frac{2}{K}\sum_{\alpha}(\Lambda_{1k}^{(\alpha)})^2\right]^{1/3}. \tag{7.48}$$

Consequently, one gets

$$P_{N,L}(K) = \sum_{k=2}^{N} \int \left|\partial^2 \mathcal{H}_N / \partial x_1^2\right|^{-1}_{x_1 = x_1^{(k)}} \delta[x_1 - x_1^{(k)}(K)]\, \mathrm{d}M_{N,L}\,, \tag{7.49}$$

with

$$\left|\partial^2 \mathcal{H}_N / \partial x_1^2\right|_{x_1 = x_1^{(k)}} \cong 3\left[\frac{2}{K^4}\sum_{\alpha}(\Lambda_{1k}^{(\alpha)})^2\right]^{-1/3}. \tag{7.50}$$

Equation (7.49) is evaluated asymptotically for large positive values of *K*. After integration over the variables x_1, $\{p_n\}$ and $\{\Lambda_{mn}^{(\alpha)}\}$, we obtain

$$P_{N,L}(K) \cong \mathcal{G}_{N,L}\,(2^{2\nu-3}(\nu+2)!)/(\beta^{\nu+1}K^{\nu+2}), \tag{7.51}$$

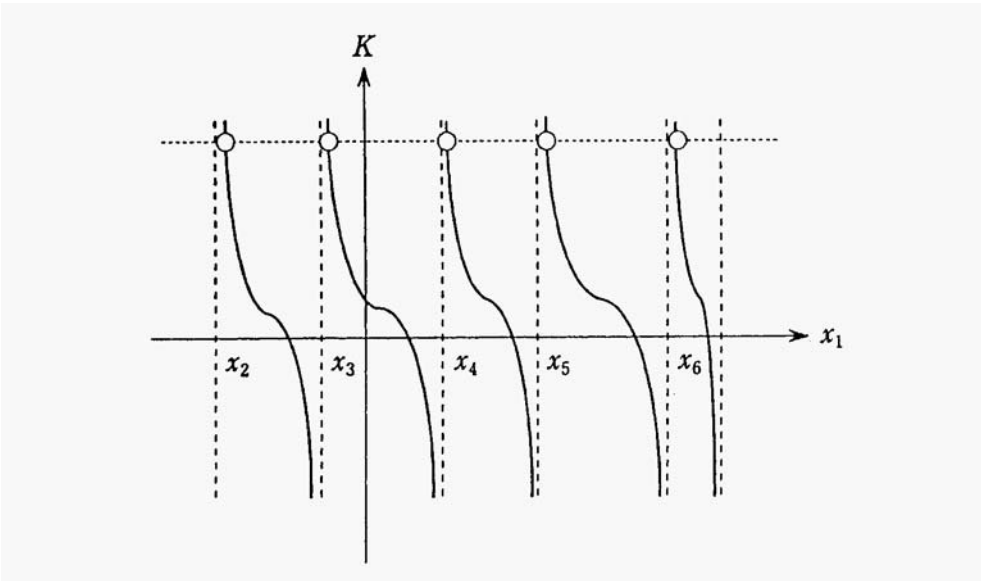

Fig. 7.6. Solutions of $K+\partial\mathcal{H}_N/\partial x_1=0$

where $G_{N,L}$ is given by the mean value over the joint probability density (7.30) as

$$G_{N,L}=\left\langle \sum_{k(\neq 1)} \frac{\delta(x_1-x_k)}{|x_1-x_k|^{\nu}} \right\rangle . \tag{7.52}$$

In the thermodynamic limit and far from the hard walls, this expression is related to spacing density at zero spacing.

Evaluation of the mean value (7.52) for a uniform spectrum of density p is quite easy. Let x_0 be any eigenvalue in a sequence of ordered eigenvalues. $<x_{-2}<x_{-1}<x_0<x_1<x_2<\cdots$. Distribution $\delta(x)$ in (7.52) is replaced by the function, $\Delta_\varepsilon(x)=0$, for $|x|>\varepsilon/2$, and $=1/\varepsilon$ for $|x|<\varepsilon/2$. Then (7.52) becomes a series of terms, each containing a pair of mean values:

$$\sum_{m=0}^{\infty}\left\{\left\langle \frac{\Delta_\varepsilon(x_0-x_{m+1})}{|x_0-x_{m+1}|^{\nu}}\right\rangle+\left\langle \frac{\Delta_\varepsilon(x_0-x_{-m-1})}{|x_0-x_{-m-1}|^{\nu}}\right\rangle\right\}. \tag{7.53}$$

The m-th term is given by

$$\rho^{\nu+1}\frac{2}{\varepsilon}\int_0^{\varepsilon/2} S^{-\nu}p_\nu^{(m)}(S)\mathrm{d}S, \qquad m=0,1,2,\cdots, \tag{7.54}$$

where $p_\nu(m)(S)$ is the the m-th order term in the spacing distribution. For m =0, $p_\nu^{(0)}$ (S) is the nearest-neighbor spacing density given by (7.43a)-(7.43c) for ν =1,2 and 4 respectively. Since $p_\nu^{(m)}(S) \cong S^{\alpha}$, with $\alpha>\nu$ for $m \geq 1$, (7.54) remains nonvanishing only for m =1 in the limit $\varepsilon \to 0$. In this limit, therefore, (7.53) becomes

$$\lim_{\substack{N,L\to\infty \\ N/L=const}} \mathcal{G}_{N,L}=\rho^{\nu+1}\lim_{S\to 0} S^{-\nu}p_\nu(S) \equiv D_\nu \rho^{\nu+1}, \tag{7.55}$$

where $p_\nu(S)=p_\nu^{(0)}(S)$ and the constants D_ν are $\pi^2/6$, $\pi^4/3$, and $2^4\pi^4/135$, for ν=1,2, and 4, respectively (see(7.43)). A similar result is available for K<0.

Finally, the tail of the curvature distribution is given for each ensemble by

$$P_{OE}(K)=(\pi^2/2)(\rho/\beta)^2\frac{1}{|K|^3}+\cdots, \tag{7.56a}$$

$$P_{UE}(K)=2^4\pi^2(\rho/\beta)^3\frac{1}{K^4}+\cdots, \tag{7.56b}$$

$$P_{SE}(K)=(2^{13}\pi^4/3)(\rho/\beta)^5\frac{1}{K^6}+\cdots \tag{7.56c}$$

for large $|K|$. We note that the powers of parameters β and ρ are consistent with the fact that $\beta K/\rho$ is the dimensionless curvature. This fact also indicates that scaling of curvature is needed in the presence of a non-uniform spectrum. The curvature distributions (7.56) are normalizable, so that they have a probabilistic interpretation. Their mean value $<K>$ is zero because densities are symmetric under the reflection $K \to -K$. The variance $<(K-<K>)2>$ is infinite for the orthogonal ensemble but finite for unitary and symplectic ensembles.

The curvature distribution in the vicinity of K = 0 is system-specific. However, Zakrzewski and Delande (1993) proposed a formula on a global feature of $P(K)$ of GUE as

$$P_{UE}(K) = (2/\pi)[1 + K^2]^{-2}, \tag{7.57}$$

which was proved valid by Oppen (1994) and Andreev and Simons (1995) for a special one-parameter family of Hamiltonians.

In this way, we can recognize why quantum spectra of classically-chaotic systems obey the same universal level distributions as in the random matrix theory. Since the statistical mechanics of a gCM system leads to the curvature distribution as well as the major issue of the random matrix theory, it is more generic than the traditional framework of random matrix theory.

7.4. Statistical Mechanics of gCS System in Intermediate Regime

While we have so far assumed the fully-chaotic systems underlying the quantum irregular spectra, most of the dynamical systems possess a mixed feature that KAM tori coexist with chaos. So it is desirable to find out intermediate statistical behaviors bridging between the Poissonian and Gaussian ensemble statistics. There is however no universal statistical behavior in the intermediate regions which is highly system-specific. Choosing the number variance which describes the long-range (rather than short-range) correlation of ensemble of levels, we shall show below one interesting channel introduced by Gaudin as early as 1966. The model certainly interpolates the Poisson and circular unitary (CUE) ensembles by a single tunable parameter z ($0 \le z \le 1$) and is described by the N-angle joint distribution

$$P(\varphi_1,\varphi_2,\cdots,\varphi_N) = C_N \prod_{j<k} \left| \frac{\varepsilon_j - \varepsilon_k}{\varepsilon_j - z\varepsilon_k} \right|^2 , \tag{7.58}$$

where φ ($0 \le \varphi < 2\pi$) stands for the eigenvalue of unitary matrix, $\varepsilon_j = \exp(2\pi i \varphi_j)$. Equation (7.58) reduces to

$$P(\varphi) = \text{const.} \tag{7.59a}$$

and

$$P(\varphi) = \prod_{j<k} |\varepsilon_j - \varepsilon_k|^2 \tag{7.59b}$$

in the limits $z \to 1$ and $z \to 0$, respectively; Equations (7.59a) and (7.59b) represent the Poisson and CUE joint distribution functions, respectively.

The expression in (7.58) can be rewritten as

$$P(\varphi_1,\varphi_2,\cdots,\varphi_N) = C'_N \prod_{j<k} \left| \frac{\sin^2(\frac{\varphi_j-\varphi_k}{2})}{1+4b\sin^2(\frac{\varphi_j-\varphi_k}{2})} \right|^2 , \tag{7.60}$$

with $b = z/(z - 1)^2$ and $C'_N = C_N(2/1 - z))^{N(N-1)}$. It should be noted that Gaudin's distribution can be derived from the partition function of the Calogero-Sutherland system (see (7.23), with the replacement (7.26)), i.e., a universal dynamical system behind periodically-pulsed quantum systems that are classically *mixed.* In fact, assume a Gibbs measure for the system in (7.29):

$$dZ = \prod_j dp_j \prod_{j<k} d\Lambda_{jk} \prod_j (d\varphi_j /2\pi) \exp(-\beta H_{CS} - \lambda Q) , \tag{7.61}$$

with the following constraint for the total "charge" :

$$Q = \sum_{j<k} |\Lambda_{jk}|^2 . \tag{7.62}$$

In (7.61) λ denotes a Lagrange multiplier. Integrating (7.61) over irrelevant variables $\{p_j\}$ and $\{\Lambda_{jk}\}$, one recovers (7.60) with a prescription $b=\lambda/\beta$. The normalization constant in (7.60) is calculated as

$$C'_N = N!^{-1}(2/(1-z))^{N(N-1)} \prod_{k=1}^{N} \frac{1-z^k}{1-z} . \tag{7.63}$$

We shall now demonstrate how the joint distribution function in (7.58) will lead to a formula of the number variance interpolating between the Poisson and CUE limits. The number of levels contained in an energy interval of length s is a stochastic variable with its average $\langle n(s)\rangle = s$, and the number variance is the fluctuation $\Sigma^2(s) := \langle\langle n(s)-n\rangle^2\rangle$. $\Sigma^2(s)$ represents a spectral rigidity and is related to the two-level cluster function as explained below.

Using Gaudin's result for the two-level correlation function,

$$R_2(\varphi_1,\varphi_2) = N(N-1)\int\cdots\int d\varphi_3\cdots d\varphi_N P(\varphi_1,\varphi_2,\cdots,\varphi_N)$$

$$= N(N-1) \; -2\Re \sum_{\lambda<\mu} \prod_{k=\lambda}^{\mu-1} \frac{1-z^k}{e^{2\pi i(\varphi_1-\varphi_2)}-z^k} \quad , \tag{7.64}$$

one obtains the two-level cluster function

$$Y_2(\xi_1,\xi_2) = 1-[N(N-1)]^{-1}R_2$$

$$= 2\,[N(N-1)]^{-1}\,\Re \sum_{\lambda<\mu} \prod_{k=\lambda}^{\mu-1} \frac{1-z^k}{e^{2\pi\, i(\xi_1-\xi_2)/N}-z^k} \quad , \tag{7.65}$$

where $\Re$ stands for "real part of' and ξ_i is the unfolded level given by $\xi = N\varphi$. Let us introduce the level separation $r = |\xi_1-\xi_2|$ *(<<N)* and parametrize z as

$$z = \exp(-2\pi a/N).$$

Then, in the limit $N \to \infty$, (7.65) reduces to

$$Y_2(r;a) \sim 2\,[N(N-1)]^{-1}\,\Re \sum_{\lambda<\mu} \exp\left[-\frac{2r\pi\, i}{N} \sum_{k=\lambda}^{\mu-1} (1-\exp(-2\pi a k/N))^{-1}\right]$$

$$\sim \left| \int_0^1 \exp[(-ir/a)\ln(e^{2\pi\, a\, x}-1)]\,dx \right|^2 . \tag{7.66}$$

The number variance Σ^2 is related to the two-level cluster function $Y_2(r)$ through

$$\Sigma^2(s;a) = s - 2\int_0^s (s-r)\,Y_2(r;a)\,dr \quad . \tag{7.67}$$

Using (7.66) in (7.67) and prescribing $v = -\ln[\exp(2\pi a)-1]$, one gets

$$\Sigma^2(s;a) \sim s - \int_v^\infty \int_v^\infty \frac{d\omega d\omega'}{(e^{\omega}+1)(e^{\omega'}+1)} \frac{\sin^2 \frac{(\omega-\omega')s}{2a}}{(\pi(\omega-\omega'))^2} \quad . \tag{7.68}$$

The asymptotic $(s \to \infty)$ behavior of (7.68) turns out to be

$$\Sigma^2(s;a) \sim [\,(1-e^{-2\pi a})/(2\pi a)]\,s$$

$$+ [(1-e^{-2\pi a})/(2\pi)]^2(\ln(s) + \text{const}) , \tag{7.69}$$

recovering the Poisson (~s) and CUE (~ ln(s)) behaviors in the special limits of $\alpha \to 0$ ($z \to 1$) and $\alpha \to \infty$ ($z \to 0$), respectively. Equation (7.69) shows that the number variance in the intermediate region ($0<\alpha<\infty$) is an arithmetic sum of the Poisson and CUE behaviors. A work in this direction was recently developed by Ma and Hasegawa (1995).

The s-linear term in (7.69) can be given an interesting interpretation by invoking a grand canonical treatment of the distribution of (7.58): In fact, Gaudin proposed an analogy with one-dimensional interacting gas, deriving from (7.58) an equation of state, with fugacity (or chemical potential) ζ:

$$\beta p = \int_0^\infty \ln(1+\zeta e^{-2\pi\alpha x}) dx \,, \tag{7.70a}$$

$$\rho = \zeta \frac{\partial}{\partial \zeta}(\beta p) = (2\pi\alpha)^{-1} \ln(1+\zeta) \,, \tag{7.70b}$$

where p and ρ are the pressure and particle density of the fictitious gas. Equation (7.70) gives rise to the compressibility of the interacting gas,

$$\frac{\partial}{\partial \rho}(\beta p) = \frac{\partial \zeta}{\partial \rho}\frac{\partial}{\partial \zeta}(\beta p) = (1 - e^{-2\pi\alpha})/(2\pi\alpha) \,, \tag{7.71}$$

which is just the coefficient of the s-linear term in (7.69). It is controversial to take the thermodynamic limit $N \to \infty$ before the integration procedure in (7.66). As a prototype of the intermediate statistical behavior between the Poisson and circular unitary ensembles, however, the analysis leading to (7.69) merits further scrutiny.

7.5. Extension to Case of Several Parameters

The gCM equation in 1+1 dimensions has been derived from the eigenvalue problem characterized by a single tunable nonintegrability parameter. No corresponding fundamental equation has yet been found, however, when several nonintegrability parameters are included in the Hamiltonian. We now consider the eigenvalue problem in this case. If several parameters are changed in the Hamiltonian, we shall see the occurrence of degeneracies of eigenvalues. Crossings of

eigenvalues have codimensions 2, 3, and 5 depending on the real, complex and quaternionic Hermitian nature of the Hamiltonian, respectively. The codimension here implies the number of independent parameters. As mentioned in the previous chapter, the formalism of quantum mechanics have some interesting features in the adiabatic limit. In particular, a fictitious gauge field is induced at the degeneracies and the wavefunction acquires a geometric phase induced by the gauge field in the adiabatic transport in $d(\geq 2)$-dimensional parameter space. Corresponding to this fact, we shall show below that in the adiabatic limit the eigenvalue problem with $d(\geq 2)$ parameters will be reduced to a field-theoretical model involving a gauge field (Nakamura *et al.,* 1992).

Suppose the Hamiltonian has a form linear in the nonintegrability parameters $\mathbf{x}=(x_1, x_2, \cdots, x_d)$:

$$H(x)=H_0+\sum_{\mu=1}^{d} x_\mu V_\mu. \tag{7.72}$$

On the r.h.s. of (7.72), the first term represents the integrable part, and the second term consists of a set of $d(\geq 2)$ nonitegrable perturbations describing, for instance, the anisotropy energy, couplings with magnetic and electric fields, etc. Further, we assume that both H_0 and $\{V_u\}$ are Hermitian $(H_0^+=H_0,\ V_u^+=V_u)$ and mutually noncommutable:

$$[H_0, V_\mu]=G_\mu, \tag{7.73}$$

$$[V_u, V_v]=G_{\mu\nu}\ . \tag{7.74}$$

From (7.73) and (7.74), G_u and G_{uv} prove to be anti-Hermitian operators $(G_u^+ =-G_u,\ G_{uv}^+=-G_{uv})$.

Consider the desymmetrized spectrum corresponding to the eigenvalue problem

$$H(\mathbf{x})|n(\mathbf{x})\rangle=\phi_n(\mathbf{x})\ |n(\mathbf{x})\rangle. \tag{7.75}$$

The spectrum is now constructed in $\mathbf{x}$ space and each eigenvalue $\{\phi_n(\mathbf{x})\}$ defines a hyper-energy surface. We can see contacts of adjacent energy surfaces at degenerate points, as well as the avoided crossings of these surfaces. In the vicinity of each degeneracy a pair of energy

surfaces constitute two sheets of a double-cone (diabolo). The diabolical point is a source of topological singularity: For a closed loop around the degeneracy in $\mathbf{x}$ space, a pair of eigenstates $|n(\mathbf{x})\rangle$ and $n+1(\mathbf{x})\rangle$ joining the double-cone acquires the global Berry phase

$$\mathrm{i}\sum_{\mu=1}^{d}\oint \langle \mathrm{n}(\mathbf{x})|\,\partial_{\mu}|n(\mathbf{x})\rangle \mathrm{d}x_{\mu}\,. \tag{7.76}$$

The formula (7.76) also applies to state $|n+1(\mathbf{x})\rangle$. The global phase (7.76) is due to the phase arbitrariness of eigenfunctions, i.e., an essential characteristics of the framework of quantum mechanics which manifests itself in the fact that eigenfunctions are multi-valued in a higher-dimensional parameter space, though of course single-valued in the configuration space. The integrand in (7.76), $\mathrm{i}\langle n(\mathbf{x})|\,\partial_{\mu}|n(\mathbf{x})\rangle$, plays the role of gauge field. As a natural extension of the treatment of the single parameter case, one may anticipate that the presence of many diabolos and avoided crossings of hyper-energy surfaces would be an indicator of quantum nonintegrability characterized by several nonintegrability parameters.

Taking $\{x_{u}\}$ as d -dimensional Euclidean *"spacetime"* coordinates, let usregard $\{\phi_{n}(\mathbf{x})\}$ and $\{|n(\mathbf{x})\rangle\}$ $(=(|1(\mathbf{x})\rangle, |2(\mathbf{x})\rangle, \bullet\bullet\bullet, |D(\mathbf{x})\rangle)$ with $\langle n(\mathbf{x})|\,n'(\mathbf{x})\rangle=\delta_{nn'}$) as internal classical vector and matrix fields, respectively. Note: $1\le\mu\le d;\ 1\le n\le D$. D may be infinite. Einstein's contraction will not be taken below. Closely following the derivation of the 1+1 dimensional Calogero-Moser system, let us take the $\mathbf{x}$ derivative of (7.75) and introduce a set of constant orthonormal vectors $\mathbf{e}_1, \mathbf{e}_2, \bullet\bullet\bullet, \mathbf{e}_d$ with $\mathbf{e}_u\ \mathbf{e}_v=\delta_{\mu\nu}$; we get

$$A_{n,\mu}=\mathrm{i}\langle n\,|\,\partial_{\mu}|\,n\rangle, \tag{7.77}$$

$$\sum_{\mu}\ \partial_{\mu}{}^{2}\phi_{n}\,\mathbf{e}_{\mu}=2\sum_{\mu}\ \sum_{m(\neq n)}\langle n|\bar{\Lambda}_{\mu}|m\rangle\langle m|\bar{\Lambda}_{\mu}|n\rangle\ (\phi_{n}-\phi_{m})^{-3}\mathbf{e}_{\mu}, \tag{7.78a}$$

$$\sum_{\mu}\ (\partial_{\mu}+\mathrm{i}A_{n,\mu})\bar{\Lambda}_{\mu}|n\rangle\mathbf{e}_{\mu}=-\mathrm{i}\sum_{\mu}\ \sum_{m(\neq n)}\ \bar{\Lambda}_{\mu}|m\rangle\langle m|\bar{\Lambda}_{\mu}\ |n\rangle\ (\phi_{n}-\phi_{m})^{-2}\,\mathbf{e}_{\mu}\,, \tag{7.78b}$$

with the nonnegative Hermitian $\bar{\Lambda}_{\mu}=\Lambda_{\mu}-\lambda_{\mu}I$ which has its unique inverse $\bar{\Lambda}_{\mu}{}^{-1}$. Here

$$\Lambda_\mu = i^{-1}[H, V_\mu] = i^{-1} G_\mu + i^{-1} \sum_{\nu(\neq\mu)} x_\nu G_{\nu\mu} \ , \tag{7.79}$$

and λ_u is the lowest eigenvalue of Λ_μ. Since Λ_μ in (7.79) does not include x_u, both λ_μ and $\bar{\Lambda}_\mu$ are x_u-independent, so that $\partial_\mu \bar{\Lambda}_\mu = 0$, which has been exploited in deriving (7.78). For the description below we should also note that $\langle n | \bar{\Lambda}_\mu | n \rangle = -\lambda_\mu$, independent of n. Some properties of $A_{n,u}$, defined in (7.77), are of interest. Contrary to the single parameter case, $A_{n,u}$ is nonvanishing in general and acts like $U(1)$ gauge field: Under the gauge transformation $|n\rangle \to |n\rangle \exp(i\chi_n)$, $A_{n,\mu}$ transforms as $A_{n,\mu} \to A_{n,u} - \partial_\mu \chi_n$ but the magnetic field $B_{n,\mu\nu} = \partial_\mu A_{n,\nu} - \partial_\nu A_{n,\mu}$ is gauge- invariant. The comparison with existing results is straightforward: For d=1 with An,u=0, (7.78) reduces to the gCM system, while for d>1 and suppressing the level dynamics (7.78), only the gauge potential (7.77) is available. (Note however that, in case of d >*s,* the degeneracies are not isolated but form lines or surfaces where nonAbelian gauge field $A^{\alpha,\beta}_{n,\mu} = i\langle n_\alpha | \partial_\mu | n_\beta \rangle$ would appear. However, we here confine ourselves to the case *d=s.*)

For illustration of the case *d=s*=3, let us reinvestigate the standard 2x2 Hamiltonian (6.11) in the previous chapter, where $H_0 = \varepsilon I$, **x=R** and $V = \frac{1}{2}\boldsymbol{\sigma}$. The eigenvalue problem $H|\pm\rangle = \phi_\pm |\pm\rangle$ has a solution which, in the present notation, can be written as

$$\phi_\pm = \varepsilon \pm \tfrac{1}{2} R \ , \tag{7.80}$$

$$|+\rangle = \mathcal{N}\{(x - iy)\mathbf{u} + (R - z)\mathbf{v}\},$$

$$|-\rangle = \mathcal{N}\{(z - R)\mathbf{u} + (x + iy)\mathbf{v}\} \ , \tag{7.81}$$

with $R = (x^2 + y^2 + z^2)^{1/2}$ and $\mathcal{N} = \{x^2 + y^2 + (R-z)^2\}^{-1/2}$. The quantities **u** and **v** are orthonormal basis functions in an **R** -independent (diabatic) representation. From the viewpoint of nonlinear dynamics, (7.80) and (7.81) should satisfy (7.78). Noting $G_x = 0$, $G_{y,x} = -i\boldsymbol{\sigma}_z/2$, and $G_{z,x} = i\boldsymbol{\sigma}_y/2$, Λ_x in (7.79) is given by $\Lambda_x = (-y\boldsymbol{\sigma}_z + z\boldsymbol{\sigma}_y)/2$, and thereby

$$\langle - | \bar{\Lambda}_x | + \rangle = \langle + | \bar{\Lambda}_x | - \rangle^+ = (yR + ixz)/[2(x + iy)]. \tag{7.82}$$

As for the gauge field, using (7.81) in (7.77), one obtains

$$A_{+x}=-2y/[R(R-z)]. \tag{7.83}$$

In a similar way, the y and z components are also available. The solution (7.80) and (7.81) prove to satisfy (7.78) only when the gauge potential in (7.83) is used together. This concrete example indicates a crucial role of the coupling of the gauge potential with level dynamics in the case $d' \geq 2$.

We now note that (7.78) with (7.77) can be obtained from a field-theoretical model. In fact, by introducing a classical Lagrangian density

$$\mathcal{L}=\mathcal{L}_0+\mathcal{L}', \tag{7.84a}$$

with

$$\mathcal{L}_0=\sum_{\mu,n}(1/2)(\partial_\mu\phi_n)^2\mathbf{e}_\mu-\mathbf{i}\sum_{\mu,n}(\partial_\mu\langle n|)\bar{\Lambda}_\mu|n\rangle\mathbf{e}_\mu$$

$$-\sum_{\mu,\nu}A_{n,\mu}(\langle n|\bar{\Lambda}_\mu|n\rangle+\lambda_\mu)\mathbf{e}_\mu \tag{7.84b}$$

and

$$\mathcal{L}'=-(1/2)\sum_{\mu}\sum_{\substack{m,n\\ m\neq n}}\langle n|\bar{\Lambda}_\mu|m\rangle\langle m|\bar{\Lambda}_\mu|n\rangle(\phi_n-\phi_m)^{-2}\mathbf{e}_\mu\ , \tag{7.84c}$$

we derive Lagrange equations from (7.84) as

$$\partial\mathcal{L}/\partial\phi_n-\sum_\mu\partial_\mu(\partial\mathcal{L}/\partial_\mu\phi_n)=0, \tag{7.85a}$$

$$\partial\mathcal{L}/\partial\langle n|-\sum_\mu\partial_\mu(\partial\mathcal{L}/\partial_\mu\langle n|)=0, \tag{7.8513}$$

$$\partial\mathcal{L}/\partial A_{n,\mu}=0. \tag{7.86}$$

As easily verified, (7.85) exactly reproduces (7.78). On the other hand, (7.86) yields the constraint given below (7.79). Noting $\partial_\mu(\bar{\Lambda}_\mu|n\rangle)=\Lambda_\mu\partial_\mu|n\rangle$ and multiplying (7.8513) or (7.7813) from the left by $\mathbf{e}_\nu\langle n|\bar{\Lambda}_\nu^{-1}$, we can recover (7.77).

In contrast with the generalized Calogero-Moser model in 1+1 dimensions for the single parameter case, we have now a novel field-theoretical model inspired by the eigenvalue problem associated with

several nonintegrability parameters. In this model, *"spacetime"* coordinates represent a set of nonintegrability parameters, and matter fields ($\{\phi_n\}$ and $\{|n\rangle\}$) are coupled with fictitious gauge fields $\{A_{n,u}\}$. The gauge fields here are composed of the matter fields themselves, as in the complex Grassmannian sigma model. We can proceed to search for instanton-like structures in (7.85) and (7.86) and to construct the statistical mechanics of (7.78), just as attempted in the gCM system.

In case where two or more parameters are varied, the quantum-mechanical signature of chaos should be the presence of many diabolical crossing points (monopoles) and avoided crossings between adjacent energy surfaces. If a single one of $d(\geq 2)$ nonintegrability parameters is changed, the resultant energy spectrum can be interpreted as a vertical cross-section of a landscape that consists of many sheets of energy surfaces piled on **x** space in $d(\geq 2)$ dimensions (see Fig. 7.7): In the spectrum, one can see only avoided crossings but no diabolical conical points (monopoles). The complicated energy spectra with

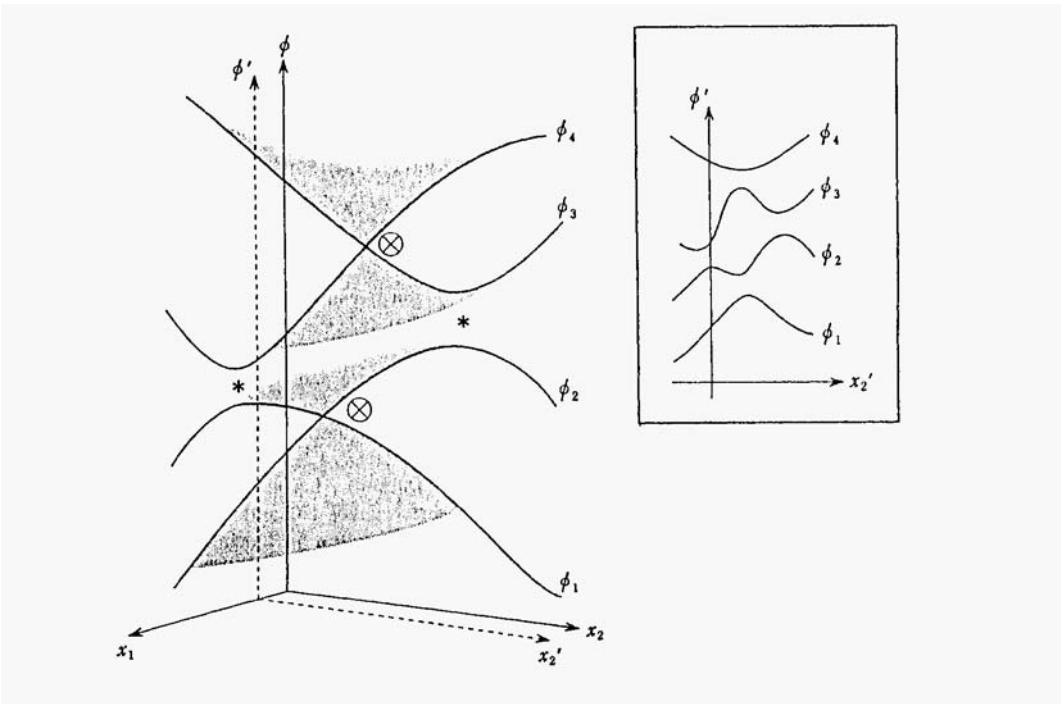

Fig. 7.7. Piled sheets of hyperenergy surfaces in case of d=2. Cross-in-circles and stars indicate diabolical degeneracy and avoided crossing, respectively. Inset: vertical intersection at $\phi' \text{-} x'_2$ plane.

many avoided crossings are therefore regarded as having a dense monopole population behind them. While, as pointed out in Chap. 1, the collapse of tori and onset of chaos are disturbing the foundations of the framework of quantum mechanics in the adiabatic limit when no quantum transition is allowed, we now understand that this framework already exhibits a very puzzling feature in the same limit.

In closing this chapter, we should emphasize: (1) The irregularity of quantum spectra and wavefunctions is caused by the incompatibility between *quantum* and *chaos*. (2) The random matrix theory describes only a very limited quantal aspect of systems that are classically chaotic. (3) The dynamical and statistical treatment of gCM/gCS systems with some constraints will provide more potential issues that are strongly and directly related to experiments.

References

Andreev, A. V., and Simons, B. D. (1995). *Phys. Rev. Lett.* **75,** 2304.

Dyson, F. J. (1962). *J. Math. Phys.* **3,** 1191.

Feynman, R. P. (1939). *Phys. Rev.* **56,** 340.

Gaspard, P., Rice, S. A., Mikeska, H. J., and Nakamura, K. (1990). *Phys. Rev.* **A42,** 4015.

Gaspard, P., Rice, S. A., and Nakamura, K. (1989). *Phys. Rev. Lett.* **63,** 930.

Gaudin, M. (1966). *Nucl. Phys.* **85,** 545.

Iu, C., et al. (1989). *Phys. Rev. Lett.* **63,** 1133.

Ishio, H., and Nakamura, K. (1992). *Phys. Rev.* **A46,** R2193.

Lanford, 0. E., and Lebowitz, J. L. (1975). *Lecture Notes in Physics* **38.** Berlin: Springer.

Ma, J. Z., and Hasegawa, H. (1995). *J. Phys. Soc. Jpn.* **64,** 2261.

Mehta, M. L. (1967). *Random Matrices and the Statistical Theory of Energy Levels.* New York: Academic.

Mehta, M. L., and Gaudin, M. (1960). *Nucl. Phys.* **18,** 420.

Mehta, M. L., and Gaudin, M. (1961). *Nucl. Phys.* **22,** 340.

Nakamura, K. (1993). *Quantum Chaos: A New Paradigm of Nonlinear Dynamics.* Cambridge: Cambridge University Press.

Nakamura, K., and Lakshmanan, M. (1986). *Phys. Rev. Lett.* **57,** 1661.

Nakamura, K., Lakshmanan, M., Gaspard, P., and Rice, S. A. (1992). *Phys. Rev.* **A46,** 6311.

Nakamura, K., and Mikeska, H. J. (1987). *Phys. Rev.* **A35,** 5294.

von Oppen, F. (1994). *Phys. Rev. Lett.* **73,** 798.

Pechukas, P. (1983). *Phys. Rev. Lett.* **61,** 943.

Rice, S. A., Gaspard, P., and Nakamura, K. (1992). In *Advances in Classical Trajectory Methods* **1,** W. L. Hase, ed. Connecticut: JAI Press.

Sinai, Y. G. (1976). *Introduction to Ergodic Theory.* Princeton: Princeton University Press.

Yukawa, T. (1985). *Phys. Rev. Lett.* **54,** 1883.

Zakrzewski, J., and Delande, D. (1993). *Phys. Rev.* **E47,** 1650.

Chapter 8

Towards Time-Discrete Quantum Mechanics

In this chapter, we shall forsake the traditional way of studying the problem of quantum versus chaos and attempt to implement my own idea of going in a radically new direction. This chapter is devoted to intensive investigation of the role of *time discretization* in both classical and quantum mechanics. Firstly, we shall comprehend how the time discretization in classical dynamics renders the time-continuous integrable system nonintegrable and chaotic. We concentrate on the phenomenon of *separatrix splitting* and a complicated homoclinic structure that constitute a symptom of chaos. Taking a time-discrete dynamical system with a double-well potential as an example, this interesting feature will be demonstrated analytically on the basis of *asymptotic expansions beyond all orders.*

Secondly, to accommodate temporal chaos also in quantum dynamics, we shall again introduce *"time difference"* Δt and propose a time-difference version of Heisenberg equation of motion. This new equation, preserving neither the unitarity nor equal-time commutation rule for (originally) conjugate operators, is demonstrated to have a chaotic solution bearing a resemblance to that of the corresponding classical dynamical equations.

8.1. Stable and Unstable Manifolds in Time-Discrete Classical Dynamics

We have arrived at a suitable point in which to abandon the traditional

way of studying the problem of quantum versus chaos, which is to apply established quantum mechanics to classically-chaotic systems. So far we have addressed a series of questions arising from the incompatibility between quantum and chaos and also hint at the necessity to conceive an alternative framework of quantum mechanics that will allow genuine chaos in quantum dynamics. The latter point was also suggested previously in the epilogue of another book of mine (Nakamura, 1993).

In this chapter, I shall try to materialize my idea to head in an altogether new direction, by discretizing *"time."* The significance of the time discretization is well recognized in classical dynamics. So let us begin with elucidating how the time discretization in classical dynamics should lead to the Birkhoff-Smale's horse-shoe.

More than one century ago Poincare' (1890) pointed out the phenomenon of separatrix splitting and a complicated homoclinic and heteroclinic structure as a symptom of chaos. The homoclinic or heteroclinic structures caused by bifurcation of separatrices lead to Birkhoff-Smale's horse-shoe mechanism generating the chaos in conservative dynamical systems. While numerical iterations of low-dimensional mappings provide easily these complicated structures, it is extremely difficult to derive them analytically. However, the difficulty will now be overcome by using the *asymptotic expansion beyond all orders.* This method was first proposed and applied to a standard map by Lazutkin and coworkers (Lazutkin *et al.,* 1988; Gelfreich et al., 1994) and to other systems (Amit *et al.,* 1992). A similar approach was developed independently by Kruskal and Segur (1991) in the context of crystal growth. The method was sharpened by being supplemented by the theoretical tools of Borel summability and Stokes phenomenon (Hakkim and Mallick, 1993; Tovbis, 1994; Tovbis *et al.,* 1996). While this updated method is still in its infancy, we shall apply it to the time-discrete dynamical system with double-well potential (Nakamura and Hamada, 1996).

We shall analyze a symplectic mapping obtained by time discretization (via *time difference* σ) of canonical equations for the dynamical system with a single degree of freedom. Consider the canonical equations of motion

$$\mathrm{d}q(t)/\mathrm{d}t=p(t), \quad \mathrm{d}p/\mathrm{d}t=-\mathrm{d}U(q)/\mathrm{d}q \ . \tag{8.1}$$

For concreteness, we choose a double-well potential

$$U(q)=(q-a)^2(q+a)^2, \tag{8.2}$$

which is often encountered in describing the phase transition phenomena.

The set of equations (8.1) with (8.2) are widely encountered in various contexts: The Duffing equation without damping and driving forces takes the identical form; it also arises if one substitutes $\Psi(x, t) = e^{iwt}\, q(x)$ in the cubic nonlinear Schrödinger equation and then replace x by t in the resultant form. While the above ordinary differential equation is integrable, we shall consider its time-difference variant obtained by discretizing time (with *time difference* σ). Among many ways of time discretization, the symplectic mapping is the most essential; it is given by

$$q_{n+1}=q_n+\sigma p_{n+1}\ ,$$
$$p_{n+1}=p_n-\sigma\, dU(q)/dq\ \big|_{q=q_n}=p_n-4\,\sigma q_n(q_n+a)(q_n-a)\ . \tag{8.3}$$

(By rescaling $\sigma p \to p$, (8.3) is reduced to the map available from a periodically-kicked system, where σ^2 plays the role of the kicking strength. In this chapter, however, we shall choose the form (8.3) for convenience.)

The Jacobi matrix corresponding to (8.3) is

$$M=\begin{pmatrix} \dfrac{\partial q_{n+1}}{\partial q_n} & \dfrac{\partial q_{n+1}}{\partial p_n} \\ \dfrac{\partial p_{n+1}}{\partial q_n} & \dfrac{\partial p_{n+1}}{\partial p_n} \end{pmatrix}=\begin{pmatrix} 1-4\sigma^2(3q_n^2-a^2) & \sigma \\ -4\sigma(3q_n^2-a^2) & 1 \end{pmatrix}. \tag{8.4}$$

The present map is area-preserving, since det M=1, and satisfies the symplecticity condition $M^TJM=J$ with $J=\begin{pmatrix} 0 & 1 \\ -1 & 0 \end{pmatrix}$. [This condition is not satisfied by the map obtained via the Euler difference which replaces the 1st line of Eq. (8.3) by $q_{n+1}=q_n+\sigma p_n$.]

The map (8.3) and its continuum (8.1) and (8.2) have common fixed points, i.e., one hyperbolic, at $(q, p)=(0,0)$, and the other two elliptic at $(q, p)= (\pm a, 0)$.

For $\sigma=0$ (i.e., in the continuum limit), phase space is occupied by regular trajectories including a separatrix, i.e., the marginal trajectory

by which localized and extended trajectories are segregated (see Fig. 8.1(a)). The separatrix is the most unstable against a perturbation and consists of a pair of degenerate manifolds: One is unstable and going away from the hyperbolic fixed point (HFP), while the other is stable and coming into HFP. On switching a perturbation arising from $\sigma \neq 0$, the splitting of the separatrix occurs, yielding an infinite number of crossing points (homoclinic points) that accumulate as HFT is approached (see Fig. 8.l(b)). The separatrix splitting and complicated

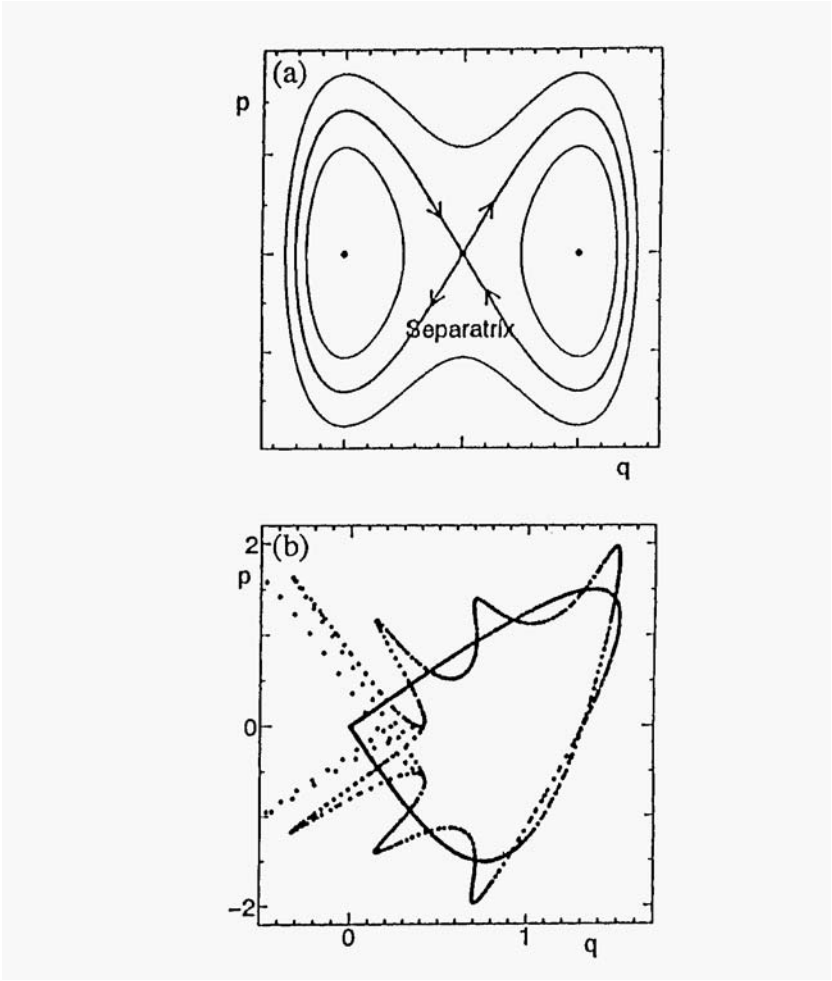

Fig. 8.1. Trajectories in phase space: (a) $\sigma=0$ Separatrices are emerging from hyperbolic fixed point at (0,0). (b) $\sigma \neq 0$. Splitting of degenerate separatrices for the right half.

homoclinic structures lead to the genesis of chaos. We shall carry out the asymptotic analytical expansion of the unstable manifold emanating from HFP at (0,0). While concentrating on the system with a double-well potential, the analysis hereafter will extend to more general systems such as those with cubic and cosine potentials.

8.2. Breakdown of Perturbation Theory

Prescribing q_n and q_{n+1} as $y(t)$ and $y(t+\sigma)$, respectively, let us concentrate on the unstable manifold $y_u(t)$ with the initial condition $\lim_{t\to-\infty} y_u(t) = 0$. For brevity, $y_u(t)$ will be taken as $y(t)$ in the following. A pair of Eqs. (8.3) are then reduced to a second-order difference equation for $y(t)$:

$$\Delta^2 y(t)/\sigma^2 = -4y(t)(y(t)-a)(y(t)+a), \tag{8.5}$$

with $\Delta^2 y(t) = y(t-\sigma)+y(t+\sigma)-2y(t)$.

Let us first attempt applying the ordinary perturbation theory 'a la Melnikov. Using Taylor's expansion as $\Delta^2 y(t) = \sigma^2 \mathrm{d}^2 y(t)/\mathrm{d}t^2 + 2\sum_{l=2}^{\infty} (\sigma^{2l}/(2l)!) y^{(2l)}(t)$, one may rewrite (8.5) as

$$\mathrm{d}^2 y(t)/\mathrm{d}t^2 = -4y(t)(y(t)-a)(y(t)+a) - 2\sum_{l=2}^{\infty} \sigma^{2(l-1)}((2l)!)^{-1} y^{(2l)}(t). \tag{8.6}$$

Taking the last term on the r.h.s. of (8.6) as a perturbation, we expand the solution $y(t)$ in a power series of σ^2:

$$y(t) = y_0(t) = y_{00}(t) + \sigma^2 y_{01}(t) + \sigma^4 y_{02}(t) + \cdots . \tag{8.7}$$

The lower index of $y_0(t)$ is used to indicate that the solution in (8.7) will turn out to be incomplete without *"terms beyond all orders."* Using (8.7) in (8.6), equations are obtained successively for each power of σ^2

$$\mathrm{d}^2 y_{00}(t)/\mathrm{d}t^2 = -4y_{00}(t)(y_{00}(t)+a)(y_{00}(t)-a), \tag{8.8a}$$

$$\mathrm{d}^2 y_{01}(t)/\mathrm{d}t^2 = -4(3y_{00}(t)^2 - a^2)y_{01}(t) - (1/12)\mathrm{d}^4 y_{00}(t)/\mathrm{d}t^4,$$

etc. (8.8b)

For the unperturbed system (8.8a), we have

$$y_{00}(t)=\sqrt{2}\,a/\cosh(2at)\,. \tag{8.9}$$

The functions $y_{0n}(t)$ for n =1,2,• • •, have the following properties: (i) They should satisfy the boundary condition ensuring that the orbit (constructed from (8.7)) will start from HFP at (0,0) :

$$\lim_{t\to-\infty} y_{0\,n}(t)=0, \qquad n=0,1,\bullet\bullet\bullet\,.$$

(ii) Their parity is even: $y_{0n}(-t)=Y_{0n}(t)$, for n=1,2,•••, because of the even-parity nature of the inhomogeneous term on r.h.s. of (8.8b) and the uniqueness of the solution for y0n(t), for n=1,2,• • •, under the unique initial condition.

The solution of (8.8b) is a sum of a general solution for its homogeneous part and the special one for the full inhomogeneous equation. The former is a linear combination of two independent solutions $v_1(t)$ and $v_2(t)$ given by

$$v_1(t)=-\frac{2\sqrt{2}a^2\sinh[2at]}{\cosh^2[2at]}\,, \tag{8.10a}$$

$$v_2(t)=-\frac{1}{8\sqrt{2}a^3}\left(\frac{6at\sinh[2at]}{\cosh^2[2at]}-\frac{3}{\cosh[2at]}+\cosh[2at]\right). \tag{8.10b}$$

Any linear combination of (8. 10a) and (8. 10b), however, cannot satisfy both (i) and (ii) at the same time: $v_1(t)$ has an odd parity and is incompatible with (ii); $v_2(t)$ diverges for $t\to-\infty$. Hence the solution of (8.8b) is inevitably provided by the latter special contribution alone, i.e.,

$$y_{01}(t)=\frac{a^3\sqrt{2}}{12\cosh^3(2at)}[9-7\cosh(4at)+2at\bullet\sinh(4at)]\,. \tag{8.11}$$

Because of the even-parity nature, the result (8.11) can lead to no splitting of the separatrix, which is not consistent with the issue of numerical iteration of the map (8.3) with $\sigma>0$.

This paradox is caused by the singularities of (8.9) and (8.11) at $t=\pm\frac{i\pi}{4a}(2m+1)$, with m=0,1,• • • , encountered in changing the time

t continuously from $t=-\infty$ to $t=+\infty$ in the complex time plane. In fact, in the neighbourhood of $t_c=\dfrac{i\pi}{4a}$,

$$y_\infty \sim \frac{c_0 i}{(t-t_c)}, \qquad \text{with } c_0=-\frac{\sqrt{2}}{2}. \tag{8.12a}$$

Similarly, reflecting the degree of the singularity of the inhomogeneous part of (8.8b), we find

$$y_{01} \sim \frac{c_1 i}{(t-t_c)^3}, \quad c_1=\frac{\sqrt{2}}{6},$$
$$\cdots\cdots\cdots\cdots\cdots$$
$$y_{0n} \sim \frac{c_n i}{(t-t_c)^{2n+1}}, \quad c_n \sim (-1)^{n+1}(2n+3)!/(2\pi)^{2n+1}, \quad \text{for } n\to\infty. \tag{8.12b}$$

The behaviour in (8.12) indicates that all orders in the expansion (8.7) give the contributions of the identical magnitude of $O(\sigma^{-1})$ at $|t-t_c|\sim\sigma$ and that the perturbation theory breaks down there. The crucial poit is that we meet the Stokes phenomenon: (i) Stokes line is emanating from $t=t_c$; (ii) a suitable odd-parity correction should be incorporated in crossing this line.

To analyze this phenomenon and to capture the *"terms beyond all orders,"* we next derive the internal equation, effective in the vicinity of $t=t_c$.

8.3. Internal Equation and Stokes Phenomenon

Let us enlarge a scale of time in the neighbourhood of $t=t_c$ and decrease the magnitude of $y(t)$ by making a transformation (see Fig. 8.2)

$$t=\frac{i\pi}{4a}+\sigma z, \tag{8.13a}$$

$$\Phi(z)=(\sigma/i)y(t). \tag{8.13b}$$

Using (8.13) in the original equation (8.5), we obtain the *internal equation*

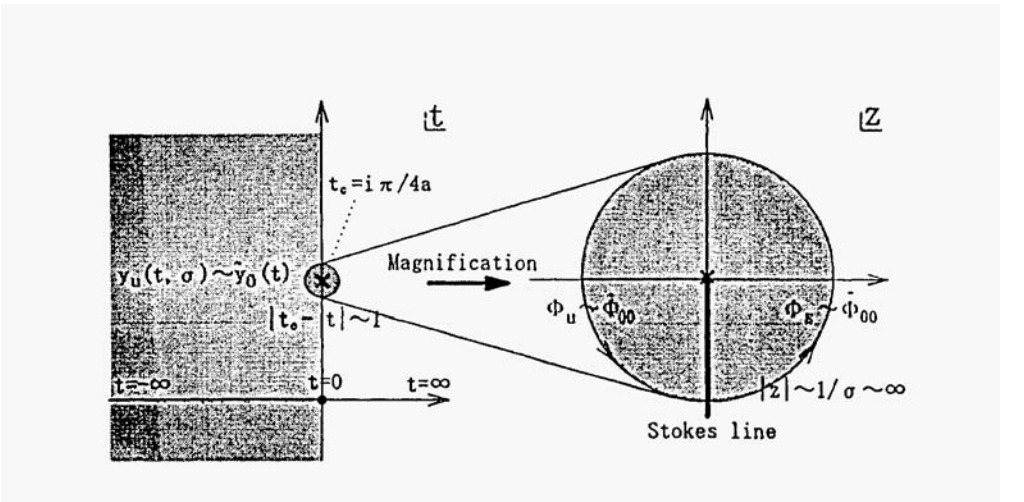

Fig. 8.2. Transformation of vicinity of $t=t_c$ from t plane to enlarged z plane.

$$\Delta^2 \Phi(z)=4(\Phi^3(z) + \sigma^2 a^2 \Phi(z)), \tag{8.14}$$

with $\Delta^2 \Phi(z)=\Phi(z+1)+\Phi(z-1)-2\Phi(z)$. Note that the tiny circle $|t-t_c|=1$ is now mapped to the big one, $|z|=1/\sigma$ $(>>1)$. By suppressing the small contribution of $O(\sigma^2)$, which gives pre-exponential corrections in the result, (8.14) becomes a σ-independent equation

$$\Delta^2 \Phi(z)=4\Phi^3(z)\,. \tag{8.15}$$

Let Φ_u and Φ_s be the solutions for unstable and stable manifolds, respectively. In the limit $z \to \infty$ with Rez <0 (Re z >0), the solution of (8.15) has an asymptotic form

$$\Phi_u(\Phi_s) \sim \Phi_{00} = \sum_{l=0}^{\infty} \frac{c_l}{z^{2l+1}}, \tag{8.16}$$

which retains the connection with the external solution (in the region with $z \to \infty, \sigma \to 0$ and $\sigma z \to 0$) (see Fig. 8.2):

$$(\sigma/\mathrm{i}) y_u(t) \sim (\sigma/\mathrm{i}) y_0(t) \sim \sum_{l=0}^{\infty} \frac{c_l \sigma^{2l+1}}{(t - \frac{\mathrm{i}\pi}{4a})^{2l+1}} = \Phi_{00}(z). \tag{8.17}$$

For any finite value of z, however, c_l grows much larger than z^{2l+1} with increasing l [$c_l \sim (-1)^{l+1}(2l+3)!/(2\pi)^{2l+1}$, as seen in (8.12b)] so that, except for $|z|=\infty$, (8.16) diverges and becomes meaningless. Since the asymptotic expansions at $z \to -\infty$ and $z \to \infty$ cannot therefore be connected smoothly so long as the finite z region is crossed, we shall take a counter-clockwise path along the lower semicircle with $|z|=\infty$. In this case, the Stokes phenomenon appears: In crossing the Stokes line at $\arg(z)=-\pi/2$, we acquire an exponentially small term responsible for the separatrix splitting that is being searched for.

In this context we shall invoke the idea of *Borel Summation.* The Borel summation fashions a convergent sum from a divergent series by resorting to the Laplace transformation. (The idea is based on the resummation of a divergent series by a suitable reordering of the terms.) The Borel or inverse Laplace transformation of (8.15) yields

$$2(\cosh[p]-1)V(p)=4V(p)*V(p)*V(p)\ , \tag{8.18}$$

where we have used the transfornations

$$\Phi(z)=\int_0^\infty e^{-pz}V(p)dp,$$

$$\Delta^2\Phi(z)=\int_0^\infty e^{-pz}2[\cosh(p)-1]V(p)dp.$$

The r.h.s. of (8.18) is a convolution defined by

$$V(p)*V(p)*V(p)=\int_0^p\int_0^{p-\tau'} V(p-\tau'-\tau)V(\tau)V(\tau')\mathrm{d}\tau\,\mathrm{d}\tau'\ .$$

The Borel transformation of the asymptotic solution (16) leads to

$$V(p)=\sum_{l=0}^{\infty}\frac{c_l}{(2l)!}p^{2l}\ . \tag{8.19}$$

Because of the convergence of coefficients $\frac{c_l}{(2l)!}$ with $l \to \infty$, the divergent series $\Phi_{00}(z)$ will become Borel summable. In terms of $V(p)$ in (8.19), solutions for stable and unstable manifolds are given by

$$\Phi_s(z)=\int_0^\infty e^{-pz}V(p)dp\ , \tag{8.20a}$$

$$\Phi_u(z)=\int_0^{-\infty} e^{-pz}V(p)dp\ . \tag{8.20b}$$

Thanks to the convergence of $V(p)$, the integrals in (8.20a) and (8.20b) are convergent in the right (Rez >0) and left (Rez<0) semi-circles, respectively. Hence both of them are Borel summable.

As recognized in (8.18), $V(p)$ has singularities at $p=\pm 2\pi i n$ (n=1,2, •••). In the Imz<0 ($|z|\to\infty$) region, $\Phi(z)$ can be obtained by taking the p-integration along the counter-clockwise path surrounding the positive imaginary p axis, and its resultant expression is given by

$$\Phi(z)=\Phi_0(z) + \Phi_1(z)e^{-2\pi iz} + \Phi_2(z)e^{-4\pi iz} + \bullet\bullet\bullet\ . \tag{8.21}$$

The expansion (8.2 1) captures exponentially small terms beyond all orders. This point will be made more explicit in terms of the difference function defined in Im z<0 as

$$\Phi_-(z)=\Phi_s(z)-\Phi_u(z)=\int_\gamma e^{-pz}V(p)dp, \tag{8.22}$$

where the integration path y is indicated in Fig. 8.3(a). The poles of $V(p)$ contribute to the integration in (8.22), leading to the converged

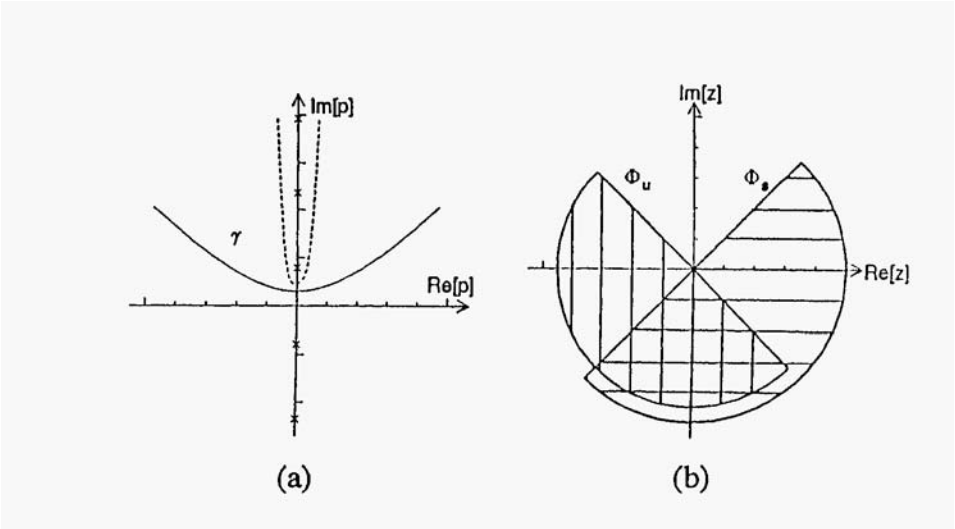

Fig. 8.3. (a) Integration path y in p plane for obtaining Φ. The path y is deformable wherever no pole distributes. (b) Regions of convergence in z plane: Vertical-, horizontal-, and cross-hatched regions for Φ_u, Φ_s, and Φ, respectively.

values of $\Phi_{-}(z)$ in the z region indicated in Fig. 8.3(b). Φ_{-} is a direct manifestation of the separatrix splitting. In the limit $|z| \to \infty$, with Imz < 0 and Re z>0, Φ_u is expressed as in (8.21) since, in this region, $\Phi_s \sim \Phi_{00}$.

The Stokes phenomenon occurs on the Stokes line at arg(z)=$-\pi/2$, where the asymptotic solution (8.21) for $|z| = \infty$ demonstrates an abrupt change. On the Stokes line, noting the relation $\Phi_u(z) = -\Phi_s(-z)$ and $\Phi_s(z^*) = \Phi_s^*(z)$, we find

$$\Phi_u(z) = -\Phi_s^*(z). \tag{8.23}$$

From (8.22) and (8.23), the equality

$$\Phi_{-}(z) = -2\mathrm{Re}[\Phi_u(z)] \tag{8.24}$$

is obtained, which means that the real part of Φ_u leads to the separatrix splitting.

We shall proceed to substitute the expansion (8.21) into the internal equation in (8.15), deriving equations successively in each power of the exponential:

$$\Delta^2 \Phi_0(z) = 4\Phi_0^{\,3}(z)\ , \tag{8.25a}$$

$$\Delta^2 \Phi_1(z) = 12\Phi_0^{\,2}(z)\Phi_1(z)\ ,$$

etc. (8.25b)

The asymptotic ($z \to \infty$) solution to the lowest order is given by

$$\Phi_0 = -\frac{\sqrt{2}}{2}\frac{1}{z} + \frac{\sqrt{2}}{6}\frac{1}{z^3} + \cdots . \tag{8.26}$$

On using $\Phi_0 \sim -\frac{\sqrt{2}}{2}\frac{1}{z}$ in (8.25b), the leading term of $\Phi_1(z)$ turns out $\sim z3$. This issue reflects that $V(p)$ has a singularity described as

$$V(p) \sim \frac{k}{(p - 2\pi\ \mathrm{i})^4}\ . \tag{8.27}$$

In fact, we observe:

$$\begin{aligned}\Phi_{-} &= \int_{\gamma} e^{-pz} V(p)dp \\ &\sim 2\pi i \mathrm{Res}[e^{-pz} \frac{k}{(p-2\pi i)^4}]_{p=2\pi i} \\ &= \lim_{p\to 2\pi i} 2\pi i k \frac{1}{(4-1)!}\frac{d^3}{dp^3}\{(p-2\pi i)^4 \frac{e^{-pz}}{(p-2\pi i)^4}\} \\ &= -2\pi k \frac{1}{3!} z^3 e^{-2\pi i z} \sim c z^3 e^{-2\pi i z} ; \end{aligned} \tag{8.28}$$

c $(=-2\pi k/3!)$ is a Stokes constant to be evaluated. Except for this numerical factor, we have succeeded to demonstrate the exponentially small term beyond all orders. By defining

$$K = \lim_{p\to 2\pi i} (p-2\pi i) B[z^{-3}\Phi_0(z)](p) , \tag{8.29}$$

one may put $c = 2\pi i K$, as recognized in (8.28). (In (8.29), $B[\bullet](p)$ implies a Borel transformation.) We shall show briefly a way to evaluate K.

Stokes Constant

This description is concerned with a technical details of calculating the Stokes constant (8.29). Readers therefore may take note of the final result below Eq. (8.39) and skip to Sec. 8.4.

To begin with, let us define

$$A(p) = B[z^{-3}\Phi_0(z)](p) . \tag{8.30}$$

Applying an elementary formula for Laplace's transformation, we find

$$A(p) = D_p^{(-3)} V(p) , \tag{8.31}$$

where $D_p^{(-3)}$ implies triple integrations over the variable p. Using in (8.31) the expansion (8.19) or its refined version,

$$V(p) = \sum_{k=0}^{\infty} v_k p^{2k} , \qquad \text{with } v_k = \frac{c_k}{(2k)!} , \tag{8.32}$$

one obtains

$$A(p) = \sum_{k=0}^{\infty} v_k \frac{(2k)!}{(2k+3)!} p^{2k+3} \equiv p^3 C(p) , \tag{8.33}$$

and the resultant expansion of $C(p)$ becomes

$$C(p)=\sum_{k=0}^{\infty} b_k p^{2k}, \tag{8.34a}$$

with

$$b_k=\frac{v_k(2k)!}{(2k+3)!}\ . \tag{8.34b}$$

Recalling the description above Eq. (8.21), $C(p)$ and $A(p)$ are seen to have the common singularities at $p=\pm 2\pi$ i. From (8.27) and (8.31), these singularities take the form $\sim(p\mp 2\pi\,\mathrm{i})^{-1}$. Therefore the following relation holds

$$C(p)=\frac{\chi}{(p/2\pi)^2+1}=\chi\,(1-(p/2\pi)^2+(p/2\pi)^4+\cdots)\ . \tag{8.35}$$

Comparing the coefficients in (8.34a) and (8.35), the equality

$$\chi=\lim_{k\to\infty}(-1)^k(2\pi)^{2k}b_k \tag{8.36}$$

obtains. Futhermore, since $\lim_{p\to 2\pi\mathrm{i}}((p/2\pi)-\mathrm{i})C(p)=\chi\lim_{p\to 2\pi\mathrm{i}}\frac{(p/2\pi)-i}{(p/2\pi)^2+1}=-1\frac{\chi}{2}$, K is related to x via

$$K=\lim_{p\to 2\pi\mathrm{i}}(p-2\pi\mathrm{i})A(p)=\lim_{p\to 2\pi\mathrm{i}}(p-2\pi\ \mathrm{i})p^3C(p)=-\frac{(2\pi)^4}{2}\chi\ . \tag{8.37}$$

Using (8.34b) and (8.36) in (8.37), K in (8.37) turns out to be expressible in terms of the limiting value of v_k as

$$K=-\frac{(2\pi)^4}{2}\lim_{k\to\infty}(-1)^k\frac{v_k(2\pi)^{2k}}{(2k+3)(2k+2)(2k+1)}\ . \tag{8.37'}$$

What remains is to derive the equation for $\{u_k\}$ and to solve it numerically. Exploiting the formula $p^{\alpha}*p^{\beta}*p^{\gamma}=\frac{\alpha!\beta!\gamma!}{(\alpha+\beta+\gamma+2)!}p^{\alpha+\beta+\gamma+2}$ with positive α,β,γ, we have

$$V(p)*V(p)*V(p)=\sum_{n=0}^{\infty}\frac{p^{2n+2}}{(2n+2)!}\sum_{j+k+l=n}v_j v_k v_l(2j)!(2k)!(2l)!\ . \tag{8.38}$$

Substituting (8.38) into the convolution equation (8.18), we get a recursion equation:

$$2\left(\frac{1}{2!}-\frac{2(2m)!}{(2m+2)!}3v_0{}^2\right)v_m=-2\sum_{\substack{j+k=m\\ k\geq 0,\,j\geq 1}}\frac{v_k}{(2j+2)!}+\frac{4}{(2m+2)!}\sum_{\substack{j+k+l=m\\ 0\leq j,k,l<m}}v_j v_k v_l(2j)!(2k)!(2l)!\ . \tag{8.39}$$

By numerical iteration of (8.39) under the initial condition $v_0=-\sqrt{2}/2$ (which is provided by (8.12) and (8.32)), vm can be evaluated for large *m,* which will determine the converged value *K* in (8.37'). Our computation has derived the value $K\sim 89.6$.

8.4. Asymptotic Expansion Beyond All Orders and Homoclinic Structures

We are now facing the task of matching the internal solution to the external one. In this context, we shall envisage the panty of the solution and the role of the Stokes constant to show up in *t*-plane.

Following the expansion of the internal solution in (8.21), the refined external solution is expected to be given by

$$\hat{y}(t,\sigma)=\hat{y}_0(t,\sigma)+S(t)[\ \hat{y}_1(t,\sigma)e^{-2\pi i t/\sigma}+\ \hat{y}_2(t,\sigma)e^{-4\pi i t/\sigma}+\ \bullet\bullet\bullet], \tag{8.40}$$

where *S(t)* describes an abrupt change of $\hat{y}(t,\sigma)$ in crossing the Stokes line at Re*t*=0 and is represented by a step function as

$$S(t)=\begin{cases}0\ , & t<0\\ \tfrac{1}{2}\ , & t=0\\ 1\ , & t>0.\end{cases} \tag{8.41}$$

The substitution of (8.40) into the original difference equation in (8.5) yields

$$\Delta^2\,\hat{y}_0(t,\sigma)=-4\sigma^2\hat{y}_0(t,\sigma)(\,\hat{y}_0(t,\sigma)+a)(\,\hat{y}_0(t,\sigma)-a)\ , \tag{8.42a}$$

$$\Delta^2 \hat{y}_1(t,\sigma) = -4\sigma^2[3(\hat{y}_0(t,\sigma))^2 - a^2]\hat{y}_1(t,\sigma) \quad . \tag{8.42b}$$

In order to obtain the lowest-order solution $y_{10}(t)$ for $\hat{y}_1(t,\sigma)$, it suffices to take the lowest-order solution $y_{00}(t) = \sqrt{2}\,a/\cosh(2at)$ for $\hat{y}_0(t,\sigma)$ $(=y_{00}(t)+\sigma^2 y_{01}(t)+\cdots)$ (see (8.9) and (8.11)). In this approximation, $y_{10}(t)$ satisfies a differential version of (8.42b):

$$d^2y_{10}(t)/dt^2 = -4[3(y_{00}(t))^2 - a^2]y_{10}(t) \quad . \tag{8.42b'}$$

As discussed in Sec. 8.2, (8.42b') has a general solution

$$y_{10}(t) = c_1 v_1(t) + c_2 v_2(t) \, , \tag{8.43}$$

where $v_1(t)$, $v_2(t)$ are already given in (8.10). Integration constants c_1, c_2 will be determined by means of matching with Φ_{10} in the neighbourhood of $t = t_c = i\pi/(4a)$. We proceed as follows.

First we introduce a small parameter $\delta = t - t_c$. Noting the identities $\sinh(2at) = i\cosh(2a\delta)$ and $\cosh(2at) = i\sinh(2a\delta)$, $v_1(t)$ and $v_2(t)$ can be rewritten as

$$v_1 = 2\sqrt{2}a^2 \frac{i\cosh[2a\delta]}{\sinh^2[2a\delta]} \quad , \tag{8.44a}$$

$$v_2 = \frac{-i}{8\sqrt{2}a^3}\left\{-\frac{6a\delta\cosh[2a\delta]}{\sinh^2[2a\delta]} - \frac{3i\pi}{2}\frac{\cosh[2a\delta]}{\sinh^2[2a\delta]} + \frac{3}{\sinh[2a\delta]} + \sinh[2a\delta]\right. \tag{8.44b}$$

As easily observed, $v_1(t)$ is an even function of δ, while $v_2(t)$ consists of both even and odd terms. Recalling the odd parity nature of Φ_{10} (see (8.2811, $y_{10}(t)$ in (8.43) should also be an odd function of δ, which is possible so long as

$$c_1 = -\frac{3\pi}{64a^5} i c_2 \tag{8.45}$$

is satisfied. The constant c_2 itself is related to the Stokes constant by matching of y_{10} with Φ_{10} on the negative imaginary axis of the z plane (i.e., on Stokes line) as

$$\frac{1}{2}\frac{\sigma}{i}y_{10}\,e^{-2\pi i t/\sigma} \sim \mathrm{Re}[\Phi_u(z)]. \tag{8.46}$$

Thanks to (8.45), $y_{10}=-\frac{i\sqrt{5}}{5}c_2\delta^3(1+O(\delta^2))=-\frac{i\sqrt{5}}{5}c_2\sigma^3 z^3(1+O(\delta^2))$. Using, in (8.46), this fact together with (8.24) and (8.28), we find

$$-\frac{\sqrt{2}}{5}c_2\sigma^4 z^3 e^{\frac{\pi^2}{2\sigma i}}e^{-2\pi i z}\sim -cz^3 e^{-2\pi i z}, \tag{8.47}$$

and hence

$$c_2=\frac{5\sqrt{2}}{2}\frac{c}{\sigma^4}e^{\frac{-\pi^2}{2\sigma i}}. \tag{8.48}$$

Since we already know the value of Stokes constant $c=2\pi$ iK (see the final result of the previous section), the value of c_2 in (8.48) is also determined.

There is an additional contribution arising from another singularity closest to the real t axis at $t=t_c^*=-\frac{i\pi}{4a}$ (see above (8.12)). This contribution is merely the complex conjugate of the existing result for $y^{10}\,e^{-2\pi i t/\sigma}$. Combining a pair of contributions, the asymptotic behavior of y_u on the real axis is finally given by

$$y_u=\sum_{n'=0}^{\infty}\sigma^{2n'}y_{0n'}+2\,S(t)\,\mathrm{Re}\Big[\sum_{n=1}^{\infty}\sum_{n'=0}^{\infty}\sigma^{2n'}y_{nn'}e^{-\frac{2n\,i\pi\,t}{\sigma}}\Big]. \tag{8.49}$$

Therefore y_u can explicitly be written up to terms $l\,(=n+n')=1$ as

$$y_u=y_{00}+\sigma^2 y_{01}+2S(t)\{c_1 v_1(t)\cos(2\pi t/\sigma)-ic_2 v_2(t)\sin(2\pi t/\sigma)\} \tag{8.50}$$

with $v_1(t)$ and $v_2(t)$ given by Eqs. (8.10).

Finally, coming back to the symplectic map in (8.3), the solution for (q_u, p_u) is constructed by the replacement

$$(q_u, p_u)=(y_u(t),\ (y_u(t)-y_u(t-\sigma))/\sigma)\ . \tag{8.51}$$

Readers will perceive in Fig. 8.4 a nice agreement between the asymptotic analytical result and the outcome of the numerical iteration of the map (8.3). The sequence of dots are obtained by numerical

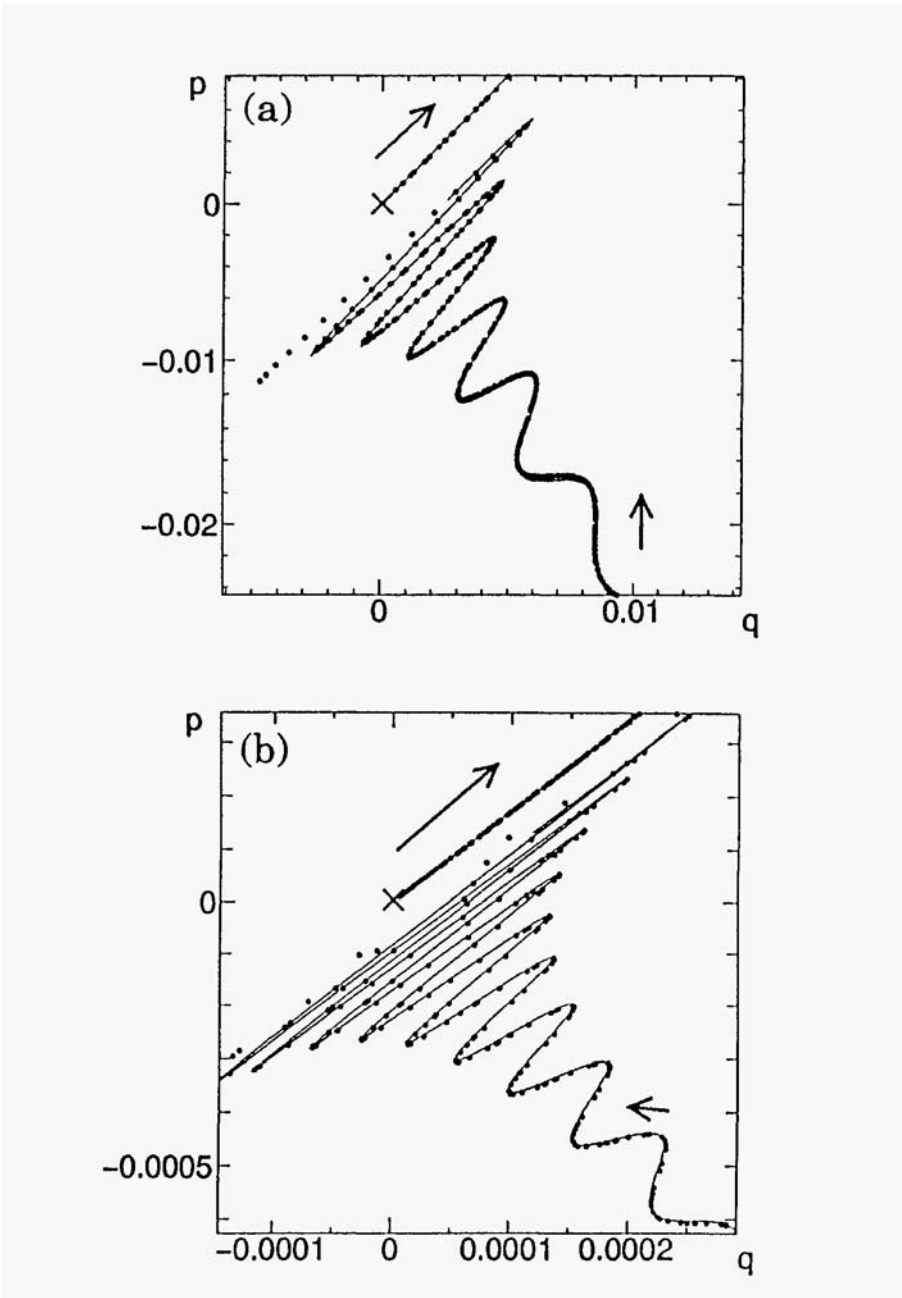

Fig. 8.4. Unstable manifold with hyperbolic fixed point (**x**). Arrow indicates direction of journey. Solid curve for analytical result and series of dots for result of numerical iteration of map: (a)a=1, σ=0.2; (b)a=1, σ=0.15

iteration of the map (8.3) for an assembly of initial points on the linearized unstable manifold at HFP (on one of the eigenvectors of the monodromy matrix (8.4)). As for the analytical result, it should be noted: If $\sigma<<1$, the complete Stokes phenomenon occurs, ensuring an abrupt change of S in (8.41) in crossing the Stokes line at Ret=0. For larger values ($\sigma\sim0.1$), we shall see a more or less incomplete Stokes phenomenon, i.e., a mild growth of $S(t)$ in a narrow region around Ret=0. However, this problem can be resolved by exploiting an appropriate constant value for $S(t)$ for $t>0$ in (8.41). In fact, with a choice of S=0.82 for $t>0$, (8.50) proves to work very well for any value of σ between 0.1 and 0.3 (see Fig. 8.4). Figures 8.4(a) and (b) are the magnification of the vicinity of HFP. The unstable manifold starting from HFP, after executing a long clockwise journey, comes back again to the vicinity of HFP, but accompanied by violent undulations. The asymptotic analytical line proves to fit the result of the numerical iteration of (8.3), describing the stretching of the area enclosed by the stable and unstable manifolds. When σ is decreased, violent undulations begin to occur in the further vicinity of HFP; see the extremely small scale unit ~10-4 for both p and q axes in Fig. 8.4(b).

Noting that the stable manifold is merely the time reversal of the unstable manifold, let us proceed to consider an angle for the intersection between the stable and unstable manifolds at the first homoclinic point t=0, where the unstable (stable) manifold begins (ceases) oscillations. Let $y_u(t)$ be divided into the even- and odd-parity parts as

$$y_u(t)=I(t)+E(t)\ , \tag{8.52}$$

where

$$I(t)=y_{00}+\sigma^2 y_{01}+\bullet\bullet\bullet\ , \tag{8.53a}$$

$$E(t)=2S(t)\{c_1 v_1(t)\cos(2\pi t/\sigma)-ic_2 v_2(t)\sin(2\pi t/\sigma)\}. \tag{8.53b}$$

Then the unstable and stable manifolds are constructed respectively by $q_u(t)=I(t)+E(t)$ and $q_s(t)=I(t)-E(t)$, with $p_u(t)$ and $p_s(t)$ expressed by (8.51). In the neighbourhood of the first homoclinic point, we shall concentrate on the small time $0<\delta t_1,\delta t_2<<\sigma<<1$, satisfying $p_u(\delta t_2)=p_s(\delta t_1)$ (see Fig. 8.5). Since $\delta t_1\sim\delta t_2\sim\delta t$, the intersection angle is given by

$$\phi=\Delta q/\Delta p=(q_s(\delta t)-q_u(\delta t))/(p_s(\delta t)-p_s(0)). \tag{8.54}$$

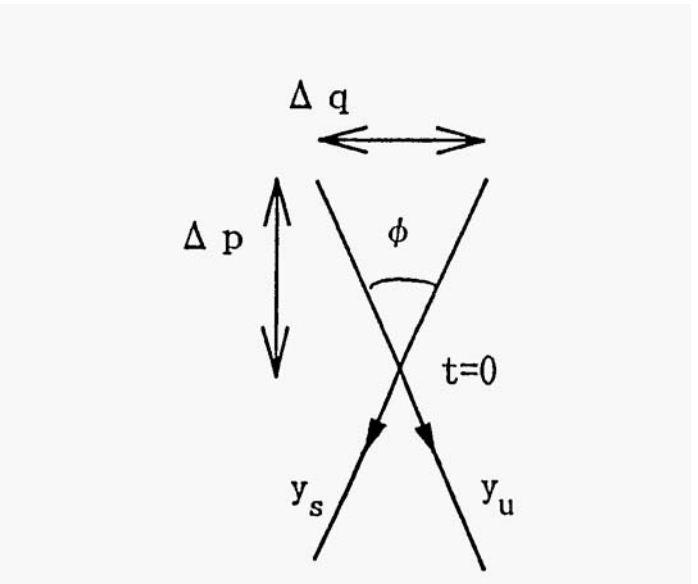

Fig. 8.5. Intersection angle ϕ.

Noting $\dot{E}(0), \dot{E}(\sigma) << \dot{I}(\sigma)$ (A means $\delta A/\delta t$), and using $S(0)=1/2$ (see (8.41)), ϕ is seen to become $\phi = 2\sigma\dot{E}(0)/\dot{I}(\sigma) = \pi\,(8a^6\sigma)^{-1}\,|c_2|$. The final result shows an essential singularity at $\sigma=0$:

$$\phi = (a_1/\sigma^{\mu})\exp[-a_2/\sigma]\,, \tag{8.55}$$

where α_1 and a_2 are positive real constants and μ is a positive integer. Their values are $(\mu, a_1, a_2)=(5,\ \sqrt{5}\pi^2 K/(8a^6),\ \pi^2/(2a))$.

In this way, we have analyzed a time-discrete classical dynamics or the symplectic map by resorting to the *asymptotic expansion beyond all orders,* based on theoretical tools of Borel summability and the Stokes phenomenon. The homoclinic structures are shown to be nicely described by the analytical expression in (8.49) and (8.50), including only l=0, 1 terms. In particular, the stretching-type oscillations appearing in the extreme vicinity of the hyperbolic fixed point recovers excellently the result of numerical iteration of the map (note the scale units~10^{-4} in Fig. 8.4(b)). Inclusion of higher-order ($l \geq 2$) terms is anticipated to derive the folding mechanism and thereby to complete the Birkhoff-Smale's horse-shoe mechanism for genesis of chaos in conservative systems. The application of the present method to other

maps, such as standard and Henon maps, is straightforward. For instance, the intersection angle for the first heteroclinic or homoclinic point is given as well by the universal form in (8.55) but with $(\mu, a_1, a_2) = (3, 24\pi^4 K, \pi^2)$ and $(8, 56\pi^2 K/3, \sqrt{2}\,\pi^2)$, respectively, for standard and Henon maps.

The present framework based on the updated method of *asymptotic expansions beyond all orders,* suffering from neither peculiarity nor any particular difficuty of the model, will be very useful for the analytical study of chaos in general, which has been investigated mostly by numerical computations or scaling arguments for long time. In this context one can also apply the present method to dissipative systems, since symplectic properties have not been used so far. It is further desirable to proceed to study analytically the quantum and semiclassical analogues of the homoclinic structures.

Thus, time discretization radically changes the nature of the time-continuous classical dynamical systems. The violent undulation of heteroclinic or homoclinic structures in the vicinity of HFP occurs for a small but nonvanishing time difference. Can we see an analogous outcome resulting from discretizing the time varivable in quantum dynamics ? We shall proceed to consider this question.

8.5. Time Discretization and Quantum Dynamics

As has been repeatedly addressed in the previous chapters, the present formalism of quantum mechanics cannot allow a genuine quantum chaos, due to the linearity of Schrödinger equation. Strictly speaking, N-body wavefunctions in open systems might have nonzero KS entropy in the limit $N \to \infty$, but it cannot have a positive Lyapunov exponent, characterizing the extreme sensitivity to initial conditions. However we have a pertinent observation on the existence of classical-quantum correspondence: If classical chaos is present, quantum chaos should also be anticipated.

Let us here review briefly how Schrödinger hit upon his idea for describing quantum dynamics. The time-dependent Schrödinger equation was first proposed in the fourth communication of his series on wave mechanics (Schrödinger, 1926). He postulated a wavefunction Ψ to satisfy the time-dependent linear differential equation

$$\partial \Psi / \partial t = -i(E/\hbar)\Psi \tag{8.56}$$

by closely following the linear equation for a classical monochromatic wave. When combined with the time-independent partner $H\Psi=E\Psi$, this form gave rise to the familiar time-dependent equation. The form (8.56), however, describes only a time-periodic or -quasiperiodic wave. So long as Schrödinger relied on (8.56) as the foundation of his thinking, the time-dependent Schrödinger equation inevitably excludes any solution representing temporal chaos or turbulence in general. The de Broglie particle to which Schrödinger referred, showing only periodic or quasi-periodic motions in the underlying classical dynamics, is indeed dual to the monochromatic wave with a characteristic frequency. For a classical particle executing chaotic motion, however, no characteristic frequency can exist. Rather the motion is characterized by a continuous broad spectrum. In constructing the corresponding quantum mechanics, therefore, one may also conceive of a nonlinear dynamical equation for Ψ (Weinberg, 1989) which will accommodate a chaotic solution.

For systems showing chaos in the underlying classical dynamics, let us investigate another possible formalism of quantum dynamics which leads to quantum chaos while recovering the existing Heisenberg or Schrödinger equation in a suitable limit.

One possibility is to discretize time *t*. The progress in nonlinear dynamics and chaos over past decades has elucidated that chaos is easily generated from the time-difference variant of the time-continuos integrable system. In previous sections of the present chapter, we have confirmed this fact. Motivated by this discovery and also by our expectation to understand more clearly the uncertainty principle between time and energy in our microscopic cosmos, let the continuous time be discretized. In this context it will be very convenient to scrutinize Heisenberg equation of motion, which has a direct correspondence with the classical equation of motion.

Our reasoning will parallel that of T. D. Lee (1987), who wrote: " For more than three centuries we have been influenced by the precept that fundamental laws of physics should be expressed in terms of differential equations. Difference equations are always regarded as approximations. I try to explore the opposite: Difference equations are more fundamental, and differential equations are regarded as approximations "

In the remaining half of this chapter we shall accept that time-discrete quantum mechanics should correspond to time-continuous classical mechanics and proceed to analyze a time-difference variant of

Heisenberg equation of motion in order to explore the possible genesis of quantum chaos.

8.6. Time-Discrete Unitary Quantum Dynamics

Several attempts to discretize the time already exist (Moncrief, 1983; Bender, 1985; Lee, 1987). Among them, the *"leapfrog"* method proposed by Moncrief is the simplest and most explicit. It will be described below.

For a system with N degrees of freedom with Hamiltonian

$$H=\sum_{k=1}^{N} p_k^2/2m + V(\mathbf{q}), \tag{8.57}$$

Heisenberg's equation of motion for the operators $\mathbf{q}=(q_1,q_2,\bullet\bullet\bullet,q_N)$ and $\mathbf{p}=(p_1,p_2,\bullet\bullet\bullet,p_N)$ are

$$dq_k/dt=(i\hbar)^{-1}[q_k,H]=p_k/m, \tag{8.58a}$$

$$dp_k/dt=(i\hbar)^{-1}[p_k,H]=-\partial V/\partial q_k=F_k\ . \tag{8.58b}$$

By introducing the time difference Δt, let us discretize the time as

$$t=j\Delta t\ , \qquad j=\bullet\bullet\bullet,-1,0,1,\bullet\bullet\bullet\ . \tag{8.59}$$

At these discrete times, $\mathbf{q}$ and $\mathbf{p}$ will be written as $\mathbf{q}(j)$ and $\mathbf{p}(j)$. With a help of auxiliary momenta $\boldsymbol{\pi}$ defined at half-integer time steps (see Fig. 8.6), consider a time-difference version of Eq.(8.58):

$$(q_k(j+1)-q_k(j))/\Delta t = m^{-1}\pi_k(j+1/2), \tag{8.60a}$$

$$[\pi_k(j+1/2)-\pi_k(j-1/2)]/\Delta t = F_k(\mathbf{q}(j)). \tag{8.60b}$$

Prescribing the momenta $\mathbf{p}(j)$ conjugate to $\mathbf{q}(j)$ as

$$p_k(j)=[\pi_k(j+1/2)+\pi_k(j-1/2)]/2 \tag{8.61}$$

and rewriting π_k in (8.60) in terms of $p_k(j)$, one finds

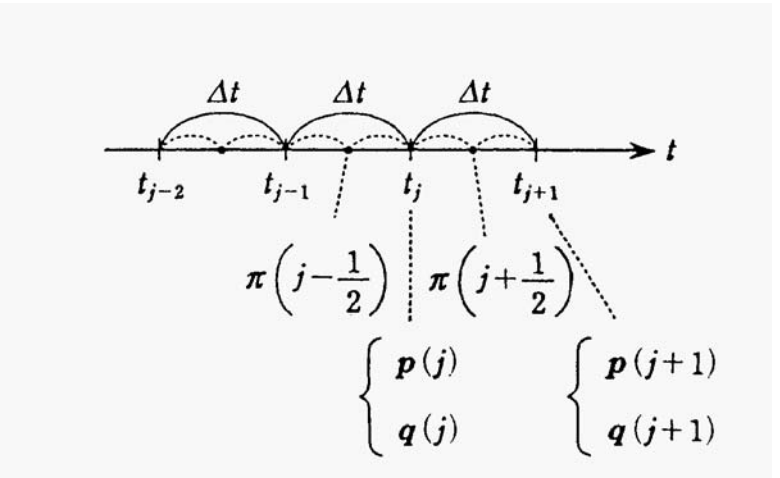

Fig. 8.6. Unitary time discretization (Moncriefs leapfrog method).

$$q_k(j+1)=q_k(j)+(\Delta t/m)[p_k(j)+(\Delta t/2)F_k(\mathbf{q}(j))], \tag{8.62a}$$

$$p_k(j+1)=p_k(j)+(\Delta t/2)F_k(\mathbf{q}(j))+(\Delta t/2)F_k(\mathbf{q}(j+1)). \tag{8.62b}$$

Equation (8.62) may be interpreted as a nonlinear symplectic mapping for matrices $\mathbf{q}(j)$ and $\mathbf{p}(j)$. (For the symplecticity, see the condition below Eq. (8.41.) The astonishing fact is that, for any nonvanishing Δt, Eq. (8.62) proves to be generated by the unitary transformation

$$q_k(j+1)=U^{+}(j)q_k(j)U(j), \tag{8.63a}$$

$$p_k(j+1)=U^{+}(j)p_k(j)U(j), \tag{8.63b}$$

with the unitary operator $U(j)$ defined by

$$U(j)=\exp[-i(\Delta t/2\hbar)V(\mathbf{q}(j))]\times\exp[-i(\Delta t/\hbar)\sum_{k=1}^{N}p_k^2(j)/2m]\times\exp[-i(\Delta t/2\hbar)V(\mathbf{q}(j))]. \tag{8.64}$$

In fact, using the identity $e^{B}Ae^{B}=A+[B,A]+(2!)^{-1}[B,[B,A]]+\cdots$, one can show that

$$\exp[\mathrm{i}(\Delta t/\hbar)\sum_{\ell} p_{\ell}^{2}(j)/2m]\, q_k(j)\, \exp[-\mathrm{i}(\Delta t/\hbar)\sum p_{\ell}^{2}(j)/2m]$$

$$= q_k(j) + (\Delta t/m) p_k(j) \tag{8.65a}$$

and

$$\exp[\mathrm{i}(\Delta t/2\hbar)V(\mathbf{q}(j))]\, p_k(j)\, \exp[-\mathrm{i}(\Delta t/2\hbar)V(\mathbf{q}(j))]$$

$$= p_k(j) + (\Delta t/2) F_k(\mathbf{q}(j)). \tag{8.65b}$$

Application of Eqs. (8.65), together with another identity

$$\mathrm{e}^{B}F(A)\mathrm{e}^{-B} = \sum_{n=0}^{\infty} \mathrm{e}^{B}(F^{(n)}(0)/n!)A^{n}\mathrm{e}^{-B} = \sum_{n=0}^{\infty} (F^{(n)}(0)/n!)(\mathrm{e}^{B}A\mathrm{e}^{-B})^{n}$$

$$= F(A + [B, A] + (2!)^{-1}[B, [B, A]] + \bullet\bullet\bullet), \tag{8.66}$$

leads to the equivalence between (8.62) and (8.63). The unitary operator (8.64) is an approximation to the true one $U^{(0)}(j) = \exp[-\mathrm{i}(\Delta t/\hbar)H(j)]$: $U(j) = U^{(0)}(j)(1 + \mathrm{O}((\Delta t)^2))$. Thanks to its unitarity, the transformation (8.62) preserves the equal-time commutation rule (ETCR) at each time step j,

$$[q_k(j), p_{k'}(j)] = \mathrm{i}\hbar\, \delta_{kk'}, \tag{8.67a}$$

$$[q_k(j), q_{k'}(j)] = [p_k(j), p_{k'}(j)] = 0, \tag{8.6b}$$

and, despite its appearance of a nonlinear symplectic mapping for matrices $\mathbf{q}(j)$ and $\mathbf{p}(j)$, it is merely a linear mapping that is unable to generate any temporal chaos. These features are in contrast with those possessed by classical symplectic mappings.

The mapping (8.62) or (8.63) can also be rewritten in the Schrödinger-Feynman's formalism. Let us prescribe $|\Psi(j)\rangle$ as a state vector at the discrete time $t_j = j\Delta t$. Using the unitary operator (8.64), a discrete variant of Schrödinger equation is given by

$$|\Psi(j+1)\rangle = U(j)\,|\Psi(j)\rangle \tag{8.68a}$$

or, in the coordinate representation, by

$$\Psi(\mathbf{q};j+1) = \int \mathrm{d}^N\mathbf{q}'\, K(\mathbf{q},\mathbf{q}')\, \Psi(\mathbf{q}';j)\,, \tag{8.6813}$$

with $\Psi(\mathbf{q};j) = \langle \mathbf{q} \,|\, \Psi(j)\rangle$ and an integration kernel

$$K(\mathbf{q},\mathbf{q}') = [m/(2\pi \mathrm{i}\hbar\,\Delta t)]^{N/2} \exp\{(\mathrm{i}/(2\hbar\,\Delta t)) \sum_k m(q_k - q'_k)^2$$

$$- (\mathrm{i}\Delta t/(2\hbar))\,(V(\mathbf{q})+V(\mathbf{q}'))\}.$$

Despite the time discretization, both the unitarity and linearity of the mapping (8.68) are obvious for any large value of Δt.

8.7. Time-Discrete Non-Unitary Quantum Dynamics

Although Moncrief s intention lies in constructing a fully consistent quantum field theory on a lattice, i.e., on Minkowsky space, let us develop further an attempt of time discretization of quantum systems exhibiting classical chaos.

Heisenberg's framework of quantum mechanics is superior to that of Schrödinger in that the former has a direct connection with the classical canonical equation, while the latter has not. Historically, the Heisenberg's framework can be traced back to Bohr's two postulates: The first is the the quantization of action (i.e., adiabatic invariant)

$$J := (2\pi)^{-1} \oint p(E)\mathrm{d}q = n\hbar\,, \qquad n=0,1,2,\bullet\bullet\bullet, \tag{8.69}$$

or its generalization to systems with $N(>1)$ degrees of freedom

$$J_k := \frac{1}{2\pi} \oint_{\Gamma_k} \mathbf{p}(E) \bullet \mathrm{d}\mathbf{q} = (n_k + m_k/4)\hbar\,, \tag{8.70}$$

with k=1,2,•••,M and nk=0,1,2,•••. Γ_k and m_k represent mutually-independent closed paths and Maslov index, respectively (see Chap. 1); the second is the frequency rule

$$E_n - E_m = \hbar\,\omega_{nm}. \tag{8.71}$$

The former rule led Born and Jordan (1925) to the discovery of a commutation rule for canonically-conjugate observables, e.g. Eq. (8.67).

Two rules are embodied in the Heisenberg equation of motion for a Hermitian operator or matrix A:

$$dA/dt=(i\hbar)^{-1}[A,H] \quad . \tag{8.72}$$

The action J in (8.70) is calculable only when each classical orbit executes a closed path on the torus.

In classically-chaotic systems, however, the collapse of tori prevents us from calculating the action on l.h.s. of (8.70) and consequently breaks the rule (8.70). The ultimate result should be that a logical foundation for the commutation rule (8.67) becomes ambiguous! It is a truth that the present-day quantum mechanics (Dirac, 1930) is constructed on the basis of two postulates (8.67) and (8.72) without any linkage to the old quantization rule in (8.69) and (8.70) and that its validity has been guaranteed by accumulation of experiments. But the foundation for the commutation rule (8.67) is traced back to (8.69) and (8.70). Although a modification of the commutation rule in chaotic systems might give rise to quantitatively small corrections in experiments, its role in the framework of quantum mechanics is beyond any conception.

Nevertheless, the ambiguity about the commutation rule is not a serious problem in our construction of a time-discrete quantum mechanics, where both conditions $\Delta t \neq 0$ and $\hbar \neq 0$ are employed. Let us discretize time as $t_j=j\Delta t\,(j=\cdots,-1,0,1,\cdots)$ in units of a fundamental time interval Δt. By replacing the time differential of a Hermitian matrix A by (Euler's) time difference,

$$dA/dt \rightarrow (A_{j+1}-A_j)/\Delta t \,, \tag{8.73}$$

(8.72) becomes

$$(A_{j+1}-A_j)/\Delta t =(i\hbar)^{-1}[A_j,H_j] \quad . \tag{8.74}$$

This form inevitably breaks the unitary property and cannot keep the equal-commutation rule preserved in the time continuum limit. Therefore neither rule nor a way will exist by which to calculate the r.h.s. of (8.74), each time we should take a single time step forward. As an attempt to overcome the difficulty and to complete the time-discrete quantum dynamics, we propose: (i) to use forcibly the commutation rule (8.67) in calculation of the r.h.s. of (8.74) at each

time step or (ii) to replace the r.h.s. of (8.74) simply by a Hermitian variant of the Poisson bracket as $(\{A_j, H_j\}+\{A_j, H_j\}^+)/2$. It should be noticed that, in some of systems including the example below, the two methods (i) and (ii) prove to yield the identical result.

We shall now concentrate upon a spin system. The advantage of the spin system is that its Hilbert space is finite-dimensional and that, for any finite magnitude of quantum spin, the Hamiltonian matrix is also finite-dimensional with no necessity of artificial matrix truncation. As a concrete example, we choose a spin system driven by the x-polarized and time-periodic magnetic field B with period $T=2\pi/\omega$, which is decribed by Hamiltonian

$$H = AS_z^2 - \mu BS_x \cos(\omega t) . \tag{8.75}$$

The 1st and 2nd terms on the r.h.s. of (8.75) represent an easy-plane anisotropy and Zeemann energy, respectively. (The δ-kick type driving field will not be considered, since our interest lies in discretization of time.)

Let us first develop the classical treatment. Using Poisson brackets

$$\{A, B\} = \sum_{\alpha\beta\gamma, j} \varepsilon_{\alpha\beta\gamma} \frac{\partial A}{\partial S_j^\alpha} \frac{\partial B}{\partial S_j^\beta} S_j^\gamma \tag{8.76}$$

and the Hamiltonian (8.75), the equation of motion for the spin S is given by

$$\begin{aligned} d\mathbf{S}/dt = \{\mathbf{S}, H\} &= \mathbf{S} \times (-\delta H/\delta \mathbf{S}) \\ &= \mathbf{S} \times (-2AS_z \mathbf{e}_z + \mu B \mathbf{e}_x \cos(\omega t)) . \end{aligned} \tag{8.77}$$

The squared spin $\mathbf{S}^2$ is a constant of motion and is taken to be unity. Then, numerically iterating (8.77), we keep trajectory values at integer-multiples of period T. By introducing polar coordinates $(S_x, S_y, S_z)=(\sin\theta\cos\phi, \sin\theta\sin\phi, \cos\theta)$, the Poincare' surface for a section in the $\theta - \phi$ plane is depicted in Fig. 8.7, which clearly exhibits a transition from tori to chaos with increasing B.

To see a quantum analog of this transition, we shall analyze Heisenberg's equation of motion for the spin matrix, by keeping time continuous. The equation of motion in the quantum case reads

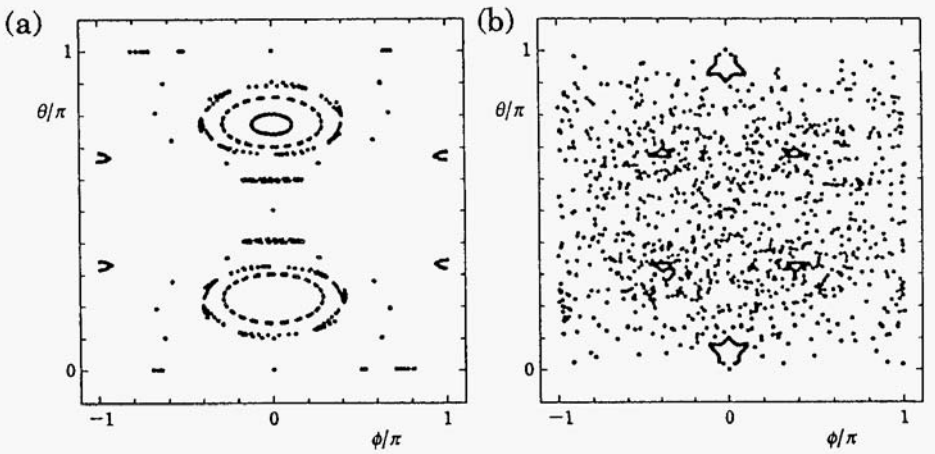

Fig. 8.7. Poincare' section for classical spin dynamics($\omega=2\pi$). Polar coordinates are defined by $\mathbf{S}=(\sin\theta\cos\varphi, \sin\theta\sin\varphi, \cos\theta)$: (a) weak field case (A=1.0, μB-0.3), (b) strong field case (A=1.0, μB=1.0). The same values are used in Figs. 8.9 and 8.10.

$$d\mathbf{S}/dt = (i\hbar)^{-1}[\mathbf{S}, H] . \tag{8.78}$$

The quantum-mechanical counterpart of Lie algebra (8.76) is the commutation rule

$$[S_\alpha, S_\beta] = i\varepsilon_{\alpha\beta\gamma}\hbar S_\gamma , \qquad \alpha, \beta, \gamma = x, y \text{ and } z. \tag{8.79}$$

From (8.78) and (8.79), we have

$$dS_x/dt = -A(S_yS_z + S_zS_y) , \tag{8.80a}$$

$$dS_y/dt = A(S_xS_z + S_zS_x) + \mu BS_z\cos(\omega t) , \tag{8.80b}$$

$$dS_z/dt = -\mu BS_y\cos(\omega t) . \tag{8.80c}$$

Choosing as bases Fock states $\{|m\rangle; m=-S,-S+1,\cdots,S-1,S\}$ with $S_z|m\rangle=\hbar m|m\rangle$, Eqs. (8.80) might be regarded as three nonlinear high-dimensional matrix equations for Hermitian matrices. It is not legitimate, however, because (8.80) keeps the commutation rule (8.79).

(The proof is given by induction.) In other words, all the matrix elements for $J_\gamma \equiv [S_\alpha, S_\beta] - i\varepsilon_{\alpha\beta\gamma}\hbar S_\gamma$ (=0) are constants of motion, whose number equals to that of the (complex) variables, i.e., matrix elements of S_x, S_y and S_z. (In the case $S=\infty$, a more rigorous argument is required.) As a consequence, any solutions of (8.80) are not chaotic but recurrent.

Following (8.73) and (8.74) together with the proposal below them, we shall now proceed to discretize the time variable as $t_j = j\Delta t$ ($j = \cdots, -1, 0, 1, \cdots$) (see Fig. 8.8) and rewrite the original Heisenberg equation of motion (8.80). The time differential on the l.h.s is taken as the Euler difference

$$(\mathbf{S}(j+1) - \mathbf{S}(j))/\Delta t\,, \tag{8.81a}$$

and expressions on the r.h.s. are replaced by using values at t_j :

$$S_z \to S_z(j)\,, \tag{8.81b}$$

$$\cos\omega t \to \cos(\omega j \Delta t)\,. \tag{8.81c}$$

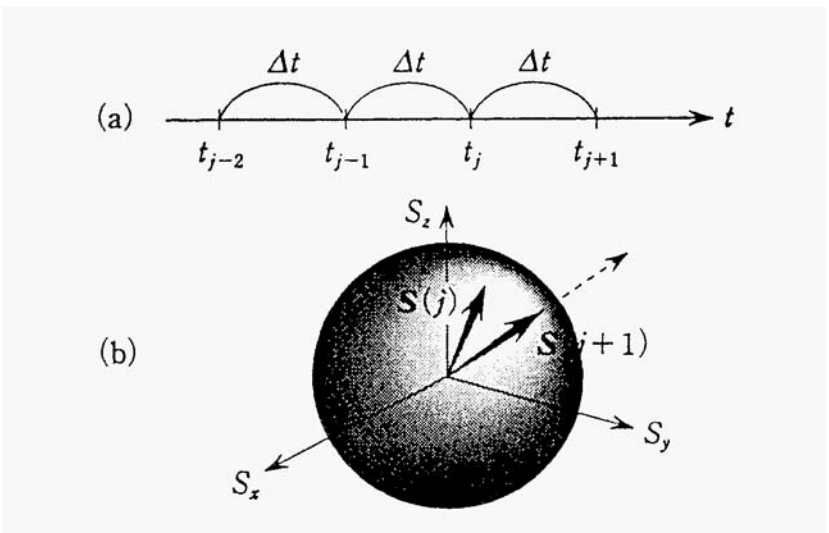

Fig. 8.8. Non-unitary time discretization: (a) time difference, (b) normalization of spin **S.**

As emphasized below (8.73) and (8.74), the time discretization like (8.81) will break the unitary property and cannot keep the equal-time commutation rule (8.79). Nevertheless, at each time step in the time evolution we shall have recourse to (8.79) to calculate the r.h.s. of (8.80). The resultant time-difference variant of (8.80) should take the following form:

$$S_x(j+1) = S_x(j) - A\Delta t\ (S_y(j)S_z(j) + S_z(j)S_y(j)) , \tag{8.82a}$$

$$S_y(j+1) = S_y(j) + A\Delta t\,(S_x(j)S_z(j)+S_z(j)S_x(j)) + \mu B\Delta t\, S_z(j)\cos(\omega t_j) , \tag{8.82b}$$

$$S_z(j+1) = S_z(j) - \mu B\Delta t\, S_y(j)\cos(\omega t_j) . \tag{8.82c}$$

Further, after each iteration of the difference equation (8.82), the replacement $(S(S+1)/\mathrm{Tr}(\mathbf{S}^2(j+1)))^{1/2}\,\mathbf{S}(j+1) \rightarrow \mathbf{S}(j+1)$ will be made so that the spin matrix should preserve the normalized magnitude $S(S+1)$ (see Fig. 8.8(b)). Amazingly, (8.82) is also valid on regarding the classical equation (8.77) as the quantal equation for Hermitian matrices and on replacing the Poisson bracket on the r.h.s. of (8.77) by its Hermitian variant.

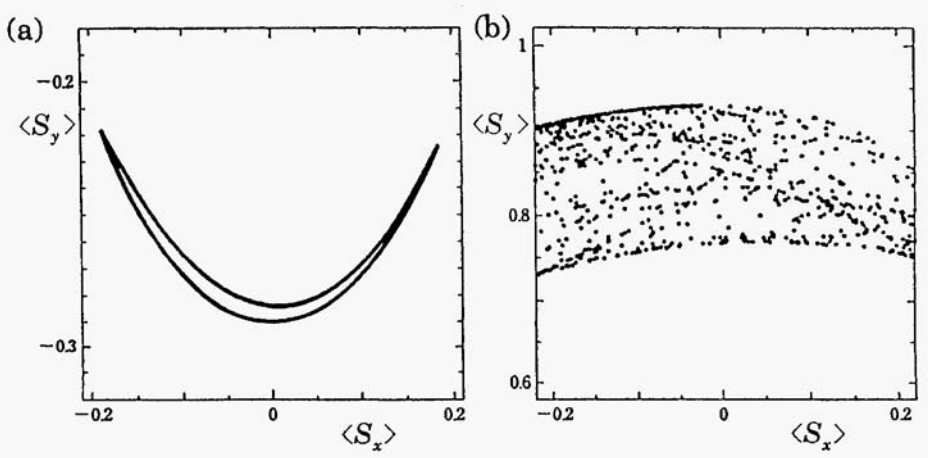

Fig. 8.9. Poincare' section of attractor for quantum spin dynamics. The spin coherent state with $\theta=2\pi/5$, $\phi=0$ is used for the representation. Time difference $\Delta t = T/3$: (a) weak field case, (b) strong field case.

Since, for S=1/2, (8.82) is a trivial linear map, we proceed to solve (8.82) numerically in the case S=1, where each component of **S** constitutes a 3 x 3 matrix. The result for valus of **S** at integer multiples of the period $T(=2\pi/\omega)$ is given in Fig. 8.9. In this figure, the expectation value of **S** in a spin-coherent state is taken. The mapping (8.82) is not area-preserving and constituting a dissipative system, which is a weak point to be improved in future. However, both Fig. 8.9 and the autocorrelation function in Fig. 8.10(a) indicate the transition from regular to chaotic behaviors with increase of the magnetic field.

An amusing feature can be found in the degree of breaking the commutation rule defined by

$$\delta^2 = \frac{1}{(2S+1)^2} \sum_{l,n} |[S_x, S_y]_{l,n} - i\hbar S_{z\,l,n}|^2 \ . \tag{8.83}$$

The time dependence of δ^2 in Fig. 8.10(b) shows small and large fluctuations corresponding to regular and chaotic behaviors of the quantum spin, respectively.

This result is sensitive to the magnitude of Δt. We find that, with decrease of Δt, the chaotic behavior is replaced by a regular one.

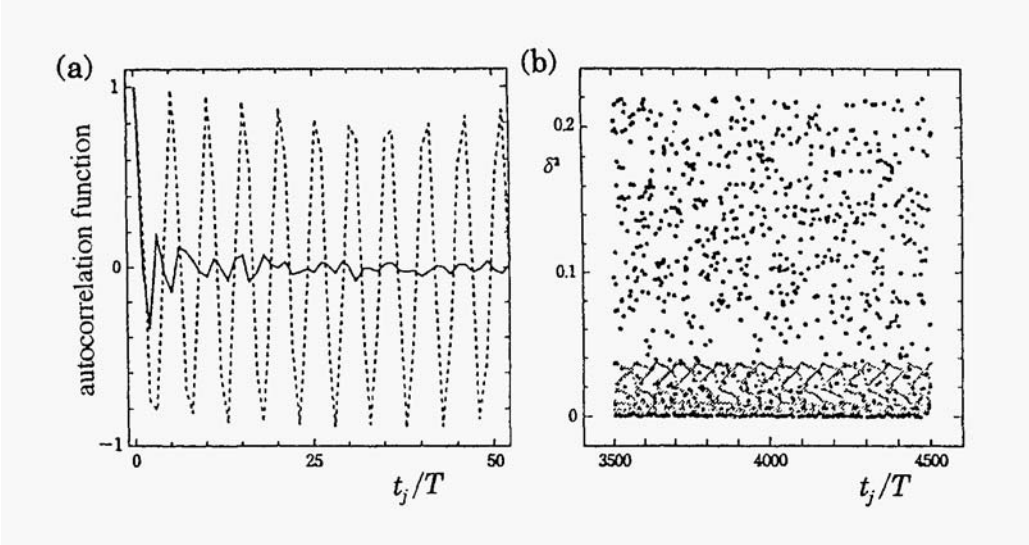

Fig. 8.10. (a) Autocorrelation function of $<S_x(j)>$. Dotted and solid lines are for weak and strong field cases, respectively. (b) Time dependence of δ^2 Gray and black dots are for weak and strong field cases, respectively.

More precisely, there exists a threshold Δt_C: Chaos emerges for $\Delta t > \Delta t_C$; Δt_C depends on the degree of quantumness ($\hbar \sim S^{-1}$) and decreases as the classical limit $S=\infty$ is approached. The phase diagram in Fig. 8.11 depicts schematically a border curve between the collapse and genesis of genuine quantum chaos. The time-discrete variant of quantum mechanics thus describes a transition from regular to chaotic behaviors of quantum variables. In the present formalism, one can move from quantum to classical mechanics by taking both limits $\Delta t \to 0$ and $\hbar \to 0$.

Since the proposed map (transformation) (8.82) is not symplectic but dissipative, one is tempted to invent an improved map. For instance,

$$\mathbf{S}(j+1)=U^{\dagger}(j)\mathbf{S}(j)U(j) \tag{8.84}$$

might be conceivable as a spin analog of the Moncrief's time-discretization scheme in (8.62) or (8.631, in terms of a unitary matrix given by

$$U(j)=\exp[-\mathrm{i}(\Delta t/2\hbar)\mu BS_x(j)\cos(\omega t_j)]\times\exp[-\mathrm{i}(\Delta t/\hbar)A(S_z(j))^2]$$
$$\times\exp[-\mathrm{i}(\Delta t/2\hbar)\mu BS_x(j)\cos(\omega t_j)]. \tag{8.85}$$

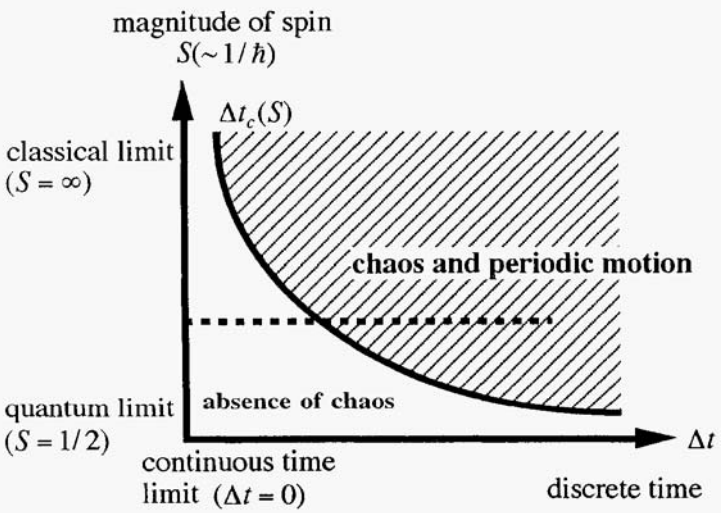

Fig. 8.11. Phase diagram for occurrence of quantum chaos.

Equation (8.85) is an approximation to the genuine unitary matrix $U^{(0)}(j)=\exp[-i(\Delta t/\hbar)H(j)]$: In fact, $U(j)=U^{(0)}(j)\ (1+O(\Delta t)^2)$. Although (8.84) with (8.85) is a quantum version of the symplectic map for the classical spin dynamics, it preserves the commutation rule (8.79). Despite exhibiting a feature of the nonlinear high-dimensional map, (8.84) with (8.85) is a linear map yielding absolutely regular orbits.

Fluctuations of Fundamental Time Step

The way of time discretization should be justified by means of *time quantization.* Meanwhile, there exists no good idea of such justification. While the fundamental time step Δt has so far been assumed constant, let us replace it by the stochastic variable Δt_i (with the mean $\langle \Delta t_i \rangle = \Delta t/2$ and the variance $\langle (\Delta t_i - \langle \Delta t_i \rangle)^2 \rangle = \Delta t^2/12$) obeying the uniform distribution defined in the region $0<\Delta t_i \leq \Delta t$. In this case, the erratic behavior of the quantum spin is anticipated without resorting to the non-unitary transformation, which will also be described below.

We reconsider the ordinary unitary transformation (8.84) for the S=1 quantum spin under a unitary operator

$$U(j)=\exp[-i\Delta t_j H(j)/\hbar]=\exp[-(i/\hbar)\,\Delta t_j(AS_z^2-\mu BS_x\cos(\omega t_j))], \tag{8.86}$$

where $t_j=\sum_{i=1}^{j}\Delta t_i$. When Δt $(=2\langle \Delta t_i \rangle = \mathrm{Max}(\Delta t_i))$ is small enough, there is no difference between the time-continuous and time-discrete quantum spin dynamics, and the quantum dynamics exhibits merely the quantum recurrence, irrespective of the magnitude of the driving field B. If At will become of the order of $T=2\pi/\omega$, however, the quantum spin dynamics shows a variety of features, depending on B. Figure 8.12 is the temporal behaviours of the expectation value Sx(j) in the same spin coherent state as used in Fig. 8.9. Although the dynamics with a fluctuating step Δt_i is identical to the one with the constant step A t in the weak field case, the discrepancy between two kinds of dynamics is serious in the strong field case. Consequently, despite the unitary property of the quantum dynamics with a fluctuating step, the theorem of the quantum recurrence is broken for the strong field case. In fact, the time series of $\langle S_x(j) \rangle$ at the successivec discrete times $t_j=\sum_{i=1}^{j}\Delta t_i$ (~ integer multiples of the period T) exhibit a transition from periodic to erratic behaviours with increasing the driving field.

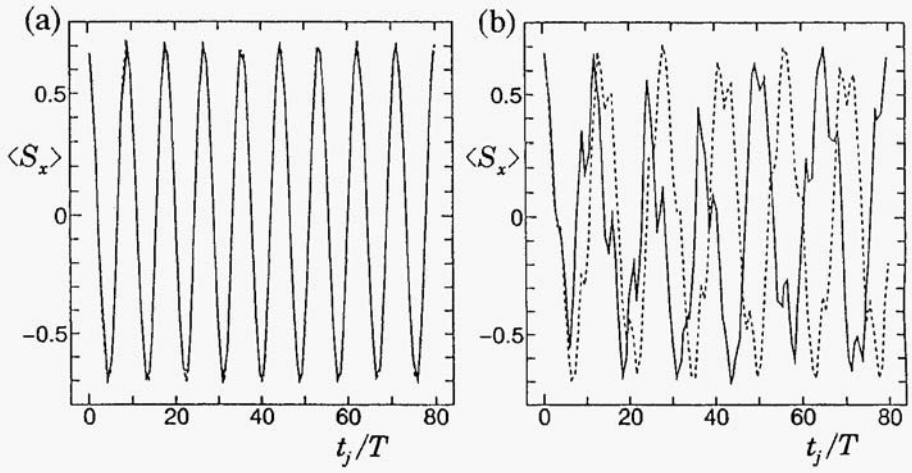

Fig. 8.12. Time series of $<S_x(j)>$ for the case of fluctuating Δt_i. $\omega=2\pi/4$ and time difference $\Delta t:=\mathrm{Max}(\Delta t_i)=T/5$ (a) weak field case (A=1.0, μB=0.05), (b) strong field case (A=1.0, μB=1.0) The same values are used in Fig. 8.13. Broken lines are for the case with no fluctuations, ie., $\Delta t_i = \Delta t$ for any i.

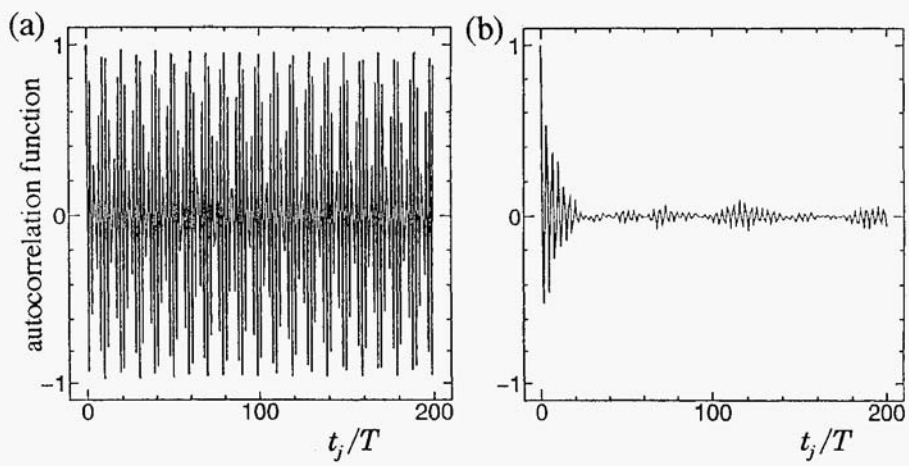

Fig. 8.13. Autocorrelation function of $<S_x(j)>$ for the case of fluctuating Δt_i: (a) weak field case, (b) strong field case.

Figure 8.13 is the autocorrelation function of $<S_x(j)>$. We see the rapid decay and persistence of the correlation for the strong and weak field cases, respectively. Therefore, the fluctuations of Δt, uncover the difference between chaotic and regular dynamics that is hidden in both the time-continuous and discrete-time unitary quantum dynamics.

Nonetheless, the apparently chaotic behavior discussed here is caused by the stochastic behavior of the fundamental time step and not by the deterministic mechanism. It is not valid to call the present erratic behaviors as the deterministic chaos. We are therefore led to a conclusion that, unless we should break the unitarity in quantum dynamics, any kind of time-difference equation could fail to yield a chaotic solution. To obtain genuine chaos in quantum mechanics, it is crucial to pursue a non-unitary time evolution.

8.8. Problems to be Examined

In this chapter, after a thoroughly comprehensive investigation into the role of time discretization in the (originally) time-continuous classical dynamics, we have analyzed various time-discrete variants of Heisenberg's matrix equation of motion. To suppress an artificial nonlinearity arising from finite truncation of infinite-dimensional matrices, we have concentrated on the spin system. Any kind of time-difference equation preserving unitarity proves to exhibit no indication of chaos, because of its reduction to the strictly linear map for the wavefunction. We have therefore proposed a non-unitary time evolution of spin matrices, displaying a numerical evidence of transition from tori to chaos, i.e., a genuine quantum chaos.

Quantum chaos is shown to appear when the fundamental time step Δt is larger than some threshold Δt_C, below which it dissappears. Δt_C itself has a maximum at the quantum limit S=l/2 and decreases as the classical limit $S=\infty$ is approached. The scheme proposed above, reducing exactly to the time-continuous Heisenberg equation of motion in the limit $\Delta t \to 0$, is compatible with the existing framework of quantum mechanics.

As for a candidate for Δt, one may point out, for instance, the time interval for a photon to traverse the electron diameter; actually it is meaningless to imagine the continuous time variation within such an unmeasurable interval. It is desirable to carry out the time-dependent measurement with high precision for the purpose of

observing quantum chaos induced by the time discretization, however difficult a task that would be. To place the present scheme on a more sound basis, there are many serious queries to be addressed: (1) We have concentrated on a special kind of non-unitary evolution. Which one is the most substantial among various kind of non-unitary time evolutions? (2) We have investigated the Heisenberg equation of motion, which is convenient for seeing relationship with the classical equation of motion. But, what will be a corresponding discrete-time evolution of wavefunctions? Is it still possible to provide a probabilistic interpretation of Ψ in the case when the unitarity is not satisfied any more? (3) Can we extend the present scheme to more general dynamical systems with variables $\mathbf{p}, \mathbf{q}$ obeying ordinary canonical commutation rules ? (4) Is it possible to improve the present trial by inventing a time-discrete *symplectic but still non-unitary* quantum dynamics ? All these questions remain to be answered.

References

Amit, C., Ching, E. S. C., Kadanoff, L. P., and Rom-Kedar, V. (1992). *J. Nonlinear Sci.* **2,** 9.

Bender, C. M., *et al.* (1985). *Phys. Rev. Lett.* **55,** 901.

Born, M., and Jordan, P. (1925). *Z. Phys.* **34,** 858.

Dirac, P. A. M. (1930). *The Principles of Quantum Mechanics.* Oxford: Clarendon Press.

Gelfreich, V. G., Lazutkin, V. F., and Svanidze, N. V. (1994). *Physica* **D71,** 82.

Hakkim, V., and Mallick, K. (1993). *Nonlinearity* **6,** 57.

Kruskal, M. D., and Segur, H. (1991). *Stud. Appl. Math.* **85,** 129.

Lazutkin, V. F., Schachmannski, I. G., and Tabanov, M. B. (1988). *Physica* **D40,** 235.

Lee, T. D. (1987). *J. Stat. Phys.* **46,** 843.

Moncrief, V. (1983). *Phys. Rev.* **D28,** 2485.

Nakamura, K. (1993). *Quantum Chaos: A New Paradigm of Nonlinear Dynamics.* Cambridge: Cambridge University Press.

Nakamura, K., and Hamada, M. (1996). *J. Phys.* **A29,** 7315.

Poincare', H. (1890). *Acta Math.* **13,** 1.

Schrödinger, E. (1926). *Ann. Phys. (Leipzig)* **81,** 109.

Tovbis, A. (1994). *Commun. Math. Phys.* **163,** 245.

Tovbis, A., Tsuchiya, M., and Jaffe, C. (1996). Preprint.

Weinberg, S. (1989). *Ann. Phys.* (N.Y.) **194,** 336.

Chapter 9

Conclusions and Prospects

As we have hitherto studied, the present framework of quantum mechanics cannot yield genuine chaos characterized by positive Lyapunov exponents. The quantum dynamics of systems with a few degrees of freedom does not exhibit temporal behaviors other than periodic or quasi-periodic oscillations characterized by discrete energy spectra. It is true that quantum dynamics of many-body open systems may have nonzero generalized KS entropy extended to systems obeying the non-commutative algebra, but such dynamics cannot be endowed with any positive Lyapunov exponent. So far much space has been devoted to the *semiclassical quantization of chaos* and *random matrix theory,* which are exploited by a growing number of researchers in the analyses of *chaos and quantum transport in mesoscopic cosmos.* In Chap. 8, we have even searched for a way to reconcile quantum with *chaos* . Let us now summarize these results and address future prospects.

Chaos and Quantum Transport in Mesoscopic Cosmos

We have developed both classical and quantum-mechanical investigations on open concave and convex billiards whose realization can be found in semiconductor microstructures. The conductance *g(B)* as a function of the magnetic field *B* in open circle *(Cl)* and stadium *(Sd)* billiards (quantum dots) has proved to be related to the feature of classical dynamics. Fluctuations of *g(B)* are shown to be dependent largely on the stability of phase space in the underlying classical dynamics of closed billiards. In the case of *Cl* billiard, the regular modulation of periodic orbits in the phase-space structure gives rise

to regular oscillations of *g(B).* On the other hand, the global chaos and genesis of successive tori with increasing *B* in the case of *Sd* billiard are responsible for slow and rapid variations of *g(B),* respectively. The theoretical result is qualitatively consistent with Marcus *et al.*'s experiment (1992). Furthermore, the classical conductance, calculated on the basis of the bouncing Larmor-orbit picture, has been shown to reproduce most of the locations of peaks in the coarse-grained version of *g(B).*

Real nanoscale structures are accompanied by extrinsic randomness, e.g., corrugation of hard walls, impurities and thermal noises. The rapid progress of advanced technology will smear out these obstacles that prevent us from comparing theory with experiment. The quantum theory of chaos is thus entering an era that will see its experimental verification by means of quantum transport in mesoscopic devices. Currently, theoretical interests are focused on a simple theme: (1) showing universality of conductance fluctuations on the basis of random matrix theory, (2) deriving the S matrices directly by extending Gutzwiller's semiclassical trace formula to open systems. Nevertheless, the observed magneto-conductance of Marcus *et al.* would demand a much deeper insight: The discrepancy of the transition point by more than order of magnitude between the theory and experiment (see Chap. 4) is very serious, and one should accept a challenge to solve this puzzle which, meanwhile, can be solved by neither the semiclassical nor the quantum theory.

For the purpose of enriching the above assertion, a comparative study on the Lyapunov exponents and magneto-conductance *G(B)* in open square and single Sinai billiards has also been made. It has been discovered that conductance fluctuations depend again on the stability of *mixed phase space* in the underlying classical dynamics. In the Sinai billiard case the classical phase space is globally stable against *B,* while for the square billiard it is globally unstable, so long as a low B-field region is concerned. Smoothed (coarse-grained) conductance G_{cg} *(B)* reveals a continuous transition between chaos and tori. In the case of a square billiard, the correlation field B_c of the smoothed conductance is shown to vary irregularly with respect to *B,* while in the case of a Sinai billiard it decreases monotonically with increasing *B.* More careful study revealed that two kinds of correlation fields B_c s are relevant: B_c of G_{cg} ***(B)*** (low frequency component) and that of *G(B)* - G_{cg}*(B)* (high frequency component) have turned out to mimic the average Lyapunov exponent $\langle\lambda\rangle$ and scaled standard

deviation of Lyapunov exponent $\delta\lambda$, respectively. The fluctuation of B_c in the case of square billiard is attributed to the *ghost orbits* with ill-converged large or small Lyapunov exponents proper to a scattering (not periodic) orbit. In the Sinai billiard case, the geometry of the billiard forms an Aharonov-Bohm ring, so that A-B oscillation is observed in a weak field region. While the A-B effect suppresses symptoms of chaos, both B_c s for $G_{cg}(B)$ and $G(B)$ - $G_{cg}(B)$ are nicely related to Lyapunov exponents and therefore capture the quantum-classical correspondence.

A pioneering experiment by Weiss *et al.* (1993) on quantum transport in mesoscopic Sinai billiards (i.e., antidot arrays) was also sketched. Despite the elegant interpretation of some of spectral properties, there remains an open question concerning the underlying low-B field anomaly, which should be interpreted on the basis of isolated unstable periodic orbits. In particular, it is possible to gain alternative insight into the fluctuations in the vicinity of zero field when the system is fully chaotic and no stable periodic orbit survives.

Semiclassical Quantization of Chaos

The semiclassical theory of chaotic scattering is a powerful tool to describe the transport properties in the zero-field regime. Its application to convex hard disk systems (whose realization can be found in finite antidot arrays at the interface of semiconductor heterojunctions) have the following advantage: (1) The systematic enumeration of all periodic orbits is possible with the help of symbolic dynamics. (2) So long as one is concerned with the case of a large degree of opening, only short periodic orbits contribute substantially to the trace formula. As a consequence, the conditional convergence of the trace formula is possible by resorting to the Ruelle zeta function, eliminating the problem of the divergence due to exponential proliferations of periodic orbits (bouncing between disks). The locations of poles (i.e., scattering resonances) of the semiclassical S matrix are in good agreement with those evaluated by the exact quantum-mechanical theory. The region void of resonances in the complex k plane is elucidated. The semiclassical theory of chaotic scattering has not only a conceptual significance for uncovering the quantum-classical correspondence, but also an advantage to be more practical than the exact quantum theory which, in applications, will be confronted with computational limitations in both c.p.u. time and memory area.

As described in Chap. 2, the autocorrelation function of the trace

formula and that of S matrices can be calculated approximately, giving insight into the transport phenomena in the mesoscopic cosmos. The semiclassical scattering theory also predicts the zero-field Lorentzian peak and the Al'tshuler-Aronov-Spivak effect in the wave-number averaged reflection probability for ballistic chaotic billiards (see Chap.4).

A serious problem, however, arises from the semiclassical scattering theory applied to quantum transport in actual mesoscopic microstructures (quantum dots), where conducting lead wires are connected to cavities. There the semiclassical quantization of chaos will be incomplete unless anomalous orbits due to wave diffraction are incorporated besides the scattering orbits. This notion holds for a series of interpretations since Jalabert *et al.* (1990) of the conductance fluctuations in the ballistic quantum transport. It is very difficult to fully describe the effect of diffraction in terms of the particle picture. (Here we have in mind the case where the trace formula is combined with the Kubo formula.)

At the same time it should also be emphasized that the semiclassical theory of chaos or Gutzwiller's trace formula would not be the ultimate theory on *"quantization of chaos."* The semiclassical theory is based on the *assumption* that the Schrödinger-Feynman framework of quantum mechanics should be effective even in systems exhibiting (classical) chaos. It is therefore not so surprizing to find a good agreement between poles of semiclassical zeta functions and those of quantum-mechanical S matrices in hyperbolic billiards without any bifurcation. So long as one stays within the framework of the Schrödinger-Feynman quantum mechanics, the trace formula indeed provides the most valuable tool for exploring many interesting topics lying on the borderline between quantum and classical mechanics of chaotic systems. However, the calculation of the trace formula applied to fully-chaotic bounded systems will encounter a serious problem of nonconvergence in the series sum due to the exponential proliferation of periodic orbits. This problem may be partly overcome either by smoothing the density of states or by inventing a way to achieve conditional convergence by means of the Ruelle zeta function. For bounded systems, however, the eigenvalues computed from the trace formula are not real! To resolve this problem, one should improve the trace formula so as to include higher-order terms in $\hbar$, which will demand more complicated mathematics. Further, in *generic and mixed systems* with elliptic islands (KAM tori) coexisting with a chaotic sea (e.g., billiards in the magnetic field), even

the symbolic coding of periodic orbits is much less obvious.

Since the fundamental law should be as simple as possible, we are here tempted to improve the Shrödinger-Feynman formalism of quantum mechanics for classically chaotic systems in order to capture a much simpler classical-quantal correspondence in the semiclassical limit. The pursuit of this kind should be guided by, and connected with, a growing number of experiments on nanoscale structures in the mesoscopic cosmos.

Random Matrix Theories

Despite an accumulation of works based on the identification of energy spectra in classically-chaotic systems and random matrix theory, there are many counter-examples: those systems possessing GOE level statistics cannot always exhibit chaos in the corresponding classical dynamics. The quantum theory of chaos has a much richer content than the random matrix theory.

We have recognized in Chap. 7 why the quantum spectra of classically-chaotic systems should obey the same universal level statistics as in random matrix theory. There exist universal classical dynamical systems, i.e., the generalized Calogero-Moser (gCM) and Calogero-Sutherland (gCS) systems, lying behind quantum systems which are in general *mixed* in the corresponding classical dynamics. The statistical mechanics of gCM (or gCS) systems is very fruitful, leading to the curvature distribution as well as the major results of the random matrix theory. It is more general than the framework of random matrix theory. As explained in Chap. 7, the statistical mechanics of gCS systems under some constraints will be able to provide the level statistics in the intermediate and mixd regime.

I have a strong criticism against the prevailing tendency to reduce the nature of chaos in quantum systems to that of random matrix theory. While many current researches concern the quantum irregular spectra mediated by fully-chaotic systems, most of the classical dynamical systems possess mixed features implying that KAM tori coexist with chaos. It is desirable to derive an intermediate statistical behavior linking the Poisson and Gaussian ensemble statistics from first principles, without being satisfied with Brody's empirical formula. There would however be no universal statistical behavior in intermediate regions, which is highly system-specific. Choosing the number variance that describes the long-range (rather than short-range) correlation of ensemble of levels, we have pointed out one interesting

channel introduced by Gaudin as early as 1966.

Dynamics beyond Born-Oppenheimer Approximation

In an attempt to construct chaotic dynamics in quantum systems within the present formalism of quantum mechanics, we have analyzed in Chap. 6 the dynamics of systems with a few degrees of freedom beyond the Born-Oppenheimer approximation. In the adiabatic limit, when time scales in the dynamics of molecular complex systems are radically different between slow (nuclear) and fast (electronic) degrees of freedom, the reaction forces (due to fictitious magnetic and electric fields) are indeed exerted on the slow (nuclear) degrees of freedom that are treated classically. But the quantum (electronic) subsystem cannot exhibit chaos. In the dynamics beyond the adiabatic approximation, however, we can see a genesis of chaos in the *quantum system* or the genuine quantum chaos in both bounded and open systems. We saw a nice example illustrated by Bulgac and Kusnezov (1995). From a viewpoint of nonlinear (classical) dynamics, most of molecular kinetics in the microscopic cosmos exhibit a possibility to generate chaos. However, if each molecular complex system were quantized at the outset, this possibility would be smeared out. Eventually, it is difficult to see chaos in quantum systems without artificial approximations. This means that the present formalism of quantum dynamics should be augmented so as to accommodate temporal chaos.

Towards a Challenge to Reconcile Quantum with Chaos

For systems showing chaos in the underlying classical dynamics, we have proposed an alternative formalism of quantum dynamics which exhibits the results of quantum chaos while recovering the existing Heisenberg or Schrödinger equation in a suitable limit.

The progress in nonlinear dynamics and chaos over past decades has revealed that chaos is easily generated from the time-difference variant of the time-continuos integrable system. Motivated by a great significance of time-discretization of the originally time-continuous classical dynamics and also by our expectation to understand more clearly the uncertainty principle between time and energy in our microscopic cosmos, we have chosen a way to discretize the time t in quantum dynamics. In this context, we have scrutinized a time-discrete variant of Heisenberg's equation of motion that has a direct correpondence with the classical equation of motion. *The new*

framework of quantum mechanics assumes both $\Delta t \neq 0$ *and* $\hbar \neq 0$ *and can be reduced to classical mechanics as well as the present formalism of quantum mechanics in suitable limits.* To be explicit, we propose a non-unitary time evolution of spin matrices, displaying a numerical evidence of transition from tori to chaos, i.e., genuine chaos characterized by a positive Lyapunov exponent. We are faced with the demand to proceed to improve the present trial by inventing a time-discrete *symplectic but still non-unitary* quantum dynamics.

The time discretization of Heisenberg equation of motion is not a unique way to generate quantum chaos. Other attempts may be conceivable to pursue the possibility of quantum chaos. Among them, we shall mention briefly (1) the extension of Liouville's equation for the density operator, i.e., a generalization of Schrödinger's equation, and (2) the method of using a time-continuous mesurement.

(1) Attempt by Prigogine's School. By resorting to the statistical description, Prigogine and coworkers (Petrosky and Prigogine, 1994) are trying to incorporate chaos into the quantum dynamics. They choose to describe the evolution of an ensemble of states by means of the Liouville operator acting on the density operator:

$$\mathrm{i}\,\partial\rho/\partial t = L\rho \ , \tag{9.1a}$$

with

$$L\rho = [H,\rho]/\hbar . \tag{9.1b}$$

This Liouville equation is identical to Shrödinger's equation for Ψ in the integrable case. In fact, we have $\rho = \sum_{k,k'} c_k c^*_{k'} |\Psi_k\rangle\langle\Psi_{k'}|$ and $\rho = \sum_k c_k c^*_k |\Psi_k\rangle\langle\Psi_k|$ for pure and mixed states, respectively. By attributing the effect of chaos to Poincare' resonance, i.e., the resonance between different degrees of freedom, Prigogine et al. assert that in the presence of Poincare' resonances the nonunitary diffusion process is combined with the reversible process. In this anomalous process the eigenvalue problem for the Liouville operator (9.1b) has a solution *outside the Hilbert space:* The solution involves a singular term breaking the time reversal symmetry. Therefore the density operator cannot be reduced to wavefunctions any more.

The elaborate attempt by Prigogine and coworkers, however, is directed towards deriving the irreversibility (or determining a direction for the arrow of time) with a help of chaos and thus is not

concerned with generating the quantum chaos characterized by a positive Lyapunov exponent.

(2) Quantum Chaos in Continuous Measurements. Bearing a photon-counting experiment in mind, we are presently investigating the possibility to envisage quantum chaos in continuous measurement. The measurement via photon-counting was originally proposed to realize the Schrödinger's cat state in the laboratory (Ueda *et al.,* 1990). Let the whole system be composed of the measured system (i.e., the subsystem to be measured) and the detector (i.e., measurement apparatus). The measured system, consisting of a two-level atom and the near-resonant photon field, is confined to a cavity. This measured system, called the Jaynes-Cummings model, is known to show chaos if the photon field could be treated classically without resorting to the rotating-wave approximation.

On switching the photon detector on at t=0, one will continue to measure photons emitted through a small hole of the cavity. The continuos read-out of the measurement information will give a continuous reaction on the subsystem and thereby lead to a non-unitary evolution of the density operator ρ of the measured system. The measurement is of either the demolishing or non-demolishing type, depending on whether each detection of a photon is possible with or without an annihilation of the photon inside the measured system. The longer the measurement is continued, the more the measured system would be forced to couple with the large degrees of freedom outside, dissipating the information and losing the quantum coherence. After all, the measured system is expected to possess a feature of the classical system which is able to show a chaotic response. In the measurement process, however, results of measurement are provided in an indeterministic way, so that one cannot predict the observed value in advance. Therefore the quantum chaos in the continuous measurement inevitably involves stochasticity. Investigations similar to ours is being made by Mensky (1995).

Among others, however, the idea developed in Chap. 8 to construct an alternative framework of quantum mechanics by time-discretization would provide the most promising way to unify quantum and chaos.

Epilogue

As we have insisted throughout the book, the genesis of chaos is disturbing the quantization condition of the adiabatic invariants

(Einstein, 1917), which is a logical foundation of modern quantum mechanics. This condition is, on the one hand, a basis for the commutation rule in the Heisenberg formalism of quantum mechanics and, on the other hand, is identical to Schrödinger equation for the wavefunction that is dual to the particle executing periodic or quasi-periodic motions. The latter statement is not changed by the probabilistic interpretation of the wavefunction. Once the framework of quantum mechanics was established, however, all questions about its very logical foundation seem to be forgotten, by our paying major attention to the application of the theory to practical results, e.g., superconductivity and quantum Hall effect. It is amazing that these essential questions remain still unanswered, despite the accumulation of fruitful and practical issues of quantum mechanics.

In this book we have explained the semiclassical theory of chaos or Gutzwiller's trace formula (Gutzwiller, 1990). While still many activities are concerned with its improvement, e.g., inclusion of diffraction effects, higher-order corrections in $\hbar$, etc, the trace formula is not the ultimate theory on quantization of chaos. This formula is based on the *assumption* that Schrödinger-Feynman's formalism of quantum mechanics should be effective even for classically-chaotic systems. The genesis of chaos, however, makes the above asumption groundless and therefore demands that we enrich or revolutionize the present framework of quantum mechanics (Nakamura, 1993).

Our considerable efforts have also been devoted to describing the quantum-classical correspondence (quantum symptoms of chaos) within the present formalism of quantum mechanics. While the description has been largely concerned with quantum transport and irregular energy spectra, wavefunction features are much less trivial. In particular, many works have elucidated (i) the suppression of chaotic diffusion in the wavepacket dynamics and (ii) the scars of unstable periodic orbits embedded in wavefunctions (Giannoni *et al.,* 1991).

However, the major interest throughout the book has centered on the pursuit of a quantum mechanism which generates chaos. So far there is no experimental report to suggest a breakdown of quantum mechanics when applied to classically-chaotic systems. This might be due to the presence of competition between fluctuations caused by determinisic chaos and those by thermal noise and random potentials. Nevertheless, there is a strong possibility to envisage a limitation of quantum mechanics which cannot accommodate chaos, owing to a

rapidly-developing high technology like (1) ultra-low-temperature technology, (2) ultra-small scale fabrication of highly-purified quantum dots and antidots, and (3) measurement on ultra-short time scales.

As candidates capable of generating chaos in quantum mechanics, we mentioned: (1) the time-discretization of Heisenberg's equation of motion, (2) a generalization of Liouville's equation so as to include dissipative process, and (3) continuous measurement, e.g., via photon counting. Other kinds of new quantum formalisms would also be conceivable which should reduce to the Hamilton-Jacobi equation in the classical limit $\hbar \to 0$. It is crucial that theoretical efforts in this direction keep stride with experimental verifications via advanced high technologies such as quantum transport in nanoscale quantum dots or antidots of high purity and with suppressed noise (Beenakkar and Houten, 1991; Akkermans *et al.,* 1995; Nakamura, 1997). To conclude, the pursuit of quantum chaos to reconcile quantum with chaos deserves an extremely great effort, comparable to the theoretical and experimental activities around the blackbody radiation of one century ago that led to the discovery of quantum mechanics.

References

Akkermans, E., Montambaux, G., Pichard, J.-L., and Zinn-Justin, J., eds. (1995). *Mesoscopic Quantum Physics, Proceedings of Les Houches Summer School.* Amsterdam: North Holland.

Beenakker, C. W., and van Houten, H. (1991). In *Solid State Physics: Advances in Research and Applications,* H. Ehrenreich and D. Turnbull, eds. New York: Academic.

Bulgac, A., and Kusnezov, D. (1995). *Chaos, Solitons and Fractals* **5,** 1051.

Einstein, A. (1917). *Verh. Dtsch. Phys. Ges.* **19,** 82.

Gaudin, M. (1966). *Nucl. Phys.* **85,** 545.

Giannoni, M. J., Voros, A., andZinn-Justin, J., eds. (1991). *Chaos and Quantum Physics, Proceedings of the NATO ASI Les Houches Summer School.* Amsterdam: North-Holland.

Gutzwiller, M. C. (1990). *Chaos in Classical and Quantum Mechanics.* Berlin: Springer.

Jalabert, R. A., Baranger, H. U., and Stone, A. D. (1990). *Phys. Rev. Lett.* **65,** 2442.

Marcus, C. M., *et al.* (1992). *Phys. Rev. Lett.* **69,** 506.

Mensky, M. (1995). *Chaos, Solitons and Fractals* **5,** 1381.

Nakamura, K. (1993). Quantum Chaos : *A New Paradigm of Nonlinear Dynamics*. Cambridge: Cambridge University Press.

Nakamura, K., ed. (1997). *Chaos and Quantum Transport in Mesoscopic Cosmos, Special issue of Chaos, Solitons and Fractals* **7.** In press.

Petrosky, T., and Prigogine, I. (1994). *Chaos, Solitons and Fractals* **4,** 311.

Ueda, M., Imoto, N., and Ogawa, T. (1990). *Phys. Rev.* **A41** , 3891.

Weiss, D., *et al.* (1993). *Phys. Rev. Lett.* **70,** 4118.

Index

Adiabatic
approximation 117,122,123
change 104
energies 109
invariant 12, 13,16
limit 104
potential surfaces 120
state 108
transport 105
Aharonov-Bohm (AB)
effect 22, 200
oscillation 48, 71, 76, 200
Allan variance 38
Al'tshuler-Aronov-Spivak effect 75
Anomalous commutation relation 118
Anomalous fluctuations 59
Anomaly phenomena 118
Antidot 70, 80, 100
arrays97, 98, 200
Aperiodic fluctuation 66
Area-preserving 5, 52, 192
Asymptotic expansions beyond all orders
162,163, 175, 180, 181
Autocorrelation function 42, 60, 71, 200
Avoided (level) crossing 102, 104, 155,156,159
multiple 127

Ballistic
conductance fluctuation (BCF) 49, 50
transport 201
Berry phase 154
Billiard
circle (Cl) 46-47, 59-63, 74, 75, 196
concave 46, 54
convex 46, 79, 80
four-disk 79, 96
hyperbolic 80,201
Sinai 23, 46, 66, 70, 75, 80, 98, 199
square 67, 71, 73, 75,199
stadium (Sd) 13,46, 47, 59-63, 74, 75, 198
Birefringence 114
Birkhoff coordinates 5 1
Blackbody cavity 12
Blackbody radiation 12, 15,207
Bloch bands 35
Bohr
magneton 108
radius 41
Bohr-Sommerfeld's quantization 11, 15
Borel
summability 163
summable 170, 171
summation 170
transformation 170,173
Born-Oppenheimer
approximation 106, 117, 121
dynamics beyond 203
force 118, 121
Brody's empirical formula 202
Brownian motion 9, 128, 129, 130
fractional 29
Bunimovich-Sinai curvature formula 91

Canonical ensemble 143
intermediate 143
Canonical transformation 2,3
Cantori 26
Circular
orthogonal ensembles (COE) 147
unitary ensembles (CUE) 151-154
Classical conductance 61
Classical distribution function 9-11
Classical-quantum correspondence 11, 181
Classical transition probability 25

Classical transmission probability 28
Coarse-grained conductance 71
Codimensions 155
Coherent state 9
Comb-like structure 67
Complex crossing point 109,110
Complex Grassmannian sigma model 159
Complex time plane 168
Conditional convergence 21, 89, 200
Conductance fluctuation 26, 73, 201
  ballistic (BCF) 49, 50
  universality of 199
Conservative systems 7
Coulomb blockade 63-65
Cross-over time 11
Crossroads 13, 80, 96
Cumulative distribution function 93, 94
Curvature distribution 147-150
Cyclotron radius 47

De Broglie
  particle 182
  relation 13
  wavelength 92
  wave-particle dualism 11
Degeneracies of eigenvalues 154
Degenerate perturbation theory 103
Degree of randomization 9
Demkov-Osherov Hamiltonian 137
Density of states 24, 85
Destructive phase interference 26
Diabatic
  representation 157
  state 110
Diabolos 156
Diamagnetic Rydberg atoms 136,139
Diffusion coefficient 82
Dirac monople 12 1
Discretized orbits 8
Double-barrier structure 31, 32, 39, 43
Double-cone 156
Double-well potential 163,166
Driven nonautonomous systems 130
Duffing equation 164
Dwelling time 67

Einstein-Brillouin-Keller (EBK)'s
  quantization rule 19
Energy resonator 12
Ensemble
  Laguerre 144
  Legendre 145
  symplectic 145
Equal-time commutation rule (ETCR) 185, 191
Eriscon's fluctuation 26
Essential singularity 180
Evanescent waves 56
Exponential proliferation 21, 25, 57, 80
  of periodic orbits 201
Exterior differentials 105

Fermi
  energy 55, 98
  level 23
  velocity 96
  wave length 66
Feynman's path- integral 16
1/f fluctuation 35
Fictitious gauge
  field 155
  potential 104, 106,107, 109, 118
Field-theoretical model 155,158
Filamentary repeller 83
Fixed points
  elliptic 5
  hyperbolic (HFP) 5, 20, 163, 177, 178
Flicker floor 38
Flux quanta 23
Fokker-Planck equation 129
Fractal conductance fluctuations 26
Fredholm determinant of an integral kernel 144
Fugacity 154
Fundamental time step 194

Gauge potential 111, 113, 158
Gauge structure 102
  global 108
  local 108
Gauge transformation 157
Gaussian
  orthogonal ensemble (GOE) 46,128, 130, 136,139,141, 202
  smoothing 10
  symplectic ensemble 147
  unitary ensemble 147
  wave packet 10
  white noise 130
Generalized Calogero-Moser (gCM) system (model)

134-136, 148, 151, 157, 158, 202
infinite 142
statistical mechanics of 142
Generalized Calogero-Sutherland (gCS) system 135, 151, 202
Genuine quantum chaos 32,196
Geometric phase 104-106,114
Ghost orbits 67, 69, 70, 76, 200
Gibbs measure 143,146,148,152
Green
function 16, 56, 58, 70, 84
theorem 56, 84

Hamilton's principle 17
Hard disks 80
Hartree
approximation 43
equation 40
Heisenberg
equation of motion 182, 183,190, 196
equation of motion for spin matrix 188
matrix mechanics 11
uncertainty principle 2, 10
Hellmann and Feynman's theorem 132
Henon maps 181
Heteroclinic structure 163
Heterostructures 39
Holonomy 106
Homoclinic
orbits 20
point 5,7
structure 7,175, 181
Hyper-energy surface 155, 156

Ill-converged 70
Impurity potentials 14
Inelastic mean free paths 66
Information dimensions 92
Intermediate distribution 139
Intermittent chaos 36, 38
Internal equation 168
Intersection angle 181
Irreducible closed contour 18

Jaynes-Cummings model 205
Joint distribution function 151,152
Joint probability density 130,144, 149

KAM tori 5, 9, 26, 46, 53, 60, 67, 136, 151,202
collapse of 4
Kicked rotator 131
Kolmogomv-Sinai(KS) entropy 1, 7, 9, 21, 32, 42, 65, 81, 181, 198
Krönig-Penny model 31
K system 46

Lagrange multiplier 152
Laminar oscillations 38
Landauer formula 70
Landau gauge 55
Landau level 98
Landau-Zener(LZ) model 108
Gaussian twisted 115,116
winding 110,111
Landau-Zener(LZ) transition 111,124, 137
Langevin equation 130
Larmor-orbit
bouncing 62, 63, 199
Larmor radius 50, 68, 83
Law of large number 38
Lead wires 70
Leapfrog method 183
Lebesgue measure 81
of periodic orbits 20
Legendre orthogonal ensembles 130
Level degeneracy 102
Level-dynamics 128
Level spacing 64
distributions 128
Liouville equation 10
extension of 204
Lyapunov exponent 7, 20, 32, 35,37, 42, 52, 55, 65, 67-69, 71, 75, 81, 82, 87, 90, 96, 181, 198, 199

Magneto-conductance 47, 49, 75, 199
Manifolds
stable 7, 170, 179
unstable 5, 7, 162, 166, 170, 179
Many-body effect 43, 47, 65
Markovian process 38
Maslov index 13, 17, 18, 25, 28, 58, 186
Maxwell-Boltzmann distribution 137
Maze-like structure 10
Mean free path 98
Mean level spacing 24
Mesoscopic
devices 13
structures 47

Mexican-hat potential 121,122
Mixed
phase 27
phase space 50, 75, 199
systems 28
Moncrief's time-discretization 193
Monodromy matrix 20, 52, 87, 90
Monopoles 159

Nanoscale structures 13
Nikitin's model 113
Noises
fractional 38
thermal 14, 63, 199
NonAbelian gauge field 157
Nonadiabatic
transitions 107,108,122
transport 108, 109
Non-Gaussian distribution 64
Nonlinear Hartree-like equation 35
Non-unitary
diffusion process 204
quantum dynamics 197,204
time evolution 196
transformation 194
Number variance 151-153

Parallel transport of quantum eigenstates 106
Pauli matrices 106,135
Peierls phase factor 70
Periodically-pulsed system 131
Periodic orbits
exponential proliferation of 30
isolated prime 87
primitive 20
scars 46
stable 20
symbolic coding of 22, 29
unstable 7, 19, 82
Perron-Frobenius operator 81
Persistent currents 22. 23
Phase coherence length 98
Phase droplet 7
Phase-integral method 110
Phase liquid 10-11
Phase space 71
Photon-counting experiment 205
Poincare'
linearized map 20, 59, 67, 87
map 5, 50-51, 58, 90
recurrence theorem 11
resonance 204
surface of section 5, 90, 188
Poisson brackets 134
Poisson distribution 137,139
Probability density function 9
Pseudo-chaos 31-32, 35, 39
Pseudo-time 132

Quantization
of action 186
of chaos 15, 19, 201
of integralsystems 17
Quantum dot 76,201
Quantum recurrence 11
Quantum transport 198, 199
ballistic 201
in superlattice 32
Quantum wires 67
Quasi-time 128,131
Quaternionic Hamiltonians 103
Quaternions 135

Random forces 129
Random matrix theory 63, 94-96, 136, 142, 144, 147, 199-202
Reaction forces 118
Recurrent phenomenon 2
Reduced action 20, 25
Resistance anomalies 98
Riemann-Siege1 type resurgence 21
Riemann's zeta function 21
Ruelle zeta function 21, 30, 89, 95, 200

Saddle-point approximation 19
Scattering
orbits 25
resonances 82, 87, 92, 93
Schrödinger equation 55, 96, 108, 120, 181,206
descrete variant of 185
nonlinear 43,164
time-dependent 40, 104, 107, 112, 131,181,182
time-independent 16
Schrödinger-like equation 114
Schrödinger's cat state 205
Schrödinger's wave mechanics 11
Semiclassical
quantization of chaos 15,200
resonance 93, 95

Sensitivity to initial conditions 1, 7, 181
Separatrix 4,164
  bifurcation of 163
  splitting 162, 163, 165,167,170,172
Shubnikov-de Haas oscillations 98
Slow degrees of freedom 117,122
Smale's horse-shoe mechanism 2, 6, 8, 10, 163, 180
S matrix 22, 25, 31, 35, 39, 55-57, 63, 83-89, 199, 200, 201
Soft wall model 98
Soliton 136
  concentration of 139
  condensation of 142
  gas of 136,142
  turbulence 136
Solitonic structures 136
Spectral rigidty 139
Spin-coherent state 192
Stability eigenvalues 5, 87
Stationary phase approximation 17, 109
Stochastic differential equation 128
Stokes
  constant 173,175, 176, 177
  line 168,172, 175, 179
  phenomenon 163,168,170,172,179
Stretching mechanism 8
Symbolic
  codings of periodic orbits 87, 202
  dynamics 97,200
Symmetry induced factorization 89
Symplectic map 163,164, 180, 194
  nonlinear 185
Symplecticity condition 164

Tangent map 67
Tight binding model 70
Time-continuous mesurement 204
Time-difference 162, 183
Time–discrete
  classical dynamics 162
  non-unitary quantum dynamics 186
  quantum dynamics 187
  sympledic but still non-unitary 197, 204
  unitary quantum dynamics 183
Time discretization 162- 164
  of Heisenberg equation of motion 204
Time quantization 194
Topological pressure functions 81
Tori
  collapse of 160
  invariant 17, 19
  nonresonant 4
  resonant 4
  stability of 3
Trace formula 19-22, 29, 57, 80, 87, 98, 206
Transfer matrix 34
Translational lattice symmetry 35
Transmission
  amplitudes 27
  coefficient 35, 57
Tunnelings
  over-barrier 33
  resonant 31-32, 39
  Zener 35, 38,108
Two-level
  cluster function 152,153
  correlation function 152

Umbilic points of curved surfaces 107
Unitary quantum dynamics 183
Unitary transformation 25
Universal conductance fluctuations (UCF) 48, 59, 66, 71

Vandermonde determinant 145

Wave diffraction 29
Wavepacket 41
  dynamics 10
Weak-localization 49
Whittaker function 56
Wiener process 128
Wien-Planck scaling formula 19
Wigner
  distribution 139,147
  level-spacing 136
  representation 10
  semicircle law 146
Winding Demkov model 113
Windingnumber 4, 18, 24

Fundamental Theories of Physics

67. Yu. L. Klimontovich *Statistical Theory of Open Systems.* Volume 1: A Unified Approach to Kinetic Description of Processes in Active Systems. 1995 ISBN 0-7923-3199-0; Pb: ISBN 0-7923-3242-3
68. M. Evans and J.-P. Vigier: *The Enigmatic Photon.* Volume 2: Non-Abelian Electrodynamics. 1995 ISBN 0-7923-3288-1
69. G. Esposito: *Complex General Relativity.* 1995 ISBN 0-7923-3340-3
70. J. Skilling and S. Sibisi (eds.): *Maximum Entropy and Bayesian Methods.* Proceedings of the Fourteenth International Workshop on Maximum Entropy and Bayesian Methods. 1996 ISBN 0-7923-3452-3
71. C. Garola and A. Rossi (eds.): *The Foundations of Quantum Mechanics - Historical Analysis and Open Questions.* 1995 ISBN 0-7923-3480-9
72. A. Peres: *Quantum Theory: Concepts and Methods.* 1995 (see for hardback edition, Vol. 57) ISBN Pb 0-7923-3632-1
73. M. Ferrero and A. van der Merwe (eds.): *Fundamental Problems in Quantum Physics.* 1995 ISBN 0-7923-3670-4
74. F.E. Schroeck, Jr.: *Quantum Mechanics on Phase Space.* 1996 ISBN 0-7923-3794-8
75. L. de la Pena and A.M. Cetto: *The Quantum Dice.* An Introduction to Stochastic Electrodynamics. 1996 ISBN 0-7923-3818-9
76. P.L. Antonelli and R. Muon (eds.): *Lagrange and Finsler Geometry.* Applications to Physics and Biology. 1996 ISBN 0-7923-3873-1
77. M.W. Evans, J.-P. Vigier, S. Roy and S. Jeffers: *The Enigmatic Photon.* Volume 3: Theory and Practice of the $\boldsymbol{B}^{(3)}$ Field. 1996 ISBN 0-7923-4044-2
78. W.G.V. Rosser: *Interpretation of Classical Electromagnetism.* 1996 ISBN 0-7923-4187-2
79. K.M. Hanson and R.N. Silver (eds.): *Maximum Entropy and Bayesian Methods.* 1996 ISBN 0-7923-4311-5
80. S. Jeffers, S. Roy, J.-P. Vigier and G. Hunter (eds.): *The Present Status of the Quantum Theory of Light.* Proceedings of a Symposium in Honour of Jean-Pierre Vigier. 1997 ISBN 0-7923-4337-9
81. *Still to be published*
82. R. Muon: *The Geometry of Higher-Order Lagrange Spaces.* Applications to Mechanics and Physics. 1997 ISBN 0-7923-4393-X
83. T. Hakioglu and A.S. Shumovsky (eds.): *Quantum Optics and the Spectroscopy of Solids.* Concepts and Advances. 1997 ISBN 0-7923-4414-6
84. A. Sitenko and V. Tartakovskii: *Theory of Nucleus.* Nuclear Structure and Nuclear Interaction. 1997 ISBM 0-7923-4423-5
85. G. Esposito, A.Yu. Kamenshchik and G. Pollifrone: *Euclidean Quantum Gravity on Manifolds with Boundary.* 1997 ISBN 0-7923-4472-3
86. R.S. Ingarden, A. Kossakowski and M. Ohya: *Information Dynamics and Open Systems.* Classical and Quantum Approach. 1997 ISBN 0-7923-4473-1
87. K. Nakamura: *Quantum versus Chaos.* Questions Emerging from Mesoscopic Cosmos. 1997 ISBN 0-7923-4557-6

KLUWER ACADEMIC PUBLISHERS -
NEW YORK / BOSTON / DORDRECHT / LONDON / MOSCOW